THE UNIVERSITY
of EDINBURGH

Characteristics of Cellular and Synaptic Function in Rodent Forebrain Neurons with Altered SynGAP Expression

Dr Lindsay A. M. Mizen
BScMedSci MBChB MRCPsych

Doctor of Philosophy,
The University of Edinburgh

2017

Declaration

This work was carried out in the Centre for Integrative Physiology, School of Biomedical Sciences at the University of Edinburgh. I hereby certify that this thesis and its composition are entirely my own work, with the exception of the following:

1. The SynGAP_GAP deletion rat model was designed by Professor Peter Kind and Dr Sally Till, Centre for Integrative Physiology, University of Edinburgh with Sigma Advanced Genetic Engineering (SAGE) Laboratories, St Louis, USA (now Horizon Discovery). SAGE then engineered the rat in the USA

2. Dr Adam Jackson, Centre for Integrative Physiology, conducted a number of the hippocampal long-term depression recordings, including all the recordings in which protein synthesis was blocked

3. Various members of the Hardingham laboratory, Centre for Integrative Physiology, prepared the WT Sprague-Dawley rat cortical cultures which I used for SynGAP isoform experiments

4. Katherine Bonnycastle, Centre for Integrative Physiology, prepared the SynGAP rat hippocampal cultures from which I recorded miniature excitatory post-synaptic currents

5. Dr Owen Dando, Centre for Integrative Physiology, mapped mRNA-seq read sets to their respective genomes, examined for novel splice junctions at the SynGAP locus and thereby identified the sequences for putative new SynGAP 5' variant forms

6. Shinjini Basu, Centre for Integrative Physiology, University of Edinburgh, conducted the RT-PCR experiments using the SynGAP isoform constructs I made

No part of the work contained in this thesis has been submitted for any other degree or professional qualification.

Signed …… Date……..

Acknowledgements

Coming from a clinical background to undertake a basic science PhD has been the most challenging thing I've ever done. The numbers of people who made this possible and more importantly who supported me through it are too many to name individually. Therefore for anyone I don't mention personally, please be assured I'm very grateful.

My thanks must start with Dr Craig Melville, University of Glasgow. Without your support, encouragement and guidance I would not have taken my first steps on the research ladder, nor would I have seriously considered applying to the PsySTAR PhD programme. Your mentorship has been much appreciated! Thank you too to Professor Anna Cooper for including me in research and related opportunities prior to my Higher Training and PsySTAR PhD applications.

Grateful thanks must also go to the funders of the Psychiatry: Scottish Training in Academic Research (PsySTAR) scheme and its directors, who granted me this wonderful opportunity to better understand the mental disorders I treat and contribute to preclinical intellectual disability research that will hopefully impact positively on patients in the future. I must also acknowledge my mentor Dr Andy Stanfield, University of Edinburgh. It was a pleasure working with you clinically Andy and I've really valued the career and research advice you've given me since then.

The exciting research into single gene disorders associated with intellectual disability and autism spectrum disorders in the laboratories of my PhD supervisors Professors David Wyllie and Peter Kind captured my imagination and provided a world class environment in which to study. I am very grateful to you both and to the other members of my thesis committee, Professor Stephen Lawrie and Dr Mandy Johnstone, for the extra guidance and support you gave me. Dr Paul Skehel, Centre for Integrative Physiology also deserves a very special acknowledgement for his never ending patience and encouragement. This extended far beyond the specific SynGAP isoform work you kindly agreed to supervise Paul and I can genuinely say there are times when I would've given up on my studies without you; 'thank you' is inadequate.

I also couldn't have completed this thesis without my fellow researchers in the Centre for the Integrative Physiology, particularly the members of the Wyllie, Kind, Hardingham, Daw, Osterweil and Jackson laboratories. I very much valued all the instruction, support, guidance and shoulders to cry on. Thank you for putting up with my silly questions and frequent frustrations and for being a captive baking audience! I really enjoyed your company and very much admire your skills and your dedication to science. Special thanks go to Dr Adam Jackson in particular; from

teaching me to patch my first cell to advising about thesis preparation you've been there from beginning to end, thank you ever so much! Similar acknowledgements must go to Owen Dando, Shinjini Basu and Katherine Bonnycastle who contributed to this body of work and for whose help I'm extremely grateful. I must also express my thanks to Richard Watson, Senior Technical Officer and to all the other technicians who had a hand in caring for the SynGAP rats over the course of my research. The experiments would've been impossible without you. Lastly in this section I must acknowledge Aoife McMahon. We only met in person once, but your thesis formed the backbone of a significant portion of my work and was an essential resource, thank you!

The support of my friends and family has also been invaluable. Cara and Caroline L, you have both been such an amazing support and wonderful company, as have Ian and Martin. Thank you so much for all the times you've listened, supported and picked up the pieces. The same goes for Caroline M, Michelle, Cat and Rachael; you have also heard more than your fair share about the trials and tribulations of research!

Mum and dad, your emotional and financial support over the years took me to medical school and beyond for which I am extremely appreciative. I hope you can take some satisfaction from the part you therefore played in helping the patients I now care for and for whom I ultimately conducted this research. Thank you too to mum and my sister Lauren for all your love and practical support during the PhD. You both know how much of a challenge it has been and having you nearby was such a help. I truly couldn't have done it without you.

Finally, I'd like to dedicate this thesis to my dear Granny Currie. As one of the early female doctors in Scotland who also worked with people with disabilities and who is a true matriarch of our family, you have been an inspiration! You have always taken such an interest in comparing and contrasting my studies and career with your clinical experiences and Grandpa's academic and clinical experiences. Visiting you regularly helps me remember the important things in life. This thesis is for you.

Abstract

Intellectual disability (ID) and autism spectrum disorders (ASDs) can have a devastating impact on an individual's functioning and quality of life. Insights from pre-clinical models of monogenic forms of ID and ASD are now revealing the biochemical pathways and aberrations in cellular and synaptic functioning involved.

One monogenic cause of ID, ASD and epilepsy is *SYNGAP1* ID which results from mutations in the *SYNGAP1* gene on human chromosome 6. Although a variety of symptoms have been reported, many affected individuals have moderate to severe intellectual impairment and severe seizure phenotypes.

Previous pre-clinical studies have mainly focussed on the effects of altered SynGAP expression in mice. This thesis is therefore the first to explore altered SynGAP expression in a rat model. It also adds to the body of research exploring the roles of SynGAP isoforms in glutamatergic synaptic function.

The SynGAP_GAP deletion rat was engineered to have a deletion encompassing the enzymatically active GTPase activating protein (GAP) domain of the protein, via which SynGAP regulates multiple biochemical pathways by enhancing the slow intrinsic hydrolysis of GTP by GTP-binding proteins. S*yngap*$^{GAP/GAP}$ rats appeared small and failed to thrive. As with *Syngap*$^{-/-}$ mice, this complete loss of WT SynGAP proved lethal, whereas *Syngap*$^{+/GAP}$ rats appeared to develop normally.

The electrophysiological data obtained from this new model reveals a reduction in the frequency of miniature excitatory post-synaptic currents (mEPSCs) in S*yngap*$^{+/GAP}$ cultured neurons. However the exaggerated hippocampal long-term depression identified in *Syngap*$^{+/-}$ mice was not seen in the rats. There was also no evidence of differences in intrinsic cell properties, excitatory and inhibitory currents or ratios of AMPAR / $GABA_AR$ and AMPAR / NMDAR between WT and heterozygous rats.

In addition to the characterisation of the SynGAP_GAP deletion rat, the impact of the previously unstudied Eα1 isoform on forebrain neuronal synaptic function was examined through mEPSC recordings. A trend towards lower mEPSC frequency was found which supports previous research showing that α1 isoforms reduce synaptic strength.

This body of work therefore adds to published evidence of isoform specific functions and provides the first evidence of the impact of SynGAP alterations in rats, the results of which show some intriguing differences from previous work in mice.

Lay summary

Learning disability or 'Intellectual disability' (ID) and autism spectrum disorders (ASDs) can have a devastating impact on a person's functioning and quality of life. Insights from rodents with deliberate changes ('mutations') in specific genes that are linked to ID and ASD in humans are now revealing abnormalities in the brain that are involved in these conditions. One cause of ID and ASD in humans, called *SYNGAP1* Intellectual Disability, results from mutations in a gene called *SYNGAP1* which is the blueprint for cells to produce a protein called SynGAP. This protein is an important regulator of signalling in the brain. Many affected individuals have moderate to severe intellectual impairment, autism spectrum disorder and severe forms of epilepsy.

Previous rodent studies have mainly focussed on the effects of altering the amount of SynGAP protein in mouse brains. This thesis is the first to explore the impact of SynGAP mutation in rats. The SynGAP_GAP deletion rat, as the new rat was named, was engineered to be missing a portion of the SynGAP protein called the GAP domain which normally acts as a brake on particular signalling pathways in the brain. Rats with the mutation in both of their two copies of the gene appeared small and failed to thrive. As had previously been shown in mice, this complete lack of normal SynGAP proved lethal, whereas rats with only one copy of the mutation appeared to develop normally.

For some experiments brain cells from the new rats were grown in dishes ('cultured') and for others, brain slices were used. Tiny electrical currents from individual or groups of cells were recorded. Surprisingly, certain findings from published research in mice were not reproduced. In mice with no SynGAP, particular electrical currents between brain cells were more frequent, thought to be because the 'brake' effect of SynGAP had been lost. However the cells of rats with two mutated copies of SynGAP this signalling was no different from rats with no mutation. Furthermore the signalling in rats with one normal and one mutated copy of SynGAP was less frequent which was somewhat puzzling. Research has previously shown that application of a drug called DHPG to brain slices from heterozygous SynGAP mice (those with only one abnormal copy of SynGAP) results in an exaggerated reduction in electrical transmission in the hippocampus, a brain region involved with learning and memory. In the heterozygous rats, this signalling was no different from rats with normal SynGAP. Other recordings were made of the electrical properties of single rat brain cells which were less directly comparable to previous work in mice. These were also no different in heterozygous rats compared to rats with normal SynGAP.

In addition to the above, cultured brain cells were manipulated to have extra Ealpha1, a previously unstudied type of SynGAP. A trend towards less frequent occurrence of certain currents passing between the cells was found. This is in keeping with previous research showing other alpha1 types of SynGAP reduce the signalling between neurons.

This body of work therefore adds to published evidence suggesting that different types of SynGAP have specific functions and provides the first evidence of the impact of SynGAP alterations in rats, the results of which show some intriguing differences from previous work in mice.

Table of Contents

List of Figures

List of Tables

Abbreviations

List of abbreviations commonly used in this thesis

AAV	Adeno-associated virus
ACSF	artificial cerebrospinal fluid
AMPA(R)	α-amino-3-hydroxy-5-methyl-4-isoxazole (receptor)
ANOVA	Analysis of variance
AP5	D(−)-2-Amino-5-phosphonopentanoic acid
ARA-C	Cytosine β-D-arabino-furanoside hydrochloride
ASD	Autism spectrum disorder
ASPA	Animal (Scientific Procedures) Act 1986
bp	Base pair
CaMKII	$Ca^{2+/}$calmodulin- dependent protein kinase II (CaMKII),
CA1	*Cornu Ammonis* 1
CA3	*Cornu Ammonis* 3
cDNA	Complementary DNA
CHX	Cycloheximide
CNQX	6-Cyano-7-nitroquinoxaline-2,3-dione
CNV	Copy number variations
DHPG	(RS)-3,5-dihydroxyphenyl-glycine
DIV	Day *in vitro*
DNA	Deoxyribonucleic acid
DNQX	6,7-dinitroquinoxaline-2,3-dione
(m)EPSC	(miniature) excitatory post-synaptic current
(m)EPSP	(miniature) excitatory post-synaptic potential
E	Embryonic day
E/I	Excitation/Inhibition
ERK	Extracellular signal-regulated kinases
FXS	Fragile X Syndrome
GABA(R)	*gamma*-Aminobutyric acid (receptor)
GAP	GTPase activating Protein
GAPDH	Glyceraldehyde 3-phosphate dehydrogenase
GEF	Guanine nucleotide exchange factor
GFP	Green fluorescent protein
GTP/GDP	Guanosine triphosphate / guanine diphosphate
HCN	Hyperpolarization-activated cyclic nucleotide–gated
ID	Intellectual disability
(m)IPSC	(miniature) inhibitory post-synaptic current
(m)IPSP	(miniature) inhibitory post-synaptic potential
KO	knock-out

Abbreviations continued:

LB	Luria broth
LEH	Long Evans Hooded
LTD	Long-term depression
LTP	Long-term potentiation
MAPK	Mitogen-activated protein kinases
mGluR	Metabotropic glutamate receptor
mPFC	Medial prefrontal cortex
NMDA(R)	N-methyl-D-aspartate (receptor)
NSID	Non-syndromal intellectual disability
P or PND	Postnatal day
PCR	Polymerase chain reaction
Pen/Strep	Penicillin / streptomycin
PH	Pleckstrin homology
PPF	Paired pulse facilitation
PSD	Post-synaptic density
PSD-95	Post-synaptic density 95
PTX	Picrotoxin
PV	Parvalbumin
qPCR	Quantitative polymerase chain reaction
RasGAP	Ras GTPase activating protein
RapGAP	Rap GTPase activating protein
RNA	Ribonucleic acid
mRNA	Messenger ribonucleic acid
RT-PCR	Reverse transcription polymerase chain reaction
siRNA	small interfering RNA
shRNA	short hairpin RNA
tRNA	transfer RNA
SNP	Single nucleotide polymorphism
SynGAP	Synaptic GTPase activating protein
SST	Somatostatin
TTX	Tetrodotoxin
WT	Wild type
ZFN	Zinc-finger nuclease

1 CHAPTER ONE: INTRODUCTION

1.1 Background

Intellectual disability (ID) and Autism Spectrum Disorders (ASDs) can have a devastating impact on an individual's life expectancy and quality of life (Patja et al. 2001; Tyrer et al. 2006; Emerson et al. 2010; Dieckmann et al. 2015, Baxter et al. 2015) and can be associated with multiple physical and mental comorbidities throughout the life span (Munir 2016; Cooper & Smiley 2009; Cooper 1999).

Despite the therefore pressing need to modulate these conditions, at present there are no drug therapies to directly target ID or autism spectrum disorder. However, preclinical research is identifying the biochemical pathways and networks that underpin the pathology in ID and ASD which will hopefully in time lead to new therapies. Studies into ID and ASD have implicated aberrations in genes associated with dendritic spine and synaptic function including in *SYNGAP1* gene (Ropers & Hamel 2005; Betancur 2011; Pinto et al. 2011; Penzes et al. 2011; Iossifov et al. 2012; de Ligt et al. 2012; Mefford, Heather C; Batshaw, ML and Hoffman 2012; Rauch et al. 2012; Penzes et al. 2013; Fitzgerald et al. 2015; Vissers et al. 2015).

This thesis therefore focusses on the mechanisms underlying *SYNGAP1* ID which is also associated with ASD and epilepsy and results from mutations in the *SYNGAP1* gene on human chromosome 6. *SYNGAP1* codes for the SynGAP protein which is one of the most abundant proteins in the post synaptic density of neurons. Its absence is lethal in mice and various aberrations have been found in the cellular and synaptic functioning of *Syngap*$^{+/-}$ mice. This thesis details the initial characterisation of the first SynGAP rat model which has a deletion encompassing the enzymatic GAP domain of the protein, the domain which normally enables it to regulate downstream signalling pathways. Previous work in our laboratory has explored the functions of the multiple different SynGAP isoforms and this thesis also expands on this work.

1.2 Intellectual Disability

In order to appreciate the relevance and importance of pre-clinical work in ID and ASD, an understanding of the two conditions is helpful. There are two main international classification systems for mental disorders, the World Health Organisation's International Classification of Disease Version 10 (ICD 10) and the fifth edition of the Diagnostic and Statistical Manual of Mental Disorders (DSM-5).

The term Intellectual Disability (ID) is defined in ICD 10 as *'a condition of arrested or incomplete development of the mind, which is especially characterized by impairment of skills manifested during the developmental period, skills which contribute to the overall level of intelligence, i.e. cognitive, language, motor, and social abilities'* (WHO 1992). In order for a diagnosis of Intellectual Disability to be made, the onset of the symptoms or impairments must occur before the age of 18 years. The severity of ID is defined by Intelligence Quotient (IQ) as follows:

- Mild (IQ 50 to 69)
- Moderate (IQ 35 to 49)
- Severe (IQ 20 to 34)
- Profound (IQ < 20)

DSM-5 (APA 2013) similarly classifies Intellectual Disability as presenting with impairments in general mental abilities that impact adaptive functioning across the following domains

1) Conceptual (e.g. language, reasoning and memory)
2) Social (e.g. interpersonal communication skills, empathy and social judgment)
3) Practical (e.g. self-management in personal care, money management, job responsibilities etc.)

It also specifies that the impairments must begin during the developmental period and in addition to IQ it also classifies the severity of the disorder by the degree of impairment in adaptive functioning.

In some countries other terms are still used to describe the same disorder. These include 'Learning Disabilities', 'Mental Retardation', 'Mental Handicap', 'Mental Disability', 'Developmental Disabilities', 'Mental Deficiency' and 'Mental Subnormalty' (WHO 2007). The prevalence of ID is somewhat uncertain, but interpretation and comparison of data gave figures of 9-14/1000 in childhood and 3-8/1000 in adults in high income countries; rates were higher in low-income countries (Cooper & Smiley 2009). A meta-analysis of population based data gave a prevalence of 10.37/1000 of the population, but it noted that studies in children and adolescents and in developing countries give higher estimates (Maulik et al. 2011).

There are hundreds of environmental causes of ID including perinatal anoxic / traumatic brain damage, foetal alcohol syndrome, infections in pregnancy (e.g. rubella, cytomegalovirus etc.), heavy metal poisoning etc. (Cooper and Smiley 2009), but genetic factors play an very important role too. The genetic mutations involved are extremely heterogeneous with more than 700 genes (X-linked, autosomal-dominant and autosomal-recessive) now linked to ID (Vissers et al. 2015). Forms of ID are defined as syndromic or non-syndromic (NSID) depending on whether additional morphological, radiologic or metabolic abnormalities over and above the ID itself are observed on physical examination, laboratory investigation and brain imaging. (Ropers & Hamel 2005; Dierssen & Ramakers 2006; Rauch et al. 2012).

1.3 Autism Spectrum Disorder

Autism was independently recognised by Leo Kanner and Hans Asperger in the 1940s. Kanner described what is thought of as 'Classical autism' (Kanner 1943) in a case series of 11 children in which he described the key deficit as being the children's "inability to relate themselves in the ordinary way to people and situations from the beginning of life". Asperger published in German in 1994 and his original paper was translated later by Uta Frith (Asperger & Frith 1991). He described a similar disorder albeit with relative preservation of language skills. It wasn't until 1987 that the syndrome named after him was recognised in the third edition of the DSM (see Murphy et al. 2016 for a review of the diagnostic classifications of autism spectrum disorders). 'Childhood Autism' as it is defined in ICD 10 is '*(a) the*

presence of abnormal or impaired development that is manifest before the age of three years, and (b) the characteristic type of abnormal functioning in all the three areas of psychopathology: reciprocal social interaction, communication, and restricted, stereotyped, repetitive behaviour' (WHO 1992). There has been growing recognition since the publication of ICD 10 that 'childhood autism' is not simply a disorder of childhood and that although the associated impairments may improve over the lifespan, the diagnostic status remains relatively stable (reviewed in Magiati et al. 2014).

DSM-5 re-defined the classification of Autism Spectrum Disorder in 2013 to:

a) Persistent disorders in social communication and social interaction across contexts, not accounted for by general developmental delays and
b) Restricted, repetitive patterns of behaviour, interests, or activities

that must be must be present in early childhood and limit and impair everyday functioning (APA 2013).

ASD is more common in those with ID than in individuals of IQ > 70 (Brugha et al. 2016) and as with ID the proposed causes are multiple. They include genetic disorders, advancing parental age, complications in pregnancy and exposure to chemicals (Lai et al. 2014).

1.4 Single gene disorders associated with ID and ASD

The aetiological complexity and phenotypic diversity of ID and ASD are challenging when trying to identify the underlying mechanisms driving them. One popular approach is therefore to study single gene disorders associated with ID and ASD. These include Fragile X Syndrome (FXS), Rett Syndrome and Tuberous Sclerosis (TS) all of which have been extensively studied in rodent models. This thesis focusses on *SYNGAP1* ID, a single gene disorder that is associated with both ID and ASD.

1.4.1 SYNGAP1 ID

The human *SYNGAP1* gene is located at Chromosome 6p 21.3 and codes for the Synaptic GTPase Activating Protein (SynGAP) protein. This protein been shown in preclinical models to be abundant in the post-synaptic density of neurons and to be

involved in synaptic signalling by regulating the insertion of excitatory α-amino-3-hydroxy-5-methyl-4-isoxa-zolepropionic acid (AMPA) receptors into the cell membrane (Chen et al. 1998; Kim et al. 1998; Krapivinsky et al. 2004; Rumbaugh et al. 2006). Further detail on the structure and function of SynGAP is presented later.

The first link between mutations in *SYNGAP1* and clinical disorders was made by researchers in Montreal in 2009. Due to the known association between intellectual disability and disruption of synaptic plasticity pathways, *SYNGAP1* was chosen as a candidate gene in a screen of *de novo* mutations in patients with non-syndromic intellectual disability (Hamdan et al. 2009). 3 of the 94 patients were identified as having *de novo* mutations in *SYNGAP1*. The three were aged between 4 and 11 years of age and all had global developmental delay, severe language impairment and hypotonia; two also had epilepsy. Since this first study several more papers identifying and / or characterising people with *SYNGAP1* mutations have followed (Table 1). Some of these individuals have mutations that only affect SynGAP and others have mutations encompassing multiple genes including *SYNGAP1* (Krepischi et al. 2010; Zollino et al. 2011; Writzl & Knegt 2013; Parker et al. 2015). The mutations were *de novo* in the majority of cases where parental data was available. Only one patient has been identified in which the mutation was inherited. This was a Danish patient in whose father the mutation was mosaic (Berryer et al. 2013).

Table 1– Timeline of papers identifying or characterising individuals with *SYNGAP1* mutations

Study	Cohort Characteristics	Patients with *SYNGAP1* mutations	New Features Noted
Hamdan 2009	94 patients with non-syndromic ID	3 females, 4-11 years	Global developmental delay, severe language impairments, hypotonia and epilepsy
Hamdan et al. 2011	95 patients with sporadic NSID	1 female, 2 males	
Krepischi et al. 2010	300 patients with ID studied by 1Mb array-CGH	6 year old male	Deletion of 18 known genes including *SYNGAP1*
Pinto et al. 2010	Single SNP microarray in 1604 people with ASD	1exonic deletion	
Vissers et al. 2010	Whole exome sequencing ten parent-proband trios	1 female	
Zollino et al. 2011	Case report of a 5 year old girl	1 female	Deletion of 4 genes including *SYNGAP1*. Gut rotation & pancreas segmentation abnormalities noted
Klitten et al. 2011	Case report of a male child	1 male	Balanced translocation with a breakpoint between exons 5 and 6 of *SYNGAP*
de Ligt et al. 2012	Exome sequencing of 100 people with severe ID	1	
Rauch et al. 2012	51 children from the German Mental Retardation Network	1 female and 1 male	
Berryer et al. 2013	16 patients with NSID and generalised epilepsy from Denmark and a similar cohort of 16 patients from Montreal with NSID	1 Dane & 2 Canadians	The Dane's father was mosaic for the mutation, required extra help at school and suffered depressive episodes
Carvill et al. 2013	Cohort of patients with epileptic encephalopathies tested with high throughput targeted sequencing	2 females, 3 males	Range of severe epilepsy phenotypes, early developmental delay and subsequent regression
Writzl & Knegt 2013	Case study of a 9 year old boy examined with comparative genomic hybridization (CGH) analysis	1 male	*de novo* 50 kb deletion encompassing four genes including *SYNGAP1*(encompassing the same genes as in the Zollino paper)
Redin et al. 2014	Targeted sequencing of protein-coding exons of 217 genes associated with ID or ASD in 106 patients with ID with or without ASD	1 male	

Table continued overleaf…

Table 1 continued…

Parker et al. 2015	7/ 10 identified from the first cohort of patients from the Deciphering Developmental Disorders Study which recruited >12,000 children across the UK 8th patient identified via routine testing at a NHS paediatric genetics clinic. Patients 9 and 10 were monozygotic twins referred for genetic evaluation	7 females, 3 males	First paper suggesting *SYNGAP1* ID is syndromic (see main text)
Stülpnagel et al. 2015	Case report of a patient with *SYNGAP1* mutation identified on next generation sequencing	A 15 year old non-dysmorphic girl	Complete EEG normalisation with eye opening
Mignot et al. 2016	*SYNGAP1 e*xome screening (n = 192) or exome sequencing (n = 59) in 251 patients with neurodevelopmental disorders	8 females, 9 males	Presented data from their own identified patients and 11 other patients from other centres plus 2 patients previously published (Rauch et al. 2012; Stülpnagel et al. 2015)
Prchalova et al. 2017	Case report of a patient with *SYNGAP1* mutation	A 31 year old female	Variant located in the broader splice donor region of intron 10

CGH = comparative genomic hybridization NHS = National Health Service

It was initially thought that *SYNGAP1* ID (also sometimes referred to as 'autosomal dominant intellectual disability type 5') was non-syndromic (Hamdan et al. 2009), but this view was challenged by a paper in 2015 describing syndromic features in 10 individuals including a pair of monozygotic twins (Parker et al. 2015). All ten had global developmental delay and moderate to severe intellectual disability. Six had a diagnosis of autism spectrum disorder and seven had seizures. The seizures were most commonly complex and generalised and included drop attacks, myoclonic seizures and absences. Seven showed generalised hyperexcitability and aggressive behaviour and all ten had sleep disturbances. This work was followed by phenotypic analysis of 17 patients with *SYNGAP1* mutations (Mignot et al. 2016). Their main clinical features are summarised in Table 2 which demonstrates that the variation in phenotypes is marked, but with distinct similarities between patients. In addition to the data in the table, Mignot and colleagues noted that all 16 patients who had undergone an EEG had abnormalities at one time or another (3 patients had multiple tests), which may suggest major brain network dysfunction. The most common abnormalities were ictal or interictal bursts of spikes, spike and waves or slow waves.

The mutations identified in Mignot's 17 patients affect most of the 19 exons of the protein, only sparing 1, 2, 9, 14, 16, 18 and 19 (Figure 1). Exons 8 and 15 are the largest and have the most mutations along with Exon 5. However no definite correlation was found between the location of the mutation on *SYNGAP1* and the clinical presentation in either Mignot et al. 2016 or Carvill et al. 2013.

The paper also collated the data of all published mutations in *SYNGAP1* to date. Of the 47 individuals reported with *SYNGAP1* mutations, three of the mutations were each found in two different patients in separate studies. As a pair of monozygotic twins were included in the 47 sample number a total of 43 mutations limited to the *SYNGAP1* gene have now been identified in published research. As panel B in Figure 1 shows, the vast majority are missense mutations and some of these have been shown to result in degradation of the SynGAP protein when transfected into HEK293 cells and N7 neuronal cells (Berryer et al. 2013).

Table 2 - Characteristics of Patients with *SYNGAP1* mutations from the Mignot et al. 2016 study

	NUMBER OF PATIENTS
Gender	
Male	9
Female	8
Level of ID	
Mild	2
Moderate	5
Severe	8
Autism diagnosis	8 of 16 assessed*
Epilepsy diagnosis	16#
Seizure categories	
Typical or atypical absences	9
Massive myoclonic jerks	7
Eyelid myoclonia	3
Clonic or tonic clonic	3
Myoclonic absences	3
Atonic	2
Seizure triggers	
Photosensitivity	5
Fixation-off sensitivity	1
Photosensitivity and fixation-off sensitivity	1
Chewing	1
Neurological examination	
Normal	2
Gait abnormalities	10
Truncal hypotonia	10
Facial hypotonia	4
Brain MRI	
Normal	13
Arachnoid cysts	2
Mild myelination delay	1
Signal abnormalities	1

*One patient too young for ASD assessment #17th patient suffered a previous febrile convulsion

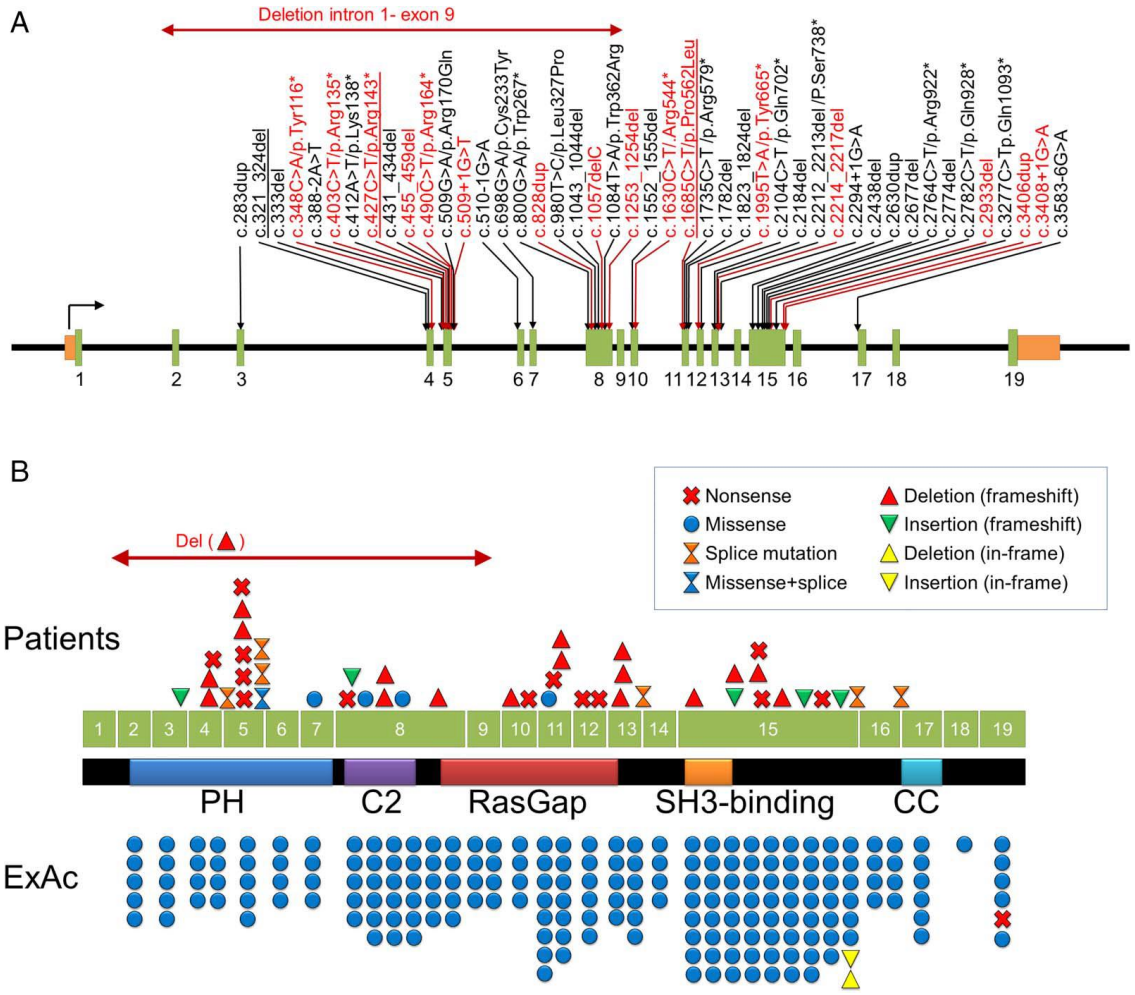

Figure 1 – There is significant diversity in the mutations on the *SYNGAP1* gene.

Adapted from Mignot et al. 2016.

(A) Location of mutations on *SYNGAP1*. Mutations in red are the patients from the Mignot study, mutations in black correspond to previously published patients and recurrent mutations are underlined

(B) Schematic representation of the mutations (above the protein schematic) and the variants present in the Exome Aggregation (ExAc) database (below the schematic) on the longest SYNGAP1 isoform (NM_006772.2) and corresponding protein domains.

1.5 Structure and Function of SynGAP

SynGAP appears to be an important protein given the severity of symptoms present when it is disrupted and the fact that it is highly conserved across species (McMahon et al. 2012). It was first identified in rat forebrain post-synaptic density (PSD) isolates where it was found to be one of the most abundant proteins, accounting for approximately 1-2% of total PSD protein (Chen et al. 1998). It is expressed strongly in the mouse cortex and hippocampus as well as at lower levels in the thalamus, amygdaloid complex, cerebellum, striatum, brainstem and olfactory bulb (Kim et al. 1998; Komiyama et al. 2002; Tomoda et al. 2004; Porter et al. 2005; Knuesel et al. 2005; Moon et al. 2008). Moon and colleagues found that 2 different isoforms of SynGAP (α1 and β) were present in all cerebral layers and in neuronal cell bodies and primary apical dendrites. In the hippocampus the highest immunoreactivity for both isoforms was in the strata radiatum and oriens of the CA1-CA3 regions and the molecular layer of the dentate gyrus; weaker immunoreactivity was evident in the stratum lacunosum-moleculare (Moon et al. 2008).

The general development and lamination of the cortex was found to be normal in *Syngap*$^{+/-}$ mice, but *Syngap*$^{-/-}$ mutants had a small reduction in cortical thickness in the posterior medial barrel sub-field and anterior snout region (Barnett et al. 2006). The same authors found that SynGAP is necessary for the development of whisker related functional modules (‘barrels’) in the somatosensory cortex which each receive specific sensory input from one of the animal’s whiskers (Barnett et al. 2006). Komiyama and colleagues found no differences in the CA1 hippocampus of *Syngap*$^{+/-}$ mice on Nissl staining with markers of synaptic-terminal or dendrites, nor with more detailed analysis of dendritic architecture (Komiyama et al. 2002). However an increase in apoptotic cells has been demonstrated in the *Syngap*$^{-/-}$ mouse hippocampus, cortical layers I–VI and the Purkinje cell layers of the cerebellum (an area the authors noted to be underdeveloped (Knuesel et al. 2005).

SynGAP protein expression changes during development and rapidly increases in the cortex and hippocampus between embryonic day 16 and post-natal day 1 (P1) (Knuesel et al. 2005). Porter and colleagues found the expression in the mouse hippocampus peaked around P7 and was then maintained throughout adulthood

(Porter et al. 2005). This is in keeping with Li et al.'s finding that the level of SynGAP mRNA in rat forebrain at 1 day and 1 week after birth was as high as the adult level (Li et al. 2001). However Clement et al. found SynGAP mRNA transcripts in mice peaked at P14 in the hippocampus (Clement et al. 2012). In the cortex Porter and colleagues found that the SynGAP protein was restricted to specific layers, rose to P7, was maintained for the second week of life and then declined in adulthood (Porter et al. 2005), but McMahon and colleagues found that its mRNA transcripts peaked at P14 (McMahon et al. 2012). In the barrel cortex SynGAP was present in neonatal homogenates and its expression increased into adulthood (Barnett et al. 2006).

Double labelling mouse hippocampal neurons with antibodies to SynGAP and the synaptic marker protein synaptophysin showed that SynGAP localises to hippocampal synapses (Kim et al. 1998). It also binds to the PDZ domains of NR1 subunit of the N-methyl-D-aspartate (NMDA) receptor, SAP102 and PSD-95 scaffolding protein via the QTRV motif on its C terminus which is only present in the α1 isoform (see below) (Chen et al. 1998; Kim et al. 1998; Araki et al. 2016).

1.5.1 SynGAP Structure

SynGAP is a complex protein which has multiple N terminal (A, B, C and E) and C terminal (α1, α2, β and γ) isoforms (McMahon et al. 2012). Between the N and C terminal isoforms there is a 'core domain' which is common to all isoforms and includes the C2, GAP and SH3 domains (see Figure 2).

SynGAP also has a Pleckstrin Homology (PH) domain which is incomplete in the C isoform of the protein. The different protein isoforms have been shown to impact differently on synaptic function, with SynGAP α1 negatively regulating synaptic strength to a varying extent depending on which N terminal isoform it is coupled with. The details of this are explored further in the introduction to chapter 3.

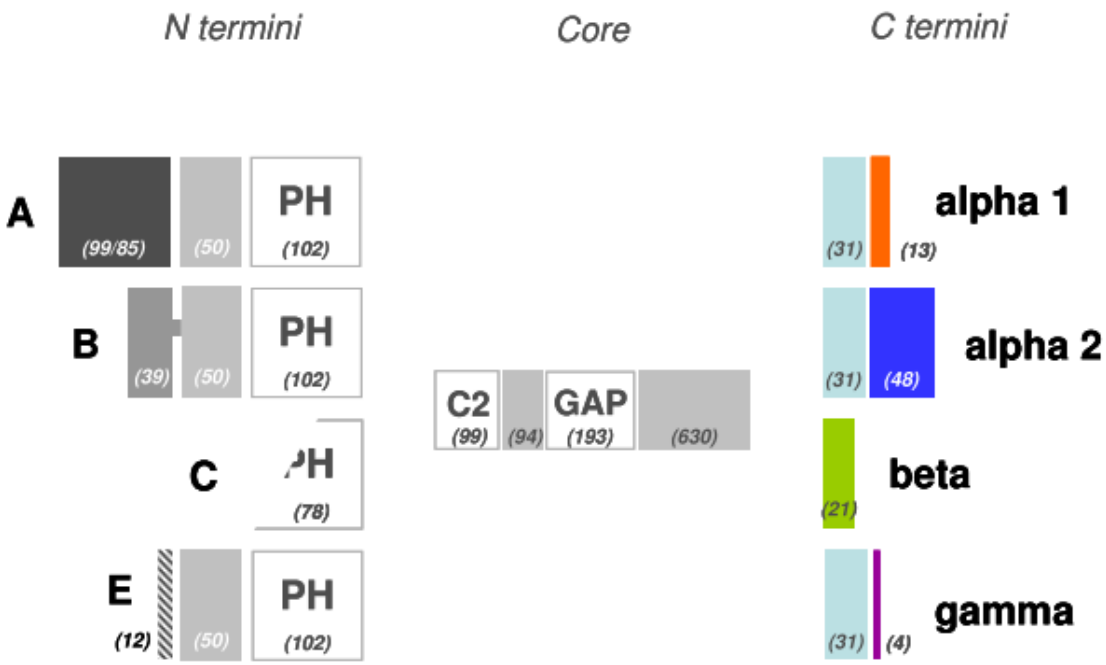

Figure 2 - Schematic of the SynGAP protein domains (McMahon 2010).

1.5.2 Functions of the SynGAP Protein Domains

Pleckstrin Homology Domain

Pleckstrin homology (PH) domains are so called because they include a ~100 amino-acid region of sequence homology that is present twice in pleckstrin (the major protein kinase C substrate in platelets). The exact function of the PH domain in the SynGAP is yet to be delineated, but the PH domains of other proteins play a role in binding to the cell's phospholipid membrane and activating lipid secondary messengers (Lemmon 2008).

C2 Domain

C2 domains are calcium dependent lipid binding domains. They have been found across a variety of proteins which are involved in diverse processes such as vesicular transport, lipid modification, protein phosphorylation and GTPase regulation (reviewed by Nalefski & Falke 1996). They have been shown to play a role in membrane binding, mediating protein-protein interactions and small molecule binding, as well as the binding of calcium (Ca^{2+}) itself. The Ca^{2+}- binding sites of different C2 domains are proposed to be specialised to provide optimized Ca^{2+}-binding parameters, changes in conformation upon Ca^{2+} binding, or docking interactions for different biological functions (Nalefski & Falke 1996). The role of the C2 domain in SynGAP has not been explored in relation to calcium binding specifically, but it was demonstrated in 2008 to be crucial for the protein's role as a RapGAP (Pena et al. 2008) which is consistent with studies of C2 domains in two other RapGAP proteins, GAP1 and RASAL RapGAP (Sot et al. 2010). This role is described in more detail below.

SH3 Domain

SH3 domains are small protein interaction modules (Saksela & Permi 2012). As described in a review by Kaneko et al., they are involved in a multitude of cellular processes including intracellular signalling and cell-environment communication, cytoskeletal rearrangements and cell movement, cell growth and differentiation, protein trafficking and degradation and immune responses (Kaneko et al. 2008).

GAP Domain

The GAP domain is the enzymatic portion of the SynGAP molecule that defines it as a GTP-ase activating protein (GAP) and mediates its function on downstream

pathways. GAPs enhance the slow intrinsic hydrolysis of GTP by GTP-binding proteins (Vetter & Wittinghofer 2001; Bernards 2003). These are proteins that can be subdivided into several families including Ras, Rap and Rho families and play a role in a diverse range of different cellular functions from cytoskeletal dynamics, cellular growth and differentiation to transmembrane signal transduction (Bernards 2003; Scheffzek & Ahmadian 2005). The GTP-binding proteins cycle between an 'on' state (GTP bound) in which downstream signalling is activated and an 'off' or deactivated state (GDP bound) which enables them to act as molecular switches. This mechanism is controlled by the opposing actions of guanine nucleotide exchange factors (GEFs) which promote the dissociation of protein bound GDP and GAPs. Some GAPs are specific to one subfamily of GTP-binding proteins whereas others have dual specificity, in particular for Ras and Rap.

SynGAP as a Ras and Rap GTPase

SynGAP has portions of sequence homologous with those previously identified in RasGAPs (Chen et al. 1998) and its 3D conformation is similar to that of other Ras and Rap GAPs p120GAP, NF1 and also Rap1B (Sot et al. 2010). In the early papers, 2 different assays confirmed its RasGAP activity. The first involved incubating GTP-bound Ras with PSD protein isolates and determining the percentage of GDP by thin layer chromatography before adding a mouse antibody against the GAP domain of SynGAP which was found to inhibit the GAP activity by 75-78% (Chen et al. 1998). In the second GTPase assay, the detection of radiolabelled phosphate in the presence of a GST fusion protein of H-ras was dramatically increased when a GST fusion protein of the RasGAP domain of SynGAP was added (Kim et al. 1998).

It was only later that SynGAP's dual Ras and Rap GTPase activity was identified (Krapivinsky et al. 2004; Pena et al. 2008; Walkup et al. 2015). Its stimulation of Rap-GTPase activity was shown to be more than 10-fold compared to its 2-fold stimulation of Ras-GTPase (Krapivinsky et al. 2004). Walkup and colleague found that the Ras and Rap GAP activity of SynGAP is independently regulated by cyclin-dependent kinase 5 (CDK5), a kinase involved in neuronal processes such as regulation of synaptic plasticity, and Ca^{2+}/ calmodulin-dependent protein kinase II

(CaMKII), a protein kinase involved in long-term potentiation through signal transduction cascades (Herring & Nicoll 2016). Both increased SynGAP's Ras and Rap GAP activity, but CDK5 phosphorylation preferentially increased the rate of SynGAP's HRas activity over its Rap1 GAP activity and CaMKII phosphorylation did the opposite (Walkup et al. 2015).

As mentioned above, other SynGAP protein domains influence the activity of its GAP domain. This is also true of the action of SynGAP phosphorylation by CDK5 and CaMKII which occurs via a number of phosphorylation sites in the carboxyl portion of the protein (Oh et al. 2004; Krapivinsky et al. 2004; Walkup et al. 2015). This differential regulation of SynGAP's GAP activity is further modified by neuronal activity as demonstrated by the application of NMDA increasing the rate of phosphorylation by CDK-5 only at specific phosphorylation sites on the SynGAP protein (Walkup et al. 2015). Moreover, radiolabelled assays demonstrated a 90% reduction in SynGAP phosphorylation following activation of NMDA receptors (NMDARs). SynGAP binds to MUPP1 a large, ubiquitously expressed scaffolding protein which also binds to CaMKII and forms a complex. It is thought that calcium flowing in through NMDARs binds to CaMKII causing it to dissociate from the complex hence reducing its ability to phosphorylate SynGAP (Krapivinsky et al. 2004).

The importance of the GAP domain in normal development has been demonstrated by the fact that a SynGAP construct with mutations in the GAP domain that markedly reduce its function could not rescue dendritic spine abnormalities seen in *Syngap*$^{-/-}$ mouse hippocampal cultures (Vazquez et al. 2004). Moreover, overexpression of a SynGAP construct with a mutated (inhibited) GAP domain had no effect on frequency or amplitude of miniature excitatory post-synaptic currents (mEPSCs) in cultured neurons in contrast to the decreased frequency and amplitude seen in overexpression of normal SynGAP (Rumbaugh et al. 2006).

1.6 Synaptic Plasticity

Neuronal synaptic plasticity is defined as the capability of synapses to modify their function, to be replaced, and to increase or decrease in number when required (Cotman & Nieto Sampedro 1984). The Synaptic Plasticity and Memory Hypothesis theorises that this ability for synapse efficacy to change, underlies learning through the storage of information (reviewed by Takeuchi et al. 2014).

1.6.1 Synaptic plasticity pathways

The trafficking of AMPAR receptors is key to this as long-term potentiation (LTP) of synaptic strength is associated with increased AMPARs at the cell surface and long-term depression (LTD) by a reduction in AMPARs (reviewed by Malinow & Malenka 2002). The trafficking of AMPARs is known to involve the small GTP binding proteins Ras and Rap (Zhu et al. 2002; Zhu et al. 2005; Derkach et al. 2007) and the mitogen activated protein kinase (MAPK) pathway, downstream of Ras (Figure 3). The pathway is triggered by calcium influx through NMDA receptor or voltage-gated calcium channels which leads to an increase in Ras and in turn to activation of Raf, mitogen- activated protein kinase / ERK kinase (MEK) and ERK (Thomas & Huganir 2004).

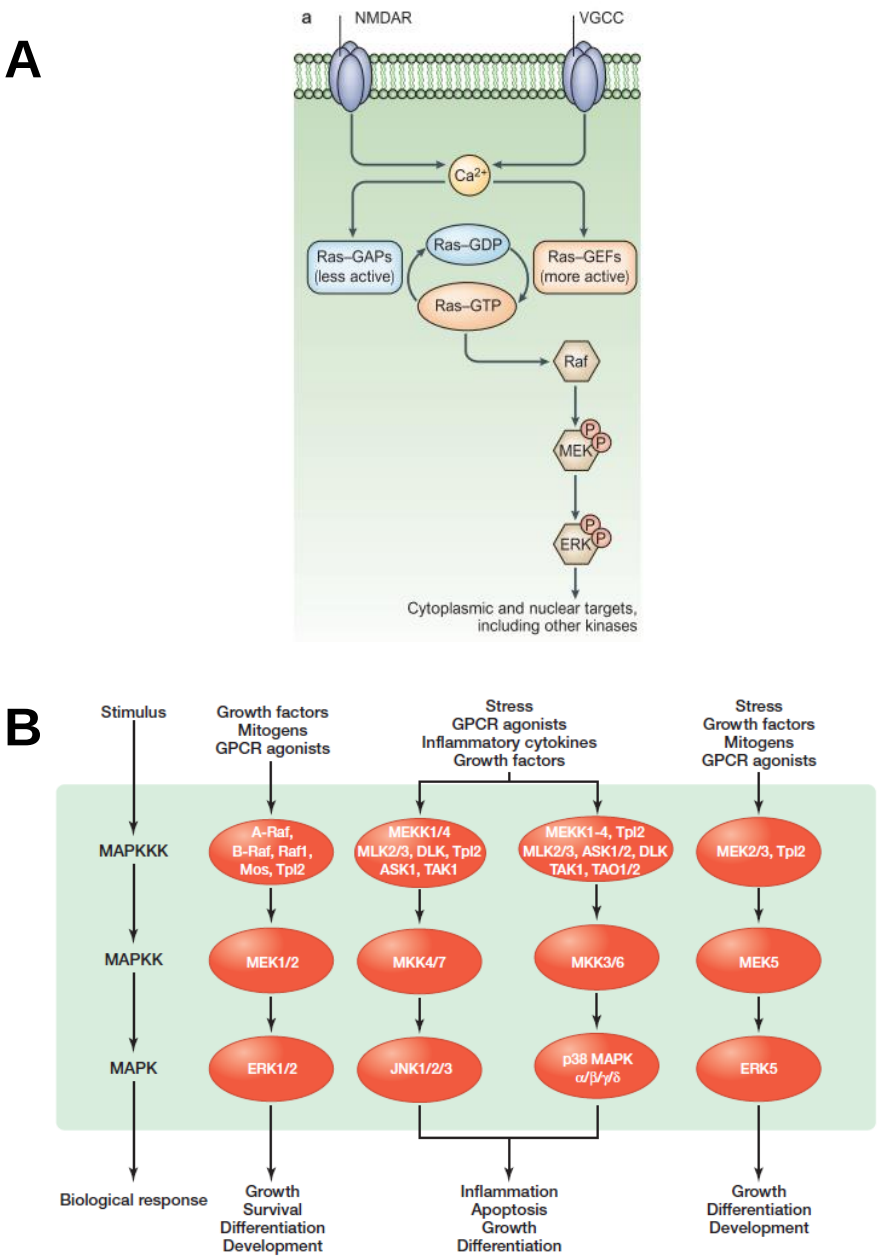

Figure 3 – Activation of extracellular signal-regulated kinase (ERK) by synaptic signalling and downstream targets.

(A) Adapted from (Thomas & Huganir 2004) Calcium influx, either through NMDA (N-methyl-D-aspartate)-type glutamate receptors or voltage-gated calcium channels triggers an increase in the levels of Ras–GTP. This leads to the activation of Raf, mitogen- activated protein kinase (MAPK)/ERK kinase (MEK) and ERK.

(B) MAPKinase pathways, from Morrison 2012.

1.6.2 The importance of AMPA receptor structure in synaptic plasticity

AMPARs have four sub-units GluR1-4 and those with long cytoplasmic tails (GluR1-, GluR2L- or GluR4) are involved in the delivery of AMPARs to the membrane during synaptic potentiation via Ras pathways (Zhu et al. 2002; Stornetta & Zhu 2011). Those with short tails (GluR2, GluR3 and GluR4c) play a role in synaptic AMPA-R removal during synaptic depression and also in the one to one recycling of AMPARs from the membrane (Zhu et al. 2002; Stornetta & Zhu 2011).

1.6.3 The role of ERK MAPKinase pathways and synaptic plasticity

The MAPKinase cascades are complicated and ERK 1/2 is only one of the four (Figure 3). Zhu and colleagues observed that the active phosphorylated form of ERK1/2 (also known as p42/44 MAPK), was enhanced in tissue expressing constitutively active Ras and decreased in tissue expressing dominant negative Ras. However constitutively active Rap resulted in increased levels of phosphorylated p38 MAPK and when p38 MAPK was blocked, the synaptic depression initiated by Rap was also blocked (Zhu et al. 2002). AMPA mediated transmission was potentiated by ~80% in cells expressing the constitutively active form of Ras, but those expressing the constitutively active form of Rap showed ~50% depression in AMPA mediated currents (Zhu et al. 2002). This therefore suggests that ERK1/2 potentiates AMPAR insertion into the cell membrane and p38 MAPK reduces it. Opposing effects of ERK1/2 and p38 MAPK have also been identified in other cell types and even inhibition of one over the other (Oh et al. 2000; Westermarck et al. 2001; Heffron & Mandell 2005).

1.6.4 SynGAP's role in synaptic plasticity

In 2000 Platenik et al. postulated that SynGAP might be a link between NMDA receptor activation and regulation of the ERK1/2 MAPKinase downstream signalling pathway through its action on Ras (Pláteník et al. 2000 and Figure 4). NMDA activation leads to influx of calcium which phosphorylates CaMKII in turn leading to phosphorylation of SynGAP (Krapivinsky et al. 2004; Walkup et al. 2015; Walkup et al. 2016; Jeyabalan & Clement 2016).

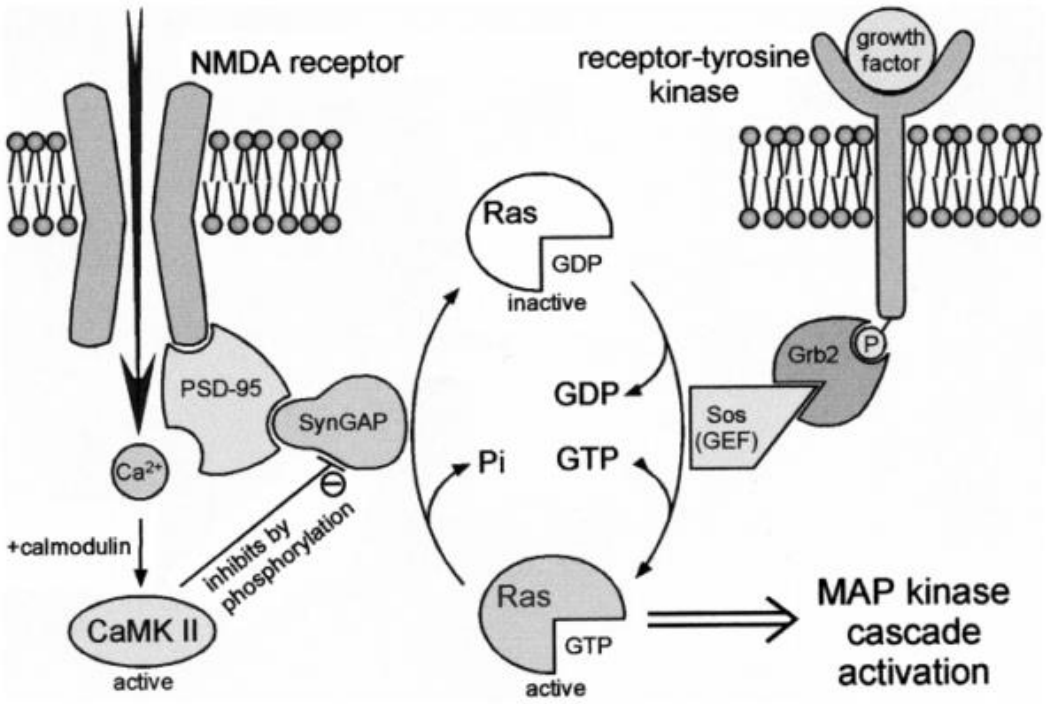

Figure 4 – Proposed model of MAP kinase cascade activation involving SynGAP.

Adapted from (Pláteník et al. 2000).

SynGAP is physically associated with the NMDA receptor through PSD-95 and under resting conditions prevents activation of Ras by other signalling pathways. This brake is released when calcium influx via NMDA receptor activates CaMKII, which can then inhibit SynGAP by phosphorylation.

As would be expected from SynGAP's role as a RasGAP, increased levels of Ras have been observed in conditions of SynGAP haploinsufficiency (Carlisle et al. 2008; Araki et al. 2015). Increased basal levels of phosphorylated (activated) ERK have also been shown in *Syngap*$^{-/-}$ cultures (Rumbaugh et al. 2006) and *Syngap*$^{+/-}$ adult mice (Komiyama et al. 2002; Ozkan et al. 2014). This level of activated ERK increased on stimulation of NMDA receptors (Komiyama et al. 2002; Rumbaugh et al. 2006), but not following theta burst stimulation (Ozkan et al. 2014). Furthermore, Ozkan et al. demonstrated deficits in LTP which is in keeping with other work in *Syngap*$^{+/-}$ mice in which LTP was stimulated with high frequency stimulation or theta burst activity (Komiyama et al. 2002; Kim et al. 2003; Ozkan et al. 2014). Berryer and colleagues explored the effects of mutations found in human *SYNGAP1* patients. They found that transfection of neurons in organotypic slice culture with WT SYNGAP1 reduced the detectable level of phosphorylated (activated) ERK, whereas transfection with certain mutations found in human patients with *SYNGAP1* mutations resulted in no difference in phosphorylated ERK in comparison with untransfected or GFP transfected cells (Berryer et al. 2013).

Komiyama went on to investigate the mechanisms underlying LTP, specifically the idea that SynGAP haploinsufficiency results in increased Ras. Somewhat surprisingly, H-Ras$^{-/-}$ mice showed enhanced AMPAR transmission following an LTP stimulation paradigm despite their lack of H-Ras. This could indicate that it is not the H-Ras form of Ras that mediates AMPAR trafficking, but doesn't preclude the involvement of other forms of Ras in this process. There is evidence that the level of Ras and Rap signalling needs to be maintained in a 'happy medium' to mediate downstream signalling and balance AMPAR trafficking (Zhu et al. 2002; McCormack et al. 2006; Stornetta & Zhu 2011). Therefore it is also possible that other forms of Ras are up-regulated in H-Ras mice to compensate for the genetic deficiency, but this wasn't investigated.

In keeping with the proposed pathway from Ras to ERK signalling (Figure 3) and the papers cited above showing opposing actions of ERK and p38 MAPK, Rumbaugh and colleagues showed that when NMDA activation occurred in rat cultured neurons

overexpressing SynGAP, there was a suppression of ERK activation and an increase in p38 MAPK activity. They also demonstrated that in knockout mouse neuronal cultures and when SynGAP was acutely knockdown with siRNA in rat neuronal cultures, there was increased ERK activation. Furthermore, basal p38 MAPK activity was significantly decreased in mouse KO neurons. Both the effect on ERK and p38 MAPK was found to be mediated by the protein's GAP domain.

In contrast, Krapivinsky and colleagues showed that mimicking activation of NMDA receptor by using TAT-blocking peptides that disrupted the SynGAP-MUPP1 interaction, significantly reduced the downstream activity of p38 MAPK with no associated change in ERK activity (Krapivinsky et al. 2004). To further complicate matters, it is possible that SynGAP may be regulating pathways that are Ras dependent but ERK independent as not all LTP induction paradigms require ERK to be successful (Watabe et al. 2000; Winder et al. 1999). However this needs further exploration.

Therefore the complexities of signalling downstream of SynGAP are still to be fully delineated, however the schematic presented by Jeyabalan et al. gives a reasonable overview of the processes involved (Figure 5).

1.6.5 The link between SynGAP and AMPAR trafficking

In addition to discrepancies in ERK MAPKinase activation in the Rumbaugh and Krapivinsky papers, Rumbaugh et al. found a reduction in the surface GluR1 AMPAR sub-unit signal which indicated fewer AMPARs on the surface in conditions of SynGAP overexpression in neuronal cultures, whereas Krapivinsky et al. found a reduction in GluR1 (as well as GluR2 and GluR3 signal) when SynGAP was knocked down. However, in agreement with Rumbaugh's findings, papers have found that GluR1 synaptic clusters are more numerous and bigger in *Syngap*$^{-/-}$ mice plus dendritic spines are larger and levels of AMPARs are concentrated (Kim et al. 2003; Vazquez et al. 2004; Carlisle et al. 2008; Araki et al. 2015). Larger GluR1 clusters and also a specific increase in the number of small clusters were also seen in adult mice in whom SynGAP was acutely knocked down using a Cre-LoxP system (Muhia et al. 2012).

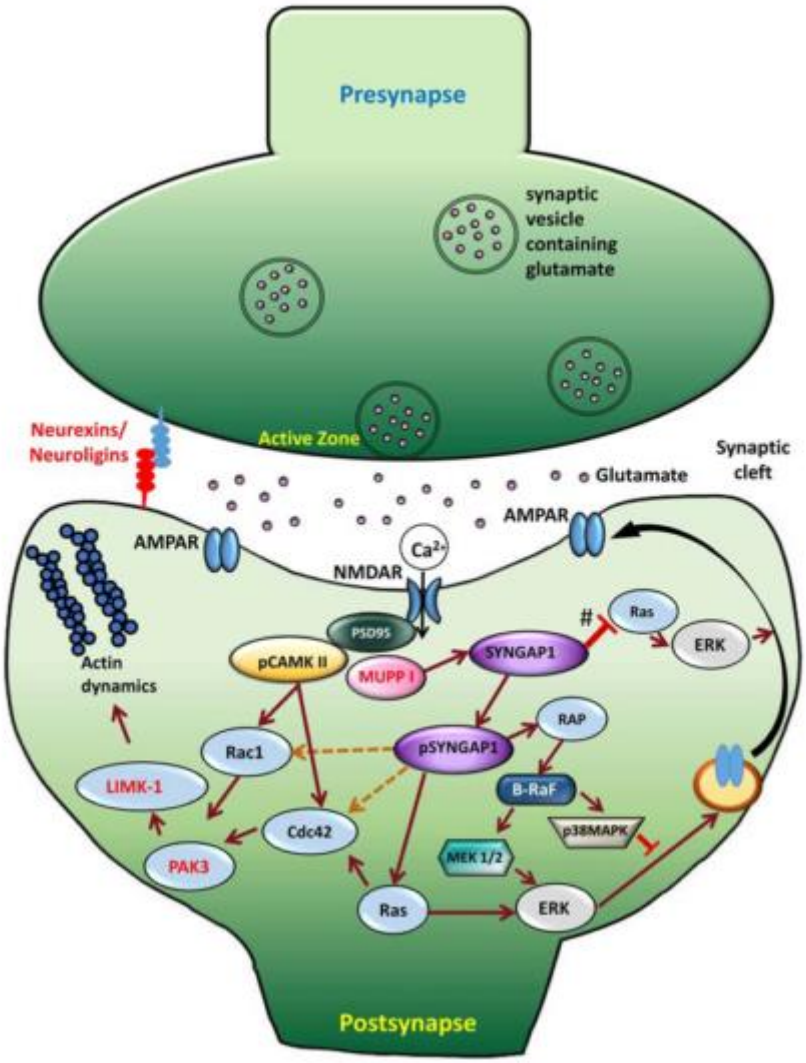

Figure 5 - Signalling mechanism upon phosphorylation of SYNGAP1.

Adapted from Jeyabalan et al. 2016.

Schematic model of the cellular events that link CaMKII activity to phosphorylation of SYNGAP1 and its regulation of downstream molecules. Upon NMDAR activation, Ca^{2+} enters the postsynaptic cytosol, triggering phosphorylation of CaMKII, which in turn phosphorylates SYNGAP1 (pSYNGAP1). pSYNGAP1 regulates Ras-GTPases controlling AMPAR insertion into the postsynaptic membrane. In Syngap1 heterozygous mutation, the inhibition of Ras activation by SYNGAP1 (shown as #) is lost, which increases Ras activity, thereby increasing AMPAR exocytosis to the postsynaptic membrane. Phosphorylation of SYNGAP1 by cyclin-dependent kinase 5 (CDK5) activates Rap1 that increases endocytosis of AMPAR. It is not clear how pSYNGAP1 regulates other SYNGAP1-associated proteins such as Cdc42, Rac1 (dotted orange lines), which are yet to be studied.

It is important to note that, in contrast with the other studies, Krapivinsky used a SynGAP–α construct throughout their experiments. Therefore they may have uncovered an isoform specific effect which perhaps also explains their observed reduction in p38 MAPK without ERK activation. Rumbaugh and colleagues did also mutate the SynGAP α1 isoform in addition to their disruption of all SynGAP isoforms and when doing this they no longer saw a reduction in GluR1 signal. This suggests α1 plays an important role in the AMPAR trafficking process, although it has been shown to have no direct effect on dendritic spine density or morphology (McMahon et al. 2012). Perhaps therefore, Krapivinsky's SynGAP-α was specifically α2 as this lacks the QRTE binding motif which facilitates binding to PDZ domains of other proteins, possibly meaning that α2 can't mediate AMPAR trafficking in the same way. Additional experiments are required to confirm this and to try to understand if this explains the different ERK MAPKinase effects seen in the Krapivinsky paper.

Further evidence for SynGAP's role in AMPAR trafficking comes from its preferential association with the NR2B subunit of NMDARs in adult brain which were shown to play a role in the removal of AMPARs containing the GluR1 subunit from the cell surface and deactivating Ras-ERK signalling (Kim et al. 2005). GluR1 AMPA subunit surface expression was ~33% lower in cells transfected with SynGAP and when SynGAP expression was blocked with RNAi, ERK expression following NMDAR activation became sustained rather than transient.

1.6.6 Other evidence linking SynGAP to synaptic plasticity

Araki et al demonstrated that following chemically induced LTP, SynGAP moved out of dendritic spines in cultured neurons in a process dependent on CaMKII activation. This dispersion still occurred during the inhibition of Ras and Rap suggesting it was upstream of SynGAP's activation of small G proteins. They noted that LTP induction resulted in increases in the size of dendritic spines as expected (Matsuzaki et al. 2004), but this increase was not maintained when CaMKII was inhibited or when the phosphorylation sites on SynGAP were mutated. This work needs further investigation though as using phospho-mutants resulted in changes in

basal function of synapses that may have influenced their ability to respond to chemical LTP induction.

Walkup et al. recently observed that phosphorylation of SynGAP α1 by CaMKII reduces its affinity for the PSD-95 protein resulting in re-organisation of the synaptic proteins as they have more opportunity to bind with PSD-95. This includes proteins such as transmembrane AMPAR regulatory proteins (TARPs) and Leucine Rich Repeat TransMembrane proteins (LRRTM) which have previously associated with glutamatergic synapse development and AMPAR trafficking (Tomita et al. 2005; Siddiqui et al. 2010; Opazo et al. 2012; Walkup et al. 2016).

Hence there are many lines of inquiry that are demonstrating the importance of SynGAP in synaptic function and in the next section, the relevance of this to animal behaviour will be explored.

1.7 Behavioural changes in SynGAP haploinsufficiency

Various studies have now linked reductions in SynGAP levels with behavioural deficits. Similar patterns have been shown in mice regardless of whether the studies use genetic knockout models (Komiyama et al. 2002; Muhia et al. 2009; Muhia et al. 2010; Clement et al. 2012; Ozkan et al. 2014; Berryer et al. 2016) or manipulate SynGAP at specific ages and in specific brain areas (Muhia et al. 2012; Ozkan et al. 2014; Berryer et al. 2016).

1.7.1 Locomotion

Once of the most prevalent findings in the literature is that of hyperactivity in *Syngap*$^{+/-}$ mice in comparison to WT animals (Guo et al. 2009; Muhia et al. 2009; Muhia et al. 2010; Muhia et al. 2012; Clement et al. 2012; Berryer et al. 2016). Berryer et al. also observed that this phenotype was not present in mice in which the *SYNGAP1* gene was conditionally deleted in only the GABAergic interneurons of the cortical, hypothalamic and mesencephalic areas (Berryer et al. 2016). Ozkan and colleagues however did observe hyperactivity in their mouse in which *SYNGAP* was conditionally knocked out in forebrain glutamatergic neurons (Ozkan et al. 2014) perhaps suggesting this is a phenotype linked more to alterations in excitatory than

inhibitory function. The picture is complicated though as they went on to show that the animals remained hyperactive in a 'rescue model' of this forebrain glutamatergic SynGAP deficient mouse (Ozkan et al. 2014), but didn't observe hyperactivity in their adult induced SynGAP global haploinsufficiency model.

1.7.2 Measures of anxiety

Several studies have demonstrated a reduced level of anxiety in *Syngap*$^{+/-}$ mice as shown by increased time in the open arms of the elevated plus maze and increased exploration of the centre area of an open field test (Guo et al. 2009; Muhia et al. 2010; Clement et al. 2012; Ozkan et al. 2014; Berryer et al. 2016). Once again this reduced anxiety was absent in Berryer's GABAergic conditional knockout mouse, but present in Ozkan's forebrain glutamatergic knockout model (Ozkan et al. 2014; Berryer et al. 2016). Furthermore, the phenotype was ameliorated by rescue of the forebrain glutamatergic model (Ozkan et al. 2014). Perhaps surprisingly a trend towards increased anxiety was seen in adult knockdown of *SYNGAP1* (Muhia et al. 2012), whereas the induction of SynGAP haploinsufficiency in adult mice by Ozkan and colleagues had no appreciable effect on the animals' performance in the elevated plus maze (Ozkan et al. 2014).

1.7.3 Learning and Memory

Komiyama et al. saw that *Syngap*$^{+/-}$ mice had a slower rate of spatial learning than WT control mice as demonstrated by more diffuse searching for a submerged platform in the Morris water maze after the platform was moved from its original location (Komiyama et al. 2002). However after extra training they were better able to locate the platform. Muhia and colleagues also observed some differences in the Morris water maze between *Syngap*$^{+/-}$ mice and WTs. Specifically, on removal of the platform *Syngap*$^{+/-}$ mutants showed a relative lack of target quadrant preference in the first 15 seconds, but thereafter there was no difference between genotypes (Muhia et al. 2010). Extinction of learning was largely no different between genotypes in either study (Komiyama et al. 2002; Muhia et al. 2010). Adult knockdown of *Syngap* also resulted in deficits in the water maze when the platform was removed (Muhia et al. 2012).

In other experiments *Syngap*$^{+/-}$ mice were observed to have significantly reduced alternation in the spontaneous alternation test in the T-maze reflecting deficits in

working memory (Deacon & Rawlins 2006; Muhia et al. 2010). This was also seen in mice in which *SYNGAP1* haploinsufficiency was induced in the first week of life and the phenotype was not modified by rescue of the genetic defect in adult mice (Clement et al. 2012). Berryer and colleagues confirmed this finding in *Syngap*$^{+/-}$ mice and in contrast with measures of hyperactivity and anxiety, also observed it in their GABAergic conditional knockout model, suggesting it may be due to deficits in inhibitory function. However, it was also noted by Ozkan and colleagues in their conditional knock out mouse in which SynGAP is lacking in excitatory forebrain glutamatergic neurons (Ozkan et al. 2014). Spontaneous alternation was indistinguishable from that of control animals in the forebrain glutamatergic rescue model and also in their adult induced SynGAP haploinsufficiency model (Ozkan et al. 2014).

Syngap$^{+/-}$ mice have also been shown to be unable to discriminate between similar contexts after a fear conditioning paradigm which the authors felt was consistent with functional deficits in the dentate gyrus (Guo et al. 2009; Clement et al. 2012). Ozkan et al. also found *Syngap*$^{+/-}$ mice and their conditional forebrain glutamatergic neuron knockout model froze less than WTs in a remote fear paradigm suggesting deficits in fear memory circuitry. The phenotype was absent in the rescue model of the forebrain glutamatergic knockout mouse and it also was not seen in their mouse in which SynGAP haploinsufficiency was induced in adulthood.

Furthermore *Syngap*$^{+/-}$ mice were observed to make more working memory errors in radial arm maze experiments which test spatial learning and memory and failed to improve over the course of training unlike WT mice (Muhia et al. 2010).

1.7.4 Social function

When presented with a stranger mouse, WT and *Syngap*$^{+/-}$ mice both spend more time exploring the stranger than an inanimate object (Guo et al. 2009; Berryer et al. 2016). However if the object is then replaced with a second stranger mouse, WT mice spend significantly more time with the new mouse, but *Syngap*$^{+/-}$ mice do not (Guo et al. 2009; Berryer et al. 2016). This was also true of Berryer's GABAergic

conditional knockout mouse. The implication is that *Syngap*$^{+/-}$ mice are unable to distinguish the second stranger from the first and so don't recognise it as novel.

1.7.5 Other behavioural findings

Guo and colleagues found that *Syngap*$^{+/-}$ mice had increased startle responses compared to WT mice and there was a suggestion that they also had a preference for social isolation (Guo et al. 2009).

Therefore the literature exploring the effects of altered SynGAP expression on mouse behaviour is complicated by the age at which the expression is altered and in which brain areas. However it seems clear that it often results in hyperactivity and deficits in learning and memory.

1.8 Altered SynGAP expression and epilepsy in mice

As well as the behavioural data presented above, there is evidence that *Syngap*$^{+/-}$ mice have widespread and frequent cortical epileptiform discharges on EEG (Ozkan et al. 2014) and a reduced seizure threshold compared to WT mice (Clement et al. 2012; Ozkan et al. 2014) which can be rescued on reversal of global SynGAP haploinsufficiency (Ozkan et al. 2014). A reduction in seizure threshold was also seen in Ozkan's forebrain glutamatergic neuron knockout mouse as well as their rescue model for this forebrain glutamatergic construct, but not in the mice in which global SynGAP haploinsufficiency was induced in adulthood. Once again this illustrates the role of age in the presence of certain phenotypes.

1.9 The advantages of rat models over mouse models

Although a number of SynGAP mouse models are already in existence, rats offer several advantages in furthering our understanding of SynGAP protein function and its relationship to human disorders. They are more intelligent and sociable (editorial by Iannaccone & Jacob 2009; Kummer et al. 2014) and quicker to complete water maze tasks with less variability in performance than mice (Whishaw 1995). This is advantageous when considering ID and ASD which affect cognition and social behaviour. There is also better spatial resolution on fMRI of a rat brain compared to a mouse brain (Ellenbroek & Youn 2016) and is it much easier to acquire reproducible brain activation upon stimulation in rats than mice (Jonckers et al.

2015). Therefore the chances of identifying disorder specific biomarkers on scanning that translate to humans may be higher in rats.

Hence, this thesis charts the initial characterisation of SynGAP_GAP deletion rat which is an exciting new tool in SynGAP research.

1.10 Mechanistic convergence between genetic causes of ID and ASD

The relevance of the work undertaken in this thesis will hopefully extend beyond the field of SynGAP specific research as there is increasing evidence of convergence of mechanisms underlying the genetic disorders associated with ID and ASD (Figure 6).

Due to SynGAP's link to the Ras/MAPKinase biochemical signalling pathways. *SYNGAP1* associated intellectual disability has now been recognised as one of a wider group of conditions known as RASopathies (Tidyman & Rauen 2016). These are medical genetics syndromes that are caused by germ-line mutations in proteins affecting the Ras/MAPKinase pathways. Several other genetic causes of ID fall into this group including Neurofibromatosis 1 (*NF1* gene), Costello Syndrome (*HRAS* gene) and Noonan Syndrome (*PTPN11* and *RAF1)*.

There is also a growing body of research pointing towards similarities in cellular processes and molecular pathways, particularly those involved in synaptic function, in different genetic causes of ID and ASD (Auerbach et al. 2012; Zoghbi & Bear 2012; Costa-Mattioli & Monteggia 2013; Krumm et al. 2014; Pinto et al. 2014; De Rubeis et al. 2014). Auerbach et al. 2012 proposed that the mechanisms underlying FXS and TS and are on a continuum. This was based on their finding that aberrations in LTD lay in opposite directions in the two syndromes and that by either manipulating mGluR5 signalling in opposite directions or by producing double mutant mice, these aberrations could be ameliorated. Recently Barnes et al. 2015 demonstrated convergence in exaggerated protein synthesis dependent LTD between mouse models of Fragile X Syndrome and SynGAP. Double mutants in this study however showed no significant differences from either single mutant model

suggesting that a common pathophysiological mechanism is at work in both FXS and SynGAP.

Therefore identification of phenotypes and understanding of cellular and synaptic deficits in the SynGAP_GAP deletion rats will be of value on several levels. Firstly it will add to the body of research investigating the function of the SynGAP protein. Secondly it will contribute to our understanding of the mechanisms underlying the deficits seen in *SYNGAP1* ID and thirdly the information gathered may be applicable to other disorders associated with ID and ASD.

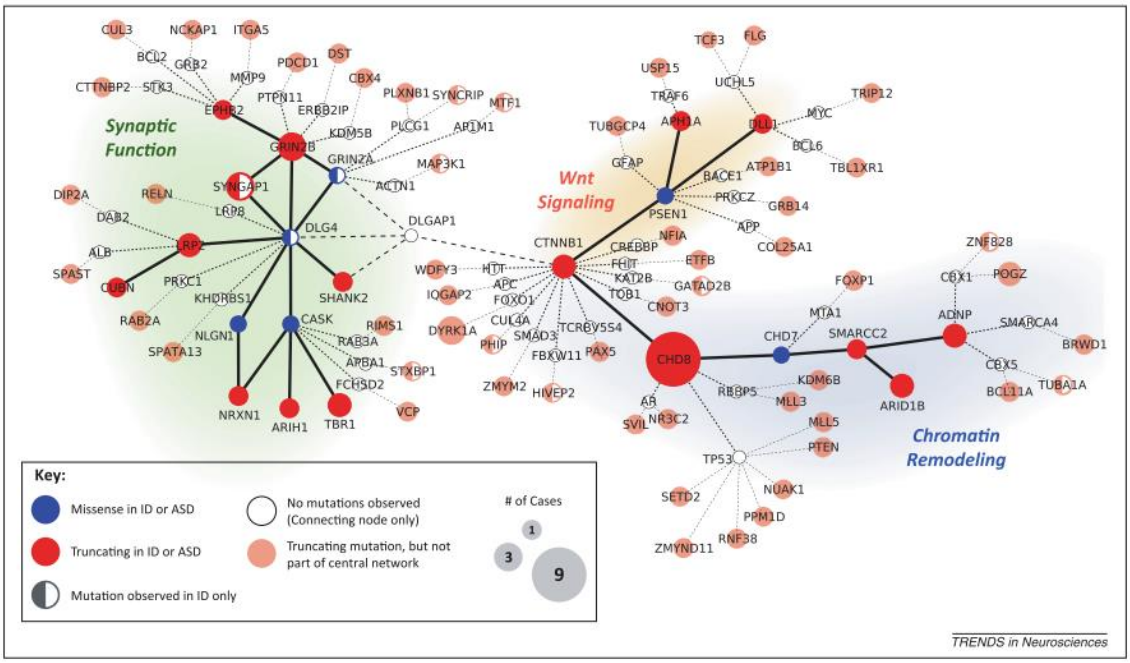

Figure 6 - The proteins disrupted by de novo mutations in autism spectrum disorder (ASD) and intellectual disability (ID) fall into similar categories of function.

Adapted from (Krumm et al. 2014).

Proteins corresponding to genes with de novo truncating mutations (red nodes) or selected missense mutations (blue nodes) in four ASD exome studies and two ID exome studies are connected using experimentally derived protein–protein interaction (PPI) data. Peripheral nodes (lighter shades) represent genes with additional truncating de novo mutations, which are separated from the central network by only a single node (white nodes).

1.11 Aims of this thesis

The broad aims of this thesis were therefore to

1) Conduct an initial characterisation of what is believed to be the world's first SynGAP rat model with particular focus on confirming its SynGAP genetic sequence and expression
2) Use electrophysiological recordings to examine measures of hippocampal and cortical function including long-term depression, intrinsic cell properties and excitatory and inhibitory currents
3) Expand on previous work suggestive of differential physiological roles of SynGAP isoforms by
    a. Examining the role of SynGAP Eα1 isoform on synaptic strength through mEPSC recordings from neurons transfected with Eα1
    b. Investigating the relative abundance of SynGAP isoforms and whether each individual isoform's expression affects that of the other isoforms

2 CHAPTER TWO: METHODS

2.1 Animal maintenance and termination

The rodents used in this thesis were group housed and bred in accordance with the United Kingdom's Animals (Scientific Procedures) Act 1986 (ASPA 1986). They were maintained in a facility that was kept on a 12:12 hour light: dark cycle with food and drink *ad libitem*.

For the preparation of rat brain slices, the rats were anaesthetised using isoflurane and decapitated either with sharp scissors or a guillotine in accordance with the Animal (Scientific Procedures) Act 1986 under the authority of Project Licence number 60/4290. Cultures were prepared from embryos which are not subject to procedures under ASPA 1986 and their mothers were decapitated by cervical dislocation, a Schedule 1 technique under ASPA 1986.

2.2 Creation of the SynGAP_GAP deletion Rat

The SynGAP_GAP deletion rat was designed in the Centre for Integrative Physiology, University of Edinburgh, but engineered in the USA by Sigma Advanced Genetic Engineering (SAGE) Laboratories, St Louis, USA (now Horizon Discovery). SAGE employed zinc-finger endonuclease technology following the brief agreed with the researchers from Edinburgh and created a 3584bp deletion in the *Syngap* gene encompassing the GAP domain of the protein. Briefly, using Sigma's CompoZr^{TM} Zinc-finger nuclease (ZFN) Technology and SAGEspeed™ animal Knockout production processes, ZFNs were designed to target the *Syngap* gene sequence above and below the GAP domain (Figure 7). These were then incorporated into a plasmid with the nuclease of the Fok-1 restriction enzyme which provides DNA cleavage activity (Figure 7). The ZFNs are endonucleases that bind to specific DNA sequences, thus by pairing them with Fok-1 activity specific DNA sites can be targeted and cleaved. The ZFNs were microinjected into the pronucleus of fertilised, one cell embryos. The cleavage of the DNA stimulated homologous recombination repair pathways to re-join the DNA creating mutant embryos that were germline transmissible. Genotyping was carried out on the pups after birth to

identify founder animals carrying the mutation, which were then bred with WT Long Evans Hooded rats to generate heterozygous F1 rats. Selection of appropriate F1 animals based on genotyping and sequencing was then carried out before further mating pairs were set up.

The founder animal for the SynGAP_GAP deletion colony used in this body of work was shown by SAGE to have a 3584 bp deletion and a 3 bp ('CAC') insertion predicted to be at NCBI coordinates 14889-18472. F2 animals were shipped to the University of Edinburgh and were inspected regularly. For a subset of litters, a digital photograph of the pups was taken as soon as it was possible to see their unique black and white markings. The pups were then weighed thrice weekly (Monday, Wednesday and Friday) from P1 to P23 (the exact ages depended on the day of the week on which the litter was born) using the photograph to identify each pup.

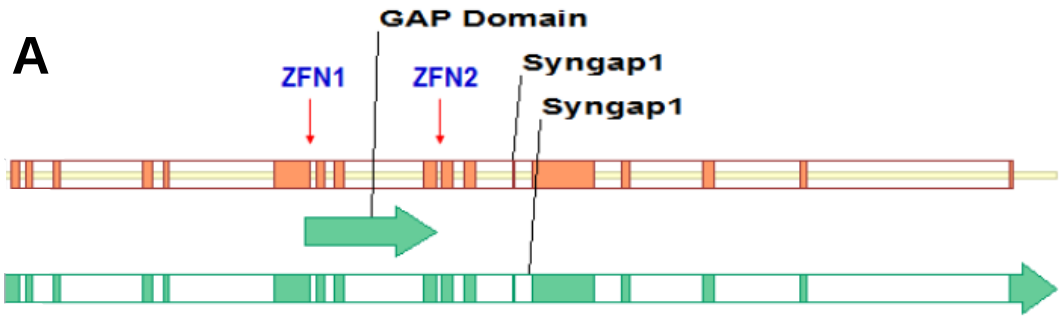

GAP domain spans 2282 bp (16083-18364; E6-E9 based on canonical isoform).

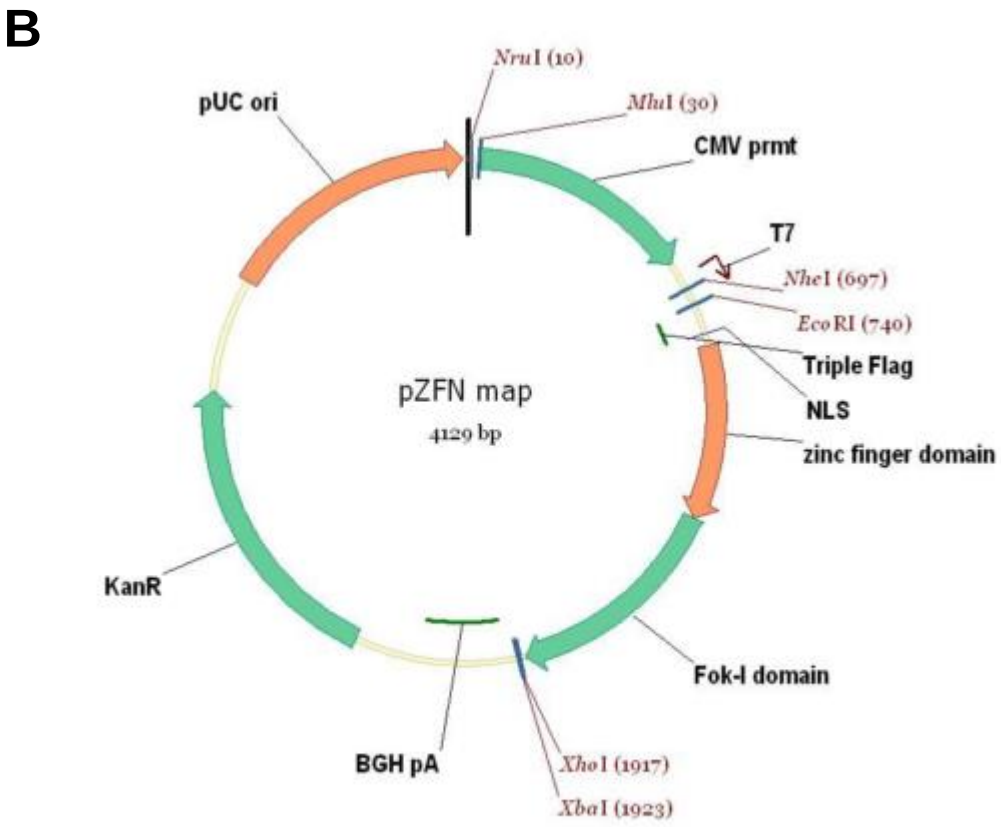

Figure 7 – Genetic engineering of the SynGAP_GAP deletion rat.

(A) Schematic of strategy to delete the GAP domain from the rat *SynGAP* gene.

(B) pZFN plasmid map**.**

Both images taken from project document entitled *Generation of SynGAP1 Knockout Rat Model:* 28DEC12 (Sigma Advanced Genetic Engineering (SAGE) Laboratories 2012).

2.2.1 Genotyping

DNA isolation

Tails/ear clips were digested in 500 µl tail buffer (100 mM Tris pH 8.5, 200mM NaCl, 0.2% SDS, 5 mM EDTA) and 5 µl proteinase K (20 mg/ ml). The Tris, NaCl and EDTA were obtained from Sigma Aldrich and the SDS from 2BScientific Ltd. Digested tails were shaken vigorously by hand, then put in a 55˚C water bath for >12 hours. The debris was pelleted by spinning at 13,000 x g in a microfuge for 10 minutes. 400 µl of the supernatant from each sample was added to 400 µl of isopropanol and shaken vigorously by hand, before being centrifuged for a further 10 minutes at 13,000 x g. The supernatant was poured off and the pellet rinsed with 1 ml 70% ethanol. 150 µl double distilled water (ddH_20) was added for ear clips or 500 µl ddH_20 for 0.5 cm tail. Once re-suspended the samples were left over night with the caps open to allow any excess ethanol to evaporate.

PCR Reactions

The genotyping protocol was designed with two assays (Figure 8). Assay 1 confirmed the absence of the deletion (i.e. identified WT alleles) because in WTs the distance between the primers is too long to amplify and so a positive result is only achieved in heterozygotes and homozygotes. As the primers for Assay 2 are both within the deletion, this assay is positive in WTs and heterozygotes, but negative in homozygotes. The primers used are shown in Table 3.

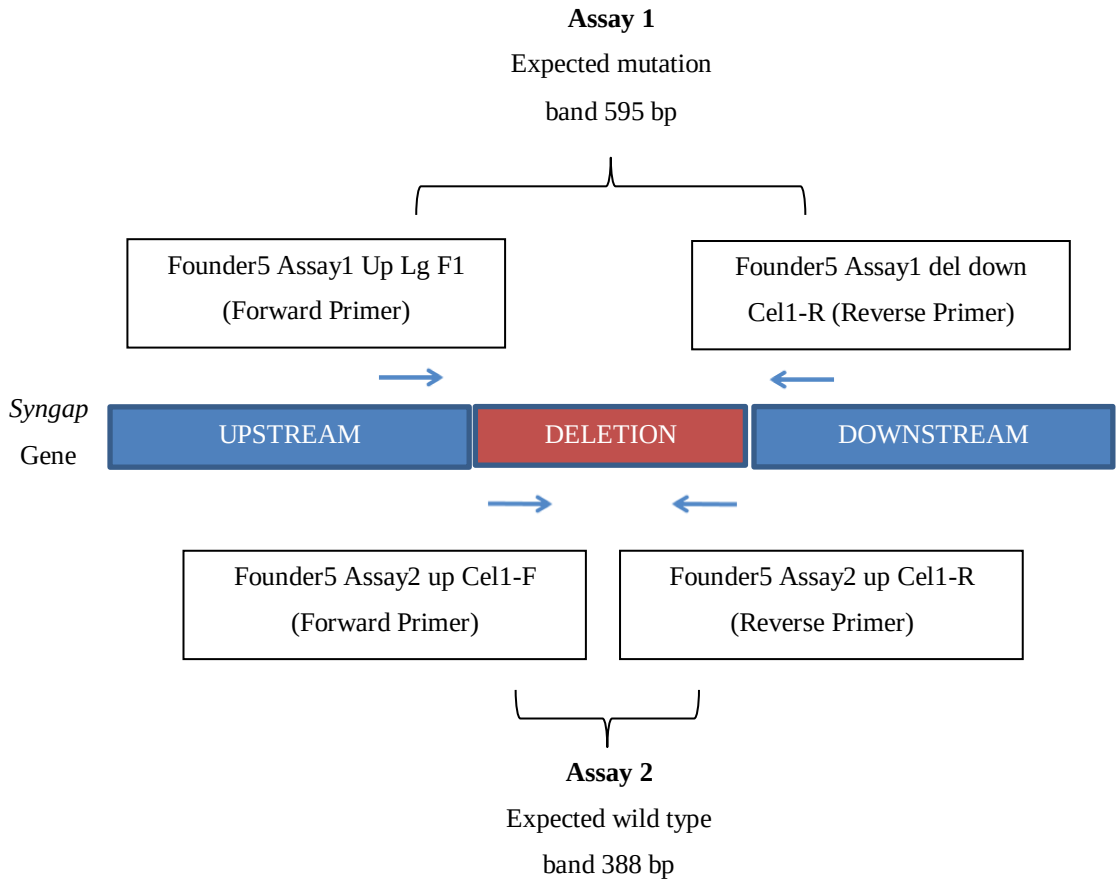

Figure 8 – Schematic of the genotyping assays for the SynGAP_GAP deletion rat.

In the absence of the deletion, the distance between the Assay 1 primers is too long to amplify. Therefore Assay 1 is only positive in heterozygotes and homozygotes. As the primers for Assay 2 are both within the deletion, this assay is positive in WTs and heterozygotes, but negative in homozygotes.

Table 3 - Primers for Genotyping the SynGAP_GAP deletion rat and confirming the deletion

Genotyping		
Assay 1		
For	Founder5 Assay 1 Up Lg F1	GGCACCTTCCCCAAGTAAGT
Rev	Founder5 Assay1 del down Cel1-R	TCACTTGGTGAGTGAGTGCC
Assay 2		
For	Founder5 Assay2 up Cel1-F	ACTGCGAGTTATGCCTGGAC
Rev	Founder5 Assay2 up Cel1-R	CTCATTGTCTGGTAACGGGC
Confirming the deletion		
For	SynGAP Rat cDNA FWD2	GACTCCATTATCAAGCCAGTACA
Rev	SynGAP Rat Exon 14 Set 3	CGAGCCATGAAGGACTGAA

The following PCR reaction was carried out for both assays

For each 20 µl reaction

- DNA template 0.5 µl
- Forward primer (final concentration 0.5 µM) 0.25 µl
- Reverse primer (final concentration 0.5 µM) 0.25 µl
- TAQ DNA polymerase (Qiagen #201203) 0.2 µl (1 unit)
- dNTP Mix, PCR Grade (Qiagen # 201901) 0.4 µl
- 10x Coral buffer from TAQ DNA Polymerase kit 2.0 µl
- ddH_20 16.4 µl
- **Total volume** **20 µl**

Thermocycling conditions:

1. 95°C for 5 minutes
2. 95°C for 30 seconds
3. 60°C for 30 seconds
4. 68°C for 1 minute
5. Go to step 2, 35 times
6. 68°C for 5 minutes
7. 10°C forever
8. END

The products were run on a 1% agarose gel with the Promega™ G2101 DNA ladder from Thermo Fisher Scientific. Images were cropped for presentation, but full gel images prior to cropping are shown in Appendix 1.

Genotyping of the rats was initially carried out in house but the results of assay 2 were unreliable so all experimental animal genotyping was outsourced to Transnetyx, Cordova, TN, USA which uses a real-time PCR method of genotyping.

2.2.2 mRNA deletion confirmation

In order to determine the exact nature of the deletion in the SynGAP_GAP rat, mRNA was extracted from whole brain tissue using the Qiagen RNeasy Mini Kit (#74104/74106). Whole brain tissue was taken from 1 adult WT and 1 adult *Syngap*$^{+/GAP}$ rat then dissected, flash frozen on dry ice and kept at -80ºC until required. The tissue was thawed on ice and the Qiagen RNeasy Mini Kit instructions followed. Briefly, approximately 30 mg of tissue was homogenised in a glass homogeniser in 600 µl Buffer RLT containing 6 µl β-mercaptoethanol. The lysate was centrifuged at full speed for 3 minutes and 1 volume of 70% ethanol added to the supernatant in a separate tube. The mix was added to an RNeasy Spin Column and centrifuged again at ≥8,000 x g for 15 seconds. 10 µl DNase I stock solution mixed with 70 µl Buffer RDD was added to the column membrane, and left at room temperature for 15 min. The column was washed twice with 350 µl Buffer RW1, centrifuging for 15 seconds between each. Two further wash steps with centrifugation were performed with 500 µl Buffer RPE containing 100% ethanol. RNA was then eluted using 25 µl RNase-free water.

cDNA was then made from the mRNA using the Invitrogen SuperScript III First-Strand Synthesis SuperMix for qRT-PCR (ThermoFisher Scientific Catalogue no. 11752-050). The following reagents were gently mixed:

- 2X RT Reaction Mix 10 µl
- RT Enzyme Mix 2 µl
- RNA (up to 1ug)
- DEPC treated water to 20 µl

and incubated at 25ºC for 10 minutes, then at 50ºC for 30 minutes. The reaction was terminated by 5 minutes at 85ºC and then chilled on ice. 1ul (2U) of *E.coli* RNase H was added and the mix was incubated at 37C for 20 minutes.

Polymerase-chain reaction (PCR) was used to amplify the cDNA using the Taq DNA Polymerase (250 U) kit (Qiagen #201203). The mix for one tube was:

- cDNA 0.5 µl
- SynGAP Rat cDNA FWD2 (Table 3) 100 nM
- SynGAP Rat Exon14 Set 3 (Table 3) 100 nM
- Coral Buffer (10X) 2.0 µl
- dNTP 0.4 µl
- TAQ polymerase (1 unit) 0.2 µl
- ddH_2O 12.9 µl

The PCR protocol used was:

1. 94ºC for 3 minutes
2. 94ºC for 30 seconds
3. 52ºC for 30 seconds
4. 72ºC for 2 minutes
5. 72ºC for 10 minutes

It was run for 25 cycles and the PCR products were run on a 1% agarose gel at 60 mV alongside a 1 kb DNA ladder (New England Biolabs #N3232S) to confirm the success of the PCR.

Extraction and Re-amplification of DNA

As no clear band was seen in WT neocortex cDNA, from this point on WT hippocampus and heterozygous whole brain were used. The Macherey-Nagel NucleoSpin® Gel and PCR Clean-up Kit (Fisher Scientific #12303368) was used. Briefly 1 volume of PCR sample was mixed with 2 volumes of buffer NTI and added to a NucleoSpin® Gel and PCR Clean-up column for centrifuging at 11,000 x g for 30 seconds. Two wash steps using 700 µl buffer NT3 with 30 second centrifugation between each. The membrane was dried by centrifuging for 1 minute with no buffer.

The column was incubated at 70ºC for 5 minutes to remove excess ethanol. Elution buffer was heated to 70ºC, added to the column and left for 5 minutes to increase the yield before centrifuging for one minute at 11,000 x g. Two elution steps were used, the first with 20 µl and the second with 15 µl of elution buffer.

The extracted products were then subjected to PCR again using the same protocol to further amplify the cDNA fragment. The products were run on a 1% gel at 65 mV for approximately 35 minutes to confirm the success of the PCR.

The Macherey-Nagel NucleoSpin® Gel and PCR Clean-up Kit was again used to purify the PCR products. The original sample (15 µL) was made up to 50 µl with ddH_20 at the start and once again two elution steps were used twice (first with 20 µl and then with 15 µl). The rest of the protocol proceeded as detailed above.

The purified PCR products were sent to Edinburgh Genomics for Sanger Sequencing using SynGAP Rat cDNA Seq For (CGTACAAAGTCACAACCCAAACC) and SynGAP Rat cDNA Seq Rev primers (TGCCAGGTTGGAAACACTAC). Using Geneious R7 (Biomatters Ltd) software, the sequence of the deletion was determined by comparison with the SynGAP rat 1308 bp transcript numbered ENSRNOT00000040859.6 on the Ensembl website (http://www.ensembl.org/Rattus_norvegicus/Transcript/ProteinSummary?db=core;g=ENSRNOG00000000483;r=20:5535432-5564437;t=ENSRNOT00000040859).

2.2.3 Western Blotting

Tissue preparation

Following decapitation as described in section 2.1, the skin was cut along the midline and the skull was peeled back using forceps to allow access to the brain. A spatula was used to remove the brain from the skull cavity and the appropriate brain regions dissected in ice cold cutting aCSF or PBS. The tissue was then snap frozen on aluminium foil laid over dry ice. If not being homogenised immediately, it was stored at -80˚C.

Tissue homogenisation

Lysis buffer was prepared by mixing protease inhibitor tablets (cOmplete™, Mini, EDTA-free Protease Inhibitor Cocktail, Sigma Aldrich), RIPA buffer (Reagents from Sigma Aldrich except when noted: 50 mM Tris-HCl, 150 mM NaCl, 1% Triton X-100, 0,5% sodium deoxycholate, 0.1% sodium dodecylsulphate (2BScientific Ltd), 1 mM EDTA) and phosphatase inhibitors (Phosphatase Inhibitor Cocktail Sets II and IV, Merck Millipore) on ice. Plastic homogenisation sticks or a mortar and pestle were used to homogenise the tissues in lysis buffer. Approximately 9 µl lysis buffer was used per 1 mg of tissue. If necessary, samples were then vortexed to complete homogenization, before a small proportion of the sample was reserved separately for the protein concentration assay. Laemlli buffer (Sigma Aldrich) was added to the remaining sample to break the disulphide bonds in the proteins and coat them in a negative charge to facilitate the western blotting. These samples were then boiled for five minutes to denature any proteases.

Protein level determination

The Pierce™ BCA Protein Assay Kit from Thermo Fisher Scientific (#23227) was used as per the kit instructions to measure the protein level in each of the samples reserved without laemlli buffer. Diluted albumin standards were prepared from the kit and the protein samples were diluted 5 or 10 fold to ensure the quantity present would fall within the range of the kit's standard sample curve. BCA working reagent was prepared by mixing Reagent A with Reagent B (50:1) and 200 µl was added to

10 µl of each albumin standard and each diluted protein sample in a 96 well plate. The plate was incubated for 30 minutes at 37°C and a FluoStar Optima plate reader (BMG Labtech) was used to read the plate at an absorbance of 570 nm. The curve plotted from the values of the BCA Protein Assay Kit standard samples was used to calculate the protein concentration of each tissue sample using Graphpad Prism for Windows (GraphPad Software) and Microsoft Excel (Microsoft) software.

Running the western blot

Before loading 12 µl of each sample into 10% Mini-PROTEAN® TGX™ Gels (Bio-Rad), they were boiled again for five minutes and briefly spun down. 5 µl of protein ladder was also loaded to each gel (SeeBlue® Plus2 Pre-stained Protein Standard or Fermentas PageRulerPlus Prestained Protein Ladder, Thermo Scientific Pierce). The gels were run at a constant current of 10 to 20 mA per gel in running buffer consisting of ddH_20 plus the following reagents (from Sigma Aldrich unless otherwise stated: 25mM Tris, 190mM glycine and 0.1% Sodium dodecylsulphate (2BScientific Ltd)).

Transfer steps

The samples were transferred to nitrocellulose membrane (Bio-Rad) in transfer buffer consisting of ddH_20, 25mM Tris (Sigma Aldrich), 190mM glycine (Sigma Aldrich) and 20% methanol (Fisher Scientific) typically at a constant current of 200 mA.

Antibody steps

The nitrocellulose membranes were rinsed three times with PBS and blocked with equal quantities of Odyssey Blocking Buffer and PBS (Sigma Aldrich) plus 0.5% Triton X-100 (Sigma Aldrich) for 10-15 minutes. Primary antibody and β-actin antibody (Table 4) were then added to the solution and left overnight at 4 °C or for 4 hours at room temperature. The membranes were then washed three times with PBS mixed with 0.5% Triton X-100 and incubated in the dark in secondary antibody (Table 4) for 45-60 minutes.

Imaging and quantification of the samples

The membranes were imaged using Li-COR Odyssey Version 5 Software and analysed using Image J Software. Densiometry of the protein bands was conducted using the gel analysis functions within the software and values from SynGAP bands were normalised to their corresponding β-actin band. The images were cropped for presentation, but the full gel images prior to cropping are shown in Appendix 1.

Western blot analysis

β-actin normalised values for heterozygous and homozygous SynGAP bands on each blot (as applicable) were compared to the mean WT values from the same membrane and expressed as a percentage ± SEM in arbitrary units. The statistical tests used are detailed in the relevant figure legends. Parametric tests were used for data that passed a d'Agostino Pearson normality test, otherwise non- parametric analyses were used.

Table 4 – Antibodies used for western blotting

Antibodies	Supplier	Catalogue No.	Dilution	SynGAP Isoform
Primary Antibodies				
SYNGAP1	Proteintech	19739-1-AP	1:2000	SynGAP A
SynGAP	Thermo Fisher Scientific/ Cambridge Biosciences	PA1-046	1:4000	All isoforms (referred to as 'Pan SynGAP')
Anti-SynGAP	Merck Millipore/ Upstate	06-900	1:2000	SynGAP alpha1
Anti-SynGAP [EPR2883Y]	Abcam	ab77235-100	1:2000	SynGAP alpha2
Anti-beta Actin	Abcam	ab8227	1:2000	n/a
Secondary Antibodies				
IRDye® 800CW Goat anti-Rabbit IgG (H + L), 0.5mg	Li-COR	926-32211	1:5000	n/a
Goat anti-Mouse IgG (H+L), Alexa Fluor® 680 conjugate	Thermo Fisher Scientific	A-21057	1:5000	n/a

2.3 SynGAP Isoform Experiments

These experiments were conceived and carried out in collaboration with Dr Owen Dando who mapped the mRNA-seq reads, Dr Paul Skehel with whom I ran PCR reactions and cleaned and further amplified the product before sequencing and Shinjini Basu who conducted the RT_PCR experiments (Centre for Integrative Physiology, University of Edinburgh).

2.3.1 SynGAP isoform construction

Owen Dando mapped mRNA-seq read sets comprising data from

1. Cortical-patterned neurons derived from human embryonic stem cells and from cultured mouse primary cortical neurons (Qiu et al. 2016)
2. Mouse and human frontal cortex tissue (Lister et al. 2013)

to their respective genomes using TopHat2, a splicing-aware read mapper (Kim et al. 2013). He then examined for novel splice junctions at the SynGAP locus and so identified putative new SynGAP 5' variant forms A1 and G in addition to the known N terminal (A, B, C, E) and C terminal (alpha1, alpha2, beta and gamma) isoforms.

Previous work in the laboratory produced constructs of the different SynGAP isoforms (McMahon et al. 2012). This involved constructing full length SynGAP constructs and ligating them into a CMV backbone from the eGFP-C1 vector (Clontech, accession number U55763) from which the eGFP gene had been removed by digestion with Age1 and BspE1 (Figure 9).

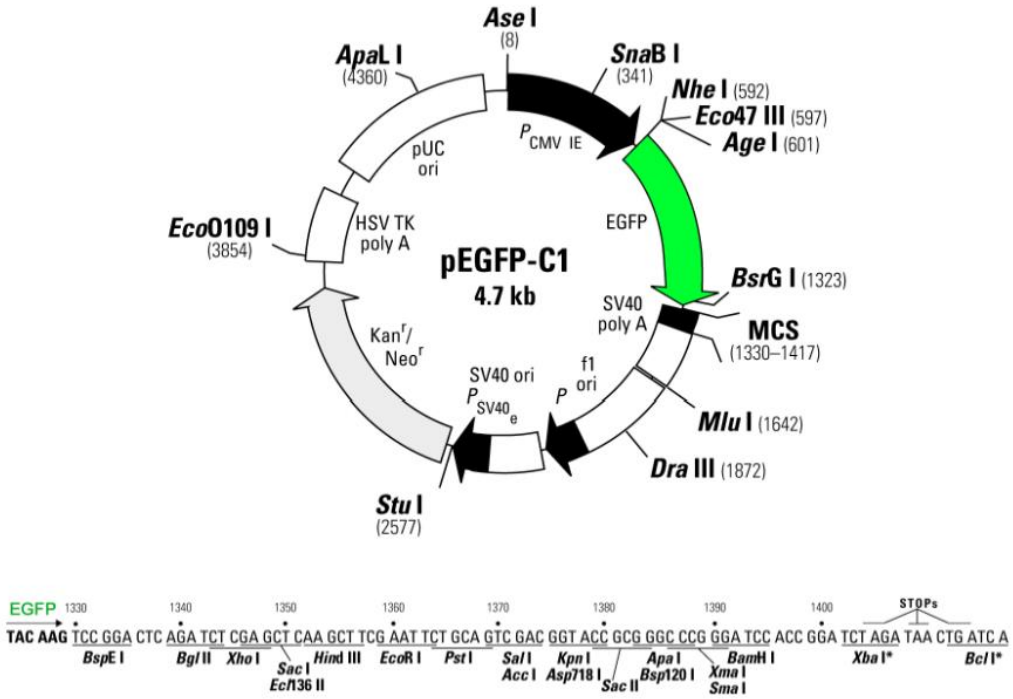

Figure 9 – eGFP-C1 vector map.

eGFP-C1 vector, Clontech, accession number U55763.

In this current new body of work PCR was used to amplify the SynGAP N terminal using McMahon's existing SynGAP Aα2 and Bα1 vectors. The rationale laid out in Figure 10 was followed. The PCR products were run on a 70% agarose gel to evaluate the result.

Reaction Mixture

- 1/20 dilution of SynGAP template 1 µl
- 10mM dNTP (Qiagen #201900) 1 µl
- Each primer (Table 5) 0.25 µg
- Phusion® HF Reaction buffer (New England Biolabs #B0518S) 10 µl
- Phusion® High-Fidelity DNA Polymerase (NEB #M0530S) 0.5µl (5 units)
- De-ionised water 37 µl
- **Total volume** **50 µl**

Thermocycling Conditions

1. 96°C for 2 minutes
2. 96°C for 30 seconds
3. 58°C for 10 seconds
4. 72°C for 10 minutes

The protocol was run with 2 holds and 20 cycles

Table 5 – SynGAP isoform construction primers

SYNGAP N AND C TERMINAL PCR PRIMERS	
Primer Name	**Sequence**
SynGAP N terminal forward SynGAP N terminal reverse	GCTTCAAGGAGTCACATTCCCAC TTCTTCCTGGGACAGCAACCTC
SynGAP C terminal forward SynGAP C terminal reverse	AAAAAACCTCCCACACCTCCCC TCAATGGGGCGGAGTTGTTAC
SYNGAP SEQUENCING PRIMERS	
Primer Name	**Sequence**
Mouse SynGAP Core Region Forward 5'-3' Mouse SynGAP Core Region Reverse 3'-5'	ATTCCCAGACTCCATCCAC CTGGCTTGATAATGGAGTCTTC

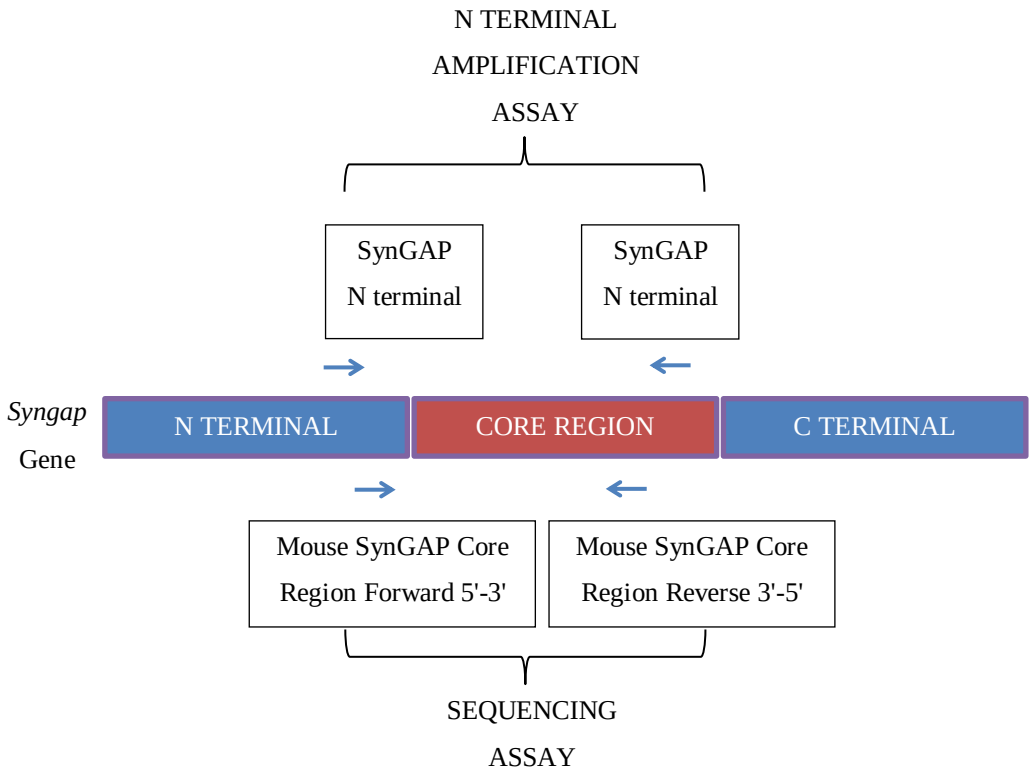

Figure 10 - Schematic of SynGAP isoform PCR and sequencing primer sites.

2.3.2 PCR purification and clean up

The PCR products were then purified using the Macherey-Nagel NucleoSpin® Gel and PCR Clean-up kit using the same protocol described above.

Gene block fragments of all N and C terminal isoforms based on the sequences identified by Owen Dando and containing T7 promoter regions were ordered from Integrated DNA Technologies. In-fusion cloning (In-Fusion® HD Cloning Kit, Clontech Laboratories Catalogue Number 638909) was then used to generate A1α1, Eα1, Gα1, A1α2, Eα2 and Gα2 SynGAP isoforms. The reagents used for the cloning were:

- 1µl linearized vector (PCR product)
- 1µl (1µg) gene block fragment
- 0.5µl 5X In-fusion HD Enzyme Premix provided with the kit

The mix was incubated at 37°C for 15 minutes and then transformed by mixing with 33 µl chemically competent cells, keeping the mix on ice for 30 minutes and then heat shocking it for 45 seconds at 42°C. It was next placed on ice for two minutes before 250 µl SOC medium was added and the cells were placed in a shaker at 150 rpm at 37°C for 45-60 minutes. The cells were plated on Kanamycin Luria Broth (LB) agar plates and incubated overnight at 37°C. 3 or 4 colonies from each plate were then picked and grown on in LB kanamycin broth overnight before being centrifuged at ~17900 x g for 30 seconds. The DNA in the recovered pellet was purified using the Qiagen QIAprep Spin Miniprep Kit (#27104) as per the kit instructions as follows. The supernatant was removed and the pellet re-suspended in 250 µl Buffer P1. 250 µl Buffer P2 was added before mixing thoroughly until the solution was a clear blue colour. 350 µl Buffer N3 was added and mixed immediately until the solution became colourless. The mix was centrifuged for 10 minutes at ~17900 x g before the supernatant was aspirated with a vacuum manifold. Washes with 500 µl Buffer PB and 750 µl Buffer PE containing ethanol were carried out with vacuum aspiration between each. The samples were centrifuged for 1 minute ~17900 x g to remove residual wash buffer and the DNA was eluted using 50 µl Buffer EB.

2.3.3 Restriction enzyme digestion

Restriction Enzyme Digestion to confirm the insertion of the isoform using KPN enzyme was conducted using the following mix which was incubated at 37°C for at least 2 hours before being run on an agarose gel:

- 2 µl DNA
- 5 units enzyme KPN 1 (New England Biolabs #R0142S)
- 1.5 µl New England Biolabs Buffer 1 (10X concentration, #B7001S)
- Water to make up to 15 µl

Following this confirmation, 5.8 µl of each purified DNA sample was mixed separately with forward and reverse SynGAP sequencing primers (Table 3) and was sent for Sanger Sequencing carried out by Edinburgh Genomics, The University of Edinburgh. The sequences were analysed and confirmed using Geneious R7 (Biomatters Ltd) software. Larger quantities of each isoform were then made from colonies grown on overnight as before using the Qiagen QIAprep Spin Maxiprep Kit. Briefly the DNA pellet obtained from centrifuging at ≥15,000 g for 5 minutes was re-suspended in 10 ml Buffer P1 solution and then mixed with 10 ml Buffer P2. 10 ml of chilled Buffer P3 was added and the solution mixed until a smooth suspension was achieved. It was then poured into a QIAfilter cartridge and left at room temperature for 20 minutes, before being filtered into a clean falcon tube. 2.5ml of Buffer ER was added to the filtered lysate and after mixing it was incubated on ice for 30 minutes. A QIAGEN-tip 500 was equilibrated by filling it with Buffer QBT and allowing the column to empty by gravity flow before the filtered lysate was applied to the QIAGEN-tip 500. The QIAGEN-tip 500 was then washed twice by filling it with Buffer QC and the DNA was eluted with 15 ml Buffer QN. 10.5 ml of room temperature isopropanol was added to precipitate the DNA before centrifugation at ≥15,000 g for 30 minutes. The supernatant was decanted and 2 ml endofree water with ethanol was used to remove the rest of the isopropanol. The supernatant was aspirated and the pellet left to air dry for 5-10 minutes before being re-suspended in 500 µl TE.

2.3.4 Real time reverse transcriptase and quantitative PCR experiments

The protocol for these experiments was as follows.

2.3.4.1 Tissue preparation

Litters of mice from SynGAP heterozygous parents were anaesthetised at P0 with inhaled isofluorane and then decapitated with sharp scissors in accordance with the Animal (Scientific Procedures) Act 1986 under project licence number 60/4290. The skin was cut along the midline and the skull was peeled back using forceps to allow access to the brain. A spatula was used to remove the brain from the skull cavity and the neocortex was dissected in ice cold cutting aCSF or PBS. The tissue was then snap frozen on aluminium foil laid over dry ice before being stored at -80˚C. Tail samples were taken for genotyping allowing total RNA extraction to be carried out on *Syngap*$^{-/-}$ mice only for the current experiments. Total RNA was extracted using the RNeasy mini-kit (Qiagen) and RNase-Free DNase set (Qiagen) and following the kit instructions. Briefly, approximately 30 mg of tissue was homogenised with a needle and syringe in 600 µl buffer RLT containing 6 µl β-mercaptoethanol. The lysate was centrifuged for 15 seconds at 16,000 x g and the supernatant transferred to a new microcentrifuge tube. 1 volume of 70% ethanol was added and mixed by pipetting before being transferred to an RNeasy spin column in a collection tube and centrifuged again for 15 seconds. 70 µl DNase I stock solution (15000 Kunitz units) mixed with 10 µl Buffer RDD was added to the column membrane, and left at room temperature for 15 min. The column was washed twice with 350 µl Buffer RW1 and twice with 500 µl buffer RPE with 15 second centrifugation between the washes. RNA was eluted in RNase free water. Total RNA concentration was measured spectrophotometricly using the Nanodrop 1000 (Thermo Scientific).

2.3.4.2 Synthetic mRNA production

Transcripts were generated from the specific plasmids made in using the mMessage mRNA kit. Briefly, the plasmids were linearised by restriction enzyme digest. The reagents for this were

- 1µg DNA
- 1µl (2000 U) EcoR1 enzyme, [# R0101S New England Biolabs, (NEB)]
- 1µl NEB4 10 x buffer (# B7004S NEB)
- H_20 to make up to 10µl.

The mix was incubated at 37°C for 2 hours.

The reaction volume was made up to 100 µl with H_20 and an equal volume of phenochloroform isoamyl alcohol (25:24:1 v/v) was added. The mix was vortexed for 30 secs to extract protein and was then centrifuged at 4°C at maximum speed for 5 minutes to separate the phases. The upper aqueous layer was separated into a new tube and further extracted with an equal volume of chloroform, and the aqueous phase recovered into another new tube. $1/10^{th}$ or 10 µl volume of 3M acid sodium acetate was added and the DNA precipitated by the addition of 200µl of 100% ethanol, and recovered by centrifuged at 4°C at maximum speed for 20mins. The supernatant was vacuum aspirated and the pellet washed in 200µl 70% ethanol. It was centrifuged again at 4°C for 5 minutes and the supernatant aspirated. The pellet was allowed to air dry for 5 minutes and then re-suspended in 11µl RNAse free H_20.

The mMESSAGE mMACHINE® Kit (Thermo Fisher Scientific #AM 1344) was used to transcribe the DNA into RNA as follows. The transcription reaction was assembled at room temperature as follows and incubated at 37°C for 1 – 2 hours.

Reaction mix

- 2X NTP/CAP 10µl
- 10X Reaction buffer 2µl
- Linear template DNA 0.2 µg
- Enzyme mix 2µl
- Nuclease-free water To 20µl

The quality and integrity of the mRNA made was determined using Agilent Genomics 2100 Bioanalyzer.

2.3.4.3 Primer design

In designing the primers, the following parameters were used as a framework in an attempt to ensure the primers would work in a comparable manner under the same experimental conditions to allow for comparisons to be made of the abundance of the different SynGAP isoforms.

- Primer length 17 – 23 bp
- Melting temperature 59 – 62.9°C
- Difference in melting temperatures of no more than 1°C
- Primer end is a cytosine or guanine
- Primers span an exon boundary
- Product (amplicon) length of 150 -250 bp
- Primers don't form hetero dimers, primer dimers, or have a secondary structure

2.3.4.4 Primer validation

Primers were designed for each of the SynGAP N terminal isoforms and for GADPH, a control gene (Table 6). A three step validation process was carried out for each primer as follows:

1. When designing the primers, any giving secondary products < 1 kb in length were discarded to minimise the amplification of non-specific products
2. One-step RT PCR was carried out for each primer using 1 µg of SynGAP isoform synthetic RNA and the products were run on a 0.7% agarose gel to confirm the amplification of just one specific product
3. Melt curve analysis was conducted at the end of each run between 55°C and 90°C. A single melting peak was taken as demonstrating one specific product. Any samples with multiple peaks were discarded from the analysis.

Table 6 – SynGAP isoform qPCR primers

SynGAP Isoform	Forward Primer	Reverse Primer
A	CGAGTCCAGCCGAAACAAAC	GGGACTCAGCAGGGACTC
A1	CGATGTCCTATGCCCCCTTC	GGGACTCAGCAGGGACTC
B	GCTCTTCTTGCTGCTTTCCG	GGGACTCAGCAGGGACTC
C	AAGTGCTGACCATGACCG	GGGACTCAGCAGGGACTC
E	TTCTCGCTGCATCTTCCGAG	GGGACTCAGCAGGGACTC
G	CGGTGCGAGATGGAGGC	GGGACTCAGCAGGGACTC
Pan Syngap	CGAAGTGCTGACCATGAC	CGGCTGTTGTCCTTGTTG
GADPH (control)	GGGTGTGAACCACGAGAAAT	CCTTCCACAATGCCAAAGTT

2.3.4.5 One-step RT PCR

The OneStep RT PCR kit (Qiagen) was used in the primer validation process. The following reagents were mixed on ice:

Reaction mix

- H_20 13.5 µl
- 5x buffer 5 µl
- dNTPs 1 µl
- Enzyme mix 1 µl
- 10 µM forward primer 1.5 µl
- 10 µM reverse primer 1.5 µl

1 µg of template RNA was added to each tube.

Thermocycling conditions

- 50°C for 30 minutes
- 25 cycles of
    - 95°C for 15 minutes
    - 94°C for 45 seconds
    - 59°C for 45 seconds
- 72°C for 1 minute
- Followed by 72°C for 10 minutes.

The reaction was then held at 4°C. The product was run on a 0.7% agarose gel. As with genotyping and western blotting, the images were cropped for presentation, but full gel images are shown in Appendix 1.

2.3.5 "Spike-in" and qPCR experiments

So called 'pan Syngap' primers (Table 6) which were previously used to amplify all known SynGAP isoforms (McMahon et al. 2012), were used in RT-PCR to check for the absence of SynGAP in the P0 homozygous mouse neocortex. Known amounts of the synthetically made mRNA of SynGAP N terminal isoforms A, B, C, E and G on the α2 c-terminal backbone were then added or 'spiked' into the total mRNA

extracted from P0 *Syngap*$^{-/-}$ mouse neocortex. qPCR was then carried out in triplicate with different quantities of each synthetic isoform. This was to establish the relative efficiencies of each primer combination and the accuracy of the qRT-PCR across the triplicates. Each synthetic isoform was also added individually ranging from 0.1 pg - 100 pg in an attempt to determine the physiological levels of isoform expression by comparing the Ct value at which the gene was detected in *Syngap*$^{-/-}$ mice versus their wild type littermates. The Ct values were all normalised to the housekeeping gene GAPDH.

First strand synthesis was performed using the First strand cDNA synthesis for RT-PCR kit (Roche). Typical reaction and reverse transcription thermal cycling conditions for these experiments were as follows:

Reaction Mix	Final Concentration
• 2 µl RNA (mouse brain RNA plus 1 µl synthetic RNA)	Varied by experiment
• 1 µl Oligo [dT] primers (50 pmol/µl)	2.5 µM
• 2 µl Random Primers (600 pmol/µl)	60 µM
• H_20	To total 13 µl

Followed by adding

- 4 µl 10x reaction buffer including 8mM final concentration of $MgCl_2$
- 0.5 µl Reverse Transcriptase (20 U/µl) — 10 U
- 2 µl Deoxynucleotides (10 mM each) — 1 mM each
- 0.5 µl RNase inhibitor (40 U/µl) — 20 U

Total volume was 20 µl

Thermocycling Conditions:

- 25°C for 10 minutes
- 55°C for 30 minutes
- 85°C for 5 minutes
- 4°C for 15 minutes

Real time RT-PCR was performed using an MJ research DNA Engine Opticon and an Applied Biosystems 7500 Real-Time PCR system with Quantitect SYBR Green PCR kit (Qiagen). A typical PCR reaction and thermal cycling conditions are shown below. 15 µl total reaction volume was used for all reactions carried out on the Applied Biosystems machine whilst 20–25 µl total reaction volumes were for reactions in the Opticon machine as the machine sensitivities varied.

Reaction Mix

- 2x QuantiTect SYBR Green PCR Mix (including Rox) 12.5 µl
- Forward Primer (300 nM final concentration) 0.75 µl
- Reverse Primer (300 nM final concentration) 0.75 µl
- H_20 10 µl
- cDNA (of appropriate concentrations) 1 µl
- **Total volume** **25 µl**

Thermocycling

Step 1: 95°C for 10 minutes

Step 2: 40 cycles of

1. 95°C for 30 seconds
2. 60°C for 40 seconds
3. 72°C for 1 minute

Step 3: Dissociation Curve

1. 95°C for 1 minute
2. 55°C for 30 seconds
3. 95°C for 30 seconds

Readings were taken at every 0.5°C temperature increase

2.3.5.1 Quality control measures

Known amounts of control cDNA from ~P90 WT mouse neocortex were used to construct a standard curve in triplicate for each SynGAP N terminal isoform primer pair and the GAPDH control primer pair. Furthermore water blank and minus reverse transcriptase controls were performed for each isoform on every run. If product was amplified in either of these controls, the corresponding experimental

data was discarded. Opticon Monitor analysis (version 1.01) or Applied Biosystems software were used to compare amplification during the log-linear phase from the dilution series of control cDNA to ensure there was similar amplification of the cDNA for each replicate sample.

2.3.5.2 Data analysis

The primer pair efficiencies were calculated using the online ThermoFisher Scientific qPCR primer efficiency calculator https://www.thermofisher.com/uk/en/home/brands/thermo-scientific/molecular-biology/molecular-biology-learning-center/molecular-biology-resource-library/thermo-scientific-web-tools/qpcr-efficiency-calculator.html and the correlation coefficient (R^2) values for the primer pairs were calculated from the standard curve data in GraphPad Prism for Windows (GraphPad Software). The Opticon Monitor analysis (version 1.01) or Applied Biosystems software automatically calculated Ct values and plotted melt curves and amplification plots.

2.4 Tissue culture

2.4.1 Preparation of SynGAP_GAP rat primary hippocampal cultured neurons

Heterozygous-heterozygous timed matings of SynGAP_GAP Long Evans Hooded rats were set up so that primary hippocampal cultures could be prepared from WT, heterozygous and homozygous embryos at embryonic day 18. The primary cultures were kindly prepared by Katherine Bonnycastle, Centre for Integrative Physiology, University of Edinburgh. Her protocol for this was as follows.

Preparation

Coverslips were coated with a mixture of 50 ml autoclaved Boric acid (100 mM, pH 8.5) and 500 µg pol-D-lysine (Sigma Aldrich, stock 5 mg / ml in water) and left overnight on a rotator. They were then washed with autoclaved pure water twice and left for 1-2 hours on the rotator before being dried on a paper towel sterilised with ethanol. One 13 mm coverslip was placed in each well of a 24 well plate. 50 µl of laminin (Sigma Aldrich) was added to 5 ml of neurobasal medium (ThermoFisher Scientific) and kept on ice. 50 µl of this mix was then pipetted on each coverslip and the plates were placed in a 37°C/ 5% CO_2 incubator. Papain powder (Worthington

Biochemical Corporation) was pre-diluted 10 units / ml and 200 µl was put straight into a 15 ml Falcon tube. One tube was used for each embryo head. The tubes were pre-warmed in the water bath at 37°C. Dulbecco's Modified Eagle Medium: Nutrient Mixture F-12 (DMEM/F12 – ThermoFisher Scientific) was supplemented with 1% penicillin/streptomycin solution and 10% Foetal Bovine Serum. This preparation was then aliquoted to give 500 µl per papain tube and 2 ml per papain tube to top up volume before centrifuging. Neurobasal medium was supplemented with 10 ml B27 (ThermoFisher Scientific), 0.5 mM (1.25 ml) L-glutamine (Sigma Aldrich) and 1% penicillin/streptomycin solution (ThermoFisher Scientific). This was then aliquoted so that 100 µl was available per head dissected plus 1 ml for every well. The aliquots of supplemented DMEM/F12 and neurobasal medium were pre-warmed in the 37°C/ 5% CO_2 incubator to let the CO_2 equilibrate.

Dissection

After the pregnant females were culled, the abdomen was sprayed thoroughly with ethanol to minimise the spread of animal dander. The skin and underlying fascia was cut around and upwards to avoid getting dander inside the abdominal cavity. The uterine horns were dissected and transferred to a petri dish. The embryos were removed from their amniotic fluid sacs and decapitated with scissors. The head and body were transferred to the same well of a 6 well plate.

The hippocampi from the chosen heads were dissected by using sharp forceps to remove the skin before gently removing the skull. The brain was scooped out using a spatula, the brainstem and cerebellum were removed and the hemispheres separated. The meninges were torn away and the hippocampus removed. To try and ensure cells were healthy, the total dissection time were restricted to no more than 75 minutes from the point of uterine horn extraction.

Tissue Digestion

Both hippocampi from each head were placed in one of the pre-warmed tubes containing 200 µl of papain and left at 37°C in a water bath for 20 minutes to digest the tissue. The excess papain was then discarded and 500 µl of the pre-warmed

DMEM/F12 was added to each tube to saturate the enzyme. The tissue was pipetted up and down approximately 25 times until it disaggregated into a single-cell suspension. The cell suspension was topped up to 2.5 ml using the rest of the pre-warmed DMEM/F12 and the tube was centrifuged at ≥15000 x g for 5 minutes. The supernatant was discarded and each tube of cells re-suspended in 100 µl of the pre-warmed neurobasal medium. 10 µl of the suspension was placed on each side of a haemocytometer and a cell count performed so that 50,000 cells/well could be plated onto the laminin spot on each pre-prepared coverslip. The cells were then left to settle for one hour before 1 ml of pre-warmed neurobasal medium was added. The plates were then kept in the 37°C/ 5% CO_2 incubator. On day 3, neurobasal medium was added to the wells with cytosine β-D-arabinofuranoside (Ara-C, Sigma Aldrich) to give a final concentration of 1 µM to stop the proliferation of glia.

Electrophysiological recordings were made at days in vitro 13-15. The analysis of the recordings was carried out whilst blind to genotype.

2.4.2 WT hippocampal tissue cultures for transfection with SynGAP isoform Eα1

Autoclaved glass coverslips were placed in 24 well culture plates and coated for 2 hours with 200 µl of poly-L-lysine (Sigma Aldrich) stock solution (10 mg / ml) per 40 ml of distilled H_20. They were coated for a further hour in 1 ml of Fibronectin (Thermo Fisher Scientific) stock solution (1 mg / 10 ml) per 10 ml of distilled H_20. Timed matings of Sprague-Dawley WT rats were set up and at day 20.5, pregnant females were culled. The mother's abdomen was sprayed with ethanol and the abdominal wall cut to enable removal of the embryos which were then decapitated with sharp scissors and placed in basal medium eagle solution (BME, Thermo Fisher Scientific) on ice.

Each pup brain was removed from the skull and hemisected before the hippocampi were dissected out in filtered HBSS (Thermo Fisher Scientific) / HEPES (Sigma Aldrich) Solution (500 ml of Hank's Based Salt Solution and 1.19 g HEPES with pH adjusted to 7.3). The hippocampi were incubated at 37°C in 2 ml Hanks / HEPES

Solution with 200 µl Trypsin (Worthington) and 20 µl DNase (Sigma Aldrich). The solution was removed and the tissue washed twice in solution that was 90% BME with 10% horse serum (Thermo Fisher Scientific) before being triturated with a fire polished pipette. The cells were counted with a haemocytometer and plated on the coverslips after the fibronectin had been washed off with BME. The following day the old media was removed and replaced with fresh serum free medium. Thereafter the cells were fed twice weekly, removing half of the old medium and replacing it with fresh serum free medium made up in 500 ml batches consisting of 500 ml BME, 8 ml of a 32.5% glucose solution (in double distilled water), 5 ml sodium pyruvate 100 mM solution (Thermo Fisher Scientific), 5 ml N2 supplement (Thermo Fisher Scientific) and 10 ml B27 supplement (Thermo Fisher Scientific). Initially 5 ml penicillin-streptomycin solution (Thermo Fisher Scientific) was also added, but in later cultures this changed to 5 ml Antibiotic-Antimycotic 1x (Thermo Fisher Scientific) due to persistent fungal contamination.

Initially the density of cultures was low and variable and it was hypothesised that this was contributing to the cells appearing unhealthy visually and on electrophysiological recording. The density of plated cells was therefore standardised to 1500 cells / mm^2.

2.4.3 WT cortical primary tissue cultures for transfection with SynGAP isoform Eα1

These cultures were kindly prepared by members of the Hardingham Laboratory, Centre for Integrative Physiology, University of Edinburgh. Their protocol was as follows:

The coverslip coating mix was prepared using 1 mg poly-lysine (BD Biosciences) and 0.375 mg laminin (Sigma Aldrich) for 75 ml. 0.4 ml coating mix was used per well in a 24 well plate and the plate was left in the 37°C incubator for ~2 hours. Dissection solution (reagents from Sigma Aldrich) was prepared by mixing 36 ml of Dissociation Medium [Na_2SO_4 1 M, $MgCl_2$ 2 M, $CaCl_2$ 1 M, HEPES 1 M, phenol red, glucose 2.5 M (45%)] in a 100 ml sterile bottle with 4 ml of 10X kynurenate magnesium (made from H_2O, phenol red, 1 M NaOH, 1 M HEPES and 2 M $MgCl_2$).

The pH of the solution was adjusted by adding drops of 0.2 M NaOH, stirring constantly. The pH was correct when the colour changed from orange (or yellow) to a rose shade of red. 9 ml of this solution was then placed in two small plastic Petri dishes (to place the cortices in after dissection). Growth medium and papain were pre-warmed in a 37°C water bath before starting dissections.

Sprague-Dawley WT rat pairings were set up in timed matings so that the pups could be dissected at embryonic day (E) 21. The mother rat was culled and ethanol sprayed on her abdomen. The abdominal wall and underlying fascia was cut and the embryonic pups removed and decapitated with sharp scissors. The number of pups required was calculated by expecting to need 1/7 cortex per 2 ml and 0.5 ml of solution per well. The brains were dissected and incisions made in the cortices to increase the surface area that interacted with the papain enzyme. The cortices were transferred to a plastic tube and as much of the dissection solution as possible was removed. A drop of 0.2 M NaOH was added to the enzyme to make it pink rather than yellow if necessary. 1 ml of papain was added to the cortices and incubated at 37°C in the water bath, stirring every 5 minutes. The coated plates were then prepared by removing the excess coating mix with a vacuum pump. They were washed once with sterile water which was then aspirated. The plates were stacked in the incubator to dry completely. All the papain was removed from the cortices tube and the tube was washed with remaining 2 ml Dissociation Medium mixed with kynurenate magnesium. The tube was washed twice with 2 ml 1% NBA growth medium (NeuroBasal A, Thermo Fisher Scientific), rat serum 1% (Harlan SeraLab Ltd), Antibiotic-Antimycotic 1x (Thermo Fisher Scientific), B-27 1x (Thermo Fisher Scientific), glutamine 1mM (Sigma Aldrich) and gently shaken to mix. 2 ml of 1% NBA was then added to the tube and the mix was pipetted up and down quickly 50-60 times to mix. A further 2 ml 1% NBA was then added and it was left for 5 minutes for all the debris to settle. The medium was gently aspirated without disturbing the tissue at the bottom and another 2 ml of growth medium was added to the tube. Again it was mixed by pipetting up and down 50 times and 2 ml more medium was added before resting for a further 5 minutes. This step was repeated until a total of 10 ml of growth medium had been used. The mix was diluted with

pre-warmed OptiMEM+ (Thermo Fisher Scientific), to achieve the required concentration of 1/7 cortex/ 2 ml. (0.0625 cortex / ml) and homogenised by further mixing with a pipette. 0.5 ml of the cell mix was plated per well of a 24-well plate and incubated for 2.5 hours at 37°C. The diluted medium was aspirated from each well and 1 ml of pre-warmed growth medium (1% NBA) was added to the wall of the well. Cells were left in the 37°C incubator to grow.

Culture maintenance:

On Days in Vitro (DIV) 4, 1 ml / well of fresh pre-warmed medium mixed with 1.2mM Cytosine β-D-arabino-furanoside hydrochloride (AraC) (Sigma Aldrich) was added to block DNA replication and stop glial cells dividing. Thereafter the cells were fed twice weekly, removing half of the old medium and replacing it with fresh serum free growth medium made up in 500 ml BME, 8 ml of a 32.5% glucose solution (in water, sterile), 5 ml sodium pyruvate 100 mM solution, 5 ml N2 supplement and 10 ml B27 supplement. As with hippocampal cultures, initially 5 ml penicillin-streptomycin solution (Thermo Fisher Scientific) was also added to the medium, but this was later changed to 5 ml Antibiotic-Antimycotic 1x (Thermo Fisher Scientific) due to persistent fungal contamination.

2.5 Transfection for electrophysiological recording for mEPSCs

SynGAP isoforms were transfected into the cultured WT Sprague-Dawley cortical and hippocampal cells on Days in Vitro (DIV) 8-10 using lipofectamine. Equal amounts of SynGAP Eα1 isoform DNA and eGFP plasmid (2 µg of each per well in a 6 well plate or 0.65 µg of each per well of a 24 well plate) were added to Opti-MEM (Thermo Fisher Scientific) (50 µl/well in a 6 well plate or 33µl/well in a 24 well plate). The eGFP was kindly provided by Katie Marwick, Hardingham Laboratory, Centre for Integrative Physiology, University of Edinburgh. Lipofectamine 2000 (ThermoFisher Scientific) was separately mixed with Opti-MEM. Initially 4µl of Lipofectamine in 50µl Opti-MEM was used for one well in a 6 well plate or 2.33µl in 33µl for one well in a 24 well plate. This was gradually reduced over successive transfections due to poor cell health. The final lipofectamine concentration used was 0.8 µl in 33µl (for one well in a 24 well plate).

Both mixtures were left on ice for 5 minutes then mixed and vortexed briefly before being left on the bench for 20 minutes. A proportion of the medium from each well of the culture plate to be transfected was removed (0.5 ml / well for a 6 well plate and 0.25 ml / well for a 24 well plate), pooled and made up to 2 ml / well for a 6 well plate or 0.5 ml / well for a 24 well plate. The Opti-MEM, DNA and lipofectamine mix was then pipetted onto the top of the well and the plate was incubated for 2 hours at 37ºC. All the media was removed from the transfected wells and replaced with the media reserved earlier. Electrophysiological recordings of miniature excitatory post-synaptic currents (mEPSCs) were made from them 16 to 25 hours later.

2.6 Preparation of Acute Hippocampal Brain Slices

The rats were anaesthetised and decapitated as described in section 2.1. The skin was cut along the midline and the skull was peeled back using forceps to allow access to the brain. A spatula was used to remove the brain from the skull cavity and 400 μm thick horizontal hippocampal brain slices were cut on a Leica VT1200S vibratome in ice-cold 'cutting' artificial cerebral spinal fluid. This was made from the following reagents (all from Sigma Aldrich and expressed in mM) and was carbogenated with 95% O_2 and 5% CO_2: NaCl 86, NaH_2PO_4 1.2, KCl 2.5, $NaHCO_3$ 25, glucose 20, sucrose 75, $CaCl_2$ 0.5, $MgCl_2$ 7. For long-term depression recordings, AMPAR / GABAR and AMDAR / NMDAR recordings, a cut was made through CA3 to prevent recurrent electrical activity from CA3 distorting the recordings.

Slices were allowed to recover for 30 minutes at 35°C in external recording solution containing the following reagents (Sigma Aldrich) in mM: NaCl 124, NaH_2PO_4 1.2, KCl 2.5, $NaHCO_3$ 25, glucose 20, $CaCl_2$ 2, $MgCl_2$ 1. Slices were then maintained at room temperature (20 - 22ºC) for a minimum of 30 minutes before recordings were made. Recordings were made from CA1 pyramidal neurons identified by their characteristic shape. The composition of the external recording solution remained as above except for the addition of certain pharmacological compounds as described below for each individual experiment. The perfusion flow rate was maintained at 3 - 5 ml / minute. The temperature of the bath was maintained at 31 ± 1°C.

For acute brain slice recordings, WT and heterozygous littermates were used and animals were chosen either at random or by another experimenter to ensure the main experimenter remained blind to genotype. The genotype was not revealed until after data analysis.

2.7 Electrophysiological methods

2.7.1 Electrophysiology recording equipment

Recording electrodes (Premium Standard Wall Borosilicate Capillary Glass with Filament, OD 1.5 mm, ID 0.86 mm) were pulled on either a Sutter P95 or P97 Micropipette Puller) to give a pipette resistance between 2 to 7 MΩ. Bipolar stimulating electrodes were made from nickel / chromium (80% / 20%) wire. Pulses were delivered by a DS3 Isolated Constant Current Stimulator (Digitimer Ltd).

For field potential experiments, recordings were acquired using WinLTP Version 2.1 (The University of Bristol), amplified 1000 times (initially with NPI electronics amplifier and then an Axoclamp-2b amplifier from Axon Instruments), filtered at 4 kHz and digitised (National Instruments BNC-2090A) at 20 kHz.

For whole cell patch-clamp recordings from acute brain slices, recordings were made using a MultiClamp 700B amplifier and a Digidata series 1440a digitiser (Molecular Devices CA 94089 USA). The samples were digitised at 20 kHz and low pass filtered at 2 kHz. The acquisition software was Clampex Version 10 software (Molecular Devices). For recordings from primary cultures the data acquisition software was WinEDR Version 3.4.3 software. The data was digitised using a National Instruments (NIDAQ-MX) Card and amplified with an AxoPatch 200B. The recordings were digitized at 10 kHz and low pass filtered at 2 kHz. Reagents used for electrophysiological experiments were sourced from Sigma Aldrich unless otherwise stated.

2.7.2 Extracellular field recordings

To measure long-term depression (LTD) in the hippocampus pairs of 200 µs current pulses 50 ms apart were delivered every 30 seconds to the Schaffer collateral axons

in post-natal day (P) 26 - 30 rats. The recording electrodes were filled with the standard external recording solution detailed above. The stimulus intensity was adjusted to give approximately 50% of the amplitude which elicited a population spike. Recordings were discarded if a stable 20 minute baseline could not be achieved. In those in which this stable baseline was achieved, 100 μM (R, S)-3, 5-Dihydroxyphenylglycine (DHPG) (Abcam) was bath applied to the slice for five minutes. The recording then continued for a further 60 minutes. For a subset of slices, 100 μM the protein synthesis inhibitor cycloheximide (CHX) (Abcam) was bath applied at least 30 minutes before application of DHPG and kept in the solution throughout the recording to evaluate whether new protein synthesis was required for LTD.

2.7.3 Intracellular recordings from hippocampal brain slices

2.7.3.1 Intrinsic cell properties

In order to examine CA1 pyramidal cell intrinsic properties, the following protocols were run after whole cell recording was established in P13 - 15 and P26 - 30 male and female rats. The recording electrodes were filled with potassium gluconate internal solution comprising (in mM) K gluconate 120, KCl 20, HEPES 10, NaCl 4, Mg ATP 4, Na_3GTP 0.3, sodium phosphocreatine 10. Firstly, 1 minute of gap-free recording was made in I=0 mode. The recording was switched to current clamp and the bridge balance was adjusted. Next a -250 pA hyperpolarising step was applied in triplicate in current clamp in order to calculate the sag, followed by a series of 25 pA current steps from -100 pA to +400 pA again in triplicate to investigate action potential properties, input resistance and resting membrane potential.

2.7.3.2 Excitatory and inhibitory current recordings

In order to examine the excitatory – inhibitory balance in hippocampal pyramidal CA1 neurons, spontaneous and miniature post synaptic currents were recorded from male and female P13-15 and P26-30 rats as follows.

The recording electrodes were filled with caesium gluconate internal solution comprising (in mM) Caesium gluconate 140, CsCl 8, HEPES 10, EGTA 0.2, Na ATP 2, Mg ATP 2, Na_3GTP 0.3. Following the establishment of whole cell recording, the cell was initially held at -70 mV and recordings of spontaneous excitatory post-synaptic currents (sEPSCs) were made for 4 minutes. The access resistance was monitored throughout using a hyperpolarising step every 1 minute. The holding potential was then changed to 0 mV and the cell was left for 4 minutes to adapt to this. Spontaneous inhibitory postsynaptic currents (sIPSCs) were then recorded for 4 minutes.

0.3 µM tetrodotoxin (TTX, supplied by Tocris) was added to the external recording solution to unmask miniature currents and the holding potential was returned to -70 mV. After 5 minutes stabilisation time, 4 minutes of miniature excitatory post-synaptic currents (mEPSCs) were recorded. The holding potential was then once again adjusted to 0 mV and after 4 minutes of adjustment time, 4 minutes of miniature inhibitory post-synaptic currents (mIPSCs) were recorded.

The receptors mediating each part of the recordings were established by the abolition of the current with the addition of 10 µM 1,2,3,4-Tetrahydro-7-nitro-2,3-dioxoquinoxaline-6-carbonitrile disodium (CNQX, Abcam), an AMPA/Kainate receptor antagonist to excitatory recordings and 100 µM picrotoxin (PTX, GABA-A receptor antagonist consisting of a 1:1 mixture of picrotoxinin and picrotin from Abcam or Hello Bio) to inhibitory recordings.

2.7.3.3 AMPAR / GABAR and AMPAR / NMDAR ratios

In P26-30 male and female rats, single 0.1 Hz current pulses were delivered every 6 seconds to the Schaffer collateral axons using a DS3 Isolated Constant Current Stimulator (Digitimer Ltd) and a bipolar electrode made from nickel / chromium

(80%/ 20%) wire. The recording electrodes were filled with caesium gluconate internal solution comprising (in mM) Cs gluconate 140, CsCl 3, HEPES 10, EGTA 0.2, Na ATP 2, MgATP 2, Na_3GTP 0.3 and QX-314 5 (Abcam). QX-314 is a Na^+ channel blocker added to the internal to improve the voltage space clamp. The stimulation required to produce a reliable current response of a minimum of approximately 100 pA amplitude at 0 mV was identified using steps of increasing stimulation (typically in the region of 40 μA to 1 mA). This was because prior to doing this, several cells were successfully recorded from at -70 mV, but when the holding potential was changed to 0 mV there was insufficient response to record inhibitory post-synaptic currents (IPSCs). The chloride reversal potential was identified by recording excitatory post-synaptic currents (EPSCs) with gradually more positive holding potentials from -70mV until clean, monosynaptic events were seen. The chloride in the internal solution was restricted to 8 mM and using the Nernst equation, the predicted chloride reversal potential at 32°C was -73.21 mV. The measured chloride reversal potential ranged from -58 mV to -68 mV. Once it had been identified, 30 consecutive EPSCs were then recorded at the chloride reversal potential. This ensured that all negative deflecting events were α-amino-3-hydroxy-5-methyl-4-isoxazole propionic acid (AMPA) receptor mediated.

The AMPA reversal potential was then identified using gradually more positive holding potentials from -10 mV until a clean monosynaptic response was identified. 30 IPSCs were then recorded. 75 - 100 μM PTX was then applied and this abolished the current demonstrating these responses were γ-Aminobutyric acid receptor (GABAR) mediated.

The cell was then held at +40 mV and 30 EPSCs were recorded. In a subset of recordings this current was altered by the application of 10 μM CNQX, an AMPA / Kainate receptor antagonist and / or 50 μM D-(-)-2-Amino-5-phosphonopentanoic acid (D-AP5, Abcam), a selective NMDA receptor antagonist. The application of both drugs together abolished the current. The holding potential was changed to -70 mV and a further 30 AMPAR mediated EPSCs were recorded. These responses were abolished when CNQX was applied to a subset of cells. Throughout the

recordings, the access resistance was monitored using a hyperpolarising step just before each 0.1 Hz pulse.

2.7.4 Intracellular recordings from cultured neurons

Once removed from the 37°C incubator at the time of recording, coverslips were continuously perfused at a flow rate of 3 - 5 ml / minute with external recording solution of the following composition (in mM) at room temperature (20-22°C): NaCl 150, KCl 3, HEPES 10, $CaCl_2$ 2.5, $MgCl_2$ 1.3, glucose 10, glycine 0.05 plus tetrodotoxin 300 nM, picrotoxin 50 μM. Magnesium was present in the external solution to ensure the voltage sensitive NMDA receptors were blocked so that any events recorded were AMPAR-mediated. WT, *Syngap*$^{+/GAP}$ and *Syngap*$^{GAP/GAP}$ hippocampal recordings were made from DIV 13 to 15. Recordings from cortical and hippocampal cultured Sprague-Dawley rat neurons transfected with SynGAP Isoform Eα1 were made from DIV 9 to 11 along with recordings from neighbouring control cells and cells from untransfected coverslips. The internal solution was composed of (in mM) Cs Gluconate 130, CsCl 10, HEPES 10, EGTA 0.1, glucose 10, sodium phosphocreatine 10, Mg ATP 4 and Na3GTP 0.5. Its pH was adjusted to 7.3 using CsOH; aiming for an osmolarity of 285 - 295 mOsm. 10 minute mEPSC recordings were made from cells with a typical pyramidal shape in voltage clamp at -70 mV. During the recordings, the perfusion was turned off to minimise the artefact from the perfusion which could mask mEPSCs. Hyperpolarising steps were programmed every minute to monitor the access resistance. A maximum of 3 cells were recorded from on each coverslip and typically coverslips were discarded after being out of the incubator for recording for 45 minutes. The number of cultures used for these recordings is shown in Table 7.

Table 7 – Number of cultures that mEPSCs were recorded from

Experiment	Brain Region	Number of Cultures
WT, *Syngap*$^{+/GAP}$ and *Syngap*$^{GAP/GAP}$ recordings	Hippocampus	3
Untransfected Sprague-Dawley hippocampal recordings	Cortex	8
	Hippocampus	8
SynGAP Isoform Eα1 recordings	Cortex	6
	Hippocampus	6

2.8 Power calculations

In general the experiments carried out in this thesis were exploratory being the first of their kind to compare WT to genetic mutants in a model of SynGAP mutation in a rat. Even those experiments investigating parameters previously measured in mouse models of SynGAP haploinsufficiency were generally not direct replicates in the rat. Therefore using published data for power calculations wasn't possible. The exceptions were the LTD experiments and the SynGAP isoform mEPSC recording experiments.

In the LTD experiments data from Barnes and colleagues *Syngap*$^{+/-}$ mouse experiments was used for power calculation as very similar experimental procedures were employed (Barnes et al. 2015). Taking Barnes' data and aiming for an effect size of 0.05 and power of 0.8, 13 animals were found to be needed per group for standard LTD experiments. For experiments comparing the effect of protein synthesis inhibition between genotypes 6 animals were found to be required per genotype group.

For the SynGAP Eα1 isoform mEPSC recordings, there was no previously published Eα1 data to refer to. Therefore power calculations were based on data from the unpublished thesis of Aoife McMahon, Centre for Integrative Physiology, University of Edinburgh (McMahon 2010). This thesis formed the basis for McMahon's subsequent paper which examined the influence of SynGAP isoforms Aα1, Bα1, Cα1, Aα2, Bα2 and Cα2 on mEPSC amplitude and frequency (McMahon et al. 2012). The most applicable data for the power calculations comes from cells

transfected with SynGAP isoforms Aα1, Bα1 and Cα1 as they have the same C terminal as those used in the current thesis (α1). If McMahon's SynGAP Aα1 data which showed the largest difference from the eGFP control is used, a group size of 23 cells is predicted to be required in order to achieve an effect size of 0.05 and power of 0.8 in the Eα1 experiments. However using her Cα1 data (which showed the smallest difference from eGFP controls), 127 per group would be required. These calculations are based on mEPSC amplitude data as McMahon presented log transformed data for mEPSC frequency and the raw values to make the calculation with weren't available.

The Biomath online power calculator was used for all the calculations described above (http://biomath.info/power/ttest.htm).

2.9 Data analysis

For all data sets, D'Agostino & Pearson normality tests were carried out. If, for two group comparisons, both groups in the analysis passed the normality test (p value of > 0.05), parametric tests were used. If not, non-parametric analysis was used. Following this rule, for the comparison of two data groups, either an unpaired t-test or Mann-Whitney test was used unless otherwise stated. The tests used to compare more than two groups are detailed under the appropriate section below. Significance was defined as $p < 0.05$ throughout and all analyses, example traces and graphs were carried out or constructed using Graphpad Prism for Windows software (GraphPad Software). Full details of the statistical tests and results are presented in the figure legends rather than the main text of this thesis. In electrophysiological recordings where more than one cell or slice was recorded from per animal/ pup, the data has been collated by both cell/ slice and animal/ pup.

2.9.1 Field recording analysis

The acquired data was exported to Microsoft Excel 2010 and plotted in Graphpad Prism for Windows (GraphPad Software). Traces in which there had been an identifiable technical issue were discarded. Mean long-term depression was calculated as the mean slope (mV / ms) value of the characteristic field potential of the first of the paired pulses, every thirty seconds for the last 10 minutes of the trace.

Slope was used as a measure rather than amplitude so that the measurement wasn't contaminated by population spikes.

2.9.2 Intrinsic cell properties analysis

Recordings were examined post-hoc and discarded if the resting membrane potential was more positive than -50 mV, or if the appearance of the action potential spikes was either indicative of a non-pyramidal cell type (e.g. fast spiking interneuron) or of the series resistance being too high (i.e. spikes with a notably short amplitude).

The following properties were analysed in Clampfit Version 10.6.2.2 (Molecular Devices LLC)**:**

- Cells had mistakenly been held at -70 pA rather than -70 mV and so baseline voltage was calculated from the first 5 current steps (all sub-threshold). All cells with a baseline voltage more positive than -64 mV or more negative than -76 mV were excluded to improve the homogeneity of the data
- Resting membrane potential was calculated by taking the mean amplitude of the one minute gap-free recording
- Input resistance was calculated from the first 5 current steps (all sub-threshold) by comparing the mean voltage recorded during the baseline 200 ms and 200 ms of each step. This was then plotted and linear regression of the slope was performed.
- Membrane time constant was measured from the +25 pA step of the protocol as the cleanest curve fitting was achieved at this current injection. A standard exponential curve was fitted by eye to the rising current and tau was automatically calculated by GraphPad Prism
- Capacitance was calculated as membrane time constant divided by input resistance
- Sag was calculated from the -250 pA steps by calculating the difference between the peak deflection and the steady state of the step
- Action potential properties were calculated at the first step at or after rheobase (i.e. the first current step with any action potentials). The first action potential generated was used for analysis and its trace was differentiated to give the change in voltage over the change in time (dV / dt). The point at which dV / dt exceeded

10 mV / ms was therefore identifiable and taken as the start of the action potential. Action potential threshold was measured here and the other action potential properties that were then calculated by the software were peak amplitude, half-width, maximum rise slope and maximum decay slope

- Action potentials per step were counted for each current step

2.9.3 Analysis of mEPSC recordings from SynGAP_GAP deletion rat cultures

The access resistance (Ra) was examined and portions of the trace with Ra > 30 MΩ or a > 20% variation in Ra were discarded. If at least 4 minutes of consecutive trace remained, further analysis was completed**.** The traces were analysed using the template detection setting in Clampfit Version 10.6.2.2 (Molecular Devices LLC). An initial template was constructed by identifying the first fifteen exemplar events of the recording. This was then used to detect events throughout the trace. The final minute of the recording was then visually examined and true events were identified as those with a fast rise time and asymmetric appearance. The Template Match Threshold of the template detection was adjusted to ensure true events were being captured whilst still avoiding false-positives. Data was gathered from 3 separate cultures for these experiments and for the second two, as the experimenter, I was blind to genotype during recording. For all three cultures I was blind to genotype whilst analysing the files.

The recordings for the three genotypes (WT, heterozygous and homozygous) did not all pass a Shapiro-Wilk Normality Test and so were analysed using a Kruskal-Wallis test. Significance was defined as $p < 0.05$.

2.9.4 Excitatory-inhibitory balance analysis

The access resistance (Ra) was examined and portions of the trace with Ra > 30 MΩ or a > 30% variation in Ra were discarded. If at least 3 minutes of consecutive trace remained, further analysis was completed**.** The traces were analysed posthoc using the template detection setting in Clampfit Version 10.6.2.2 (Molecular Devices LLC) in the same manner as the analysis of mEPSCs described above.

2.9.5 AMPAR / GABAR and AMPAR / NMDAR ratio analysis

The traces were analysed posthoc using Clampfit Version 10.6.2.2 (Molecular Devices LLC). Cells were discarded if the access resistance was >30 MΩ or if it varied by more than 20% during the recording. The 30 EPSCs or IPSCs in each recording were averaged and the baseline for the average trace adjusted. For AMPAR / GABAR ratios each average event was integrated to give the total charge transfer. The AMPA charge transfer was then divided by the GABA charge transfer in Microsoft Excel 2010. For AMPAR / NMDAR ratios, the peak of the traces recorded at -70 mV was divided by the average amplitude from 80-85 ms post stimulus of the traces recorded at +40 mV. 80 – 85 ms post stimulus was chosen as by this time in the -70 mV recordings, all the AMPA traces had decayed to < 3% of their peak amplitude, so the contribution of the AMPA receptors to the response at 80 - 85 ms post stimulus in the +40mV traces was minimal.

2.9.6 SynGAP isoform Culture mEPSC recording analysis

The access resistance (Ra) was examined and portions of the trace with Ra > 30 MΩ or a > 20% variation in Ra were discarded. Further analysis was completed using Minianalysis Version 6 Software (Synaptosoft Inc.). Root mean squared (RMS) noise was analysed and portions of the trace with noise > 4 RMS were excluded. If at least 5 minutes of consecutive trace remained, for the majority of files the software's in built AMPA EPSC detection template was used to identify mEPSCs, for the remainder settings were manually adjusted to try and capture true events whilst excluding false positives. The extracted events were then manually reviewed to ensure they were fast rising and asymmetric. Any anomalous events were discarded and missed events added and the final pool of identified events was filtered to remove any with time to rise or time to decay of < 0.5 ms.

3 CHAPTER THREE: GENERATION OF THE SYNGAP_GAP DELETION RAT

3.1 Key findings

- Exons 8 to 12 inclusive are deleted in the *Syngap* gene in the SynGAP_GAP deletion rat model. This is predicted to encompasses the C2 and GAP domains of the protein
- *Syngap*$^{GAP/GAP}$ rats are smaller than their littermates and homozygosity of the mutant SynGAP allele is fatal in the first few days of life
- Hippocampal WT SynGAP protein expression in the SynGAP_GAP deletion rat colony increases from P7 to P28, whereas mutant protein increases from P7 to P14 before stabilising by P28
- WT and mutant SynGAP protein are both expressed in visual and hippocampal brain tissue at P20 and can be detected with all four existing SynGAP isoform antibodies

3.2 Introduction

Although there are several mouse models of SynGAP haploinsufficiency in existence, the greater intelligence and sociability of the rat (editorial by Iannaccone & Jacob 2009; Kummer et al. 2014) is advantageous when conducting research related to ID and ASD, as explained in the introduction to this thesis. On this premise, the SynGAP_GAP deletion rat was engineered and this chapter pertains to its generation using Zinc Finger Technology and confirmation of the mutation using genotyping, mRNA analysis and western blotting. The rationale for deleting the GAP domain of the SynGAP protein comes from the multitude of studies that have linked the GAP domain function to SynGAP's ability to regulate downstream signalling events (Chen et al. 1998; Kim et al. 1998; Krapivinsky et al. 2004; Vazquez et al. 2004; Rumbaugh et al. 2006; Pena et al. 2008; Walkup et al. 2015).

Confirmation of the genetic abnormality in the rats was the first priority as understanding exactly what the disruption to the SynGAP protein was formed the basis for the interpretation of all other findings in this thesis. Thereafter, assessment

of the general characteristics of the SynGAP_GAP deletion rat pups was important given the wealth of detail available about the development of *Syngap*$^{+/-}$ and *Syngap*$^{-/-}$ mice.

3.2.1 SynGAP mouse models

The first SynGAP mutant mice were generated by Komiyama et al. 2002 by disrupting the C2 and GAP domains of the protein in C57BL/6 mice with a vector comprised of a hemagglutinin (HA) epitope tag, internal ribosomal entry site, lacZ gene and polyA tail. Kim et al. 2003 also generated a SynGAP mouse line by disrupting exons 7 and 8 (part of the PH and part of the C2 domain) with a neo^{R} cassette again in C57BL/6 mice. This site was chosen as it is the first common methionine site in the shortest SynGAP isoform (SynGAP C) and the resulting mice have low levels of SynGAP remaining at approximately 120 kDa on immunoblotting whereas the other mouse models have no SynGAP remaining. Vazquez et al. 2004 inserted a Neo cassette flanked by LoxP sites into intron 3 of the SynGAP gene and an additional downstream LoxP site within intron 9. Therefore expression of Cre recombinase results in deletion of SynGAP exons 4 to 9 (part of the PH domain, the C2 domain and a portion of the GAP domain) in this model which was backcrossed onto a C57BL/6 background. The design of the SynGAP_GAP deletion rat was such that the C2 and GAP domains of the protein would be lost, similar to the Komiyama mouse model.

From a breeding and development point of view, the inheritance of their SynGAP mouse lines was found by Komiyama et al. 2002 and Kim et al. 2003 to follow a Mendelian pattern and heterozygotes were fertile and developed without overt signs of abnormality. However *Syngap*$^{-/-}$ pups died, mostly within 48 hours of life (Komiyama et al. 2002; Kim et al. 2003; Vazquez et al. 2004; Porter et al. 2005; Knuesel et al. 2005). Vazquez et al. 2004 observed them to be initially smaller in size at P0 than their littermates and to appear to fail to thrive in comparison with their heterozygous and WT littermates. They were noted to weaken and to display impaired motor skills and trembling before death. In contrast, homozygous cultured neurons appear healthy *in vitro* (Komiyama et al. 2002; Vazquez et al. 2004).

3.3 Hypothesis

It is predicted that deleting a portion of the SynGAP protein in rats will lead to death in homozygotes. It is also predicted that the mutant SynGAP will be present in various brain regions including the hippocampus and will be found to be comprised of multiple SynGAP isoforms when examined by western blotting.

3.4 Results

3.4.1.1 Confirmation of the mutation

Genotyping of heterozygous SynGAP_GAP deletion rats revealed bands of the predicted size, namely ~600 bp for assay 1 (to detect the absence of the deletion) and ~400 bp for assay 2 (to detect a WT band) (Figure 11). mRNA extracted from an adult heterozygous SynGAP_GAP deletion rat was converted to cDNA and amplified with PCR. As Figure 12 shows, the resultant band was faint and sequencing of it was unsuccessful. The PCR product was therefore re-amplified before being cleaned up and sent for Sanger sequencing at Edinburgh Genomics. The sequence confirmed that the SynGAP_GAP deletion mutant rats have a deletion encompassing exons 8 to 12 of the *Syngap* gene resulting in a truncated protein, predicted to be lacking its C2 and GAP domains (Figure 12).

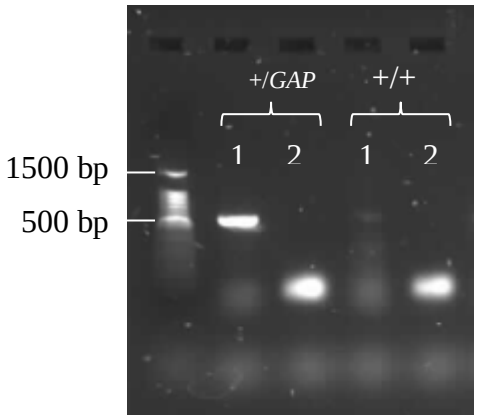

Figure 11- Genotyping of SynGAP_GAP deletion rats.

Syngap$^{+/GAP}$ (left) and WT (WT) (right) rat genotyping with assays 1 and 2 for each.

In the absence of the deletion, the distance between the Assay 1 primers is too long to amplify. Therefore Assay 1 is only positive in heterozygotes and homozygotes. As the primers for Assay 2 are both within the deletion, this assay is positive in WTs and heterozygotes, but negative in homozygotes.

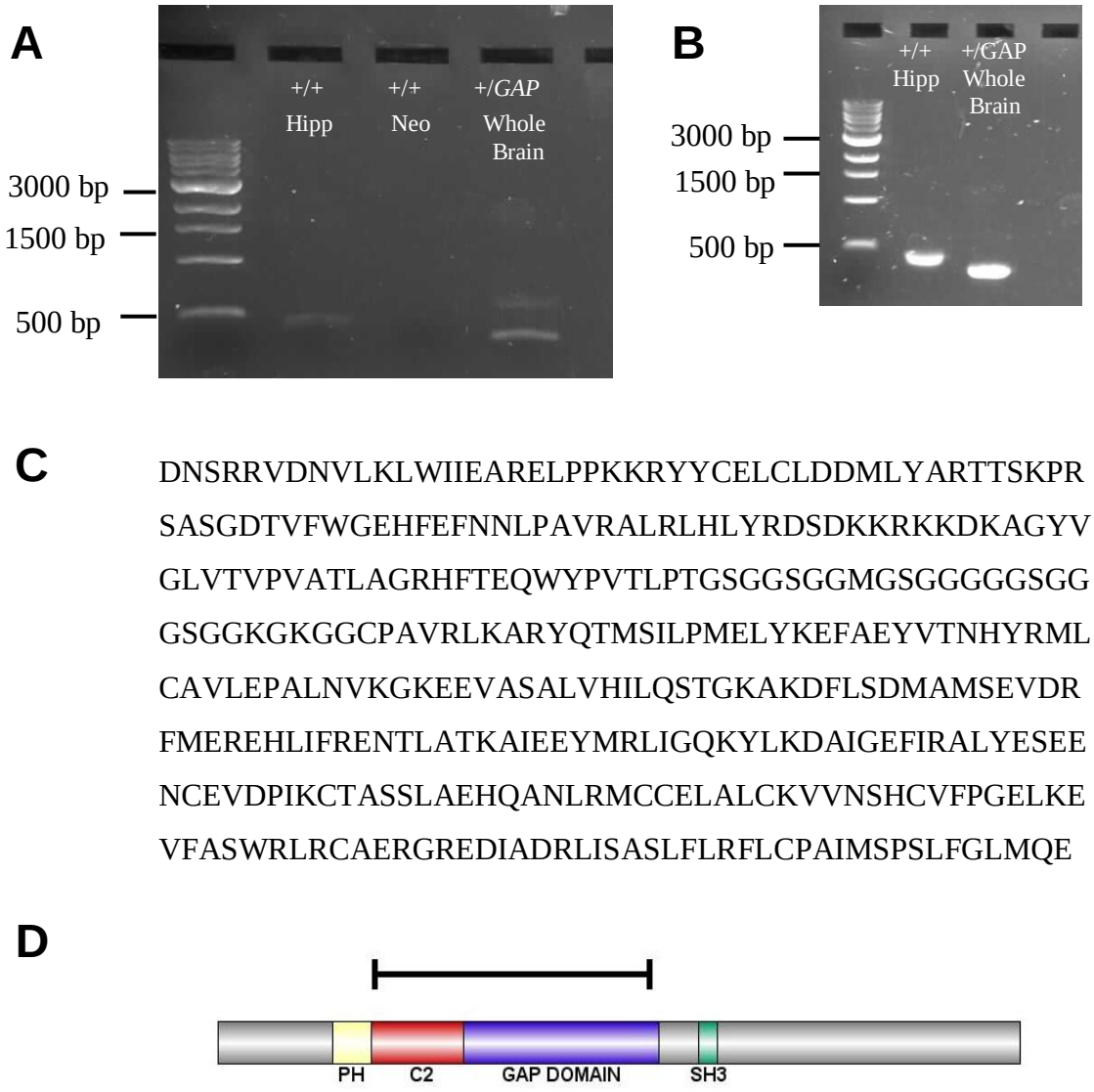

Figure 12 – The amino acid deletion in the *Syngap*$^{+/GAP}$ rats encompasses exons 8 to 12 of the SynGAP protein.

(A) Bands show successful amplification of WT hippocampal and *Syngap*$^{+/GAP}$ whole brain samples.

(B) Bands show successful re-amplification of the WT and *Syngap*$^{+/GAP}$ samples from panel (A) following further PCR amplification.

(C) Amino acid sequence of the *Syngap* deletion in the *Syngap*$^{+/GAP}$. This corresponds to exons 8-12 inclusive which is a deletion of 451 amino acids.

(D) Schematic of the rat SynGAP protein. The black line indicates the deletion in the SynGAP_GAP deletion rat which corresponds to the loss of the C2 and GAP domains in this model.

3.4.2 Colony characterisation

Of the first 120 pups born from WT (WT) – *Syngap*$^{+/GAP}$ pairings, 56 were WT and 64 were *Syngap*$^{+/GAP}$. 8 litters from *Syngap*$^{+/GAP}$ - *Syngap*$^{+/GAP}$ pairings were born, but 4 of these had one or more pups missing (presumed cannibalised) before samples could be taken for genotyping. Of the 4 litters where the genotype for all pups was known, there were 9 WT, 17 *Syngap*$^{+/GAP}$ and 11 *Syngap*$^{GAP/GAP}$. Therefore the breeding appears to follow a Mendelian pattern. WT and *Syngap*$^{+/GAP}$ pups were indistinguishable clinically with specifically no noticeable difference in activity levels in their home cages (although this wasn't formally tested) in contrast to *Syngap*$^{+/-}$ mice which are consistently noted to be hyperactive in comparison to WT mice (Guo et al. 2009; Muhia et al. 2009; Muhia et al. 2010; Muhia et al. 2012; Clement et al. 2012; Ozkan et al. 2014; Berryer et al. 2016).

The first *Syngap*$^{+/GAP}$ - *Syngap*$^{+/GAP}$ litter was closely observed due to the lethality of homozygosity in *Syngap*$^{-/-}$ mice. 1 pup appeared ill (smaller and markedly less mobile than its littermates) at P2 and so it was culled along with an unaffected littermate for comparison. The ill pup proved to be heterozygous and the littermate was WT. All 9 remaining pups still appeared well at P10 when they were taken for western blot samples. However, despite moving normally and apparently eating well (an abdominal milk spot was evident) 4 of the remaining 9 were much smaller than their littermates and on genotyping were found to be homozygotes. This first *Syngap*$^{+/GAP}$ - *Syngap*$^{+/GAP}$ litter proved to be somewhat of an anomaly as homozygous pups from subsequent *Syngap*$^{+/GAP}$ - *Syngap*$^{+/GAP}$ pairings appeared to become ill or die in the first few days of life. This is depicted in the survival plot in Figure 13.

In accordance with the conditions of the UK government project licence granted under Animals (Scientific Procedures) Act 1986 that these animals were bred under, any ill animals had to be culled as soon as possible. Therefore the survival plot includes animals that were culled because they looked as if they were ill or dying. Typically they had reduced head and limb movements, and no longer had a visible milk spot. Furthermore, it wasn't possible to capture the information about pups that were found to be missing (presumed cannabilised) as they had not yet been

genotyped. The apparent death of animals at P10 is artificial as they were taken for experiments as described.

89 pups from 10 litters were longitudinally weighed thrice weekly (Monday, Wednesday and Friday) from P1 to P23 (depending on which day of the week they were born). The weights of heterozygote animals paralleled that of WTs in both genders. When comparing all three genotypes at P10 (the point at which there was the most data for homozygous pups), a significant difference was found on a 1 way ANOVA between WT, *Syngap*$^{+/GAP}$ and *Syngap*$^{GAP/GAP}$ rats (WT = 18.91 ± 0.57g, *Syngap*$^{+/GAP}$ = 16.27 ± 0.53g and *Syngap*$^{GAP/GAP}$ = 8.50 ± 0.29g; Figure 13). Although the numbers of homozygous pups was too small to pass a normality test, ANOVA was used rather than the non-parametric Kruskal-Wallis test as weight is well established as a normally distributed variable.

As the genders of the one litter with P10 homozygous pups was not established, it wasn't possible to determine definitively if this is due to sex differences. However on comparing the P10 WT and *Syngap*$^{+/GAP}$ rats for which gender was recorded, there was a significant difference due to genotype, but not gender on 2 way ANOVA analysis. By P22 this effect had disappeared and there was no significant difference on a 2 way ANOVA test at this age between genotype nor gender (Animals from 3 litters: WT males = 32.75 ± 6.047 g n = 4, WT females = 41.5 ± 2.446 g n = 6, *Syngap*$^{+/GAP}$ males = 31.8 ± 5.285 g n = 5, *Syngap*$^{+/GAP}$ females = 36.2 ± 1.535 g n = 9; 2 way ANOVA with *post hoc* Bonferroni corrections for multiple comparisons, gender effect: $F_{(1,\ 20)}$ = 0.3541, p < 0.0745; genotype effect: $F_{(1,\ 20)}$ = 0.7915, p = 0.3842; gender x genotype interaction: $F_{(1,\ 20)}$ = 0.3822, p = 0.5434).

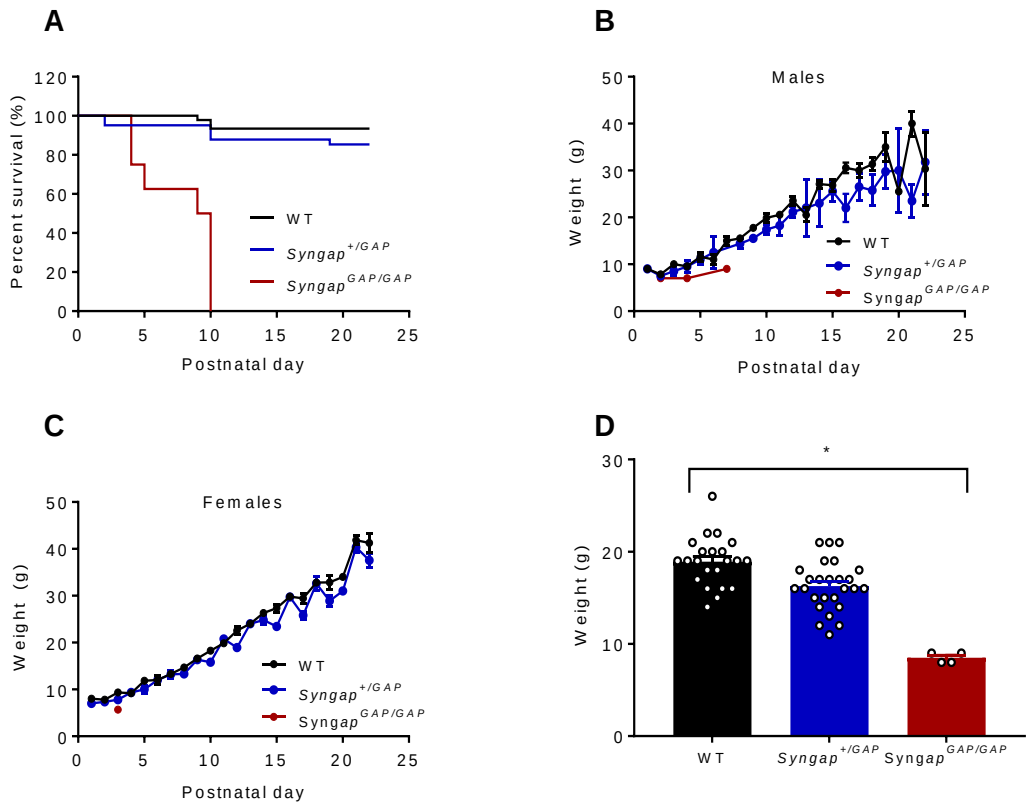

Figure 13 – *Syngap*$^{GAP/GAP}$ rats are smaller than their littermates and die in the first few days of life.

(A) Survival plot showing mutant *Syngap* homozygosity was lethal in the first few days of life. One litter with 4 homozygotes survived until P10 at which point it was taken for experiments.

(B) Male and (C) Female WT and *Syngap*$^{+/GAP}$ rats grow at a similar rate, but *Syngap*$^{GAP/GAP}$ littermates are smaller.

(D) The weights of pups from 6 litters at P10 were significantly different between genotypes (WT = 18.91 ± 0.573 g n = 22, *Syngap*$^{+/GAP}$ = 16.27 ± 0.53 g n = 26, *Syngap*$^{GAP/GAP}$ = 8.5 ± 0.29 g n = 4; 1 way ANOVA with *post hoc* Bonferroni corrections for multiple comparisons, F = 27.93, p < 0.0001).

3.4.3 Western blotting results

Western blotting of protein from a litter with WT, *Syngap*$^{+/GAP}$ and *Syngap*$^{GAP/GAP}$ P10 rats revealed two protein bands in heterozygotes corresponding to one WT allele at ~140 kDa (which is correct for WT SynGAP) and a mutant allele at ~ 90 kDa (Figure 14). The Bioinformatics Protein Molecular Weight Calculator (http://www.bioinformatics.org/sms/prot_mw.html) predicts the molecular weight of the deleted portion of amino acid sequence to be 40.27 kDa which is therefore in keeping with the difference in allele size on western blotting. Crucially, no mutant SynGAP was detected in WT animals and no WT SynGAP in homozygotes.

These blots also revealed the presence of SynGAP in both the neocortex and hippocampus in WT and heterozygous animals (Figure 14). This is in keeping with studies showing that SynGAP is expressed strongly in the mouse cortex and hippocampus as well as at lower levels in the thalamus, amygdaloid complex, cerebellum, striatum, brainstem and olfactory bulb (Kim et al. 1998; Komiyama et al. 2002; Tomoda et al. 2004; Porter et al. 2005; Moon et al. 2008).

Furthermore, although the mutant allele band appeared less intense that that of the WT band in the mutant, it was not statistically hypomorphic as its intensity was not significantly different from the 50% normalised intensity which would be expected for one allele in a WT animal or 100% expected in homozygotes (Figure 14). In hippocampal blots, the mutant band in *Syngap*$^{+/GAP}$ animals was 19.73 ± 2.69% of WT and in *Syngap*$^{GAP/GAP}$ it was 37.02 ± 3.39%. The beta actin loading control was not significantly different between genotypes (WT = 5350.8 ± 48.4 n = 2, *Syngap*$^{+/GAP}$ = 3839.8 ± 405.1 n = 3, *Syngap*$^{GAP/GAP}$ = 4873.4 ± 294.4 n = 4, Kruskal-Wallis test p = 0.1556).

In neocortex samples, the mutant was again not significantly different from the 50% intensity which would be expected for one allele in a WT animal (Figure 14). As before, the beta actin loading control was not significantly different between genotypes (WT = 2399.4 ± 686.8 n = 2, *Syngap*$^{+/GAP}$ = 2810.1 ± 233.5 n = 3, *Syngap*$^{GAP/GAP}$ = 1890.2 ± 91.9 n = 4, Kruskal- Wallis test p = 0.1683).

Hippocampal SynGAP expression changed over the course of the first 28 days of life. WT rat protein increased in abundance from P0 to P28, whereas *Syngap*$^{+/GAP}$ rat mutant protein appeared to increase from P0 to P14 and then decrease somewhat by P28 (Figure 15). However, closer inspection of the data and the original blot (Appendix 1) revealed that one heterozygous rat had markedly higher normalised protein levels at P14 due to having a considerably lower intensity β actin band. There was no obvious experimental error to account for this. If this rat is excluded from the analysis, the levels of WT and mutant SynGAP in heterozygotes rise from P0 to P14 and are then maintained at a comparable level at P28 (with outlier excluded, P14: *Syngap*$^{+/GAP}$ WT band = 27.7 ± 0.9% *n* = 2, *Syngap*$^{+/GAP}$ mutant band = 17.5 ± 1.0% *n* = 2, At P28: WT = 100.0 ± 8.5% *n* = 3, *Syngap*$^{+/GAP}$ WT band = 23.5 ± 1.8% *n* = 3, *Syngap*$^{+/GAP}$ mutant band = 16.7 ± 0.8% *n* = 3). This data and the fact that the WT levels continued to rise at P28, suggests that SynGAP expression levels may peak later in the SynGAP_GAP deletion rats than in mice. Porter et al. 2005 found the expression of SynGAP in the mouse hippocampus peaked around post-natal day seven (P7) using X-gal staining to identify the β-galactosidase reporter gene which was introduced in this mouse model to monitor the cellular expression pattern of the SynGAP gene. Porter's study showed that SynGAP levels were then maintained throughout adulthood. SynGAP mRNA transcripts in mice have been found to peak at P14 in both the hippocampus (Clement et al. 2012) and cortex (McMahon et al. 2012).

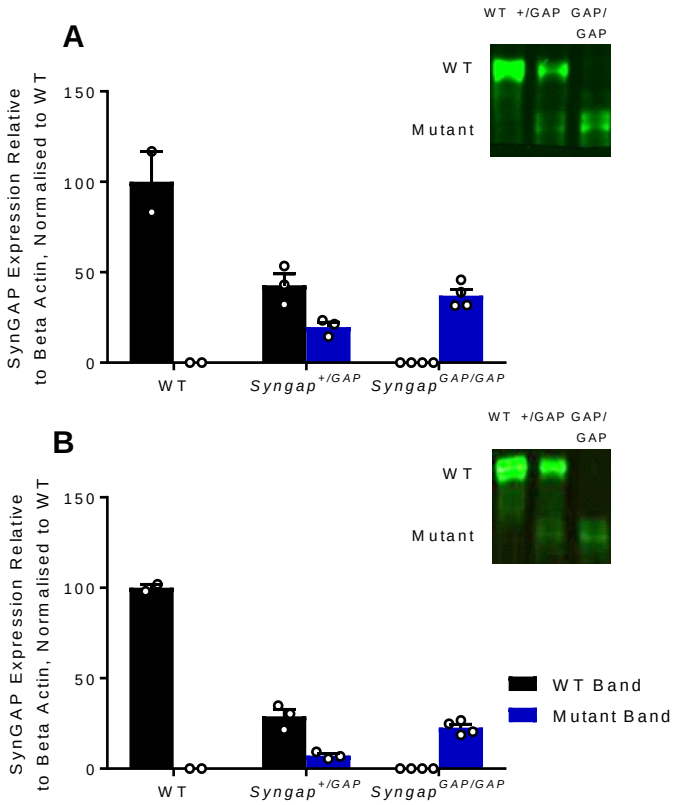

Figure 14 – WT and mutant bands are seen on western blotting of the *Syngap*$^{+/GAP}$ rat hippocampus and neocortex at P10.

(A) Western blot labelled with pan SynGAP antibody which labels all SynGAP isoforms and normalised to the WT mean. WT band ~135-140 kDa and heterozygous band ~95-100 kDa. Hippocampus (WT band in WT = 100 ± 16.81% *n* = 2, WT band in *Syngap*$^{+/GAP}$ = 42.87 ± 6.14% *n* = 3, Mutant band in *Syngap*$^{+/GAP}$ = 19.73 ± 2.69% *n* = 3, Mutant band in *Syngap*$^{GAP/GAP}$ = 37.02 ± 3.39% *n* = 4; Wilcoxon signed rank test: WT band in *Syngap*$^{+/GAP}$ theoretical median = 50, actual median = 43.06, *p* = 0.5, Mutant band in *Syngap*$^{+/GAP}$ theoretical median = 50, actual median = 21.27, *p* = 0.25, Mutant band in *Syngap*$^{GAP/GAP}$ theoretical median = 100, actual median = 35.35, *p* = 0.1250).

(B) Neocortex (WT band in WT = 100 ± 1.88% *n* = 2, WT band in *Syngap*$^{+/GAP}$ = 28.93± 3.90% *n* = 3, Mutant band in *Syngap*$^{+/GAP}$ = 7.18 ± 1.11% *n* = 3, Mutant band in *Syngap*$^{GAP/GAP}$ = 22.65 ± 1.87% *n* = 4; Wilcoxon Signed Rank Test: WT band in *Syngap*$^{+/GAP}$ theoretical median = 50, actual median = 30.33, *p* = 0.25, Mutant band in *Syngap*$^{+/GAP}$ theoretical median = 50, actual median = 6,79, *p* = 0.25, Mutant band in *Syngap*$^{GAP/GAP}$ theoretical median = 100, actual median = 22.62, *p* = 0.1250).

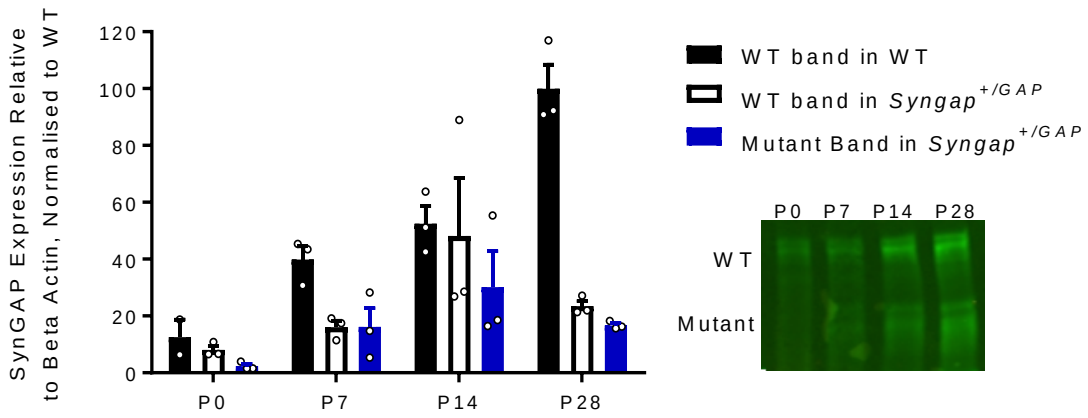

Figure 15 – Hippocampal SynGAP protein levels in *Syngap*$^{+/GAP}$ rats rise from P0 to P14 and then decrease by P28.

Representative image shown is from heterozygous animals. Western blot was labelled with pan SynGAP antibody which labels all SynGAP isoforms and values were normalised to WT at P28. WT bands ~135-140 kDa and heterozygous band ~95-100 kDa.

P0: WT = 12.6 ± 6.2% *n* = 2, *Syngap*$^{+/GAP}$ WT band = 8.0 ± 1.4% *n* = 3, *Syngap*$^{+/GAP}$ mutant band = 2.3 ± 0.8% *n* = 3. P7: WT = 39.8 ± 4.6% *n* = 3, *Syngap*$^{+/GAP}$ WT band = 16.0 ± 2.3% *n* = 3, *Syngap*$^{+/GAP}$ mutant band = 16.1 ± 6.6% *n* = 3. P14: WT = 52.5 ± 6.1% *n* = 3, *Syngap*$^{+/GAP}$ WT band = 48.1 ± 20.4% *n* = 3, *Syngap*$^{+/GAP}$ mutant band = 30.1 ± 12.6% *n* = 3. P28: WT = 100.0 ± 8.5% *n* = 3, *Syngap*$^{+/GAP}$ WT band = 23.5 ± 1.8% *n* = 3, *Syngap*$^{+/GAP}$ mutant band = 16.7 ± 0.8% *n* = 3.

SynGAP expression at P20 was explored in the hippocampus and visual cortex using 4 SynGAP antibodies which label different SynGAP isoforms - SynGAP A, SynGAP α1, SynGAP α2 and the antibody referred to as 'pan SynGAP' as it labels all known isoforms.

All 4 antibodies labelled SynGAP in both the hippocampus (Figure 16) and visual cortex (Figure 17) confirming the presence of multiple SynGAP isoforms in the SynGAP_GAP deletion rat at P20. The pattern of expression was similar throughout and at this age, the expression of the mutant allele was again not found to be statistically hypomorphic. Several of the alleles in these blots show multiple bands which are indicative of different SynGAP isoforms. No antibodies exist for SynGAP N terminal isoforms so exploring this further by western blotting is not possible at this time.

Once again, there was no significant difference in β actin intensity across genotypes for any of the four antibodies (Table 8).

Table 8 – Beta actin intensities for P20 hippocampus and visual cortex western blots

Isoform Labelled	**WT (mean ± SEM)**	***Syngap*$^{+/GAP}$ (mean ± SEM)**	**Mann-Whitney test (P value)**
Hippocampus			
SynGAP A	6972.0 ± 374.2 *n* = 3	6420.7 ± 762.0 *n* = 5	0.5714
All isoforms ('Pan SynGAP')	6460.4 ± 287.8 *n* = 3	5252.8 ± 929.4 *n* = 5	0.5714
SynGAP alpha1	7775.6 ± 321.7 *n* = 3	7325.6 ± 621.6 *n* = 5	0.3929
SynGAP alpha2	5898.2 ± 193.3 *n* = 3	6304.0 ± 619.1 *n* = 5	>0.9999
Visual Cortex			
SynGAP A	2713.7 ± 503.0 *n* = 3	1425.4 ± 492.1 *n* = 5	0.2500
All isoforms ('Pan SynGAP')	3660.2 ± 737.7 *n* = 3	2117.1 ± 539.8 *n* = 5	0.2500
SynGAP alpha1	2315.3 ± 16.1 *n* = 3	2240.1 ± 293.9 *n* = 5	0.7857
SynGAP alpha2	2687.0 ± 202.9 *n* = 3	2695.0 ± 483.7 *n* = 5	0.7857

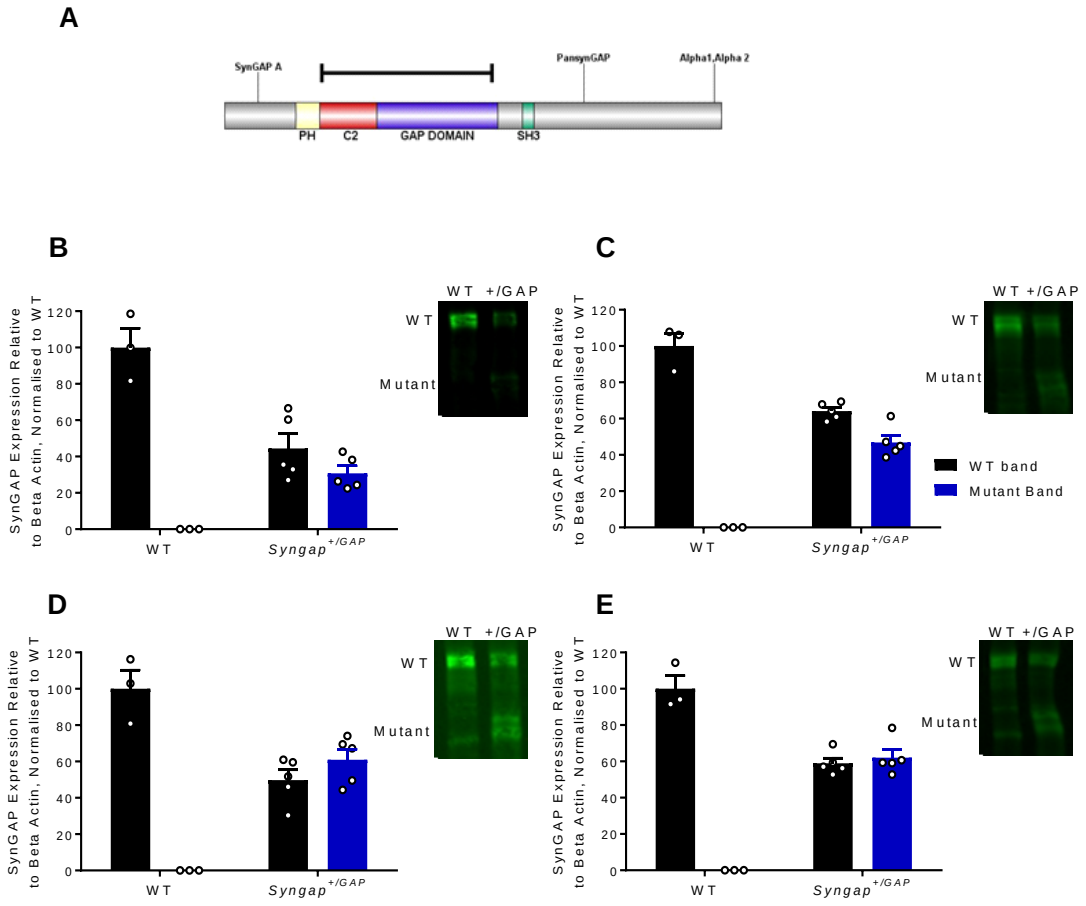

Figure 16 – The *Syngap*$^{+/GAP}$ WT and mutant alleles include SynGAP A, α1 and α2 isoforms in the hippocampus at P20.

All data is normalised to the mean WT value of that western blot. WT bands ~135-140 kDa and heterozygous band ~95-100 kDa.

(A) Schematic of the SynGAP protein with black line depicting the deletion in SynGAP_GAP deletion rat and labels showing the location of different antibody epitopes on the protein.

(B) SynGAP A isoform N terminal antibody (WT band in WT = 100 ± 10.67% n = 3, WT band in *Syngap*$^{+/GAP}$ = 44.49 ± 7.91% n = 5, Mutant band in *Syngap*$^{+/GAP}$ = 30.8 ± 4.04% n = 5, Wilcoxon signed rank test: WT band in *Syngap*$^{+/GAP}$ theoretical median = 50, actual median = 35.52, p = 0.4375, Mutant band in *Syngap*$^{+/GAP}$ theoretical median = 50, actual median = 26.37, p = 0.0625).

Legend continued overleaf…

Figure 16 legend continued…

(C) Pan SynGAP antibody which labels all isoforms (WT band in WT = 100 ± 6.99% n = 3, WT band in *Syngap*$^{+/GAP}$ = 64.13 ± 2.06% n = 5, Mutant band in *Syngap*$^{+/GAP}$ = 46.87 ± 3.89% n = 5, Wilcoxon signed rank test: WT band in *Syngap*$^{+/GAP}$ theoretical median = 50, actual median = 61.14, p = 0.0625, Mutant band in *Syngap*$^{+/GAP}$ theoretical median = 50, actual median =44.89, p = 0.6250).

(D) SynGAP alpha1 isoform C terminal antibody (WT band in WT = 100 ± 10.30% n = 3, WT band in *Syngap*$^{+/GAP}$ = 49.77 ± 5.55% n = 5, Mutant band in *Syngap*$^{+/GAP}$ = 60.93 ± 5.87% n = 5, Wilcoxon signed rank test: WT band in *Syngap*$^{+/GAP}$ theoretical median = 50, actual median = 51.77, p > 0.9999, Mutant band in *Syngap*$^{+/GAP}$ theoretical median = 50, actual median = 67.28, p = 0.3125).

(E) SynGAP alpha2 isoform C terminal antibody (WT band in WT = 100 ± 7.21% n = 3, WT band in *Syngap*$^{+/GAP}$ = 58.97 ± 2.83% n = 5, Mutant band in *Syngap*$^{+/GAP}$ = 62.03 ± 4.32% n = 5, Wilcoxon signed rank test: WT band in *Syngap*$^{+/GAP}$ theoretical median = 50, actual median = 57.02, p > 0.0625, Mutant band in *Syngap*$^{+/GAP}$ theoretical median = 50, actual median = 59.29, p = 0.0625).

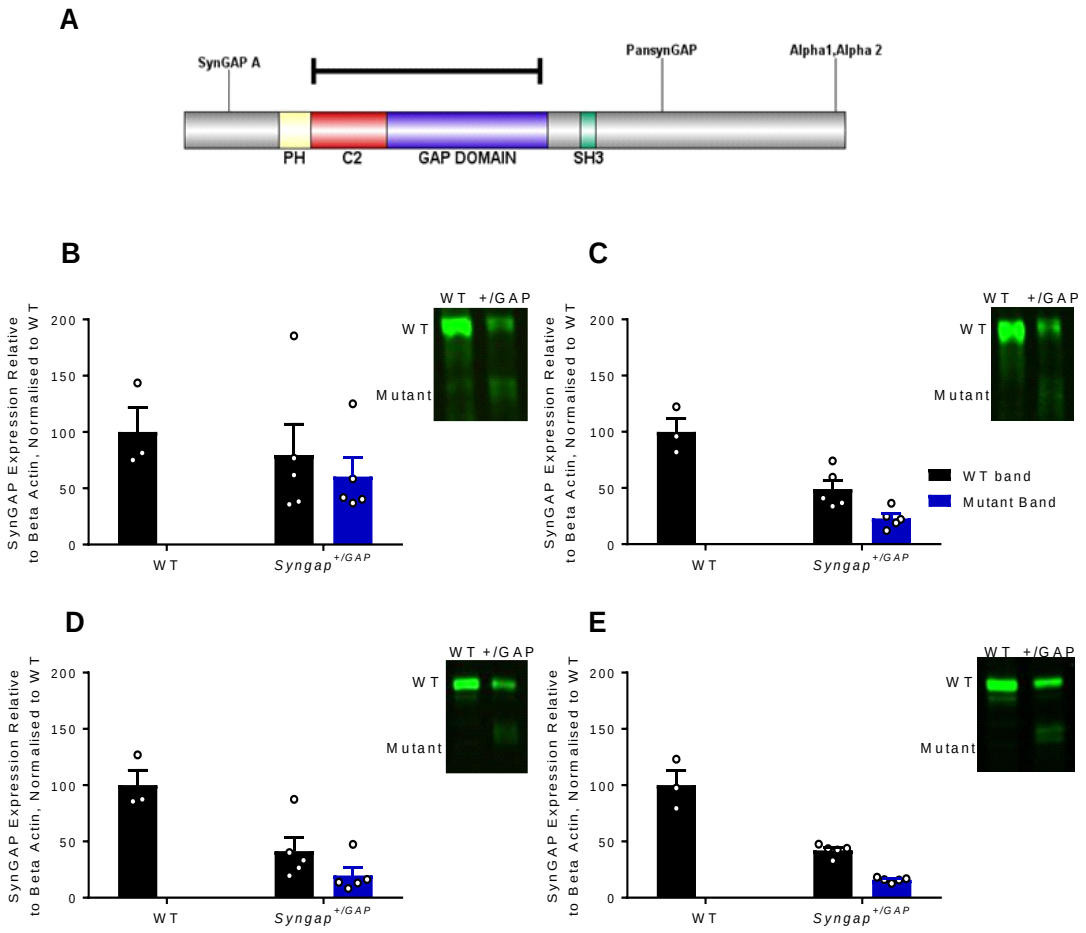

Figure 17 - The *Syngap*$^{+/GAP}$ WT and mutant alleles include SynGAP A, α1 and α2 isoforms in the visual cortex at P20.

All data is normalised to the mean WT value of that western blot. WT bands ~135-140 kDa and heterozygous band ~95-100 kDa.

(A) Schematic of the SynGAP protein with black line depicting the deletion in SynGAP_GAP deletion rat and labels showing the location of different antibody epitopes on the protein.

(B) SynGAP A isoform N terminal antibody (WT band in WT = 100 ± 21.83% n = 3, WT band in *Syngap*$^{+/GAP}$ = 79.59 ± 27.53% n = 5, Mutant band in *Syngap*$^{+/GAP}$ = 60.44 ± 16.59% n = 5, Wilcoxon signed rank test: WT band in *Syngap*$^{+/GAP}$ theoretical median = 50, actual median = 61.82, p = 0.4375, Mutant band in *Syngap*$^{+/GAP}$ theoretical median = 50, actual median = 41.68, $p > 0.999$).

Legend continued overleaf…

Figure 17 legend continued…

(C) Note example image has been flipped horizontally to show WT on the left and *Syngap*$^{+/GAP}$ on the right. Pan SynGAP antibody which labels all isoforms (WT band in WT = 100 ± 11.82% n = 3, WT band in *Syngap*$^{+/GAP}$ = 49.05 ± 7.71% n = 5, Mutant band in *Syngap*$^{+/GAP}$ = 22.85 ± 3.99% n = 5, Wilcoxon signed rank test: WT band in *Syngap*$^{+/GAP}$ theoretical median = 50, actual median = 40.97, $p > 0.9999$, Mutant band in *Syngap*$^{+/GAP}$ theoretical median = 50, actual median = 22.15, $p = 0.0625$).

(D) SynGAP alpha1 isoform C terminal antibody (WT band in WT = 100 ± 13.46% n = 3, WT band in *Syngap*$^{+/GAP}$ = 41.39 ± 12.02% n = 5, Mutant band in *Syngap*$^{+/GAP}$ = 19.73 ± 7.04% n = 5, Wilcoxon signed rank test: WT band in *Syngap*$^{+/GAP}$ theoretical median = 50, actual median = 33.21, $p = 0.6250$, Mutant band in *Syngap*$^{+/GAP}$ theoretical median = 50, actual median = 13.81, $p = 0.0625$).

(E) SynGAP alpha2 isoform C terminal antibody (WT band in WT = 100 ± 12.69% n = 3, WT band in *Syngap*$^{+/GAP}$ = 42.08 ± 2.47% n = 5, Mutant band in *Syngap*$^{+/GAP}$ = 15.98 ± 0.90% n = 5, Wilcoxon signed rank test: WT band in *Syngap*$^{+/GAP}$ theoretical median = 50, actual median = 43.52, $p > 0.0625$, Mutant band in *Syngap*$^{+/GAP}$ theoretical median = 50, actual median = 16.15, $p = 0.0625$).

3.5 Discussion

This chapter details basic characteristics of the SynGAP_GAP deletion rat. The sequence of the deleted amino acids in the SynGAP protein was confirmed by extracting mRNA from homogenised brain tissue, converting it to cDNA and sequencing it using Sanger Sequencing. This is a reliable method and the results were in keeping with the western blot experiments as the predicted molecular weight of the missing portion of protein corresponded with the difference in protein weight (kDa) between WT and mutant bands on western blotting. The exons deleted correspond with the C2 and GAP domains of the protein, but it should be acknowledged that no formal testing was carried out to confirm the loss of these regions. A GTPase assay in particular would be valuable to confirm that the enzymatic activity of the mutant SynGAP is lost in these rats.

The general characterisation of the SynGAP_GAP deletion rat colony is in keeping with previous reports indicating that the development of *Syngap*$^{+/-}$ mice is grossly similar to that of WT mice whereas homozygous mice do not develop well and die prematurely (Komiyama et al. 2002; Kim et al. 2003; Vazquez et al. 2004; Porter et al. 2005; Knuesel et al. 2005). However, the details of the data in this current chapter raise a number of points of discussion as follows.

3.5.1 Validity of the SynGAP_GAP deletion rat

Engineering the SynGAP rats to have a deletion encompassing the C2 and GAP domains has construct validity in terms of investigating the role of different parts of the protein in the regulation of downstream signalling cascades. However, does it have face validity for using the model to make inferences about human *SYNGAP1* ID? The vast majority of people with mutations in *SYNGAP1* have missense mutations rather than deletions in the protein (Mignot et al. 2016) and these are often found to result in truncation of the SynGAP protein (Hamdan et al. 2009; Hamdan et al. 2011; Berryer et al. 2013). Only one person with a deletion limited to SynGAP (rather than encompassing other genes too) has been identified and has a deletion of Exons 1 to 9 (Mignot et al. 2016). Therefore, the SynGAP_GAP deletion rat is likely to be more useful for assessing the function of the protein rather than as a direct comparison to human *SYNGAP1* ID.

3.5.2 Why did the first litter of *Syngap*$^{GAP/GAP}$ pups live apparently healthily until P10 when later homozygous pups died earlier?

As the first homozygous pups lived healthily for longer than those in subsequent litters they may have been anomalous. In keeping with homozygotes from later litters they were noticeably smaller than their WT and heterozygous littermates (Figure 13) suggesting a detrimental effect of the mutation, but otherwise appeared well until they were taken for experiments at P10 unlike subsequent homozygous pups which sickened before this time. It is possible that the SynGAP_GAP Deletion mutation was not present in every cell (i.e. they were mosaic for the mutation) of the first litter containing homozygotes, but this was not formally confirmed.

3.5.3 Why was it not possible to be more specific about the age at which *Syngap*$^{GAP/GAP}$ rats naturally die?

As this was a newly genetically modified rat line, all litters that could include homozygous rat pups were monitored on a daily basis for any signs of pain, suffering or distress in light of the lethality of SynGAP homozygosity in mice. In accordance with Animals (Scientific Procedures) Act 1986 licence conditions, pups were culled as soon as possible if these signs (typically identified by reduced limb or head movements and lack of milk spot) were noted. As described above, the first *Syngap*$^{+/GAP}$ - *Syngap*$^{+/GAP}$ litter (later found on genotyping to include 4 homozygotes) appeared healthy with no signs of distress. They were therefore allowed to live until they were taken for western blot experiments at P10. However, homozygous pups from subsequent litters became ill and died earlier than this (Figure 13).

3.5.4 Limitations of the colony characteristics data

Although it seems clear from the graphs in Figure 13 that there was little difference between WT and heterozygous pup weights, but homozygotes were smaller, it is acknowledged that using the ANOVA statistical test to compare the weights of pups from different genotypes is crude. It does not take into account other variables that may influence pup weight such as the identity of the mother, how well she nursed her

pups, what the litter size was, whether any pups were lost early in life giving others access to proportionately more milk etc. More in depth analysis of the pup characteristics could be carried out in the future using a Generalised Linear Mixed Model which could take these other factors into account. However it is reassuring that similar to the pattern shown in the rats, Knuesel and colleagues found that *Syngap*$^{+/-}$ conditional knock out mice in which the level of SynGAP was 40-50% of standard heterozygotes, were smaller than their littermates and also died prematurely (Knuesel et al. 2005).

3.5.5 Limitations of the western blot data

Western blotting of SynGAP_GAP deletion rat brain tissue repeatedly revealed two separate bands in the heterozygous rats which corresponded with the weight of the WT SynGAP protein (~135-140 kDa) and the predicted weight of the mutant SynGAP allele (~95–98 kDa). Careful attempts were made to control the experimental conditions to allow semi-quantitative assessment of the amount of protein present in difference genotypes. Firstly the mass of total protein in each sample was measured using a bicinchoninic acid assay (BCA) Protein Assay. This is a colorimetric assay which enables measurement of protein concentration in samples using a spectrophotometer. This meant that the volume of sample required to load 10 µg of protein into each lane could be calculated. Secondly, a loading control protein was measured (β-actin). The utility of a loading control is two fold

1) It confirms the presence of protein in that lane
2) It allows the abundance of the protein of interest to be normalised to the loading control which is believed to be relatively constantly expressed. This enables comparisons of protein quantity to be made between different samples which may have been subject to differential loading errors or differential blot transfer (Aldridge et al. 2008)

β-actin was the loading control chosen for the SynGAP_GAP deletion rat western blots and is one of the most commonly used (Li & Shen 2013). The intensity of β-actin signal was compared between WT and heterozygous rat samples to ensure that it did not vary between experimental conditions as some doubt has been cast on the premise that β-actin and other 'housekeeping' genes are constantly expressed in

different conditions (Dittmer & Dittmer 2006; Li & Shen 2013). No significant difference was found between the intensity of β-actin in WT, heterozygous or homozygous rats which was reassuring. However as β-actin is a high-abundance protein whereas the protein of interest (in this case SynGAP) is often less abundant, it may not be possible to detect variations in β-actin between samples in the small protein concentrations used in western blotting. Therefore, it is not possible to be completely certain that the β-actin remained unchanged between genotypes. Furthermore, there appeared to be an anomalous data point in a heterozygous rat at P14 due to a considerably lower intensity β actin band as discussed in paragraph 3.4.3 .

Hence consideration should be given to repeating the western blots with larger numbers of samples (so that individual anomalies have less impact on the mean data) and using other methods of assessing the consistency of protein levels in each lane e.g. normalising to total protein concentration (Aldridge et al. 2008).

The western blot data also reveals that at least 1 SynGAP N terminal isoform (A) and 2 C terminal isoforms (α1 and α2) expressed in the hippocampus and visual cortex at P20 (Figure 16 and Figure 17). Unfortunately further examination of N terminal isoforms is not possible using western blots as no antibodies exist to probe for them.

3.6 Chapter summary

Zinc finger techniques were used to modify the SynGAP gene in Long-Evans Hooded rats resulting in a deletion of 5 exons, including the portion of the gene that codes for the C2 and enzymatic GAP domains of the protein. This results in homozygous rats that are smaller than their littermates and die in the first few days of life. Western blotting revealed that the mutant SynGAP protein is present in the hippocampus, neocortex and visual cortex and is comprised of at least one N terminal and two C terminal isoforms (A, α1 and α2). This model is likely to be most useful for assessing the function of the SynGAP protein.

4 CHAPTER FOUR: SYNGAP_GAP DELETION RAT ELECTROPHYSIOLOGICAL EXPERIMENTS

4.1 Key findings

- There is no significant difference in long-term depression between WT and *Syngap*$^{+/GAP}$ rats including when new protein synthesis is inhibited
- There is no significant difference in paired-pulse ratio in hippocampal fEPSP recordings between WT and *Syngap*$^{+/GAP}$ rats
- There is no significant difference in intrinsic properties at P13-15 or P26-30
- There is a reduction in the frequency of mEPSCs in *Syngap*$^{+/GAP}$ hippocampal cultured neurons
- At P13-15 sEPSCs and mEPSCs from *Syngap*$^{+/GAP}$ rats tended to be larger amplitude and higher frequency events
- At P26-30 sEPSCs and mEPSCs from *Syngap*$^{+/GAP}$ rats tended to be of larger amplitude, but were less frequent than in WTs
- At P26-30 there were no significant differences between AMPAR / $GABA_AR$ and AMPAR / NMDAR ratios in *Syngap*$^{+/GAP}$ rats compared to WT rats

4.2 Introduction

Electrophysiology has revealed differences in hippocampal long-term depression (LTD) and excitatory-inhibitory balance in previous models of SynGAP haploinsufficiency and the experiments in this chapter explore these in the SynGAP_GAP deletion rats.

4.2.1 Long-term depression, SynGAP and intellectual disability

The link between LTD and neuropsychiatric disorders came with the observation that hippocampal mGluR LTD was exaggerated and independent of new protein synthesis in a mouse model of Fragile X Syndrome (FXS), a single gene cause of ID and ASD in humans (Huber et al. 2002). This led to the mGluR Theory of FXS (Bear et al. 2004) which described Fragile X Mental Retardation Protein (FMRP), the protein missing in FXS, as normally functioning as ‘a brake’ on the synthesis of new synaptic proteins which stabilise LTD following stimulation of Group 1 mGluRs; therefore in its absence LTD was exaggerated.

Aberrations in mGluR mediated hippocampal plasticity have now been identified in other rodent models of neurodevelopmental disorders that lead to ID, ASD and epilepsy phenotypes in humans including Tuberous Sclerosis and Rett Syndrome (reviewed by Senter et al. 2016). Most topically for this thesis, exaggerated mGluR dependent LTD has been identified in the CA1 of the hippocampus in *Syngap*$^{+/-}$ mice between the ages of P26-P32 (Barnes et al. 2015). This is felt to phenocopy the exaggerated LTD in FXS as *Syngap*$^{+/-}$, like FMRP acts on the ERK/MAPK biochemical pathways. This mGluR dependent form of LTD was not seen in adult *Syngap*$^{+/-}$ mice (Komiyama et al. 2002; Kim et al. 2003), but impairments in NMDA induced LTD were identified in 6 to 12 week old *Syngap*$^{+/-}$ mice (Carlisle et al. 2008).

It is well established that new protein synthesis is required for the successful maintenance of mGluR hippocampal LTD in WT animals (Huber et al. 2000). However this new protein synthesis was not required for LTD maintenance in a mouse model of Fragile X Syndrome (Nosyreva et al. 2006), nor in *Syngap*$^{+/-}$ mice (Barnes et al. 2015). It is therefore postulated that dysregulation of metabotropic glutamate/ ERK dependent protein synthesis may be a common feature of a subset of neurodevelopmental disorders (Barnes et al. 2015).

4.2.2 Excitatory Inhibitory Balance in SynGAP

It has been proposed that ASD in humans could result from an increased ratio of excitation/inhibition (E/I) in various systems in the brain (reviewed by Rubenstein & Merzenich 2003). This would also help to explain the overlap between ASD and epilepsy which is thought to arise due to a relative excess of excitation over inhibition. As SynGAP haploinsufficiency in humans is associated with ASD and epilepsy and SynGAP is known to regulate excitatory pathways (e.g. ERK/MAPK), this theory is of relevance and interest when investigating pre-clinical models of SynGAP mutations. There is mounting evidence of exaggerated excitation in SynGAP haploinsufficiency from the whole organism level down to specific cellular functions. *Syngap*$^{+/-}$ mice, both those that are globally haploinsufficient and a model in which SynGAP is knocked down only in forebrain excitatory glutamatergic neurons have been shown to have reduced seizure threshold (Clement et al. 2012;

Ozkan et al. 2014). At a network level, photostimulated signals from the dentate gyrus have been shown to be progressively attenuated in WT animals, but not in *Syngap*$^{+/-}$ mice (Clement et al. 2012) and signals from *Syngap*$^{+/-}$ mice were significantly larger than those from WT mice on fast voltage-sensitive dye imaging of the cortex in acute brain slices (Ozkan et al. 2014).

In *Syngap*$^{-/-}$ mouse cultures increased hippocampal and forebrain mEPSC frequency (Vazquez et al. 2004; Rumbaugh et al. 2006) and hippocampal mEPSC amplitude (Vazquez et al. 2004) have been shown. In *Syngap*$^{+/-}$ mice, an increased AMPA / NMDA ratio has been found in thalamocortical slices at P5 and in mPFC slices at P8 (Clement et al. 2013) and increases in mEPSC amplitude and frequency in *Syngap*$^{+/-}$ mice > 9 weeks of age (but not at P14) in layer 2/3 pyramidal neurons of the mPFC have been observed (Ozkan et al. 2014). When SynGAP haploinsufficiency was induced in adult mice using a Cre-LoxP system the amplitude of spontaneous EPSCs was shown to be smaller, but their frequency increased (Muhia et al. 2012).

Ozkan et al. also found that mPFC layer 2/3 neurons were hyperexcitable in response to evoked neurotransmitter release in *Syngap*$^{+/-}$ mice and that the excitatory / inhibitory balance was shifted towards excitation when isolated excitatory and inhibitory currents were measured. Moreover they examined the inhibitory function and found a decrease in mIPSC amplitude in adult *Syngap*$^{+/-}$ mice and significantly decreased firing rate of parvalbumin positive (PV+) cells at 6 weeks (but not P14 or 9 weeks) of age.

Clement et al. 2012 examined hippocampal function in *Syngap*$^{+/-}$ mice and found that at ~P14 there were increases synaptic transmission (as measured by medial perforant path field EPSPs), the ratio of AMPA / NMDA currents in dentate gyrus granule neurons (and the AMPA / NMDA current ratio in a Cre LoxP model of induced haploinsufficiency) and in mEPSC amplitude and frequency at P14 all of which normalised by P21. They also identified a significant increase in mIPSC frequency and amplitude at P14 and felt this might be a compensatory response to the increase

in excitation. Furthermore the intrinsic excitability of dentate gyrus neurons was increased in heterozygotes at P8-9 but had resolved by P14.

With regards to inhibitory function, mice with SynGAP haploinsufficiency selectively in inhibitory cells originating from the medial ganglionic eminence [PV+ and Somatostatin+ (SST+) cells], have significantly longer mIPSC mean inter-event intervals in layer 2-3 pyramidal cells in the somatosensory cortex and hippocampal CA1 pyramidal cells (Berryer et al. 2016). Targeted expression of the light sensitive Channel rhodopsin-2 via Cre also revealed reduced amplitude of evoked IPSCs in Layer 5 pyramidal cells. Both findings are suggestive of a shift towards excitation. However in contrast to these mice, there was no significant difference in mIPSC inter-event interval in germ-line deletion of SynGAP (i.e. in *Syngap*$^{+/-}$ mice), which the authors felt could be due to compensatory developmental changes.

Manipulation of SynGAP expression in cultured neurons also lends support to the hypothesis that there is a shift towards excitation in conditions of reduced SynGAP expression. A significant increase in mEPSC amplitude was recorded following knockdown of alpha SynGAP in DIV 11-16 cultured cortical neurons which could be rescued by co-expression of WT SynGAP (Wang et al. 2013). Overexpression of GFP-tagged SynGAP (Cα1isoform) resulted in a marked decrease in both amplitude and frequency of AMPAR mediated mEPSCs (Rumbaugh et al. 2006). However deletion of the C terminal portion of SynGAP including the PDZ binding domain and also separate mutation of the GAP domain resulted in no difference in amplitude and frequency from untransfected neurons. This therefore implies the need for a functioning GAP domain and the ability to interact via its PDZ binding domain for SynGAP to influence mEPSC frequency and therefore excitatory function.
The data presented here from the SynGAP_GAP deletion rats mainly focusses on hippocampal function and explores both cellular and synaptic properties.

4.2.3 Hypothesis

Taken together, the research presented above leads to the hypothesis that in *Syngap*$^{GAP/GAP}$ rats there will be an increase in mEPSC amplitude and frequency. In *Syngap*$^{+/GAP}$ rats, there will be exaggerated protein synthesis independent mGluR mediated hippocampal LTD and changes in cellular and synaptic function indicative of increased excitability.

4.3 Results

4.3.1 Long-term depression recordings in acute hippocampal slices

mGluR LTD in the CA1 of the hippocampus of SynGAP_GAP deletion rats was induced between P26-30 by bath application of the mGluR agonist DHPG (100 μM) to horizontal hippocampal slices for 5 minutes. For some animals results were available for more than one slice, but no significant difference was found between WT and *Syngap*$^{+/GAP}$ slices regardless of whether the unit of analysis was 'animal' (WT = 78.7 ± 3.1% *n* = 12, *Syngap*$^{+/GAP}$ = 73.5 ± 3.3% - Figure 18) or 'slice' (WT = 78.9 ± 3.3% *n* = 14, *Syngap*$^{+/GAP}$ = 75 ± 3.4% **-** Figure 19). The requirement for new protein synthesis for LTD maintenance was then examined by applying 100 μM cycloheximide (CHX) prior to the induction of LTD. As was shown in *Syngap*$^{+/-}$ mice (Barnes et al. 2015) there was no significant difference in LTD between *Syngap*$^{+/GAP}$ rats exposed to CHX and those that weren't (*Syngap*$^{+/GAP}$ = 72.8 ± 4.0%, *Syngap*$^{+/GAP}$ CHX 72.7 ± 9.1% - Figure 20) this implies LTD in these rats is independent of new protein synthesis. However, unexpectedly there was also no significant difference between WT rat slices with and without cycloheximide (WT 82.4 ± 2.3%, WT CHX 89.9 ± 4.8% - Figure 20) and therefore between the WT rats and *Syngap*$^{+/GAP}$ rat slices exposed to CHX (WT CHX 89.9 ± 4.8%, *Syngap*$^{+/GAP}$ CHX 72.7 ± 9.1% - Figure 20). This appears to be because WT rat LTD was also independent of new protein synthesis. This significant confounder unfortunately prevents interpretation of the effect of the SynGAP mutation.

Paired pulse facilitation was calculated from the pairs of fEPSPs stimulated throughout the LTD experiments. No differences were seen between WT and *Syngap*$^{+/GAP}$ rats (at baseline: WT = 1.5 ± 0.05, *Syngap*$^{+/GAP}$ = 1.6 ± 0.04; after LTD: WT = 1.6 ± 0.05, *Syngap*$^{+/GAP}$ = 1.7 ± 0.05, 2 way ANOVA with *post hoc* Bonferroni

corrections, LTD x genotype interaction: $F_{(1,\ 28)} = 1.234$, $p = 0.2760$). This is consistent with published findings in *Syngap*$^{+/-}$ mouse hippocampal recordings at P14 (Clement et al. 2012) and in adulthood (Komiyama et al. 2002; Kim et al. 2003; Ozkan et al. 2014). As alterations in PPF are indicative of pre-synaptic changes (Zucker 1973), this suggests there is no measurable difference in pre-synaptic function between WT and *Syngap*$^{+/GAP}$ rats.

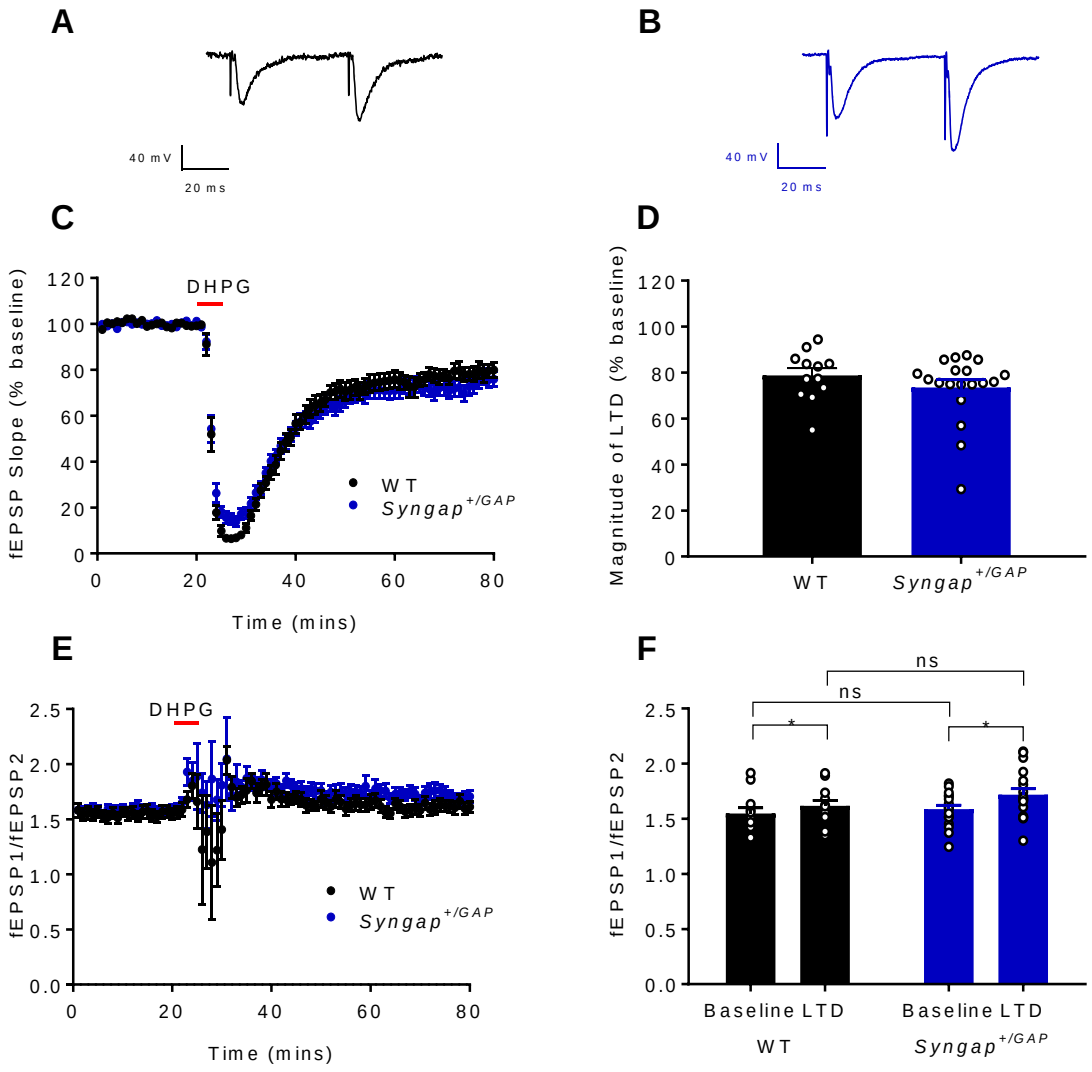

Figure 18 – There is no significant difference in hippocampal mGluR LTD or PPR between P26-33 WT and *Syngap*$^{+/GAP}$ rats when the data is collated by animal.

(A) WT and (B) *Syngap*$^{+/GAP}$ example traces.

(C) and (D) There is no significant difference in LTD induced with 100 µM DHPG between WT and *Syngap*$^{+/GAP}$ rats**.** LTD was measured as the mean value between 70 and 80 minutes. (WT = 78.7 ±3.1% n = 12, *Syngap*$^{+/GAP}$ = 73.5 ± 3.3% n = 19, Mann-Whitney test p = 0.3889).

(E) and (F) Paired pulse ratio is facilitated after LTD, but there is no significant difference between WT and *Syngap*$^{+/GAP}$ rats. (At baseline WT = 1.5 ± 0.05 n = 12, *Syngap*$^{+/GAP}$ = 1.6 ± 0.04 n = 18, after LTD WT = 1.6 ± 0.05 n = 12, *Syngap*$^{+/GAP}$ = 1.7 ± 0.05 n = 18, 2 way ANOVA with *post hoc* Bonferroni corrections for multiple comparisons, LTD effect: $F_{(1, 28)}$ = 12.46, p < 0.0015; genotype effect: $F_{(1, 28)}$ = 1.289, p = 0.2659; LTD x genotype interaction: $F_{(1, 28)}$ = 1.234, p = 0.2760).

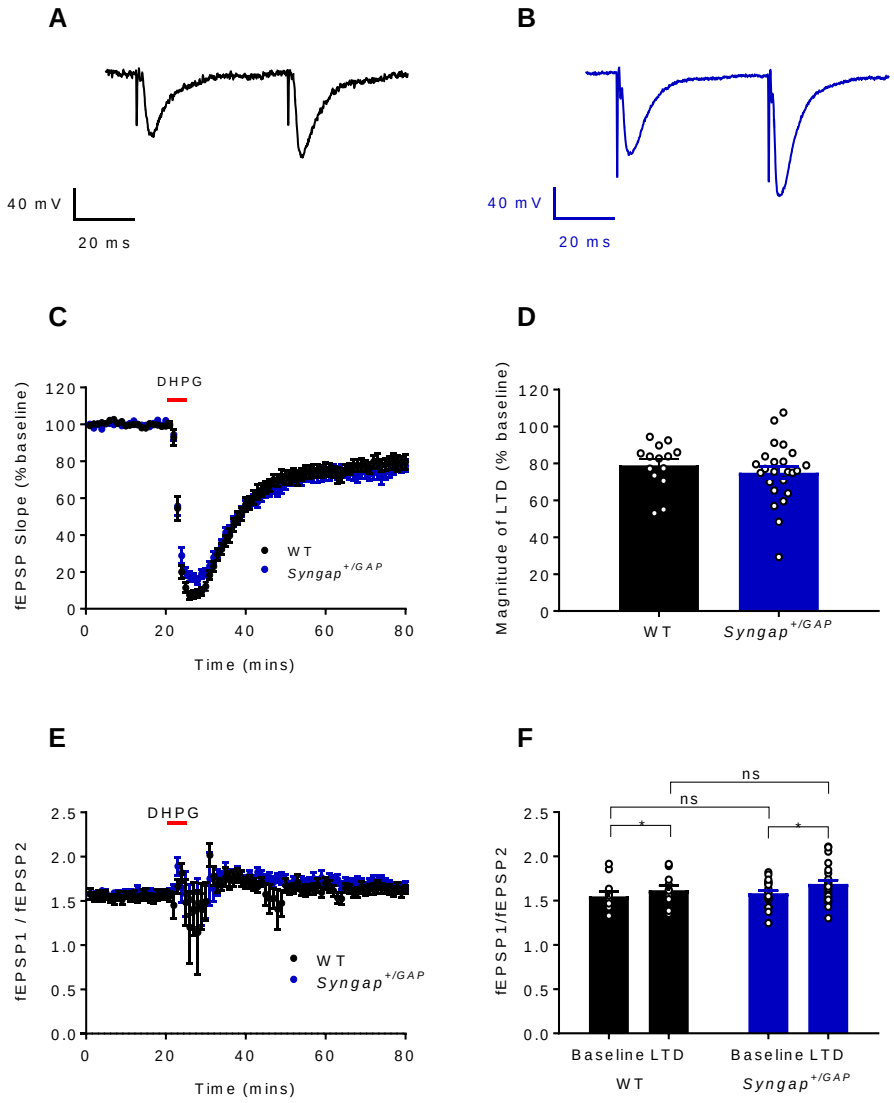

Figure 19 – There is no significant difference in hippocampal mGluR LTD or PPR between P26-33 WT and *Syngap*$^{+/GAP}$ rats when the data is collated by slice.

(A) WT and (B) *Syngap*$^{+/GAP}$ example traces.

(C) and (D) There is no significant difference in LTD induced with 100 µM DHPG between WT and *Syngap*$^{+/GAP}$ rats**.** LTD was measured as the mean value between 70 and 80 minutes. (WT = 78.9 ± 3.3% n = 14, *Syngap*$^{+/GAP}$ = 75 ± 3.4% n = 24, Unpaired t test p = 0.4457).

(E) and (F) Paired pulse ratio is facilitated after LTD, but there is no significant difference between WT and *Syngap*$^{+/GAP}$ rats. (At baseline WT = 1.5 ± 0.05 n = 12, *Syngap*$^{+/GAP}$ = 1.6 ± 0.03 n = 23, after LTD WT = 1.6 ± 0.05 n = 12, *Syngap*$^{+/GAP}$ = 1.7 ± 0.04 n = 23, 2 way ANOVA with *post hoc* Bonferroni corrections for multiple comparisons, LTD effect: $F_{(1, 33)}$ = 10.61, p < 0.0026; genotype effect: $F_{(1, 33)}$ = 0.8964, p = 0.3506; LTD x genotype interaction: $F_{(1, 33)}$ = 0.4712, p = 0.4972).

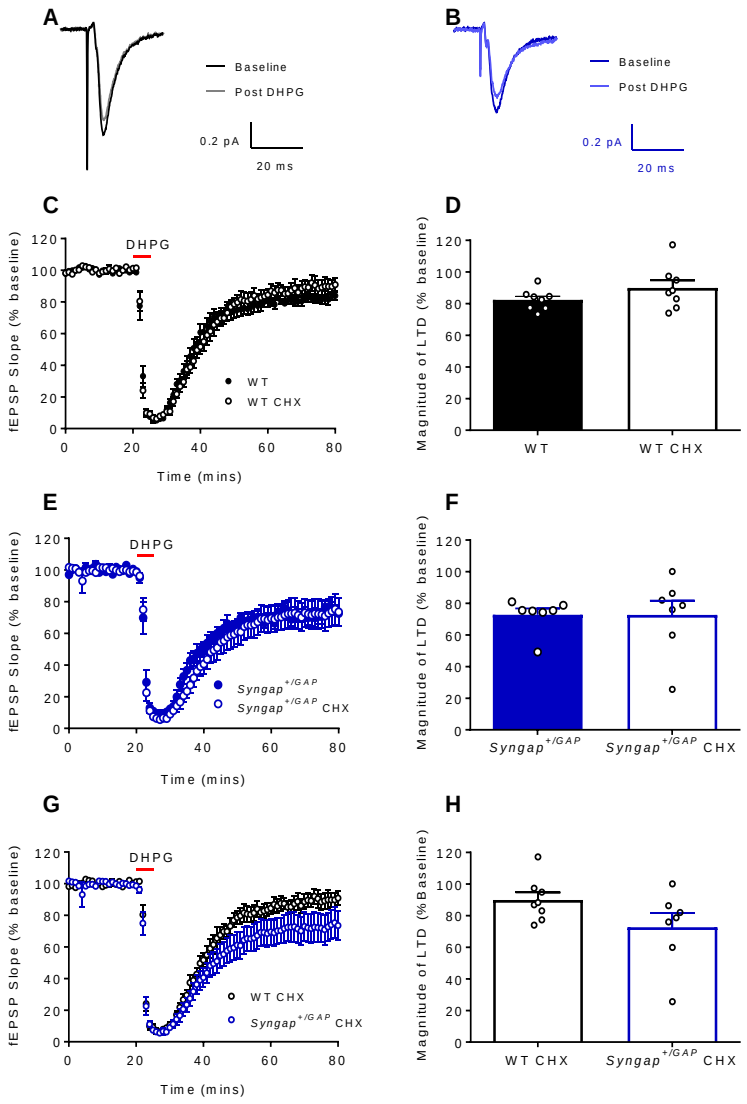

Figure 20 - There is no significant difference in LTD between Syngap$^{+/GAP}$ and WT recordings when new protein synthesis is inhibited.

(A) WT and (B) *Syngap*$^{+/GAP}$ example traces in the presence of 100 µM CHX.

(C) and (D) There is no significant difference in LTD between WT recordings with and without CHX (WT = 82.4 ± 2.3% n = 8, WT CHX 89.9 ± 4.8% n = 8, paired t-test p = 0.1472).

(E) and (F) There is no significant difference in LTD between *Syngap*$^{+/GAP}$ recordings with and without CHX (*Syngap*$^{+/GAP}$ = 72.8 ± 4.0% n = 7, *Syngap*$^{+/GAP}$ CHX 72.7 ± 9.1% n = 7, Wilcoxon matched-pairs signed rank test = 0.8125).

(G) and (H) There is no significant difference in LTD between WT and *Syngap*$^{+/GAP}$ recordings with CHX (WT CHX 89.9 ± 4.8% n = 8, *Syngap*$^{+/GAP}$ CHX 72.7 ± 9.1% n = 7, Mann-Whitney test p = 0.1520).

LTD was measured as the mean value between 70 and 80 minutes. Data was collected from one drug free and one CHX slice per animal.

4.3.2 Intrinsic cell property recordings in acute hippocampal slices

Intrinsic cell properties were examined by injecting a series of 25 pA current steps from -100 to +400 pA during CA1 pyramidal cell whole cell recordings in current clamp.

There was no significant difference in resting membrane potential, membrane time constant, input resistance, or capacitance between WT and Syngap+/GAP recordings at P13-15 and P26-30 when the unit of analysis was 'animal' (Figure 21 and Figure 25). Furthermore there was no significant difference in action potential properties or firing rate when the unit of analysis was 'animal' at either age (Figure 22, Figure 23, Figure 26 and Figure 27). There was however a trend towards a higher input resistance in Syngap+/GAP recordings at P26-30 (Figure 25). Perhaps with a larger sample size this would have become statistically significant. Physiologically, with higher input resistance less current is required to elicit the same depolarisation of a neuron. This would therefore represent a shift towards excitation.

However, certain statistically significant differences were seen when the data was analysed with n = cell. An increase in rheobase (WT = 125 ± 12.09 pA, Syngap+/GAP = 160.1 ± 7.674 pA, unpaired t test p = 0.0186) , maximum rise rate (WT = 226.7 ± 19.19 mV / ms, Syngap+/GAP = 316.9 ± 25.61 mV / ms, Mann-Whitney test p = 0.0124) and maximum decay rate (WT = -65.49 ± 3.982 mV / ms, Syngap+/GAP = -75.17 ± 3.164 mV / ms, Mann-Whitney test p = 0.0480) were observed in Syngap+/GAP rats at P13-15 (Figure 22). At P26-30 an increase in membrane time constant (Figure 25 - WT = 12.83 ± 1.03 ms, n = 24, Syngap+/GAP = 14.29 ± 0.70 ms, unpaired t test p = 0.0481) and action potential half width (WT = 0.94 ± 0.04 ms, Syngap+/GAP = 1.09 ± 0.05 ms, Unpaired t test p = 0.0135) and a decrease in action potential maximum decay rate (WT = -108.50 ± 4.11 mV / ms, Syngap+/GAP = -91.92 ± 4.78 mV / ms, unpaired t test p = 0.0119) (Figure 26) were seen in Syngap+/GAP rats. This is likely to be a pseudo-replication effect as there is no significant difference when the unit of analysis is 'animal'. This means that the statistical interpretation of the data is inflated to significance because the use of n = cell fails to take into account the increased similarity and the lack of independence between cells from the same animal which introduces bias into the analysis (Lazic

2010; Sikkel et al. 2013). I therefore believe the correct results are those analysed by n = animal. Furthermore, the 'significant' differences seen when the unit of analysis is 'cell' are in the direction of inhibition over excitation as they would result in fewer action potentials in a given period of time (except for the increase in maximum rise rate at P13-15 and increase in maximum decay rate at P26-30) which is not in keeping with the published literature on SynGAP mutations. Whilst clearly this is not a reason in itself to doubt the result, when considered alongside the lack of independence of multiple cells from individual animals this strikes me as a further illustration of the unhelpful effects of pseudo-replication.

Hyperpolarising (-250 pA) current steps were injected into each cell in order to measure the 'sag' in current produced by the opening of hyperpolarisation-activated cyclic nucleotide-gated (HCN) channels. This is of interest because HCN channels open in response to membrane hyperpolarisation and have roles in the maintenance of resting membrane potential, input resistance, dampening of synaptic potentials, neural oscillations and temporal dendritic summation (reviewed by Benarroch 2013; He et al. 2014). CaMKII and p38-MAPK pathways and glutamatergic signalling via both AMPA and NMDA receptors have been postulated as modulators of HCN channel expression and HCN channel dysfunction has been implicated in epilepsy (reviewed by He et al. 2014). Therefore given SynGAP's link to epilepsy, its role in AMPA trafficking and its interactions with CaMKII and p38-MAPK it was possible that differences in sag would be identified between the rat genotypes. However, no significant differences were found between the Sag in either age group when comparing WT and *Syngap*$^{+/GAP}$ rat recordings (P13-15: Figure 24 and P26-30: Figure 28).

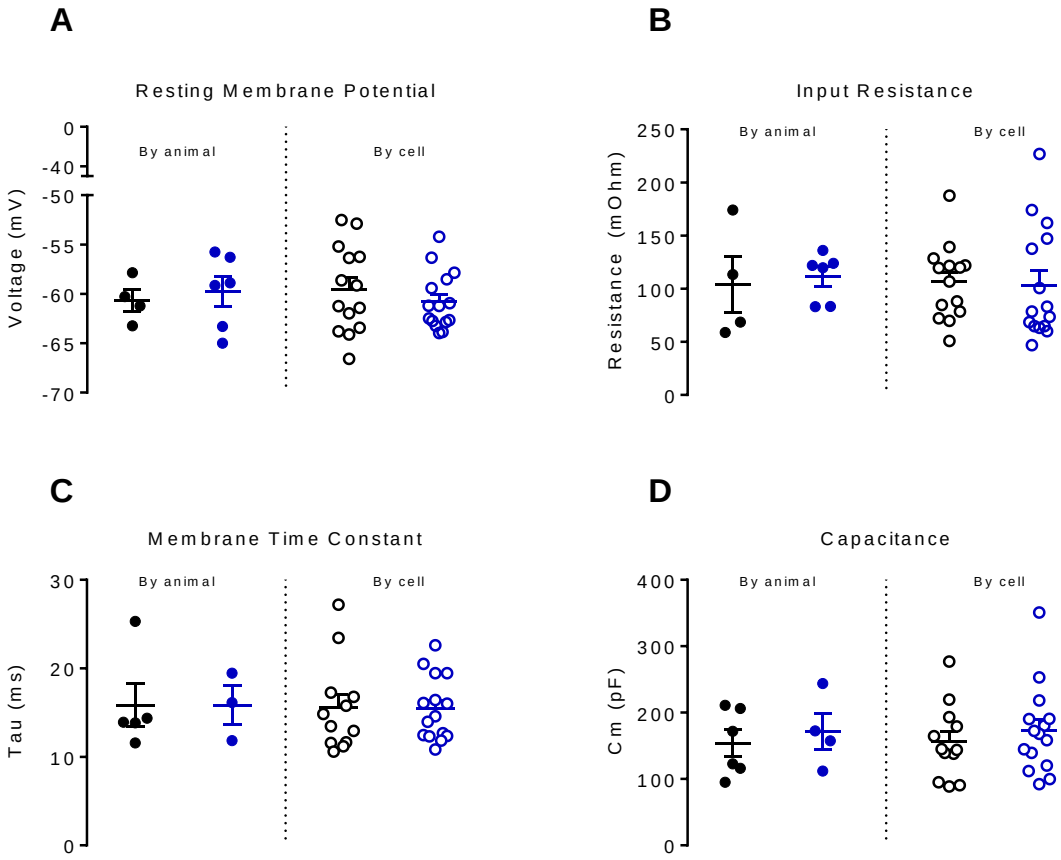

Figure 21 – At P13-15 passive cell properties are not significantly different WT and *Syngap*$^{+/GAP}$ recordings.

WT shown in black, *Syngap*$^{+/GAP}$ shown in blue.

(A) Resting membrane potential (analysed by n = animal: WT = -59.73 ± 1.518 mV, *n* = 6, *Syngap*$^{+/GAP}$ = -60.65 ± 1.113 mV, *n* = 4, Mann-Whitney test *p* = 0.6952; analysed by n = cell: WT = -59.53 ± 1.174 mV, *n* = 14, *Syngap*$^{+/GAP}$ = -60.77 ± 0.7521 mV, *n* = 15, Unpaired t test *p* = 0.3766).

(B) Input resistance (analysed by n = animal: WT = 111.4 ± 9.203 MΩ, *n* = 6, *Syngap*$^{+/GAP}$ = 103.7 ± 26.26 MΩ , *n* = 4, Mann-Whitney test *p* = 0.4476; analysed by n = cell: WT = 106.4 ± 9.421 MΩ , *n* = 14, *Syngap*$^{+/GAP}$ = 103.5 ± 13.72 MΩ , *n* = 15, Unpaired t test *p* = 0.8644).

(C) Membrane time constant (analysed by n = animal: WT = 15.81 ± 2.427 ms, *n* = 5, *Syngap*$^{+/GAP}$ = 15.81 ± 2.203 ms, *n* = 3, Mann-Whitney test *p* = 0.7857; analysed by n = cell: WT = 15.56 ± 1.479 ms, *n* = 1,2 *Syngap*$^{+/GAP}$ = 15.44 ± 0.9356 ms, *n* = 15, Mann-Whitney test *p* = 0.9436).

(D) Capacitance (analysed by n = animal: WT = 153.8 ± 20.18 pF, *n* = 6, *Syngap*$^{+/GAP}$ = 171.4 ± 27.37 pF, *n* = 4, Mann-Whitney test *p* = 0.7524; analysed by n = cell: WT = 156.1 ± 16.07 pF, *n* = 12, *Syngap*$^{+/GAP}$ = 172.7 ± 17.09 pF, *n* = 15, Mann-Whitney test *p* = 0.4769).

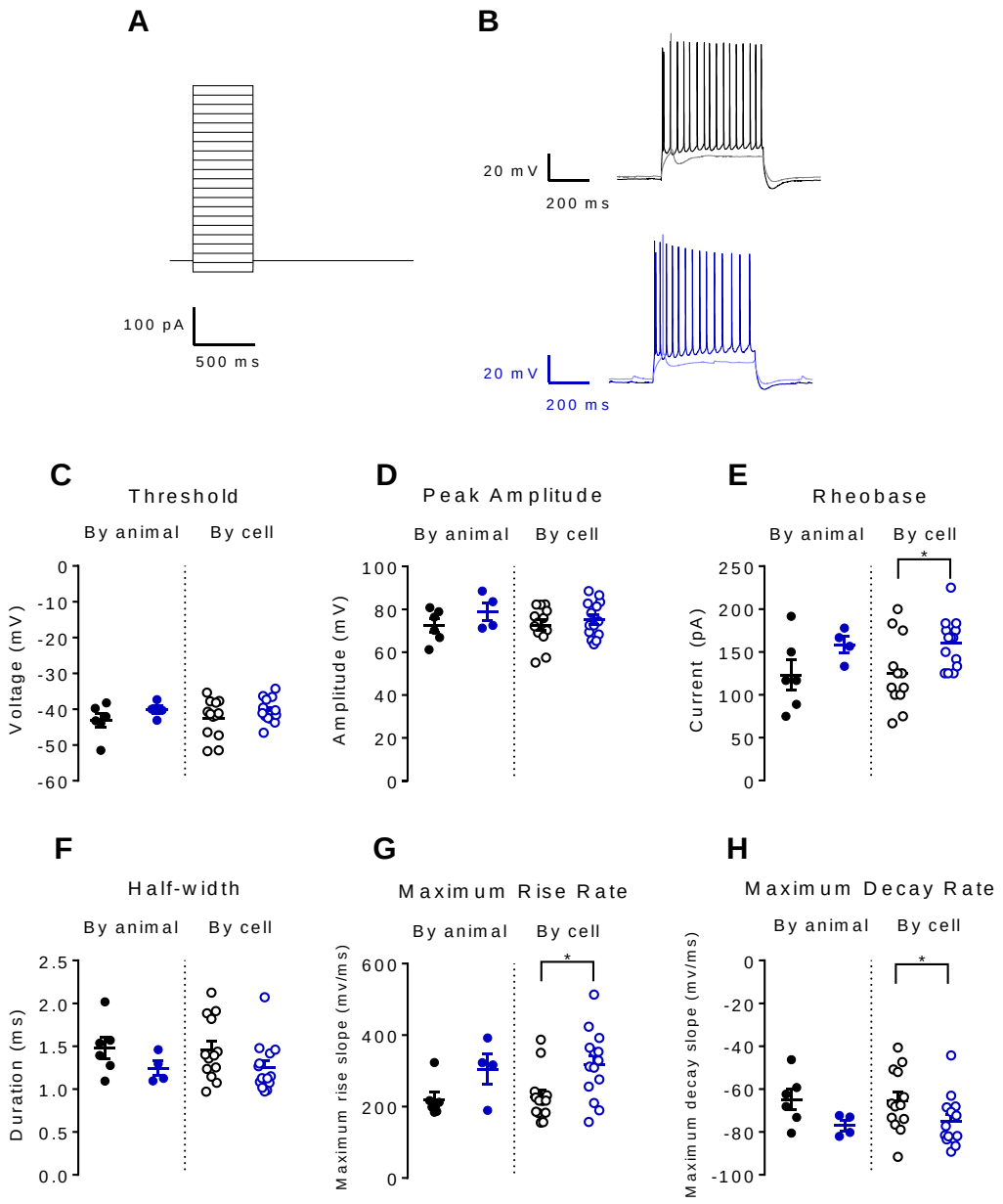

Figure 22 - Action potential properties are not significantly different between P13-15 WT and *Syngap*$^{+/GAP}$ rats.

WT shown in black, *Syngap*$^{+/GAP}$ shown in blue.

(A) Current step protocol with 25 pA current steps from -100 pA to +400 pA

(B) Representative traces of WT and *Syngap*$^{+/GAP}$ recordings.

Legend continued overleaf…

Figure 22 Legend continued…

(C) Action potential threshold (analysed by n = animal: WT = -43.12 ± 1.89 mV *n* = 6, *Syngap*$^{+/GAP}$ = -40.19 ± 1.17 mV *n* = 4 Mann-Whitney test *p* = 0.3524; analysed by n = cell: WT = -42.54 ± 1.446 mV, *n* = 13, *Syngap*$^{+/GAP}$ = -40.50 ± 0.8944 mV, *n* = 14 Unpaired t test *p* = 0.2340).

(D) Action potential peak amplitude (analysed by n = animal: WT = 72.35 ± 3.10 mV *n* = 6, *Syngap+/GAP* = 78.93 ± 4.22 mV *n* = 4 Mann-Whitney test *p* = 0.2571; analysed by n = cell: WT = 72.59 ± 2.445 mV, *n* = 13, *Syngap*$^{+/GAP}$ = 75.17 ± 2.225 mV, *n* = 4, Unpaired t test *p* = 0.4411).

(E) Action potential rheobase (analysed by n = animal: WT = 123.10 ± 17.31 pA *n* = 6, *Syngap*$^{+/GAP}$ = 158.60 ± 9.48 pA *n* = 4, Mann-Whitney test *p* = 0.1524; analysed by n = cell: WT = 125 ± 12.09 pA *n* = 14, *Syngap*$^{+/GAP}$ = 160.1 ± 7.674 pA *n* = 13, Unpaired t test *p* = 0.0186).

(F) Action potential half-width (analysed by n = animal: WT = 1.48 ± 0.13 ms *n* = 6, *Syngap*$^{+/GAP}$ = 1.24 ± 0.08 ms *n* = 4, Mann-Whitney test *p* = 0.3333; analysed by n = cell: WT = 1.462 ± 0.09969 ms *n* = 14, *Syngap*$^{+/GAP}$ = 1.252 ± 0.07784 ms *n* = 14, Mann-Whitney test *p* = 0.1680).

(G) Action potential maximum rise rate (analysed by n = animal: WT = 220.10 ± 21.25 mV / ms *n* = 6, *Syngap*$^{+/GAP}$ = 305.20 ± 42.20 mV / ms *n* = 4, Mann-Whitney test *p* = 0.3333; analysed by n = cell: WT = 226.7 ± 19.19 mV / ms *n* = 13 , *Syngap*$^{+/GAP}$ = 316.9 ± 25.61 mV / ms *n* = 14, Mann-Whitney test *p* = 0.0124).

(H) Action potential maximum decay rate (analysed by n = animal: WT = -64.97 ± 4.847 mV / ms *n* = 6, *Syngap*$^{+/GAP}$ = -76.92 ± 2.465 mV / ms *n* = 4, Mann-Whitney test *p* = 0.1714; analysed by n = cell: WT = -65.49 ± 3.982 mV / ms *n* = 13, *Syngap*$^{+/GAP}$ = -75.17 ± 3.164 mV / ms *n* = 14, Mann-Whitney test *p* = 0.0480).

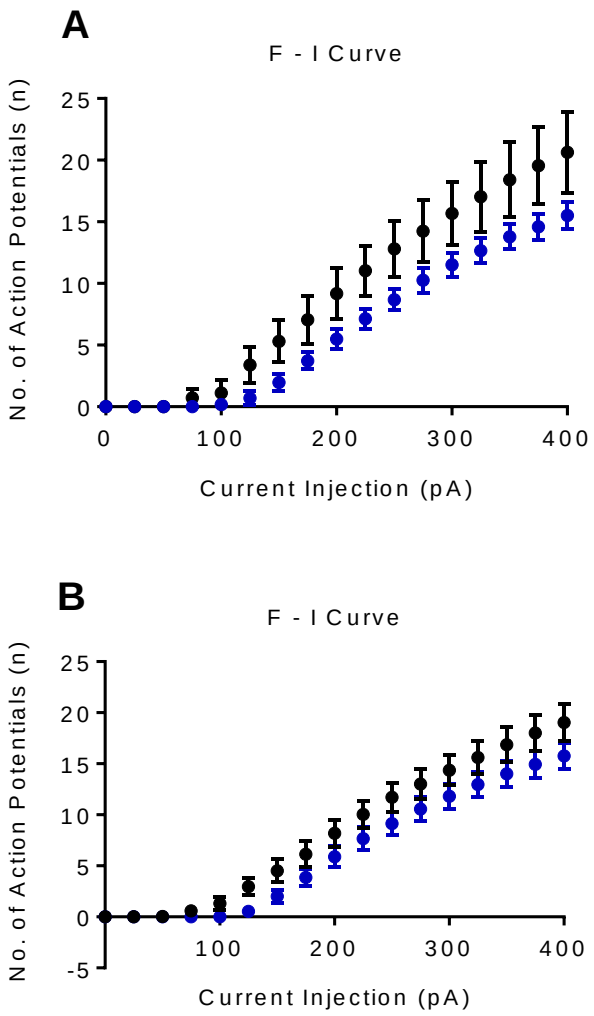

Figure 23 – There is no significant difference in action potential firing rate in *Syngap*$^{+/GAP}$ rats compared to WT rats at P13-15.

WT shown in black, *Syngap*$^{+/GAP}$ shown in blue.

(A) Firing rate vs Input with data collated by n = animal (2 way ANOVA with *post hoc* Bonferroni corrections for multiple comparisons, current injection effect: $F_{(16, 128)}$ =78.1 , p < 0.0001; genotype effect: $F_{(1, 8)}$ = 1.677, p = 0.2314; current injection x genotype interaction: $F_{(16, 128)}$ = 1.479, p = 0.1171).

(B) Firing rate vs Input with data collated by n = cell (2 way ANOVA with *post hoc* Bonferroni corrections for multiple comparisons, current injection effect: $F_{(16, 400)}$ = 206.2, p < 0.0001; genotype effect: $F_{(1, 25)}$ = 2.396, p = 0.1342; current injection x genotype interaction: $F_{(16, 400)}$ = 1.521, p = 0.0886).

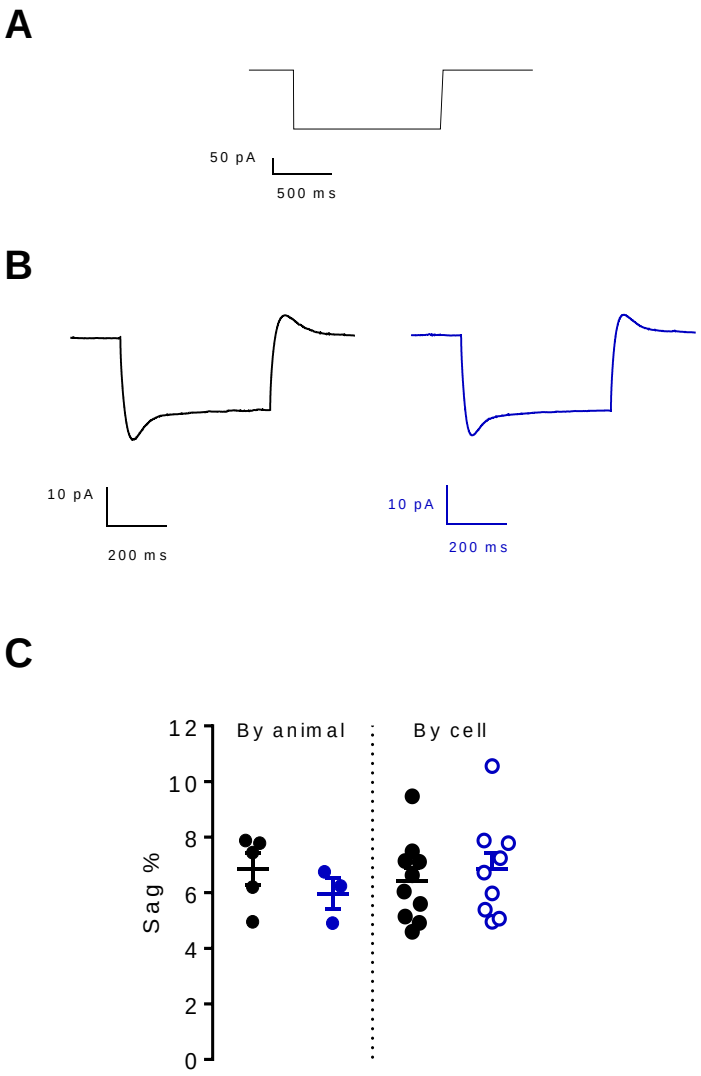

Figure 24 - Current sag is not significantly different between P13-15 WT and *Syngap*$^{+/GAP}$ rats.

WT shown in black, *Syngap*$^{+/GAP}$ shown in blue.

(A) Sag -250 pA step protocol applied 6 times for each cell.

(B) WT (black) and *Syngap*$^{+/GAP}$ (blue) example traces.

(C) Sag with n = animal (WT = 6.854 ± 0.5613%, n = 5, *Syngap*$^{+/GAP}$ = 5.967 ± 0.5479%, n = 3, Mann-Whitney test p = 0.3571), sag with n = cell (WT = 6.413 ± 0.4655%, n = 10, *Syngap*$^{+/GAP}$ = 6.842 ± 0.5950%, n = 9, unpaired t test p = 0.5738).

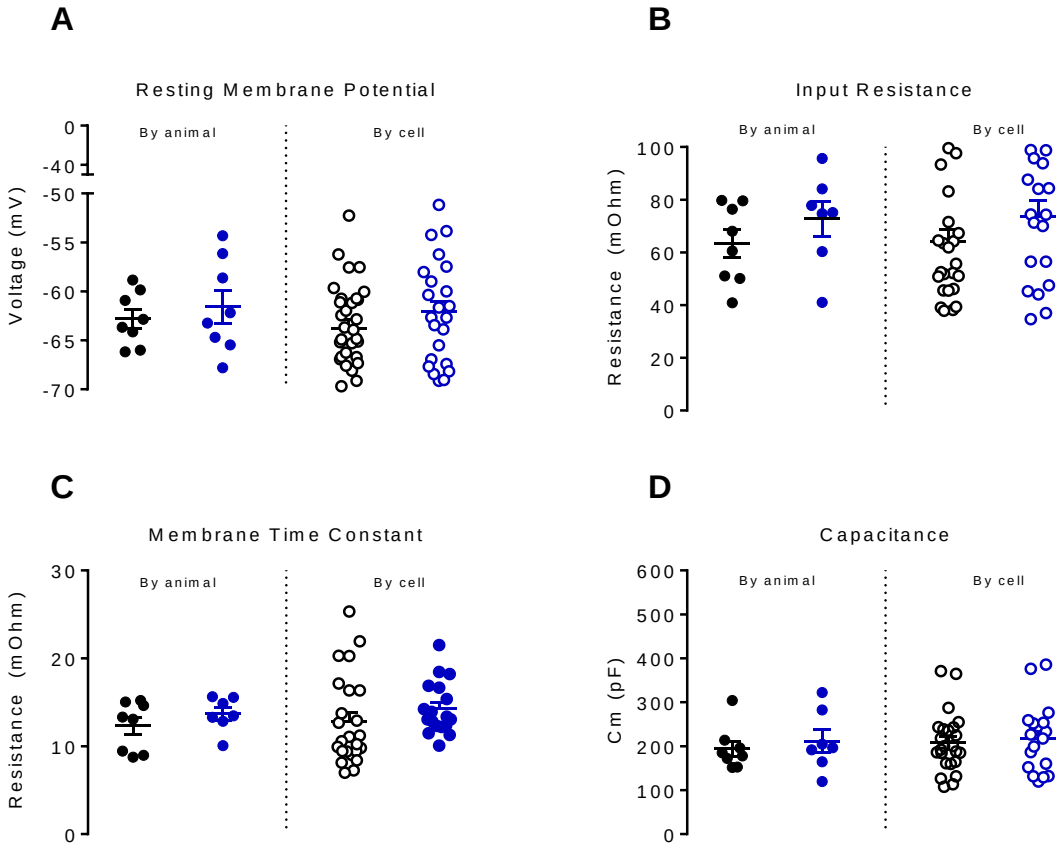

Figure 25 – At P26-30 passive cell properties are not significantly different WT and *Syngap*$^{+/GAP}$ recordings.

WT shown in black, *Syngap*$^{+/GAP}$ shown in blue.

(A) Resting membrane potential (analysed by n = animal: WT = -62.81 ± 0.96 mV, *n* = 8, *Syngap*$^{+/GAP}$ = -61.56 ± 1.68 mV, *n* = 8, unpaired t test *p* = 0.6454; analysed by n = cell: WT = -63.78 ± 0.9171 mV, *n* = 31, *Syngap*$^{+/GAP}$ = -62.11 ± 1.102 mV, *n* = 23, Unpaired t test *p* = 0.4447).

(B) Input resistance (analysed by n = animal: WT = 63.3 ± 5.28 MΩ , *n* = 8, *Syngap*$^{+/GAP}$ = 72.70 ± 6.63 MΩ , *n* = 7, Mann-Whitney test *p* = 0.3969; analysed by n = cell: WT = 63.97 ± 4.710 MΩ , *n* = 25, *Syngap+/GAP* = 73.57 ± 6.215 MΩ , *n* = 19, unpaired t test *p* = 0.2583).

(C) Membrane time constant (analysed by n = animal: WT = 12.31 ± 0.99 ms, *n* = 8, *Syngap*$^{+/GAP}$ = 13.67 ± 0.74 ms, *n* = 7, Mann-Whitney test *p* = 0.3357; analysed by n = cell: WT = 12.83 ± 1.03 ms, *n* = 24, *Syngap*$^{+/GAP}$ = 14.29 ± 0.70 ms, *n* = 18, unpaired t test *p* = 0.0481).

(D) Capacitance (analysed by n = animal: WT = 194.2 ± 17.34 pF, *n* = 8, *Syngap*$^{+/GAP}$ = 211.7 ± 26.13 pF, *n* = 7, Mann-Whitney test *p* = 0.5358; analysed by n = cell: WT = 207.5 ± 13.75 pF, *n* = 24, *Syngap*$^{+/GAP}$ = 218.7 ± 18.35 pF, *n* = 18, unpaired t test *p* = 0.5543).

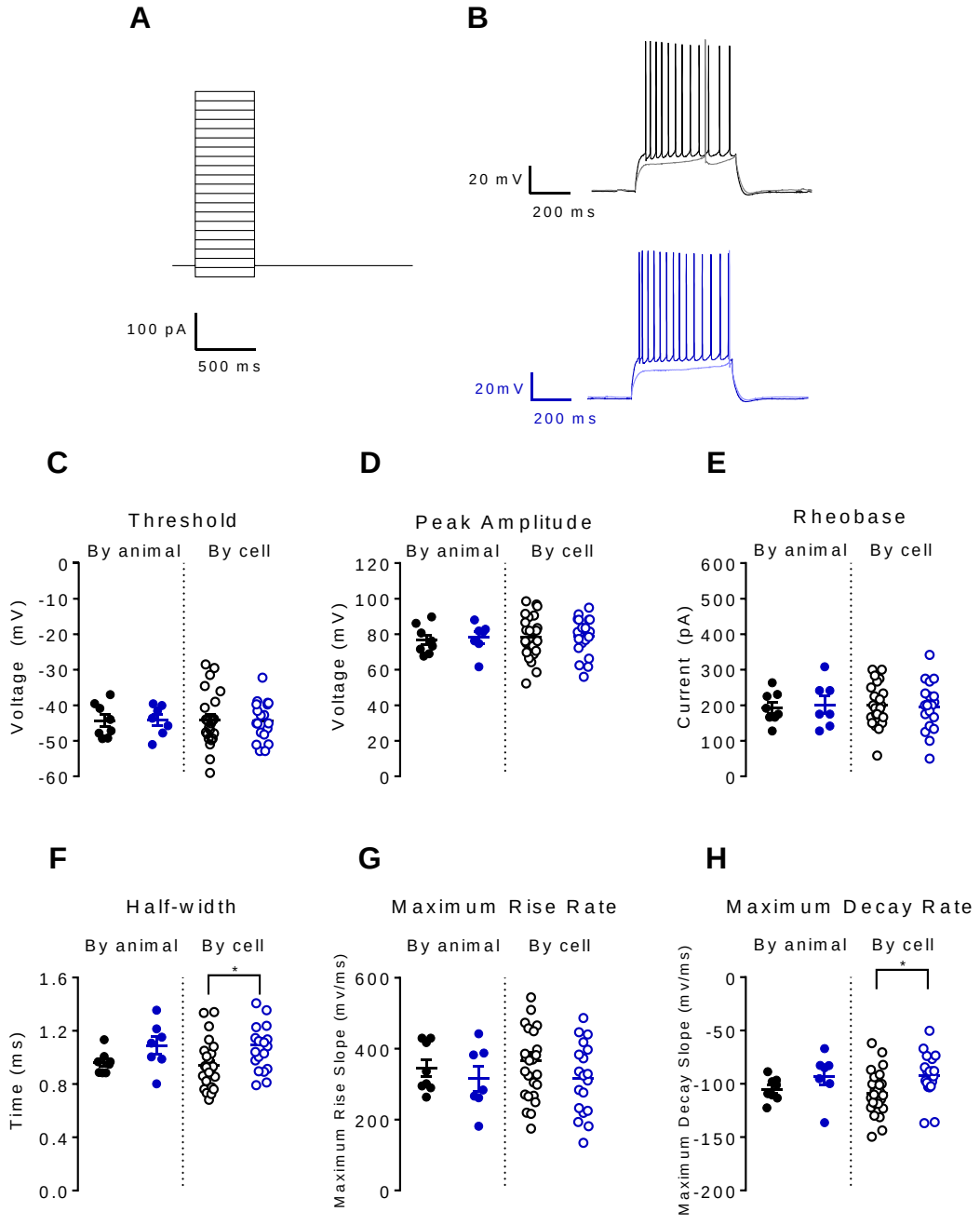

Figure 26 – Action potential properties are not significantly different between P26-30 WT and *Syngap*$^{+/GAP}$ rats.

WT shown in black, *Syngap*$^{+/GAP}$ shown in blue.

(A) Current step protocol with 25 pA current steps from -100 pA to +400 pA.

(B) Representative traces of WT (black) and *Syngap*$^{+/GAP}$ (blue) recordings.

Legend continued overleaf…

Figure 26 legend continued…

(C) Action potential threshold (analysed by n = animal: WT = -44.37 ± 1.68 mV *n* = 8, *Syngap*$^{+/GAP}$ = -44.21 ± 1.60 mV *n* = 7 Mann-Whitney test *p* = 0.9551; analysed by n = cell: WT = -44.01 ± 1.50 mV *n* = 25, *Syngap*$^{+/GAP}$ = -44.31 ± 1.27 mV *n* = 19 unpaired t test *p* = 0.8833).

(D) Action potential peak amplitude (analysed by n = animal: WT = 76.79 ± 2.839 mV *n* = 8, *Syngap*$^{+/GAP}$ = 78.1 ± 3.2 mV *n* = 7 Mann-Whitney test *p* = 0.5358; analysed by n = cell: WT = 78.40 ± 2.37 mV *n* = 25, *Syngap*$^{+/GAP}$ = 78.7 ± 2.49 mV *n* = 19 unpaired t test *p* = 0.9319).

(E) Action potential rheobase (analysed by n = animal: WT = 193.3 ± 15.44 pA *n* = 8, *Syngap*$^{+/GAP}$ = 201.6 ± 24.43 pA *n* = 7, Mann-Whitney test *p* = 0.7983; analysed by n = cell: WT = 200.3 ± 11.47 pA *n* = 25, *Syngap*$^{+/GAP}$ = 196.1 ± 15.85 pA *n* = 19, unpaired t test *p* = 0.8234).

(F) Action potential half-width (analysed by n = animal: WT = 0.96 ± 0.03 ms *n* = 8, *Syngap*$^{+/GAP}$ = 1.09 ± 0.07 ms *n* = 7, Mann-Whitney test *p* = 0.0939; analysed by n = cell: WT = 0.94 ± 0.04 ms *n* = 25, *Syngap*$^{+/GAP}$ = 1.09 ± 0.05 ms *n* = 19, unpaired t test *p* = 0.0135).

(G) Action potential maximum rise rate (analysed by n = animal: WT = 345.3 ± 24.57 mV / ms *n* = 8, *Syngap*$^{+/GAP}$ = 315 ± 34.51 mV / ms *n* = 7, Mann-Whitney test *p* = 0.3969; analysed by n = cell: WT = 365.20 ± 23.81 mV / ms *n* = 25, *Syngap*$^{+/GAP}$ = 315.2 ± 22.98 mV / ms *n* = 19, unpaired t test *p* = 0.1475).

(H) Action potential maximum decay rate (analysed by n = animal: WT = -104.9 ± 3.84 mV / ms *n* = 8, *Syngap*$^{+/GAP}$ = -92.69 ± 8.29 mV / ms *n* = 7, Mann-Whitney test *p* = 0.0721; analysed by n = cell: WT = -108.50 ± 4.11 mV / ms *n* = 25, *Syngap*$^{+/GAP}$ = -91.92 ± 4.78 mV / ms *n* = 19, unpaired t test *p* = 0.0119).

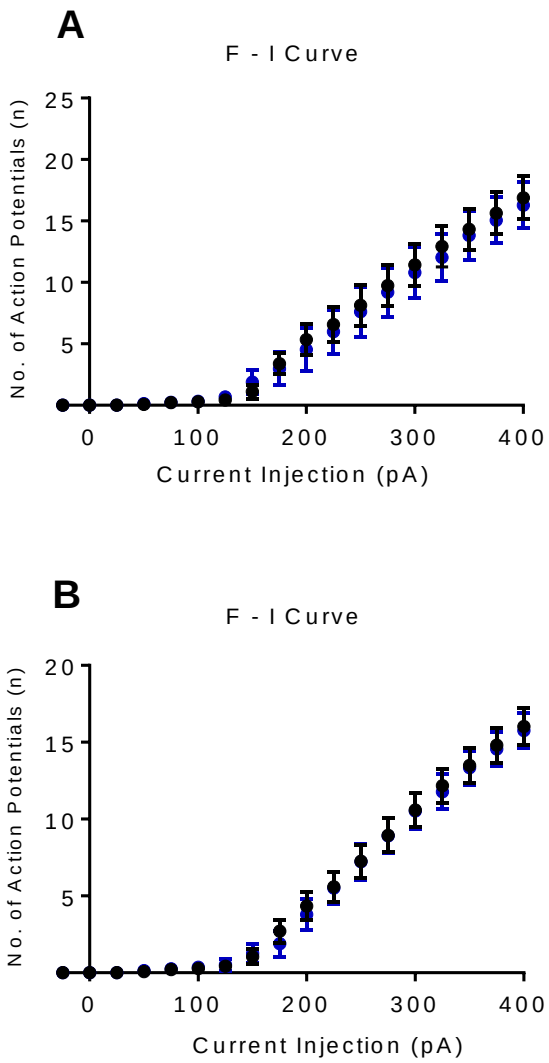

Figure 27 – There is no significant difference in action potential firing rate in *Syngap*$^{+/GAP}$ rats compared to WT rats at P26-30.

WT shown in black, *Syngap*$^{+/GAP}$ shown in blue.

(A) Firing rate vs Input when analysed by n = animal (2 way ANOVA with *post hoc* Bonferroni corrections for multiple comparisons, current injection effect: $F_{(17, 221)} = 95.43$ $p < 0.0001$; genotype effect: $F_{(1, 13)} = 0.03826$, $p = 0.8479$ current injection x genotype interaction: $F_{(17, 221)} = 0.1255$, $p > 0.9999$).

(B) Firing rate vs Input when analysed by n = cell (2 way ANOVA with *post hoc* Bonferroni corrections for multiple comparisons, current injection effect: $F_{(17, 731)} = 213.5$, $p < 0.0001$; genotype effect: $F_{(1, 43)} = 0.01825$, $p = 0.8932$ current injection x genotype interaction: $F_{(17, 731)} = 0.1062$, $p > 0.9999$).

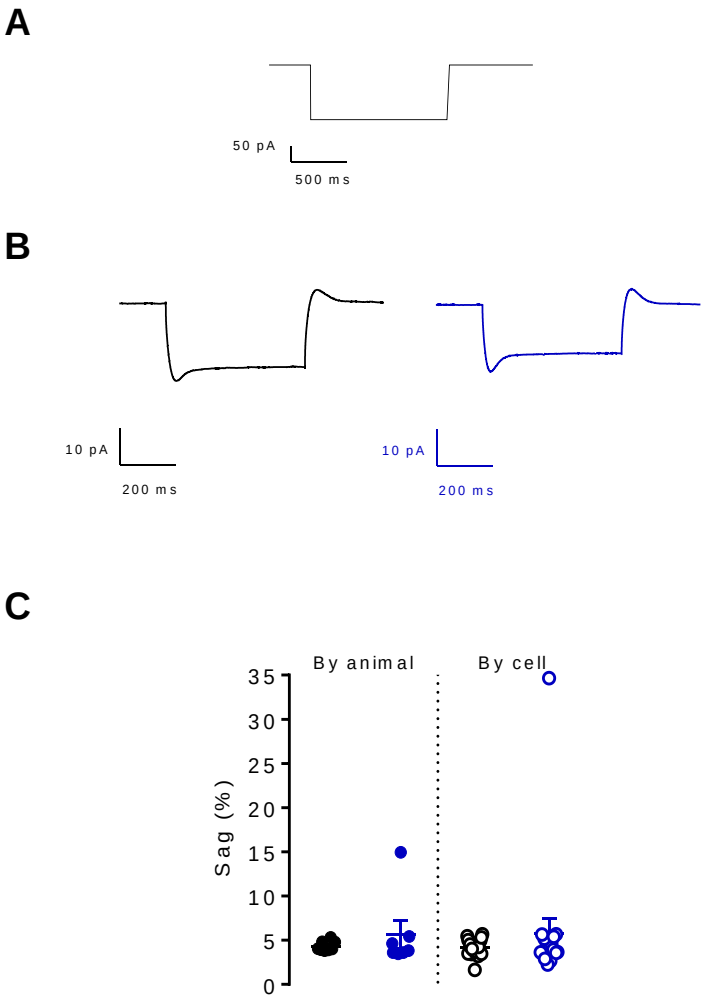

Figure 28 – Current sag is not significantly different between P26-30 WT and *Syngap*$^{+/GAP}$ rats.

WT shown in black, *Syngap*$^{+/GAP}$ shown in blue.

(A) Sag -250 pA step protocol applied 6 times for each cell.

(B) WT (black) and *Syngap*$^{+/GAP}$ (blue) example traces.

(C) Sag (WT = 4.324 ± 0.1974%, n = 5, *Syngap*$^{+/GAP}$ = 5.641 ± 1.572%, n = 3, Mann-Whitney test p = 0.5917), sag (WT = 4.171 ± 0.1914 %, n = 9, *Syngap*$^{+/GAP}$ = 5.752 ± 1.716%, n = 10, Mann-Whitney test p = 0.8111).

4.3.3 mEPSC recordings in cultured neurons

Due to the lethality of homozygous SynGAP mutation, the only way to examine electrical properties of homozygous neurons was to record from cultured neurons. Recordings were made in the presence of TTX (300 nM) and picrotoxin (50 μM) to block spontaneous, action potential driven activity in order to unmask the miniature events. As Figure 29 shows, there is no difference in mEPSC amplitude across genotypes, which is illustrated by the cumulative distribution plots of the amplitude for each genotype as well as the histogram graphs. The histograms also demonstrate the expected positive skew in mEPSC amplitude (Bekkers et al. 1990; McBain & Dingledine 1992; Wyllie et al. 1994).

Kruskal-Wallis testing of the mean frequency of mEPSC events across WT, *Syngap*$^{+/GAP}$ and *Syngap*$^{GAP/GAP}$ recordings revealed a significant difference when the unit of analysis was 'n = pup' (WT = 2.54 ± 1.44 Hz, *Syngap*$^{+/GAP}$ = 0.58 ± 0.09 Hz, *Syngap*$^{GAP/GAP}$ = 1.29 ± 0.21 Hz, Kruskal-Wallis test statistic 6.102, p = 0.0473) and also when the unit of analysis was 'n = cell' (WT = 2.02 ± 0.91, *Syngap*$^{+/GAP}$ = 0.78 ± 0.14 Hz, *Syngap*$^{GAP/GAP}$ = 2.01 ± 0.51 Hz, Kruskal-Wallis test statistic 7.389, p = 0.0249). Dunn's correction revealed on both analyses that the statistically different result on Kruskal-Wallis testing was due to heterozygous recordings having a significantly lower event frequency than recordings from homozygotes. The cumulative distribution plots of the inter-event frequencies illustrate this difference (Figure 29).

This finding of reduced frequency of mEPSCs in *Syngap*$^{+/GAP}$ rat recordings which is evaluated in more detail in the discussion section below, is unexpected as previously an increase in frequency has been seen in *Syngap*$^{-/-}$ mice (Vazquez et al. 2004; Rumbaugh et al. 2006).

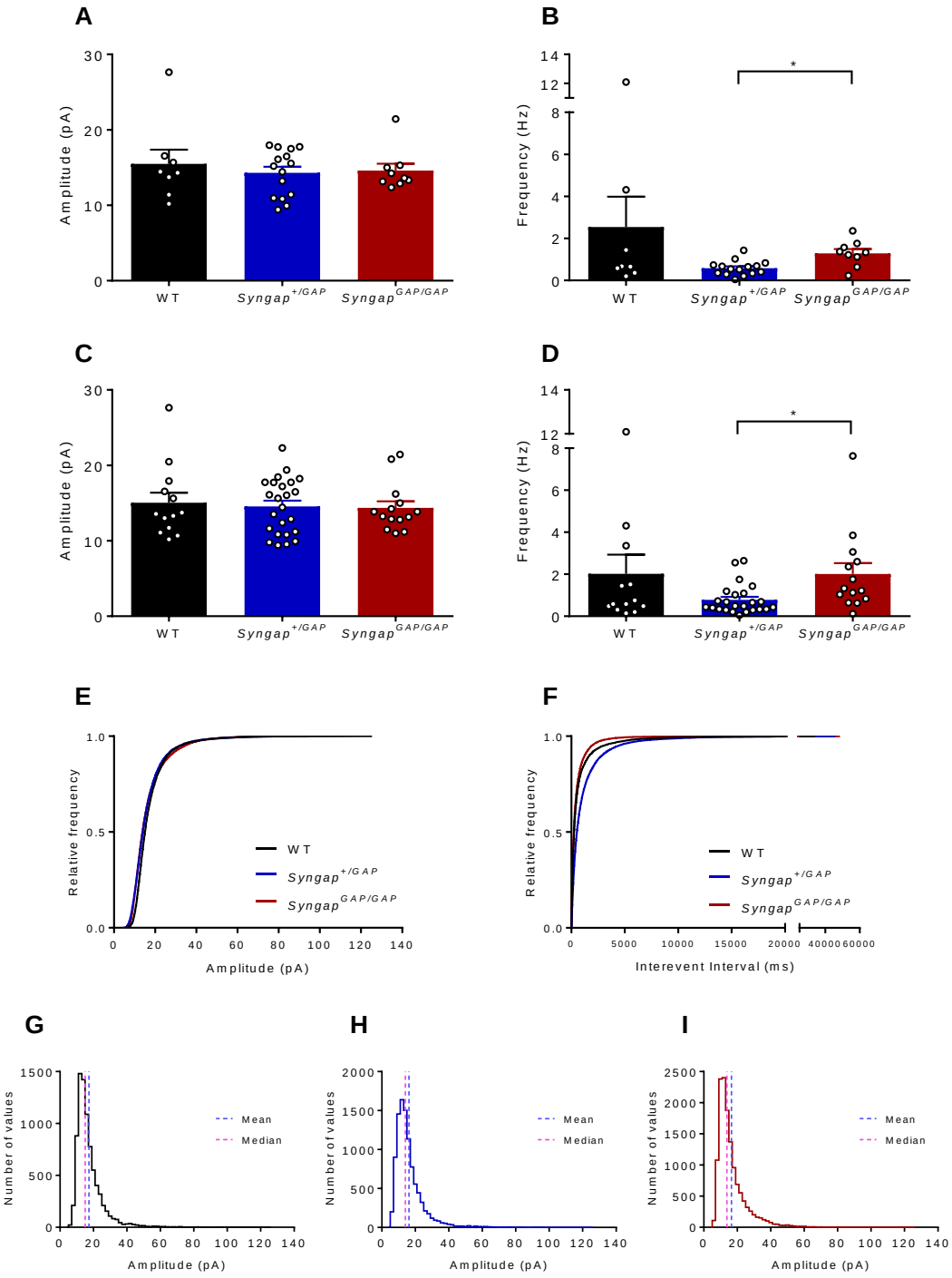

Figure 29 - mEPSC frequency is significantly decreased in *Syngap*$^{+/GAP}$ and *Syngap*$^{GAP/GAP}$ rat hippocampal DIV 13-15 cultures.

Legend overleaf…

Figure 29 legend:

(A) There is no significant difference in mEPSC amplitude between genotypes when the unit of analysis is 'pup' (WT = 15.5 ± 1.88 pA *n* = 8, *Syngap*$^{+/GAP}$ = 14.30 ± 0.80 pA *n* = 15, *Syngap*$^{GAP/GAP}$ = 14.59 ± 0.91 pA *n* = 9, Kruskal Wallis Test with Dunn's correction for multiple testing; Kruskal-Wallis statistic 0.2057, *p* = 0.9023).

(B) There is a significant difference in mEPSC frequency between genotypes when the unit of analysis is 'pup' (WT = 2.54 ± 1.44 Hz *n* = 8, *Syngap*$^{+/GAP}$ = 0.58 ± 0.09 Hz *n* = 15, *Syngap*$^{GAP/GAP}$ = 1.29 ± 0.21 Hz, *n* = 9, Kruskal Wallis Test with Dunn's correction for multiple testing; Kruskal-Wallis statistic 6.102, *p* = 0.0473. Dunn's testing: WT vs. *Syngap*$^{+/GAP}$ Mean Rank Difference 5.504, not significant; WT vs. *Syngap*$^{GAP/GAP}$ Mean Rank Difference -4.063, not significant; *Syngap*$^{+/GAP}$ vs. *Syngap*$^{GAP/GAP}$ Mean Rank Difference -9.567 significant).

(C) There is no significant difference in mEPSC amplitude between genotypes when the unit of analysis is 'cell' (WT = 15.04 ± 1.34 pA *n* = 13, *Syngap*$^{+/GAP}$ = 14.56 ± 0.75 pA *n* = 24, *Syngap*$^{GAP/GAP}$ = 14.37 ± 0.85 pA *n* = 14, Kruskal Wallis Test with Dunn's correction for multiple testing; Kruskal-Wallis statistic 0.0101, *p* = 0.9950).

(D) There is a significant difference in mEPSC frequency between genotypes when the unit of analysis is 'cell' (WT = 2.02 ± 0.91 Hz *n* = 13, *Syngap*$^{+/GAP}$ = 0.78 ± 0.14 Hz *n* = 24, *Syngap*$^{GAP/GAP}$ = 2.01 ± 0.51 Hz, *n* = 14, Kruskal Wallis Test with Dunn's correction for multiple testing; Kruskal-Wallis statistic 7.389, *p* = 0.0249. Dunn's testing: WT vs. *Syngap*$^{+/GAP}$ Mean Rank Difference 5.569, not significant; WT vs. *Syngap*$^{GAP/GAP}$ Mean Rank Difference -8.005, not significant; *Syngap*$^{+/GAP}$ vs. *Syngap*$^{GAP/GAP}$ Mean Rank Difference -13.57 significant).

(E) mEPSC Amplitude and (F) mEPSC frequency cumulative frequency distributions.

(G) WT, (H) *Syngap*$^{+/GAP}$ *and* (I) *Syngap*$^{GAP/GAP}$ recordings display the typical positively skewed distribution that is expected in mEPSC recordings (WT median = 15.05, WT mean = 17.28 pA, *Syngap*$^{+/GAP}$ median = 14.01 pA, *Syngap*$^{+/GAP}$ mean = 16.20 pA, *Syngap*$^{GAP/GAP}$ median = 13.79 pA, *Syngap*$^{GAP/GAP}$ mean = 16.51 pA).

4.3.4 Excitatory and inhibitory recordings in acute hippocampal slices

To investigate excitatory and inhibitory currents, recordings were made from pyramidal cells in acute hippocampal slices at the ages of P13-15 and P26-30. Firstly, spontaneous excitatory currents (sEPSCs) were recorded at -70 mV, followed by spontaneous inhibitory currents (sIPSCs) at 0 mV. TTX and PTX were then bath applied and further recordings made at -70 mV and 0 mV to capture miniature EPSCs (mEPSCs) and miniature IPSCs (mIPSCs). Example traces for P13-15 and P26-30 are shown in Figure 30 and Figure 31.

In a subset of recordings, CNQX was washed on at -70 mV to demonstrate through the abolition of events that these currents were AMPAR mediated. In other recordings, picrotoxin was washed on at 0 mV to demonstrate through abolition of events that these currents were $GABA_AR$ mediated (Figure 32).

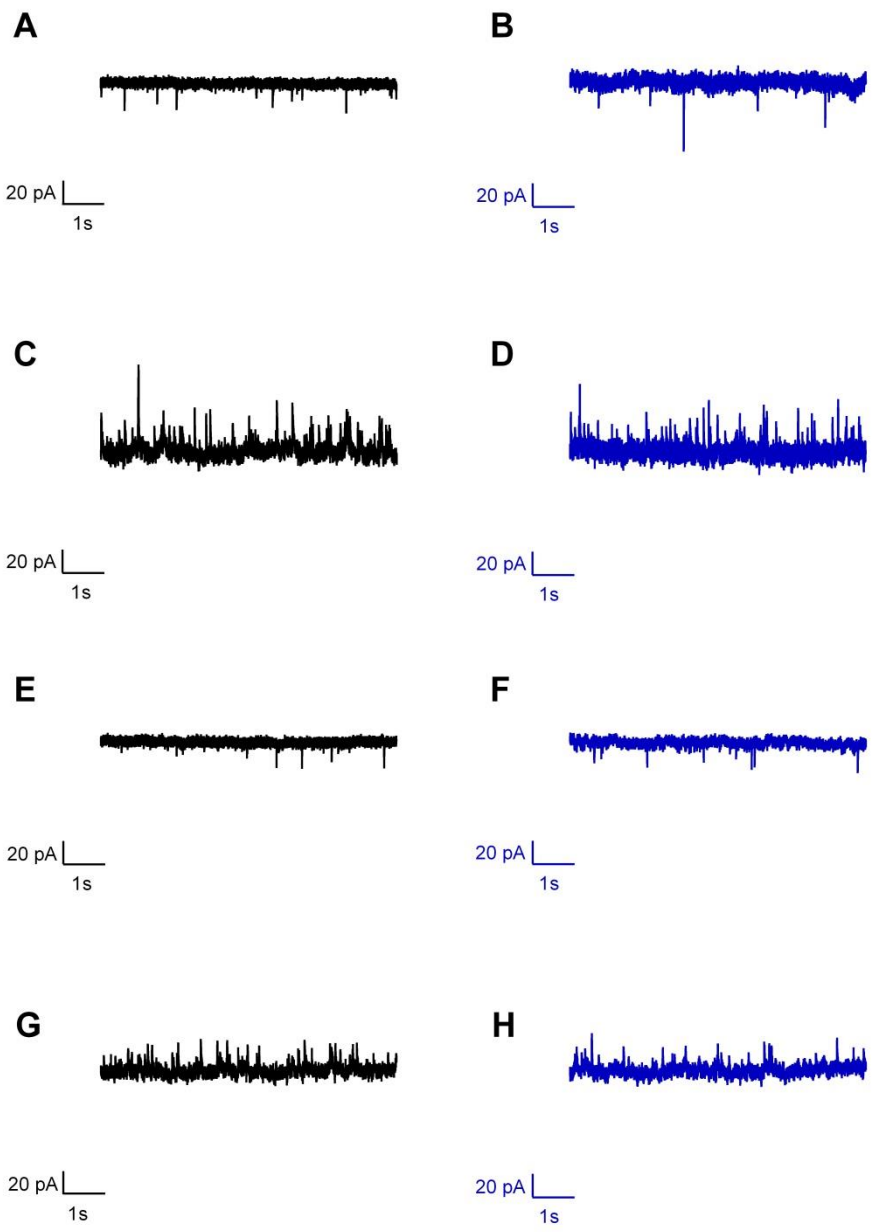

Figure 30 – P13-15 example traces from excitatory and inhibitory current recordings.

(A) WT sEPSC, (B) *Syngap*$^{+/GAP}$ sEPSC, (C) WT sIPSC, (D) *Syngap*$^{+/GAP}$ sIPSC, (E) WT mEPSC, (F) *Syngap*$^{+/GAP}$ mEPSC, (G) WT mIPSC, (H) *Syngap*$^{+/GAP}$ mIPSC.

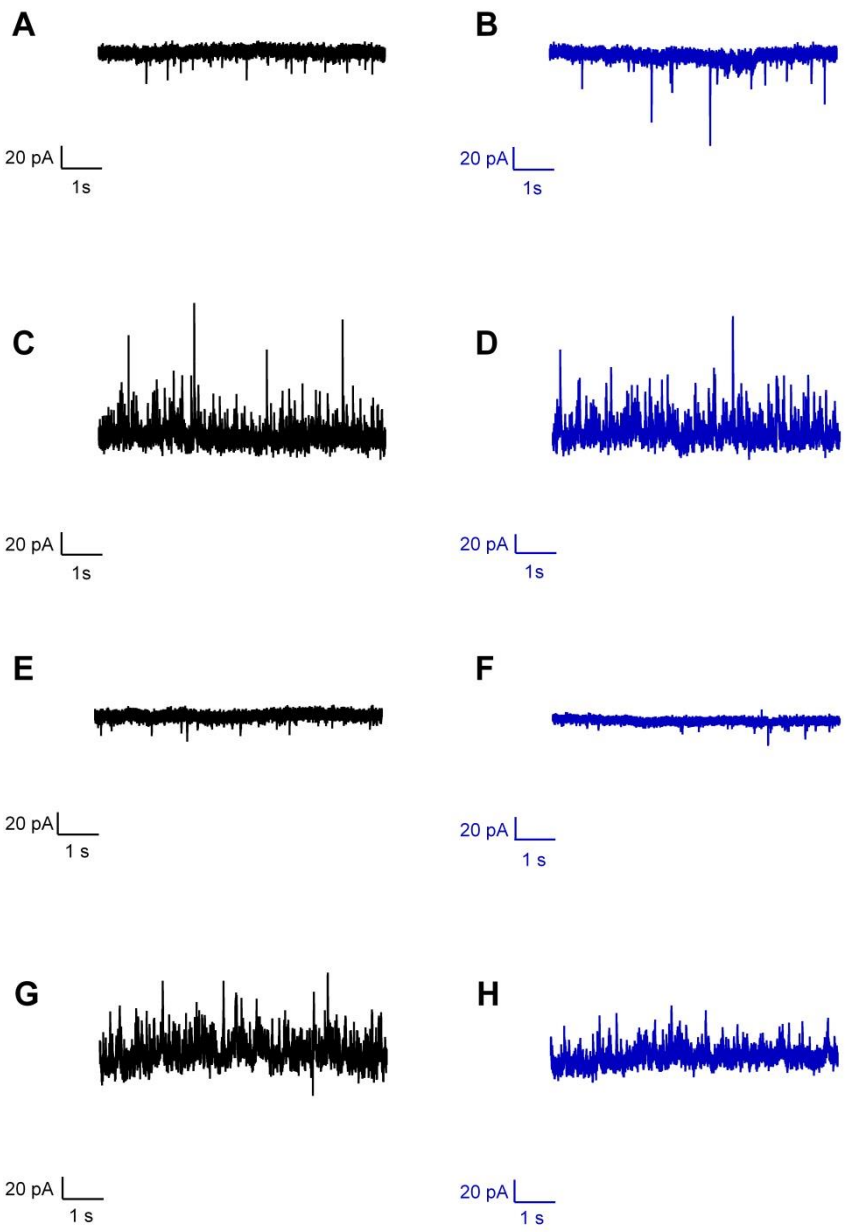

Figure 31 – P26-30 example traces from excitatory and inhibitory current recordings.

(A) WT sEPSC, (B) *Syngap*$^{+/GAP}$ sEPSC, (C) WT sIPSC, (D) *Syngap*$^{+/GAP}$ sIPSC, (E) WT mEPSC, (F) *Syngap*$^{+/GAP}$ mEPSC, (G) WT mIPSC, (H) *Syngap*$^{+/GAP}$ mIPSC.

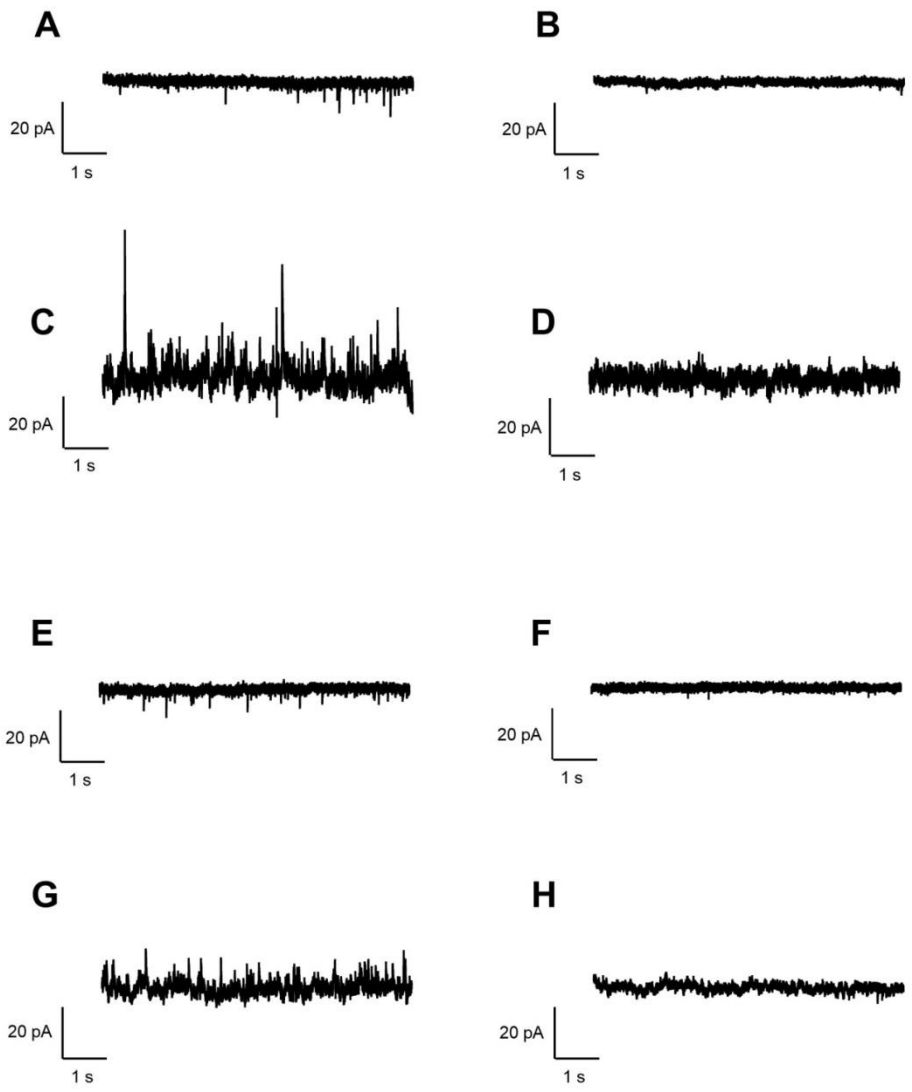

Figure 32 – The abolition of excitatory currents with CNQX and inhibitory currents with PTX in P26-30 recordings demonstrates they are mediated by AMPARs and GABARs respectively.

Application of 10 µM CNQX, abolishes the sEPSC and mEPSC currents demonstrating that they are AMPAR mediated (A) sEPSC no drug (B) sEPSC with CNQX, (E) mEPSC with TTX only, (F) mEPSC with TTX and CNQX.

Application of 50 µM PTX abolishes the sIPSC and mIPSC currents demonstrating that they are GABAR mediated (C) sIPSC no drug (D) sIPSC with PTX, (G) mIPSC with TTX only, (H) mIPSC with TTX and PTX.

The mean results were similar for the experiments conducted at P13-15 and P26-30, namely that there was no significant difference between sEPSC, sIPSC, mEPSC or mIPSC mean amplitude nor frequency between WT and Syngap+/GAP rats regardless of whether the unit of analysis was 'animal' (Figure 33 and Figure 36) or 'cell' (Figure 34 and Figure 37). The numbers in each group when collated by animal were however small and perhaps with larger sample sizes differences in sEPSC amplitude and frequency would have been seen between genotypes. The numbers of experimental subjects was low in some of the groups, particularly in WT sEPSC recordings at P26-30. This was due to discarding cells during post-hoc analysis as they did not meet the inclusion criteria (e.g. holding current, access resistance etc). This was an unfortunate limitation explored further in the discussion. The amplitudes of both genotypes showed the expected positively skewed distribution of excitatory (Bekkers et al. 1990; Cormier & Kelly 1996; McBain & Dingledine 1992; Wyllie et al. 1994) and inhibitory (Edwards et al. 1990; De Simoni et al. 2003) spontaneous and miniature events in both age groups (P13-15: Figure 34 and Figure 35 and P26-30: Figure 37 and Figure 38).

Examination of the cumulative frequency distributions of the P13-15 recordings revealed that the sEPSCs and mEPSCs from *Syngap*$^{+/GAP}$ rats tended to be larger amplitude and higher frequency events. In contrast, there was little difference in the cumulative frequency distributions of sIPSCs and mIPSCs between WT and *Syngap*$^{+/GAP}$ rats (Figure 35). Therefore the overall effect was of a shift towards excitation over inhibition in the CA1 pyramidal cells of *Syngap*$^{+/GAP}$ rats.

At P26-30 the cumulative frequency distributions show that the sEPSCs and mEPSCs from *Syngap*$^{+/GAP}$ rats still tended to be of larger amplitude, but tended to be slightly less frequent than in WTs (Figure 37). The distributions of sIPSCs and mIPSCs between WT and *Syngap*$^{+/GAP}$ rats showed much smaller differences as they had done in the younger animals (Figure 38). Therefore although it would be less marked than at P13-15, the overall effect would still be of a shift towards excitation over inhibition in the CA1 pyramidal cells of *Syngap*$^{+/GAP}$ rats at P26-30 as a change in either amplitude or frequency is sufficient to modify synaptic strength (Rumbaugh et al. 2006).

Many authors have published research suggestive of a shift to excitation in models of SynGAP haploinsufficiency (Vazquez et al. 2004; Rumbaugh et al. 2006; Clement et al. 2012; Clement et al. 2013; Wang 2013; Ozkan et al. 2014; Berryer et al. 2016) so whilst the mean data presented here is not necessarily in keeping with the literature, the trends in cumulative frequency data are.

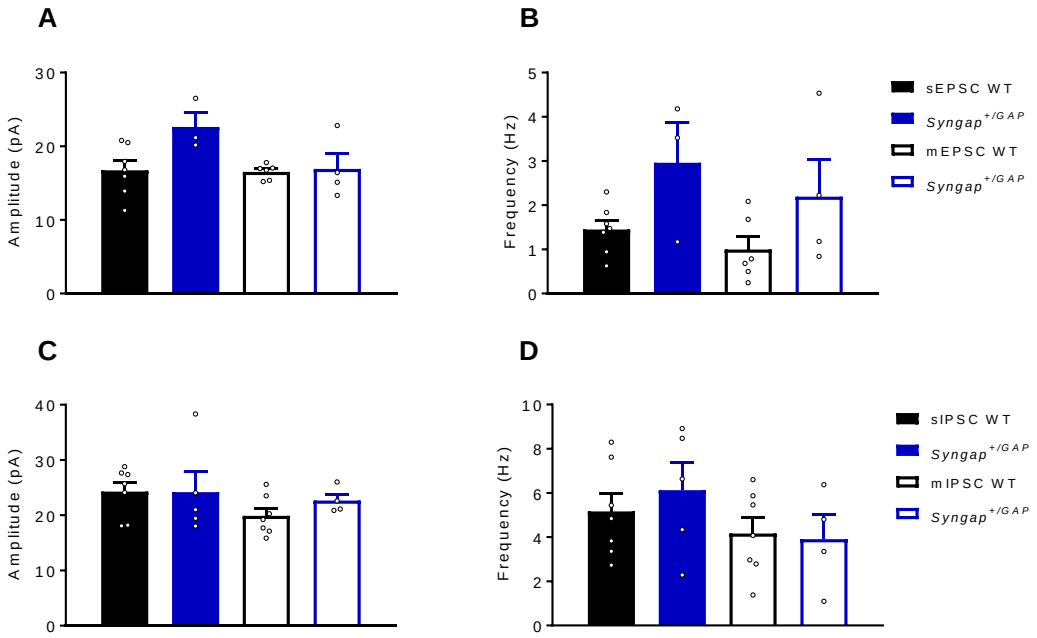

Figure 33 – At P13-15 the amplitude of excitatory and inhibitory currents are not significantly different between WT and *Syngap*$^{+/GAP}$ recordings when the unit of analysis is 'animal'.

(A) There is no significant difference in the sEPSC or mEPSC amplitude between WT and *Syngap*$^{+/GAP}$ hippocampal brain slices (WT sEPSC = 16.74 ± 1.29 pA n = 7, *Syngap*$^{+/GAP}$ sEPSC = 22.62 ± 1.97 pA n = 3, Mann-Whitney test p = 0.0667, WT mEPSC = 16.52 ± 0.42 pA n = 6, *Syngap*$^{+/GAP}$ mEPSC = 16.91 ± 2.07 pA n = 4, Mann-Whitney test p = 0.4762).

(B) There is no significant difference in the sEPSC or mEPSC frequency between WT and *Syngap*$^{+/GAP}$ hippocampal brain slices (WT sEPSC = 1.45 ± 0.21 Hz n = 7, *Syngap*$^{+/GAP}$ sEPSC = 2.96 ± 0.91 Hz n = 3, Mann-Whitney test p = 0.2667, WT mEPSC = 1.0 ± 0.29 Hz n = 6, *Syngap*$^{+/GAP}$ mEPSC = 2.19 ± 0.83 Hz n = 4, Mann-Whitney test p = 0.1143).

(C) There is no significant difference in sIPSC or mIPSC amplitude between WT and *Syngap*$^{+/GAP}$ hippocampal brain slices (WT sIPSC = 24.27 ± 1.68 pA n = 7, *Syngap*$^{+/GAP}$ sIPSC = 24.18 ± 3.68 pA n = 5, Mann-Whitney test p = 0.5303, WT mIPSC = 19.89 ± 1.34 pA n = 7, *Syngap*$^{+/GAP}$ mIPSC = 22.65 ± 1.19 pA n = 4, Mann-Whitney test p = 0.1636).

(D) There is no significant difference in sIPSC or mIPSC frequency between WT and *Syngap*$^{+/GAP}$ hippocampal brain slices (WT IPSC = 5.16 ± 0.80 Hz n = 7, *Syngap*$^{+/GAP}$ sIPSC = 6.13 ± 1.25 Hz n = 5, Mann-Whitney test p = 0.5303, WT mIPSC = 4.16 ± 0.72 Hz n = 7, *Syngap*$^{+/GAP}$ mIPSC = 3.90 ± 1.12 Hz n = 4, Mann-Whitney test p = 0.9273).

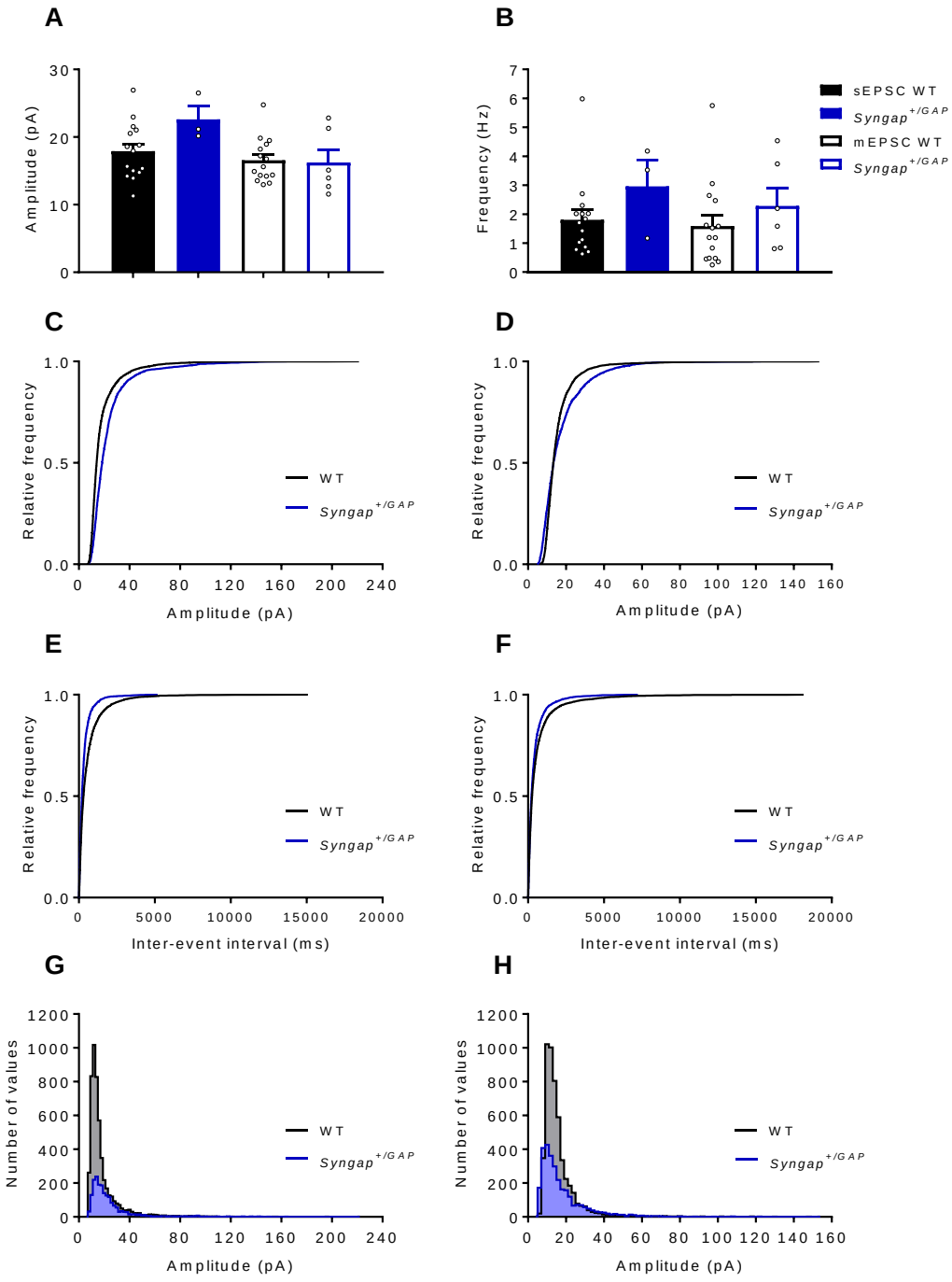

Figure 34 – At P13-15 there is a shift in the cumulative distributions of both sEPSCs and mEPSCs in *Syngap*$^{+/GAP}$ hippocampal slices towards larger amplitude and more frequent events.

Legend overleaf….

Figure 34 legend:

(A) There is no significant difference in the mean amplitude of excitatory recordings between WT and *Syngap*$^{+/GAP}$ hippocampal brain slices when the unit of analysis is n = cell (WT sEPSC = 17.91 ± 1.07 pA *n* = 15, *Syngap*$^{+/GAP}$ sEPSC = 22.62 ± 1.97 pA *n* = 3, Mann-Whitney test *p* = 0.1299, WT mEPSC = 16.56 ± 0.84 pA *n* = 15, *Syngap*$^{+/GAP}$ mEPSC = 16.23 ± 1.91 pA *n* = 6, Mann-Whitney test *p* = 0.6222).

(B) There is no significant difference in the mean frequency of excitatory recordings between WT and *Syngap*$^{+/GAP}$ hippocampal brain slices when the unit of analysis is n = cell (WT sEPSC = 1.81 ± 0.34 Hz *n* = 15, *Syngap*$^{+/GAP}$ sEPSC = 2.96 ± 0.91 Hz *n* = 3, Mann-Whitney test *p* = 0.2034, WT mEPSC = 1.59 ± 0.37 Hz *n* = 15, *Syngap*$^{+/GAP}$ mEPSC = 2.28 ± 0.63 Hz *n* = 6, Mann-Whitney test *p* = 0.3023).

(C), (D), (E) and (F) Cumulative frequency distributions of sEPSC amplitude, mEPSC amplitude, sEPSC inter-event interval, and mEPSC inter-event interval respectively.

(G) The frequency distributions of the pooled sEPSC amplitudes from WT and *Syngap*$^{+/GAP}$ recordings display the positive skew expected in spontaneous sEPSC recordings (WT median = 14.02, WT mean = 18.00 pA, *Syngap*$^{+/GAP}$ median = 18.33 pA, *Syngap*$^{+/GAP}$ mean = 23.25 pA).

(H) The frequency distributions of the pooled mEPSC amplitudes from WT and *Syngap*$^{+/GAP}$ recordings display the positive skew expected in mEPSC recordings (WT median = 13.35, WT mean = 15.68 pA, *Syngap*$^{+/GAP}$ median = 13.37 pA, *Syngap*$^{+/GAP}$ mean = 17.23 pA).

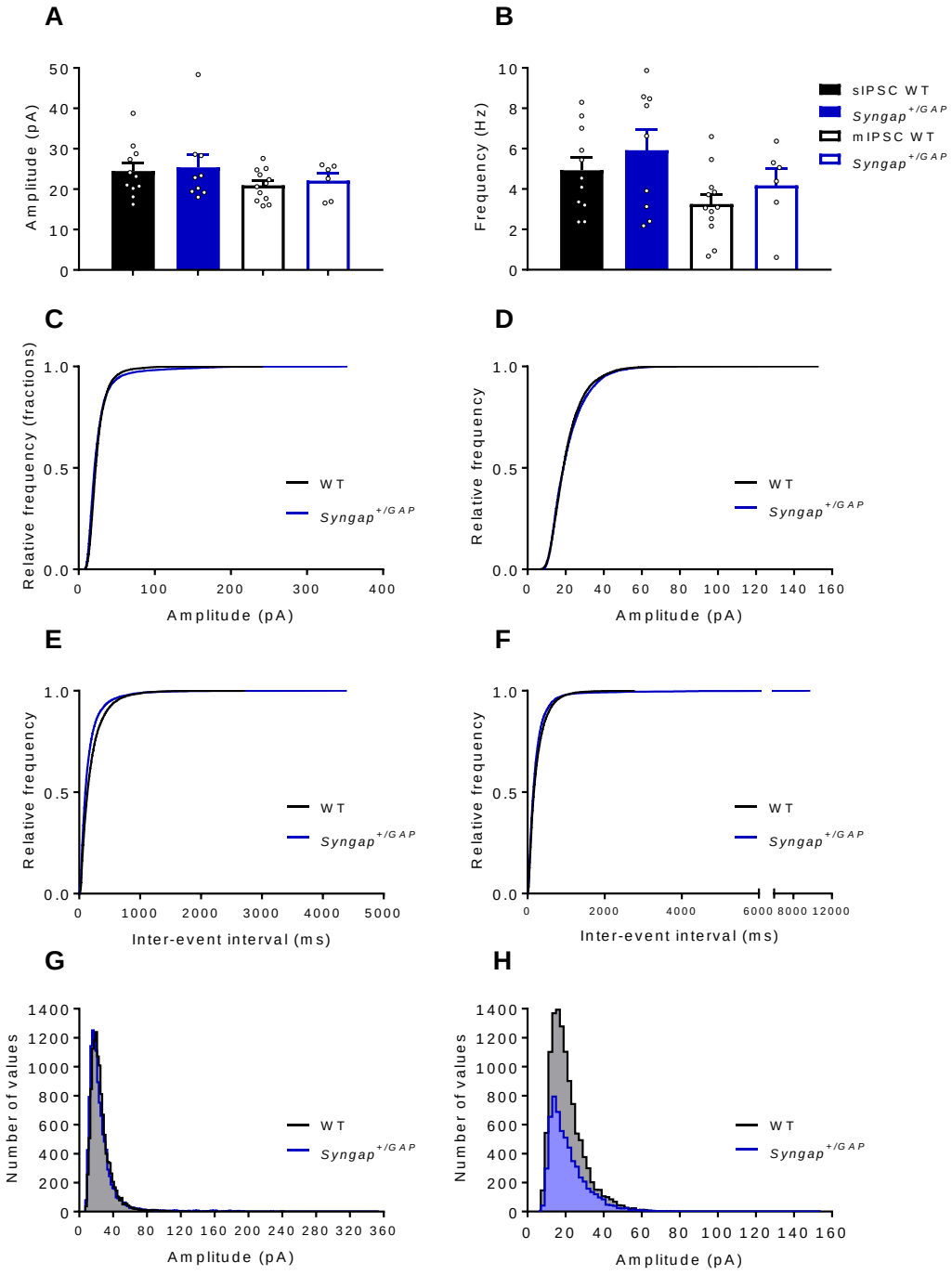

Figure 35 – At P13-15 the distributions of both sIPSCs and mIPSCs are similar between WT and *Syngap*$^{+/GAP}$ hippocampal slices.

Legend overleaf…

Figure 35 legend:

(A) There is no significant difference in the mean amplitude of inhibitory recordings between WT and *Syngap*$^{+/GAP}$ hippocampal brain slices when the unit of analysis is n = cell (WT sIPSC = 24.47 ± 1.97 pA n = 11, *Syngap*$^{+/GAP}$ sIPSC = 25.38 ± 3.14 pA n = 9, Mann-Whitney test p = 0.8238, WT mIPSC = 20.94 ± 1.11 pA n = 12, *Syngap*$^{+/GAP}$ mIPSC = 22.1 ± 1.76 pA n = 6, Mann-Whitney test p = 0.4936).

(B) There is no significant difference in the mean frequency of inhibitory recordings between WT and *Syngap*$^{+/GAP}$ hippocampal brain slices when the unit of analysis is n = cell (WT sIPSC = 4.93 ± 0.63 Hz *n* = 11, *Syngap*$^{+/GAP}$ sIPSC = 5.92 ± 1.01 Hz *n* = 9, Mann-Whitney test *p* = 0.2034, WT mIPSC = 1.6 ± 0.4 Hz *n* = 15, *Syngap*$^{+/GAP}$ mIPSC = 2.3 ± 0.6 Hz *n* = 6, Unpaired t test *p* = 0.3967).

(C), (D), (E) and (F) Cumulative frequency distributions of sIPSC amplitude, mIPSC amplitude, sIPSC inter-event interval, and mIPSC inter-event interval respectively.

(G) The frequency distributions of the pooled sIPSC amplitudes from WT and *Syngap*$^{+/GAP}$ recordings display the positive skew expected in spontaneous IPSC recordings (WT median = 22.36 pA, WT mean = 25.51 pA, *Syngap*$^{+/GAP}$ median = 20.82 pA, *Syngap*$^{+/GAP}$ mean = 21.8 pA).

(H) The frequency distributions of the pooled mIPSC amplitudes from WT and *Syngap*$^{+/GAP}$ recordings display the positive skew expected in mIPSC recordings (WT median = 18.73 pA, WT mean = 20.89 pA, *Syngap*$^{+/GAP}$ median = 18.81 pA, *Syngap*$^{+/GAP}$ mean = 21.32 pA). The apparent difference in numbers of values between genotypes simply reflects the fact that the number of WT cells recorded from was double that of *Syngap*$^{+/GAP}$cells (12 WT and 6 *Syngap*$^{+/GAP}$*)*.

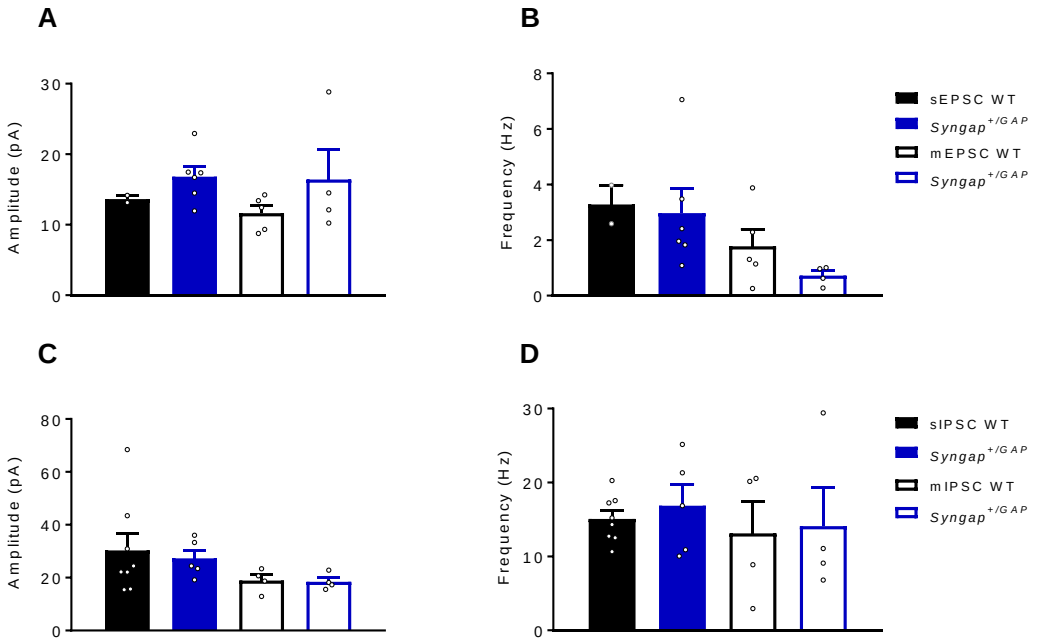

Figure 36 - At P26-30 the amplitude of excitatory and inhibitory currents is not significantly different between WT and *Syngap*$^{+/GAP}$ recordings when the unit of analysis is 'animal'.

(A) There is no significant difference in the mean amplitude of recordings between WT and *Syngap*$^{+/GAP}$ hippocampal brain slices (WT sEPSC = 13.64 ± 0.52 pA n = 2, *Syngap*$^{+/GAP}$ sEPSC = 16.82 ± 1.50 pA n = 6, Mann-Whitney test p = 0.2857, WT mEPSC = 11.64 ± 1.10 pA n = 5, *Syngap*$^{+/GAP}$ mEPSC = 16.42 ± 4.23 pA n = 4, Mann-Whitney test p = 0.4127).

(B) There is no significant difference in the frequency of sEPSC and mEPSC recordings between WT and *Syngap*$^{+/GAP}$ hippocampal brain slices (WT sEPSC = 3.28 ± 0.69 Hz n = 2, *Syngap*$^{+/GAP}$ sEPSC = 2.97 ± 0.88 Hz n = 6, Mann-Whitney test p = 0.4286, WT mEPSC = 1.77 ± 0.62 Hz n = 5, *Syngap*$^{+/GAP}$ mEPSC = 0.72 ± 0.17 Hz n = 4, Mann-Whitney test p = 0.1905).

(C) There is no significant difference in the amplitude of sIPSC and mIPSC recordings between WT and *Syngap*$^{+/GAP}$ hippocampal brain slices (WT sIPSC = 30.33 ± 6.31 pA n = 8, *Syngap*$^{+/GAP}$ sIPSC = 27.27 ± 3.18 pA n = 5, Mann-Whitney test p = 0.7242, WT mIPSC = 18.91 ± 2.22 pA n = 4, *Syngap*$^{+/GAP}$ mIPSC = 18.45 ± 1.55 pA n = 4, Mann-Whitney test p = 0.6857).

(D) There is no significant difference in the frequency of sIPSC and mIPSC recordings between WT and *Syngap*$^{+/GAP}$ hippocampal brain slices (WT sIPSC = 15.06 ± 1.20 Hz n = 8, *Syngap*$^{+/GAP}$ sIPSC = 16.86 ± 2.9 Hz n = 5, Mann-Whitney test p = 0.8329, WT mIPSC = 13.12 ± 4.34 Hz n = 4, *Syngap*$^{+/GAP}$ mIPSC = 14.10 ± 5.18 Hz n = 4, Mann-Whitney test p > 0.9999).

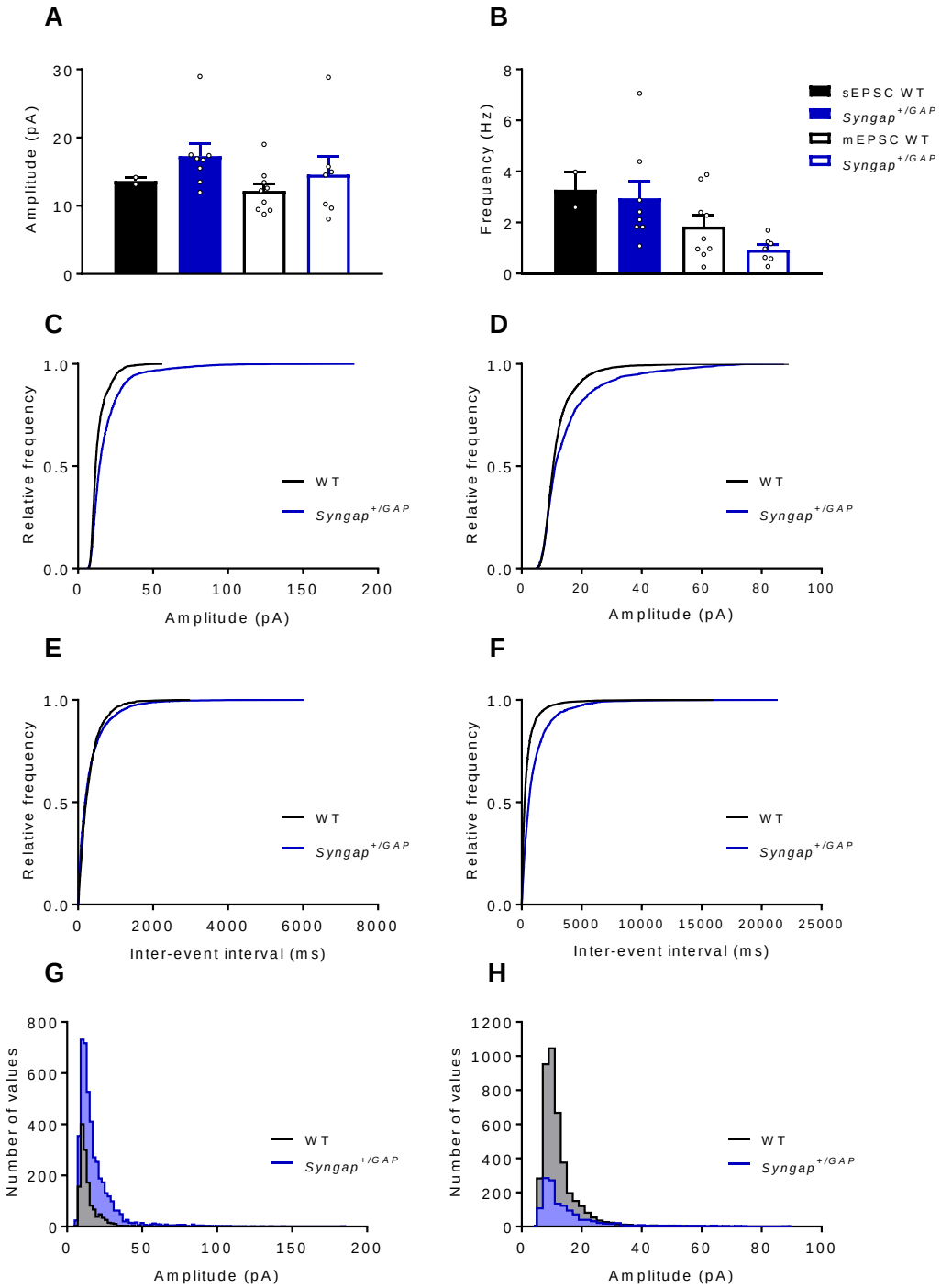

Figure 37 – At P26-30 there is a shift in the cumulative distributions of both sEPSCs and mEPSCs in *Syngap*$^{+/GAP}$ hippocampal slices towards larger but less frequent events.

Legend overleaf…

Figure 37 legend:

(A) There is no significant difference in the mean amplitude of excitatory recordings between WT and *Syngap*$^{+/GAP}$ hippocampal brain slices when the unit of analysis is n = cell (WT sEPSC = 13.64 ± 0.52 pA *n* = 2, *Syngap*$^{+/GAP}$ sEPSC = 17.29 ± 1.81 pA *n* = 8, Mann-Whitney test *p* = 0.2667, WT mEPSC = 12.19 ± 1.07 pA *n* = 9, *Syngap*$^{+/GAP}$ mEPSC = 14.57 ± 2.63 pA *n* = 7, Mann-Whitney test *p* = 0.4698).

(B) There is no significant difference in the mean frequency of excitatory recordings between WT and *Syngap*$^{+/GAP}$ hippocampal brain slices when the unit of analysis is n = cell (WT sEPSC = 3.28 ± 0.69 Hz *n* = 2, *Syngap*$^{+/GAP}$ sEPSC = 2.95 ± 0.68 Hz *n* = 8, Mann-Whitney test *p* = 0.5333, WT mEPSC = 1.84 ± 0.43 Hz *n* = 9, *Syngap*$^{+/GAP}$ mEPSC = 0.94 ± 0.18 Hz *n* = 7, Mann-Whitney test *p* = 0.2105).

(C), (D), (E) and (F) Cumulative frequency distributions of sEPSC amplitude, mEPSC amplitude, sEPSC inter-event interval, and mEPSC inter-event interval respectively.

(G) The frequency distributions of the pooled sEPSC amplitudes from WT and *Syngap*$^{+/GAP}$ recordings display the positive skew expected in spontaneous sEPSC recordings (WT median = 11.70 pA, WT mean = 13.69 pA, *Syngap*$^{+/GAP}$ median = 14.29 pA, *Syngap*$^{+/GAP}$ mean = 18.58 pA).

(H) The frequency distributions of the pooled mEPSC amplitudes from WT and *Syngap*$^{+/GAP}$ recordings display the positive skew expected in mEPSC recordings (WT median = 10.48 pA, WT mean = 12.13 pA, *Syngap*$^{+/GAP}$ median = 11.18 pA, *Syngap*$^{+/GAP}$ mean = 15.23 pA).

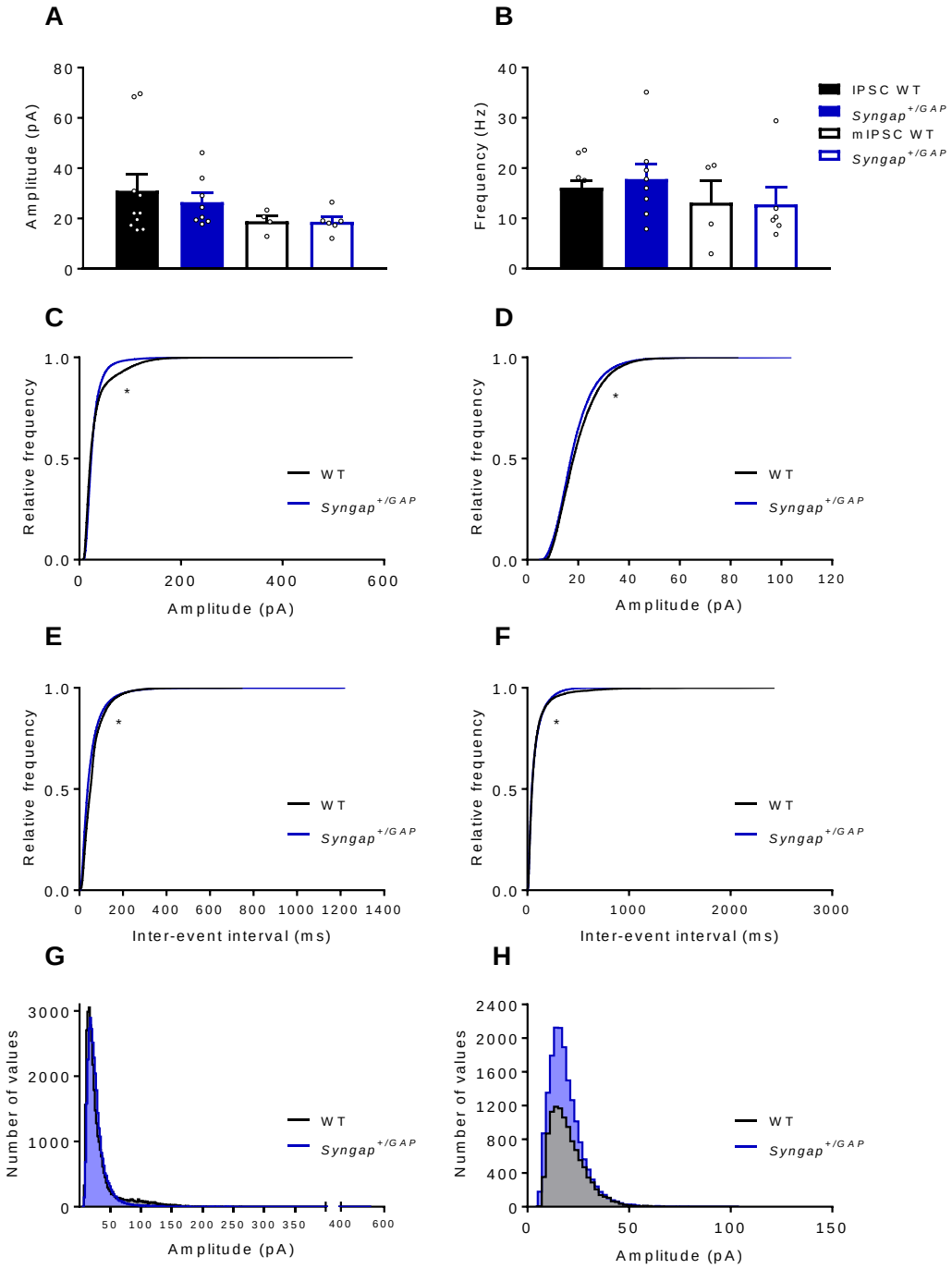

Figure 38 - At P26-30 the distributions of both sIPSCs and mIPSCs are similar between WT and *Syngap*$^{+/GAP}$ hippocampal slices.

Legend overleaf…

Figure 38 legend:

(A) There is no significant difference in the mean amplitude of inhibitory recordings between WT and *Syngap*$^{+/GAP}$ hippocampal brain slices when the unit of analysis is n = cell (WT sIPSC = 31.05 ± 6.54 pA n = 10, *Syngap*$^{+/GAP}$ sIPSC = 26.53 ± 3.56 pA n = 8, unpaired t test p = 0.5806, WT mIPSC = 18.91 ± 2.22 pA n = 4, *Syngap*$^{+/GAP}$ mIPSC = 18.69 ± 1.89 pA n = 6, Mann-Whitney test p = 0.7619).

(B) There is no significant difference in the mean frequency of inhibitory recordings between WT and *Syngap*$^{+/GAP}$ hippocampal brain slices when the unit of analysis is n = cell (WT sIPSC = 16.13 ± 1.39 Hz *n* = 10, *Syngap*$^{+/GAP}$ sIPSC = 17.82 ± 2.93 Hz *n* = 8, unpaired t test *p* = 0.5861, WT mIPSC = 13.12 ± 4.34 Hz *n* = 4, *Syngap*$^{+/GAP}$ mIPSC = 12.79 ± 3.40 Hz *n* = 6, unpaired t test *p* > 0.9999).

(C), (D), (E) and (F) Cumulative frequency distributions of sIPSC amplitude, mIPSC amplitude, sIPSC inter-event interval, and mIPSC inter-event interval respectively.

(G) The frequency distributions of the pooled sIPSC amplitudes from WT and *Syngap*$^{+/GAP}$ recordings display the positive skew expected in spontaneous sIPSC recordings (WT median = 21.81, WT mean = 32.02 pA, *Syngap*$^{+/GAP}$ median = 23.36 pA, *Syngap*$^{+/GAP}$ mean = 28.14 pA).

(H) The frequency distributions of the pooled mIPSC amplitudes from WT and *Syngap*$^{+/GAP}$ recordings display the positive skew expected in mIPSC recordings (WT median = 18.14, WT mean = 19.88 pA, *Syngap*$^{+/GAP}$ median = 17.14 pA, *Syngap*$^{+/GAP}$ mean = 18.73 pA).

4.3.5 GABAR/AMPAR and AMPAR/NMDAR recordings in acute hippocampal slices

Measurements of GABAR/AMPAR ratios were made in P26-30 hippocampal brain slices from WT and *Syngap*$^{+/GAP}$ rats by delivering 0.1 Hz current pulses every 6 seconds to the Schaffer collateral axons and recording 30 consecutive events at the chloride reversal potential and the AMPA reversal potential. Picrotoxin (100 μM) was then bath applied to block the $GABA_AR$ mediated responses as demonstrated in Figure 39, before 30 AMPAR mediated events were recorded at -70 mV and 30 NMDAR and AMPAR mixed events were recorded at +40 mV.

In a subset of cells the nature of the current at +40 mV was demonstrated by the application of 10 μM CNQX and 50 μM D-(-)-2-Amino-5-phosphonopentanoic acid (D-AP5), a selective NMDA receptor antagonist. The current was altered by the application of either drug alone and abolished by the application of both together showing the current is mediated by both AMPARs and NMDARs. In a further subset of cells, CNQX (10 μM) was applied during recordings at -70 mV in the presence of PTX which abolished the current confirming it was AMPAR mediated (Figure 39).

No significant differences were found between WT and *Syngap*$^{+/GAP}$ recordings when the GABAR charge transfer was divided by the AMPAR charge transfer to give the GABAR / AMPAR ratio. This was regardless of whether the unit of analysis was 'animal' or 'cell' (Figure 40). No significant differences were found in AMPAR/NMDAR ratio between genotypes either (Figure 40).

Alterations in AMPA / NMDA currents in SynGAP haploinsufficiency were identified at P14 in the *Syngap*$^{+/-}$ mouse hippocampus (Clement et al. 2012). However, this had resolved by 6 weeks of age. Given that synaptic transmission and mEPSC amplitude and frequency which were also increased at P14 had resolved by P21, it may be the case that a difference would've been evident in the AMPA/ NMDA ratio in the SynGAP_GAP deletion rats at a younger age.

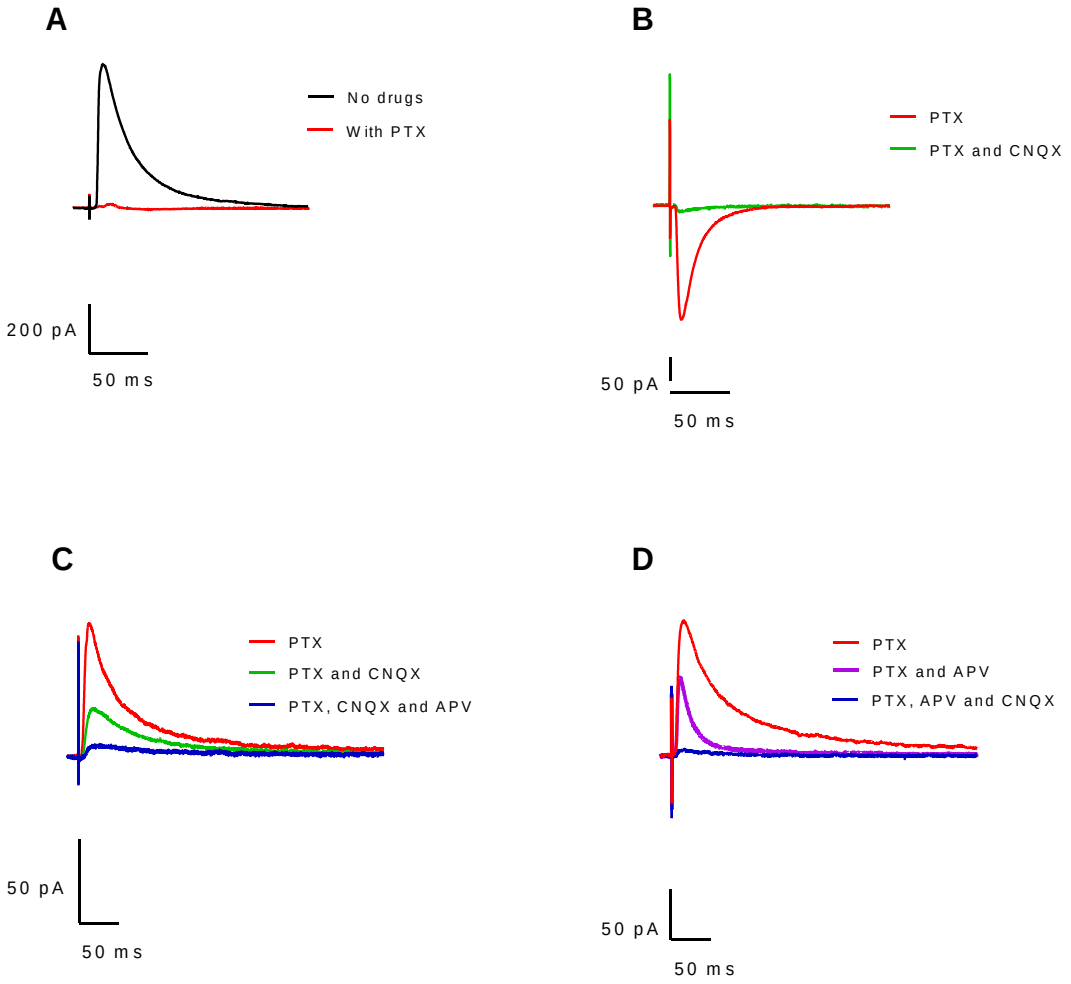

Figure 39 – The pharmacological modification of the currents recorded in GABAR / AMPAR and AMPAR / NMDAR experiments demonstrates the receptors that mediate the currents.

(A) Application of 75-100 µM PTX during a recording at the AMPA reversal potential (100 µM PTX applied at +14mV in this case) abolishes the current. This demonstrates that responses recorded at the AMPA reversal potential were $GABA_AR$ mediated.

(B) Application of 10 µM CNQX to a recording at -70mV in the presence of PTX abolishes the current. This demonstrates responses recorded at -70mV in the presence of PTX are AMPAR mediated.

(C) and (D) The current at +40 mV is both AMPAR and NMDAR mediated as demonstrated by the application (in the presence of PTX) of 10 µM CNQX and 50 µM D-APV singly and in combination. Applying either drug alone in the presence of PTX changes the waveform, but only in the presence of both is the current abolished.

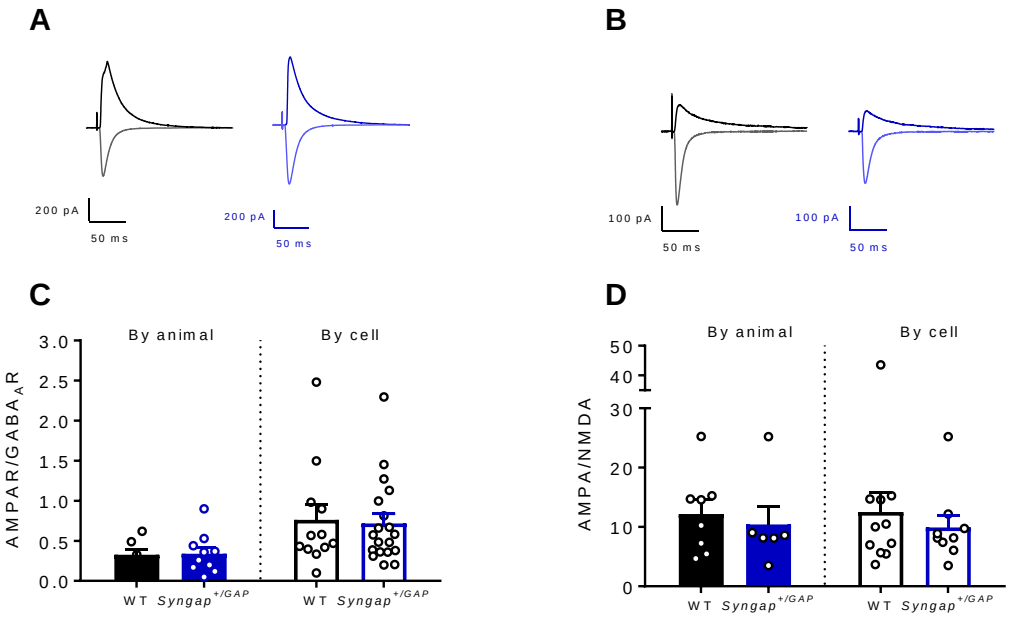

Figure 40 - There is no difference in AMPA / $GABA_A$ and AMPA / NMDA receptor ratios in P26-30 rats when the unit of analysis is 'animal'.

(A) WT (black) and *Syngap*$^{+/GAP}$ (blue) GABA : AMPA example traces.

(B) WT (black) and *Syngap*$^{+/GAP}$ (blue) AMPA : NMDA example traces.

(C) AMPA receptor to $GABA_A$ receptor ratio was unchanged in *Syngap*$^{+/GAP}$ rats compared to WT rats when analysed by animal (WT = 0.3271 ± 0.06372 *n* = 7, *Syngap*$^{+/GAP}$ = 0.34 ± 0.07806 *n* = 10, Mann-Whitney test *p* = 0.9811) and by cell (WT = 0.7622 ± 0.1886 *n* = 12, *Syngap*$^{+/GAP}$ = 0.7156 ± 0.1199 *n* = 19, Mann-Whitney test *p* = 0.9776).

(D) AMPA receptor to NMDA receptor ratio was also unchanged in *Syngap*$^{+/GAP}$ rats compared to WT rats when analysed by animal (WT = 12.18 ± 2.398 *n* = 8, *Syngap*$^{+/GAP}$ = 10.44 ± 3.069 *n* = 6, Mann-Whitney test *p* =0.5481) and by cell (WT = 12.51 ± 3.333 *n* = 11, *Syngap*$^{+/GAP}$ = 9.920 ± 2.071 *n* = 9, Mann-Whitney test *p* = 0.7463).

4.4 Discussion

This body of work presents the first comprehensive analysis of cellular and synaptic electrophysiological properties in SynGAP_GAP deletion rats. Somewhat surprisingly, the predicted protein synthesis independent exaggeration in hippocampal mGluR LTD was not observed despite this being a strong phenotype in similar *Syngap*$^{+/-}$ mouse experiments. Furthermore, the hypothesis that there would be a shift towards excitation in electrophysiological measurements was unsubstantiated by mean data, but the cumulative distributions of excitatory and inhibitory currents pointed in the direction of excitation as predicted.

On examination of CA1 pyramidal cells, no significance differences were seen between WT and *Syngap*$^{+/GAP}$ recordings of passive cellular properties or action potential properties (when analysed by n = animal). Although dentate gyrus cells and Layer 2/3 pyramidal neurons have been shown to be hyperexcitable in *Syngap*$^{+/-}$ mice neurons, systematic evaluation of the properties of CA1 pyramidal neurons in models of SynGAP have not been presented before. The current data suggests that in this brain region at P13-15 and P26-30, there is no distinct cellular phenotype. As no overt anatomical, developmental or behavioural differences were noted between WT and *Syngap*$^{+/GAP}$ rats, it is perhaps reasonable to expect that any cellular phenotype would be relatively mild as gross changes in the functions of individual cells could severely and noticeably impact on the functioning of the rat as a whole. The lack of difference between genotypes may also be a function of the age ranges at which recordings were made as the previous hyperexcitability identified in the *Syngap*$^{+/-}$ hippocampus (albeit in the dentate gyrus) was noted at P8-9 but had resolved by P14 (Clement et al. 2012). The influence of experimental age is discussed in full below.

Although on examination of the synaptic function in these rats no differences were seen in GABAR/ AMPAR or AMPAR/ NMDAR ratios or in the mean amplitude or frequency of excitatory or inhibitory currents, there was a shift in the cumulative distributions of excitatory currents suggestive of an imbalance between excitation and inhibition in favour of excitation. It is possible that with higher experimental numbers a difference between genotypes would've been delineated. This is in

keeping with evidence in the literature suggestive of increased excitation in SynGAP haploinsufficiency (Vazquez et al. 2004; Rumbaugh et al. 2006; Clement et al. 2012; Clement et al. 2013; Wang et al. 2013). However my finding that the frequency of mEPSCs from cultured *Syngap*$^{+/GAP}$ rat CA1 pyramidal neurons was reduced is at odds with this.

To explore the validity of the data and consider why certain experiments gave unexpected results it is helpful to consider two categories of variable. The first is variables that may be common to every experiment, namely experimental model, gender, background rat strain, experimental age and sample size. The second are the factors that are relevant to particular experiments only.

4.4.1 Common variables

Experimental model

The SynGAP rat is different from previous SynGAP mouse studies because the mutant allele still results in translation of a truncated form of SynGAP, whereas the mutant allele in two of the most extensively studied mouse models is fully knocked out resulting in no protein production (initial papers using these models were by Vazquez et al. 2004; Rumbaugh et al. 2006). The mouse designed by Kim and colleagues (Kim et al. 2003) does have low levels of SynGAP remaining (as described in paragraph 3.2.1), but there are fewer publications pertaining to it. When attempting direct comparison between the current work and previous publications this difference in model should therefore be born in mind.

When considering the lack of exaggerated hippocampal mGluR LTD in the *Syngap*$^{+/GAP}$ rats compared to the findings of Barnes et al. 2015, could it be that the remaining 'mutant' SynGAP in heterozygous rats is sufficient to mediate an indistinguishable level of LTD from WT rats? This seems unlikely as the rats lack the portion of the SynGAP gene that codes for the protein's enzymatic GAP domain which is thought to influence LTD by regulating both Ras and Rap (Chen et al. 1998; Kim et al. 1998; Krapivinsky et al. 2004; Walkup et al. 2015). Ras and Rap in turn modulate the surface expression of AMPARs (Zhu et al. 2002; Zhu et al. 2005;

Derkach et al. 2007), a reduction in which leads to LTD (Carroll et al. 1999; Lüscher et al. 1999; Luthi et al. 1999; Man et al. 2000; Xiao et al. 2001; Snyder et al. 2001). Furthermore, the degree of LTD has been shown to correlate with mEPSC amplitude and frequency in the hippocampus (Zhang et al. 2005) and increased mEPSC amplitude has been shown to be due to enhanced by incorporation of the GluR2-lacking type of AMPAR into the cell membrane (Wang et al. 2013). Therefore the results in *Syngap*$^{+/GAP}$ rats are puzzling as not only would loss of the GAP domain be predicted to result in the increased LTD seen by Barnes et al. which isn't seen in the *Syngap*$^{+/GAP}$ rats, the assumption would be that AMPAR currents would be increased as was seen in *Syngap*$^{-/-}$ mouse mEPSC amplitude (Vazquez et al. 2004) and frequency (Vazquez et al. 2004; Rumbaugh et al. 2006). The decrease in mEPSC frequency in *Syngap*$^{+/GAP}$ rat recordings found in this body of work (Figure 29) is more in keeping with overexpression of SynGAP (Rumbaugh et al. 2006) and the lack of difference in the mean amplitude and frequency of AMPAR mediated sEPSCs, mEPSCs or AMPAR / NMDAR ratios in *Syngap*$^{+/GAP}$ rat hippocampal slices was also not as predicted. Could this mean that despite the deletion of the coding region for the GAP domain, there is somehow sufficient GAP function in the SynGAP_GAP deletion rat for SynGAP to fulfil its role as a brake on downstream pathways? This would seem to be highly unlikely and would still not explain the reduced frequency of mEPSCs from *Syngap*$^{+/GAP}$ rats. A GTPase assay to assess GAP activity would establish whether there is residual GAP activity in *Syngap*$^{+/GAP}$ and *Syngap*$^{GAP/GAP}$ rats.

Compensatory Mechanisms

In genetically altered models it is possible that compensatory mechanisms have developed to counteract the negative impact of the genetic mutation. This could in theory result in a balancing of function so that for example, electrophysiological recordings do not reveal a difference between genotypes. However, exaggerated mGluR LTD and alterations in excitatory and inhibitory currents have been identified in mouse models of *Syngap* haploinsufficiency as described. There is no obvious reason to explain why genetically modified rats would achieve equilibrium in function through compensatory mechanisms when genetically modified mice did not. Comparing the results found in transgenic animals with models of acute knockdown

of SynGAP is one way of exploring compensatory mechanisms further. When this was done in mice it was found that siRNA disruption of the SynGAP protein after synaptogenesis produced the same phenotypes of an increase in mEPSC frequency and increased ERK pathway activation as was seen in transgenic *Syngap*$^{-/-}$ mouse cultures (Rumbaugh et al. 2006). Furthermore, the increase seen in dentate gyrus AMPAR / NMDAR ratio in heterozygous SynGAP mice was recapitulated by acute knockdown of SynGAP at postnatal day 1 in a Cre LoxP conditional mouse, but not in adult mice (Clement et al. 2012). This suggests these are direct effects of the loss of SynGAP and not related to compensatory mechanisms. Interestingly though, significantly lower levels of phosphorylated p38 found in Syngap$^{-/-}$ cultured mouse neurons when synaptic activity had been blocked weren't replicated by siRNA knockdown of SynGAP (Rumbaugh et al. 2006). It is possible that this is due to compensatory mechanisms leading to the phenotype in the transgenic mice. Acute knockdown experiments could be planned in the SynGAP_GAP deletion rats to investigate the role of compensatory mechanisms further.

Sex differences

Both male and female animals were used in the SynGAP_GAP deletion rat experiments despite some evidence in the literature of differences in hippocampal function between male and female rats. Most of the reported gender differences have been in adult rats (Maren 1995; Yang et al. 2004; Oberlander & Woolley 2016) which were not examined in this current body of SynGAP work. The exception was the paper by Maren et al. which found greater perforant path - dentate gyrus LTP and burst depolarisation in male rats in adult and pre-pubescent animals (35 days) in comparison with younger animals (Maren et al. 1994). This was not seen in female rats. This suggests there may be gender specifics differences in hippocampal function just a few days later than recordings were made in the current experiments (the latest being P30). However there is no published literature of gender differences in hippocampal function at the age ranges used in this thesis (P13-15 and P26-30).

It is reasonable to expect that hormonal changes at puberty might mark the beginning of a greater divergence between male and female function and so knowing when puberty is in Long-Evans Hooded rats could be important when considering the

SynGAP rat data. Papers use different methods to indicate puberty onset in female rats. Ojeda & Skinner 2006 used first ovulation as a marker which they stated occurs in most laboratory rat stocks between P35 and P45. This time window is in keeping with reports using vaginal opening as a marker of puberty onset (Kakeyama et al. 2008; Hovey et al. 2011). However there are studies showing earlier vaginal opening (Keeley et al. 2015; Stanko et al. 2016) including one with mean vaginal opening at 30.6 days in Long-Evans rats (Gray et al. 1997). Keeley et al. 2015 showed that puberty in Long-Evans male rats was later (between 35 and 40 days). This data suggest it is unlikely that even the older animals in the SynGAP experiments (P26-30) were pubertal and so subjected to surges in hormones that could potentially results in differences between the genders. Furthermore, when the LTD data was analysed by gender there was no significant difference between males and females (WT male = 79.0 ± 3.6% n = 10, WT female = 77.2 ± 6.6% n = 2 *Syngap*$^{+/GAP}$ male = 74.4 ± 3.8% n = 15, *Syngap*$^{+/GAP}$ female = 70.2 ± 7.4% n = 4; Kruskal Wallis test p = 0.6960, Dunn's multiple comparisons test showed no significant differences). This interpretation does require some caution though given small numbers of females. The other experimental datasets in this thesis included fewer animals and so the validity of sub-dividing the results by gender would have been dubious and so has not been done.

It is important to note when considering the current results in the context of published research, that the use of both male and female animals has been common in the SynGAP electrophysiology research community (Rumbaugh et al. 2006; Clement et al. 2012; Clement et al. 2013; Ozkan et al. 2014; Berryer et al. 2016). Reassuringly, gender specific data has generally not been presented as the authors found no significant difference between males and females. The exception is a small reduction in mEPSC amplitude in parvalbumin positive interneurons found only in male mice (Ozkan et al. 2014). Therefore I do not believe the use of both male and female SynGAP rats has significantly impacted on the observations made in this thesis.

Background strain

Background strain has been recognised as a potential influence in rodent hippocampal experiments for many years (Manahan-Vaughan 2000; Nguyen et al. 2000; Bowden et al. 2012; Kamal et al. 2014). With regards to rodent LTD in particular, certain low frequency stimulation protocols that induce LTD in some strains (Wistar and Sprague-Dawley) don't result in LTD in Lister-Hooded rats (Manahan-Vaughan 2000). When considering this in relation to the current *Syngap*$^{+/GAP}$ WT Long-Evans hooded rat LTD experiments, it is a notable advantage to be able to compare the results to the previously published LTD experiments carried out in our laboratory with very similar protocols and equipment (Till et al. 2015). The most notable difference between the experiments was the background strain of the rats, as those used by Till and colleagues were Sprague-Dawley animals rather than the Long-Evans Hooded strain of the SynGAP_GAP deletion rats. It is therefore interesting that Till and colleagues present a mean value of 78.64 ± 3.7% for LTD in WT rats which is very similar to the 78.7 ± 3.1% found in the WT animals from the SynGAP rat colony. However Till et al. found that in contrast to the SynGAP_GAP Deletion WT rats (but in keeping with Barnes and colleague's *Syngap*$^{+/-}$ mouse data), LTD was not maintained in WT animals in the presence of protein synthesis inhibition by cycloheximide. This suggests that the protein synthesis dependence may somehow relate to the background strain of the rats. However, published data has shown the same loss of LTD maintenance in the presence of protein synthesis inhibitors in WT Long-Evans Hooded rats at a similar age P21-30 (Huber et al. 2000) suggesting background strain is not to blame. The explanation may therefore be specific to the Long-Evans hooded strain of rats used in the SynGAP colony as it has been noted that variability can occur within a given strain when different breeding practices have been followed (Kacew & Festing 1996).

Further examination of LTD in different rat strains is therefore warranted before firm conclusions can be drawn about the influence of the SynGAP_GAP Deletion mutation on LTD and in particular, its dependence on new protein synthesis.

Experimental age

The age at which some of the experiments in this thesis were conducted may have affected the likelihood of revealing certain phenotypes given the pattern of results seen in the literature. WT SynGAP expression in the mouse is known to increase from early in life and peak around P7 (Porter et al. 2005) to P14 (Clement et al. 2012; McMahon et al. 2012) and I have shown in this thesis that levels of SynGAP protein also increased during the first month of life in SynGAP_GAP Deletion (Figure 15). This suggests SynGAP may play a particularly critical role during development. Supporting this idea is the fact that many of the electrophysiological phenotypes in the *Syngap*$^{+/-}$ mouse were identified during the first two weeks of life and later resolved (Clement et al. 2012; Clement et al. 2013; Ozkan et al. 2014). For example, in the hippocampus the significant differences in heterozygous mice were mostly at P14 (increased mEPSC amplitude and frequency, synaptic transmission and AMPAR/ NMDAR ratio) and had resolved by P21 (Clement et al. 2012). In keeping with this was the absence of alterations in NMDAR or AMPAR mediated currents in 14 – 20 week old *Syngap*$^{+/-}$ mice (Komiyama et al. 2002). As noted above, acute knockdown experiments have shown mixed results, but interestingly in an adult Cre LoxP conditional mouse acute SynGAP knockdown did not show the increased AMPAR / NMDAR ratios seen after knockdown at P1 (although did reveal increased intrinsic excitability in dentate gyrus neurons) (Clement et al. 2012) and induced global haploinsufficiency in mature animals using a conditional knockout SynGAP mouse line resulted in no change in mEPSC amplitude or frequency in Layer 2/3 pyramidal neurons or in measures of animal behaviour (Ozkan et al. 2014). This adds weight to the idea of SynGAP acting mainly during development, but some electrophysiological differences have been identified in older *Syngap*$^{+/-}$ mice. These are comprised of a decrease in adult hippocampal mEPSC amplitude and increased frequency following acute *SynGAP1* deletion in a Cre LoxP mouse model (Muhia et al. 2012), an increase in mPFC mEPSC amplitude and frequency in *Syngap*$^{+/-}$ mice > 9 weeks of age and a decrease in the firing of parvalbumin positive cells at 6 weeks of age (Ozkan et al. 2014).

In the present rat work, hippocampal slice experiments were conducted at P13-15 and P26-30 which should have allowed observations of early phenotypes that then

resolve to be made. The exceptions to this were the LTD experiments (as the age range for them was chosen based on the corresponding mouse literature) and the GABAR/AMPAR and AMPAR/NMDA ratios. It would therefore certainly be informative to explore the AMPAR/NMDA ratios in particular at the P13-15 in the SynGAP_GAP deletion rats with the hypothesis that they would be increased in *Syngap*$^{+/GAP}$ rats.

Sample size and variability

The size of the final datasets in the SynGAP_GAP deletion rat experiments suffered due to the number of recordings that had to be discarded post-hoc for not meeting inclusion criteria (e.g. resting membrane potential, holding current etc.) and so being potentially indicative of unhealthy or unstable cells/ tissue. This was compounded at times by a lack of available animals due to insufficient pregnancies (despite breeding pairs being set up) or maternal cannibalism of litters early in life.

I am aware from personal correspondence with researchers working with SynGAP mice and from (Guo et al. 2009) that breeding can be difficult depending on the background strain of the animals and so it is possible that this might be a factor in the SynGAP rat colony, but cannot be confirmed without a comparable genetic mutation on another rat background strain. It is also possible that for some as yet unidentified reason, mutation in the SynGAP protein has an adverse effect on breeding in rats. However it did not appear on informal observation that *Syngap*$^{+/GAP}$ dams had more difficulty conceiving, carrying pups to term or levels of cannibalism than their WT counterparts. Over the course of the experiments in this thesis, other animals housed with the SynGAP rat colony also went through periods of failing to breed well which was suggestive of an unidentified environmental effect within the animal house.

These factors have resulted in sample sizes in this thesis that are smaller than would be ideal statistically. As described in the methods section normality tests were used in an attempt to standardise the analysis. However with $n \leq 7$, the GraphPad Prism Software is unable to perform normality tests and in such cases non-parametric

analysis was used to try and prevent over-interpretation of the data. Furthermore, as the Statistics Guide within GraphPad Prism notes, normality tests are less powerful with small sample sizes so even though when it was mathematically possible to conduct one, it may not have helpful.

On the face of it, this appears to be a limitation, but many of the datasets in this thesis were expected to have non-Gaussian distributions e.g. mEPSCs, sEPSCs, sIPSCs, mIPSCs etc. so non-parametric analysis could be appropriate. In this thesis, parametric analysis was however used when a normality test was passed which is in keeping with the use of parametric analysis in the SynGAP literature (Vazquez et al. 2004; Rumbaugh et al. 2006; Clement et al. 2012; Clement et al. 2013; Ozkan et al. 2014).

The variability within samples in the SynGAP_GAP deletion rat experiments presented could also be statistically problematic as the standard error of the mean (SEM) within each group is often markedly different in a given dataset. To give just one example, the data for the mEPSC recordings from SynGAP rat brain cultures shows a difference in SEM of nearly 7 fold (WT SEM = 1.44 Hz, $Syngap^{GAP/GAP}$ = SEM 0.21 Hz). One of the premises of parametric t-tests is that the data points are sampled from populations of equal variance. Furthermore non-parametric Mann-Whitney test tests determine if the distribution of ranks is different (which it may well be if the variance is different), so the unequal variances may make the interpretation of results here more difficult. Larger sample sizes and transformation of datasets e.g. log transformation could help to address this in future experiments.

4.4.2 Discussion of the results and variables relevant to specific experiments

4.4.2.1 Hippocampal mGluR LTD Experiments

Due to the number and complexity of variables that may have specifically impacted on the LTD experiments, they are presented here under sub-headings for clarity.

Experimental setup

The finding of no significant difference in long-term depression between WT and *Syngap*$^{+/GAP}$ rats was somewhat surprising given the robust exaggeration in LTD found in *Syngap*$^{+/-}$ mice by Barnes et al. 2015. The explanation is unlikely to lie in the equipment used as the recordings were made on the same electrophysiological rigs (albeit with a change of amplifier) with the same experimental set up and with the aid of Dr Adam Jackson who was the third author on the Barnes paper. There was a slight difference in the age of the animals (P25-32 in the mice and P26-30 in the rats), but the external and internal solutions used (prior to the addition of drugs) were identical and the temperature was very similar (31 ± 1°C in the rat experiments vs 30°C with the mice), as was the flow rate (3-5 ml / min in the rat experiments vs 4 ml / min with the mice).

A higher concentration of DHPG (100 μM vs 50 μM) was used in the rat experiments due to personal correspondence from Dr Adam Jackson that this resulted in more reliable induction of LTD in other rat LTD recordings. This is in keeping with the known dose response effect of DHPG in rats (Huber et al. 2001).

The use of picrotoxin

One potentially more significant difference was the fact that Barnes and colleagues bathed their slices in 50 μM picrotoxin during their recordings, which was not done in the SynGAP rat experiments. This was because inhibitory blockade was not felt to be necessary in the rats to elicit fEPSPs to record from. Palmer et al. 1997 found that DHPG induced hippocampal LTD was facilitated (both the number of successful inductions of LTD and the magnitude of the depression) using picrotoxin. However this was not observed when comparing the magnitude of LTD in the WT SynGAP rat experiments to that in the WT mice in Barnes' paper (78.9% in the rat and 77% in the mouse), but caution is required when comparing directly across species as other authors have reported differences even when experimental protocols are identical (Huber et al. 2002) so this may be a species issue.

Palmer et al. 1997 also found that in the presence of picrotoxin, the NMDA receptor antagonist AP5 had little effect on LTD induction or magnitude whereas in conditions where the amount of Ca^{2+} entering the cell was more reliant on NMDA receptors (e.g. in Mg^{2+} free medium) AP5 significantly reduced LTD. This therefore suggested that in the presence of picrotoxin, a NMDA independent mechanism was working. However, for this to explain the lack of significant difference in LTD magnitude in the *Syngap*$^{+/GAP}$ rat versus mouse experiments, a difference in NMDA LTD function would be needed between genotypes and between species. Carlisle et al. 2008 noted reduced NMDA induced LTD in *Syngap*$^{+/-}$ mice, but only in a high calcium solution which doesn't apply to the current experiments. Huber et al. 2002 did find differences in NMDA mediated LTD between species, but her results showed a greater LTD magnitude in WT rats over mice which is contrary to the SynGAP findings. Therefore it seems unlikely that the absence of picrotoxin resulting in altered LTD mechanism is the explanation for lack of LTD phenotype in the rats.

Choice of protein synthesis inhibitor

Cycloheximide was the drug used to inhibit protein synthesis in the SynGAP rat LTD experiments rather than anisomycin which Barnes et al. 2015 used, but the two mechanisms of action are very similar as both drugs bind to the large 60S subunit of the ribosome and inhibit translation. Specifically, anisomycin binds to the 60S t-RNA A-Site and inhibits the binding of the aminoacyl-tRNA molecules (t-RNA bound to an amino acid molecule) whereas cycloheximide disrupts the protein synthesis further downstream by binding to the 60S t-RNA E-site stalling the ribosome during ongoing translation (Garreau De Loubresse et al. 2014; Rodnina & Wintermeyer 2016). There is no obvious reason why this minor difference in action would result in a lack of dependence on new protein synthesis in the WT rats.

Sample Size

Power calculations for the LTD experiments based on the *Syngap*$^{+/-}$ mouse LTD data (Barnes et al. 2015) indicated a group size of 13 would be required for a power of 0.8 and with a significance level of 0.05. The data presented here did not quite reach this

threshold in both experimental groups (WT n = 19, *Syngap*$^{+/GAP}$ n = 12) and so the experiment was slightly underpowered for the heterozygous animals, but it seems unlikely that one extra animal in the Syngap group would have changed the result as the LTD for that hypothetical extra animal would've had to have been particularly exaggerated. Only 6 animals were needed per genotype to reach statistical significance for the protein synthesis experiments. The data from the SynGAP rats came from 8 WT and 7 heterozygotes indicating statistical significance was not an issue.

Summary

Although there are several factors that could potentially have resulted in the unexpected LTD and protein synthesis results in the *Syngap*$^{+/GAP}$ rats in addition to the common variables described in section 4.4.1, the background strain of the rats appears to be particularly important. Although it does not obviously explain the lack of statistically exaggerated LTD in heterozygotes compared with WT, it would seem to be behind the unexpected result in WT rat protein synthesis experiments. Therefore if the underlying mechanisms for LTD are somehow mediated differently by this particular Long-Evan Hooded rat strain, interpretation of the added effect of a SynGAP mutation is extremely difficult. Further experiments to compare and contrast LTD in these rats with LTD in other WT rat strains will be required to definitively investigate this. Furthermore, it may be informative to specifically quantify new protein synthesis following the application of DHPG as basal protein synthesis was shown to be elevated in *Syngap*$^{+/-}$ mice (Barnes et al. 2015).

4.4.2.2 Intrinsic cell properties and action potential properties

There is a paucity of published evidence of intrinsic properties in models of SynGAP haploinsufficiency. To date the notable findings in *Syngap*$^{+/-}$ mice have been greater excitability of dentate gyrus neurons compared to WT mice at P8-9, (Clement et al. 2012) a reduction in layer 2/3 parvalbumin positive interneuron firing at 6 weeks of age (Ozkan et al. 2014) and an increase in action potential width in Layer 2/3 somatostatin positive interneurons in adult mice (Ozkan et al. 2014). Therefore it isn't possible to directly compare the parameters measured in the current CA1 pyramidal cell SynGAP_GAP deletion rat recordings with those in the literature.

However, when considering the quality of recordings and data obtained, it is helpful to compare the WT values with other published data. Although papers publish slightly different parameters, Table 9 and Table 10 enable at least some comparison between the WT data from the current experiments with published rat CA1 pyramidal data. For some values estimates have by necessity, been taken from graphed data as the raw values are not presented. The variability in some of the parameters across the published data is notable and comparison limited by different experimental factors (age, background strain etc.), but generally the current data is in keeping with the range of values seen in the literature which suggests the cells were a) hippocampal pyramidal neurons and b) reasonably healthy. Membrane time constant was the notable exception as it was shorter in the current experiments and the reasons for this are unclear as changes in other parameters e.g. action potential per current sweep might have been expected to be seen in tandem with a shorter membrane time constant. The method used to define the time constant (single mono-exponential curve fitting using appropriate software) is a recognised method, but identifying the point at which the curve plateaued in order to set the parameters for the curve fitting was done by eye. This could therefore represent an experimenter error. As capacitance was calculated by dividing the membrane time constant by the input resistance, it is not surprising that the capacitance values are also low compared to the literature. Changes in capacitance can of course reflect differences in cell size, but given the potential methodological difficulties with calculation of capacitance here, no comment can be made on cell size.

Table 9 – WT passive cell properties from the current SynGAP rat experiments is in keeping with published WT rat hippocampal slice data

Study	Experimental details	Resting membrane potential (mV)	Input resistance (MΩ)	Membrane time constant (ms)	Sag % (ratio)	Capacitance (pF) #
WT rats from SynGAP colony	**P13-15 both genders, HHS**	**-59.73**	**111.4**	**15.81**	**6.85 (0.93)**	**153.8**
WT rats from SynGAP colony	**P26-30 both genders, HHS**	**-62.81**	**63.3**	**12.31**	**4.32 (0.96)**	**194.2**
Baraban & Schwartzkroin 1995	P25-35, both genders, SD, HHS or THS	-61.7	49.4	30.1	Not given	609.3117
Staff et al. 2000	2-9 week old, Wistar, THS (gender not given)	-66.2	119.8	40	(0.79)	333.8898
Thibault et al. 2001	3-5 month old, male, Fischer, THS	-58.7	58.9	Not given	Not given	
Gu et al. 2007	4-7 week old, male, Wistar, THS	-68.2	40.7	Not given	Not given	
Kaczorowski et al. 2007	P14-28, male Wistar, THS	-60	72	Not given	(0.76)	
Routh & Johnston 2009	5-7 week old , male, SD, HHS	-64.6	65.6	22.4	Estimated (0.91)	341.4634
Malik & Chattarji 2011	P36, male SD, THS	-64.8	100.6	27.9	Only given in voltage	277.336
Graves 2013	P21-28, males from Charles River (strain not given), THS	-65.8 RS 66.2 BS	55 RS 33.7 BS	Not given	0.84 RS 0.74 BS	

SD = Sprague-Dawley, HHS = horizontal hippocampal slices, THS = transverse hippocampal slices RS = regular spiking, BS = burst spiking, 'Estimated' = estimated from graphed data in the published paper as no exact values given, #values from published studies calculated from membrane time constant / input resistance

Table 10 – WT action potential properties from the current SynGAP rat experiments are in keeping with published WT rat hippocampal slice data

Study	Experimental Details	Threshold (mV)	Peak amplitude (mV)	Rheobase (pA)	Half width (ms)	Maximum rise rate (mV / ms)	Maximum decay rate (mV / ms)
WT rats from SynGAP colony	**P13-15, both genders, HHS**	**-43.12 WT**	**72.35 WT**	**123.1 WT**	**1.48 WT**	**220.1 WT**	**-64.97 WT**
WT rats from SynGAP colony	**P26-30 both genders, HHS**	**-44.37 WT**	**76.79 WT**	**193.3 WT**	**0.96 WT**	**345.3 WT**	**-104.9 WT**
Baraban & Schwartzkroin 1995	P25-35, both genders, SD, HHS or THS	Not given	71.0	Not given	Not given	Not given	Not given
Staff et al. 2000	2-9 week old, Wistar, THS (gender not given)	-46.3	112	213	0.95	381	-94.8
Thibault et al. 2001	3-5 month, male, Fischer, THS	Not given	83.8	151	Not given	Not given	Not given
Kaczorowski et al. 2007	P14-28, male Wistar, THS	-53	103	1249	Not given	Not given	Not given
Routh & Johnston 2009	5-7 week old, male SD, HHS	-48 estimated	90.5 estimated	Not given	0.9 estimated	400 estimated	Not given
Chu et al. 2010	2-3 week old, male SD, THS	-39.2	96.3	122	1.2	Not given	Not given
Malik & Chattarji 2011	P36, male SD, THS	-51.5 (where reached -40mV/mS)	120.1	700	1.6	420	Not given

SD = Sprague-Dawley, HHS = horizontal hippocampal slices, THS = transverse hippocampal slices RS = regular spiking, BS = burst spiking, 'Estimated' = estimated from graphed data in the published paper as no exact values given

Baseline voltage

During intrinsic cell property experiments, cells were mistakenly been held at -70 pA rather than -70 mV. Therefore, in order to improve the homogeneity of the data, cells with a baseline voltage more positive than -64 mV or more negative than -76 mV were excluded. A more strict exclusion limit would have severely reduced the number of cells that could be included in the analysis. Hence the passive and action potential property data is acknowledged to come with the caveat that some cells were held at a potential 12 mV more negative than others. The level to which some conductances are active or inactive may therefore differ between recordings and so potentially influence the data. Ideally the experiments would therefore be repeated with all cells maintained at -70 mV.

4.4.2.3 mEPSC recordings in homozygous SynGAP rat hippocampal cultures

Vazquez et al showed in 2004 that at DIV 10, mEPSCs in hippocampal neurons had significantly larger amplitudes and frequency in *Syngap*$^{-/-}$ mice, than in WT mice. In 2006, Rumbaugh and colleagues compared AMPA mEPSC recordings from WT and *Syngap*$^{-/-}$ mouse forebrain neuronal cultures (between DIV 12-19) and also found a significant increase in the frequency of mEPSCs in homozygous mice, but no change in amplitude. In homozygous neurons which had been transfected with GFP tagged SynGAP (Cα1 isoform), the mEPSC frequency was rescued to WT levels, whereas the amplitude was decreased to lower levels than that seen in WT cultures (Rumbaugh et al. 2006).

However, in unpublished work from our laboratory, Aoife McMahon did not find a significant difference in mEPSC amplitude or frequency between WT and Syngap$^{-/-}$ mouse cultured cortical and hippocampal cells at DIV 9-11 and 13-14. Nor did she find any alterations in AMPAR or NMDAR mediated currents. Clearly the finding of a decrease in mEPSC frequency in the *Syngap*$^{+/GAP}$ rat cultures is at odds with these previous results. Presented below is a discussion of the factors which could explain the current findings.

Culture health

The cultured neurons looked healthy when compared informally with other culture plates. Recordings were typically discarded if the holding current dropped below -100 pA. Furthermore, portions of each trace during which the access resistance was found to have exceeded 30 MΩ or varied by more than 20% were discarded. Traces with less than 4 minutes of recording remaining were also discarded. These measures should therefore have excluded unstable recordings which might indicate poor cell health.

Were the currents recorded typical of mEPSCs?

As Figure 29 shows the mEPSCs recorded were the expected asymmetric shape with a positive skew in their amplitude distribution (Bekkers et al. 1990; McBain & Dingledine 1992; Wyllie et al. 1994). The mean amplitude and frequency of WT recordings in this thesis (15.5 pA and 2.54 Hz) are in keeping with the published literature on mEPSC amplitude (11 -15 pA) and frequency (0.2 – 2.5 Hz) in rat culture or slice recordings (Turrigiano et al. 1998; De Simoni et al. 2003; Zhang et al. 2005; Sutton et al. 2006). Therefore I am confident that true mEPSCs were recorded.

Research protocol

The protocols for preparation of the cultured *Syngap*$^{GAP/GAP}$ hippocampal neurons in this thesis and the *Syngap*$^{-/-}$ of Vazquez et al. 2004 and Rumbaugh et al. 2006 (who took their method from a previous study - Banker & Cowan 1977) are compared in Table 11.

The *Syngap*$^{GAP/GAP}$ rat protocol is more similar to that of Vazquez et al. and yet despite the methodological differences between Vazquez et al. and Rumbaugh et al. (e.g. brain region, age at culture preparation and recording, plating density, and solution composition) it is the work of these two published studies that shows the same phenotype. This suggests that the methodological differences across all three bodies of work do not explain the different phenotype seen in the *Syngap*$^{GAP/GAP}$ rats.

Unlike the SynGAP rat experiments, the other authors did not add AraC (which blocks glial cell proliferation) to their cultures. AraC has been shown to increase neuronal damage in the presence of glutamate and kill post-mitotic neurons with an EC_{50} of 50 µm (Martin et al. 1990; Ahlemeyer et al. 2003). However, no exogenous glutamate was added to the cultures in the SynGAP rat experiments and the concentration of 1 µM AraC used was not toxic to neurons in the Martin et al. paper. Therefore it seems unlikely that the addition of AraC itself would explain the difference in phenotype between the SynGAP rat experiments and previous studies.

Rumbaugh et al. specifically encouraged glial growth with glia conditioned media so it could be postulated that the absence of glia was important in their finding of increased mEPSC frequency. However Vazquez et al. published similar results and they included B27 in their culture medium which has been shown to result in near absence of glial cells (Brewer et al. 1993). Therefore I am confident that the difference in phenotype seen in the SynGAP rat cultures is not because of a lack of glia.

Table 11 – A comparison of *Syngap*$^{GAP/GAP}$ and *Syngap*$^{-/-}$ hippocampal culture preparation

Study	Species	Brain region	Age at preparation	Medium components	Density of plating (mm^2)*	Age at recording (Days in Vitro)	Was glial proliferation blocked?	External recording solution (mM)	Internal recording solution
SynGAP Rats	Rat	Hippocampus	E18	Neurobasal medium, B27, L-glutamine and penicillin/ streptomycin solution	250	13-15	Yes with AraC	150 NaCl, 3 KCl, 10 HEPES, 2.5 $CaCl_2$, 1.3 $MgCl_2$, 10 Glucose, 0.05 Glycine, 0.0005 TTX, 0.05 PTX pH 7.3	130 Cs Gluconate, 10 CsCl, 10 HEPES, 0.1 EGTA, 10 glucose, 10 Na phosphocreatine, 4 MgATP, 0.5 Na_3GTP. pH 7.3
Vazquez et al. 2004	Mouse	Hippocampus	E16-17	Neurobasal medium, B27, glutamate, and glutamax-I	200	9-10	No	145 NaCl, 5 KCl, 5 HEPES, 2 $CaCl_2$, 0.5 $MgCl_2$, 10 Glucose 0.0005 TTX, 0.03 PTX pH 7.4	145 K gluconate, 10 KCl, 5 NaCl, 2 $MgCl_2$, 0.1 $CaCl_2$, 5 EGTA, 5 HEPES, 2 ATP. pH 7.2
Rumbaugh et al. 2006	Mouse	Forebrain	P1	Neurobasal media, equine serum, B27, glutamax and pen/strep	357	12-19	No, fed with glia conditioned media twice a week	150 NaCl, 3.1 KCl, 10 HEPES, 2 $CaCl_2$, 1 $MgCl_2$, 0.1 APV, 0.005 strychnine, 0.1 PTX, and 0.001 TTX pH 7.3–7.4	135 Cs-MeSO4, 10 CsCl, 10 Hepes, 5 EGTA, 2 $MgCl_2$,4 Na-ATP, 0.1 Na-GTP. pH 7.2

*Information regarding dish surface area to enable calculation of density taken from https://www.thermofisher.com/uk/en/home/references/gibco-cell-culture-basics/cell-culture-protocols/cell-culture-useful-numbers.html

4.4.2.4 Excitatory – Inhibitory Balance Experiments

Although the mean values for spontaneous and miniature excitatory and inhibitory currents were not significantly different between genotypes in the SynGAP_GAP deletion rat colony, there was a trend towards increased excitation over inhibition which is in keeping with published data.

The factors which may have influenced the recordings are inevitably similar to those presented for intrinsic cell properties and mEPSCs in culture and so some repetition is required when considering why there was no definite shift towards excitation as had been hypothesised.

Is the WT data in keeping with the published literature?

Table 12 presents data from the small number of published studies with spontaneous and miniature current data in WT rat hippocampal slices alongside the data recorded in WT SynGAP_GAP Deletion colony rats. The relative lack of studies for comparison is problematic especially as they differ in experimental age and background strain in particular and not all studies publish the same parameters. Furthermore, estimates of mean values are sometimes by necessity, again taken from graphed data as the raw values are not presented. Only two studies documenting spontaneous sEPSC amplitude were found and although their values differed widely, the current SynGAP data reassuringly fell between the two. sEPSC frequency was also in keeping with the literature. Only one study with sIPSC amplitude was identified which had markedly higher amplitudes than that found in the SynGAP rat experiments. The sIPSC frequency found in the SynGAP rat colony at P13-15 was in keeping with published studies, but the frequency at P26-30 was substantially higher in the SynGAP rat colony dataset. mEPSC data and mIPSC amplitude was consistent with the wider body of research, but the mIPSC frequencies found in the SynGAP rat colony were higher. None of the published studies made recordings in Long-Evans Hooded rats though so it is impossible to delineate whether these differences relate to this or other experimental procedures.

In the absence of easily comparable literature, is therefore reassuring that the events recorded had asymmetric appearances and fast rise times as would be expected. Furthermore the cumulative frequency distributions show the expected positive skew (Edwards et al. 1990; Bekkers et al. 1990; Cormier & Kelly 1996; McBain & Dingledine 1992; Wyllie et al. 1994; De Simoni et al. 2003).

Recording procedure

Similar to other experiments, recordings were typically excluded if the holding potential was > 100 pA, if the access resistance was above >30 MΩ or if it varied by more than 30%. This should have removed unstable recordings that might be indicative of poor cell / slice health. Furthermore, caesium gluconate was included in the internal solution to try to maximise the voltage clamp.

The protocol allowed for the sequential recording of sEPSCs, mEPSCs, sIPSCs and mIPSCs from each cell, although in practice for any given cell it was rare for the recording from all 4 current types to meet the inclusion criteria described above. It was also relatively common for cells to die before reaching the end of mIPSC recordings (or earlier). By the time mIPSC recording was reached, the recording had been underway for a considerable time and so it is possible that the health of the cell may have been poorer compared to that at the start of the recording. As described, having thresholds for acceptable ranges of access resistance and holding potential attempted to mitigate this.

On examination of the variance in recordings (Table 13), the standard error of the mean (SEM) for sIPSC and mIPSC recordings was typically higher than that of the sEPSCs and mEPSCs. As the example traces shown in Figure 30 and Figure 31 illustrate, the inhibitory current recordings were somewhat noisier than their excitatory counterparts, particularly at P26-30 where the frequency of inhibitory events is higher. This may have contributed to the variability in the datasets for sIPSC and mIPSCs as distinguishing true from erroneous events is more difficult in the presence of noise. This noise is likely due to low level background interference from NMDA receptor activity at 0 mV. If future recordings were to be made, the

excitatory and inhibitory currents could be recorded from different slices. Not only would this reduce the length of time a cell was subject to recording procedures (a maximum of 29 minutes in the current experiments), it would allow the pharmacological isolation of excitatory and inhibitory currents i.e. excitatory recordings could be done in the presence of picrotoxin to block $GABA_AR$ and inhibitory in the presence of CNQX and AP5 to block AMPAR and NMDAR. This would be particularly advantageous for reducing the noise and potentially the variability in inhibitory recordings.

Preliminary experiments were conducted to time the wash in of the bath applied drugs against the noticeable change in the recording trace that would signify that the drug was taking effect. Hence 4 minutes was chosen as sufficient time for drug wash in, but this is a rather crude method, particularly for establishing if spontaneous activity has been blocked by TTX. It is possible that 4 minutes may have been insufficient and so this would have meant there was potentially a mix of spontaneous and true miniature events in the early stages of mEPSC and mIPSC recordings. Making spontaneous and miniature recordings from separate slices so would overcome this difficulty as the slices for miniature recordings could be bathed in TTX throughout the experiment.

Table 12 – The current SynGAP rat WT excitatory and inhibitory current data is in keeping with the published literature

Study	Experimental Details	sEPSC Amp (Freq)	sIPSC Amp (Freq)	mEPSC Amp (Freq)	mIPSC Amp (Freq)
SynGAP Rats	**P13-15**	**16.74 (1.45)**	**24.27 (5.16)**	**16.52 (1.0)**	**19.89 (4.16)**
SynGAP Rats	**P26-30**	**13.64 (3.28)**	**30.33 (15.06)**	**11.64 (1.77)**	**18.91 (15.05)**
Hershkowitz et al. 1993	P16-23 SD, THS	11.9 (0.22)		13.2pA (0.33)	
De Simoni et al. 2003	Various ages, male SD	(1.5 at P14) (5.6 at P21)		Estimated P14: 8 pA (0.1) Estimated P21: 6.5 pA (0.2)	Estimated P14: 19.5 pA (1) Estimated P21:17 pA (2.75)
Zhang et al. 2005	2-3 week old Wistar rats, coronal HS			11.54 (0.093)	
Parfitt & Madison 1993	200-300g SD rats, slice orientation not given			9 pA (range 0.8-5)	
Malik & Chattarji 2011	P36, male SD, THS			22.4 (0.28)	
Pitler & Alger 1992	200-300g, male SD rats, slice orientation not given		Median = 150 to 200 pA range (2.8-8 Hz estimated depending on internal $Ca2^{+}$)		
Karlsson et al. 2011	P14-40, both genders, Wistar, THS	(1.9)	(3.5)		
Katchman et al. 1994	P21-28 SD rats, THS				22.6 (0.42 estimated)
Tian et al. 2012	P18-21, male SD, THS	34.60 pA (0.65)		25.49 pA (0.77)	

Amp = amplitude (in pA), Freq = frequency (in Hz), SD = Sprague Dawley, THS = transverse hippocampal slice, 'Estimated' = estimated from graphed data in the published paper as no exact values given

Sample Size

Could the lack of shift in mean excitation / inhibition be because the experiment was underpowered? As this is the first exploration of SynGAP mutation in a rat, directly comparable data were not available to conduct a power calculation prior to recording. When examining the SynGAP _GAP deletion data post-hoc using the power calculation and sample size software at http://biomath.info/power/ttest.htm, it was possible to assess how small a difference between the means could be identified for an significance level of 0.05 and power 0.8. As Table 13 reveals, only three of the observed differences (P13-15 sEPSC amplitude and frequency and P26-30 sEPSC amplitude) were larger than the minimum detectable difference between WT and *Syngap*$^{+/GAP}$ means. There was also a wide range in sample size for different recordings from n = 2 to n = 8 due to post-hoc discarding of cells that did not meet the inclusion criteria. It is therefore possible that the present body of work is underpowered meaning a larger sample size may have shown a statistical difference between the excitatory and inhibitory currents across the two genotypes. However, given the often large differences in standard error of the mean between the WT and *Syngap*$^{+/GAP}$ data and the non-Gaussian distribution of the data, drawing definitive conclusions from the use of such calculations is questionable. This is because standard power calculations assume that the data is a) normally distributed and b) sampled from populations with similar variance, neither of which is the case in the current dataset. The huge variation in the numbers of animals needed per group going forward if this current data is used for a power calculation likely reflects this. Clearly it is not ethical or practical to be using hundreds or thousands of animals per group, but it is possible that future datasets might be less variable for example if excitatory and inhibitory currents were recorded separately as discussed above. Smaller sample sizes would therefore be needed to achieve a robust level of statistical power.

If the variance in the *Syngap*$^{+/GAP}$ data was consistently in the same direction compared to WT rats, this might be informative, but the direction of variation changes from dataset to dataset; for some, WT data is more variable and for others

Syngap$^{+/GAP}$ data is more variable. The variance does not therefore appear to be related to the SynGAP mutation.

Finally, it is worthy of note that it had been hoped that a comparison of action potential bursts from CA3 could be made between genotypes during the recordings; hence CA3 was left intact when the hippocampal slices were prepared. However, bursting only occurred in two WT recordings at P13-15 (one sEPSC and one sIPSC) plus three WT recordings (one sEPSC and two sIPSC) and one *Syngap*$^{+/GAP}$ (sEPSC) at P26-30 (Figure 41). Therefore the very small number of cells in which it was seen prevented any formal analysis of this. This lack of bursting may relate to the extent to which the preparation of hippocampal slices damages CA3 cell dendritic arbours (Li et al. 1994). The absence of bursting in cells bathed in TTX was reassuring as the drug's action potential blocking effect should preclude any action potential driven activity.

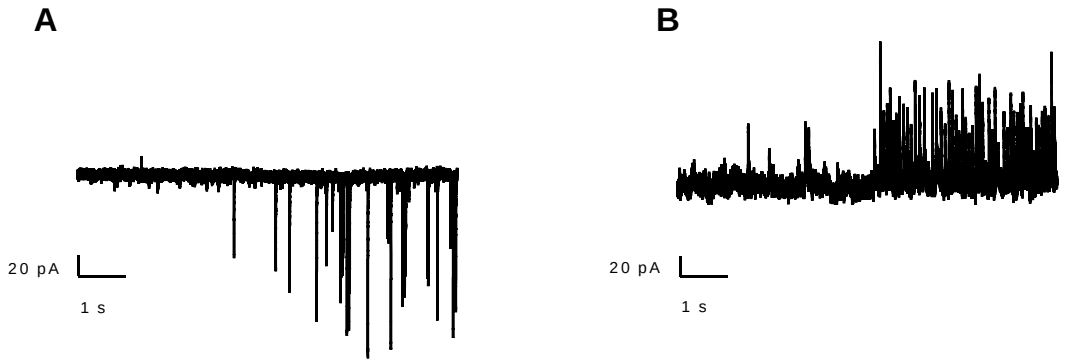

Figure 41 - Examples of sEPSC and sIPSC recordings discarded due to recurrent electrical activity from CA3.

Example of the onset of bursting activity in (A) a sEPSC and (B) a sIPSC trace.

Table 13 – Size of detectable difference in excitatory and inhibitory current amplitude and frequency and future sample size calculations based on the current SynGAP rat data

Parameter	WT SEM and (sample size)	*Syngap*$^{+/GAP}$ SEM and (sample size)	Size of statistically detectable difference between groups*	Size of observed difference in means between groups	Sample Size (n) required per group if current data is used for power calculation
P13-15 sEPSC Amp (pA)	1.29 (7)	1.97 (3)	5.5	5.88	7
P13-15 sEPSC Freq (Hz)	0.21 (7)	0.91 (3)	0.91	1.51	<6
P13-15 mEPSC Amp (pA)	0.42 (6)	2.07 (4)	1.8	0.39	111
P13-15 mEPSC Freq (Hz)	0.29 (6)	0.83 (4)	1.3	1.19	7
P13-15 sIPSC Amp (pA)	1.68 (7)	3.68 (5)	7.2	0.09	38218
P13-15 sIPSC Freq (Hz)	0.8 (7)	1.25 (5)	3.4	0.97	77
P13-15 mIPSC Amp (pA)	1.34 (7)	1.19 (4)	5.7	2.74	28
P13-15 mIPSC Freq (Hz)	0.72 (7)	1.12 (4)	3.1	0.26	840
P26-30 sEPSC Amp (pA)	0.52 (2)	1.5 (6)	2.9	3.18*	<6
P26-30 sEPSC Freq (Hz)	0.69 (2)	0.88 (6)	3.9	0.31	158
P26-30 mEPSC Amp (pA)	1.1 (5)	4.23 (4)	4.9	4.78	6
P26-30 mEPSC Freq (Hz)	0.62 (5)	0.17 (4)	2.8	1.05	29
P26-30 sIPSC Amp (pA)	6.31 (8)	3.18 (5)	27	3.06	536
P26-30 sIPSC Freq (Hz)	1.2 (8)	2.9 (5)	5.1	1.8	57
P26-30 mIPSC Amp (pA)	2.22 (4)	1.55 (4)	10	0.46	1464
P26-30 mIPSC Freq (Hz)	3.88 (4)	5.18 (4)	18	0.95	1049

Amp = amplitude, Freq = frequency, SEM = standard error of the mean, SD = standard deviation
*calculated using http://biomath.info/power/ttest.htm

4.4.2.5 AMPAR / $GABA_AR$ and AMPAR / NMDAR data

AMPAR / $GABA_AR$ and AMPAR / NMDAR ratios were calculated from CA1 pyramidal cells recordings between the ages of P26-30 as a further measure of excitatory / inhibition. As with other datasets, the research protocols were designed to ensure only healthy, stable recordings were included by discarding cells if the access resistance was >30 MΩ or if it varied by more than 20% during the recording. Care was taken to identify clean monosynaptic evoked responses to reduce the likelihood of recording a mixed current response. The relevant reversal potentials were carefully identified too so that at the chloride reversal potential all negatively deflecting events were AMPAR mediated and at the AMPA reversal potential all positively deflecting events were GABAR mediated.

No significant difference was seen in the AMPAR / $GABA_AR$ ratio between WT and *Syngap*$^{+/GAP}$ recordings and as there is no published evidence of AMPAR / $GABA_AR$ ratios in the SynGAP literature this is a novel finding. Fewer papers have investigated inhibitory function in SynGAP models, but as noted in the introduction to this chapter, mice with SynGAP haploinsufficiency specifically in inhibitory cells originating from the medial ganglionic eminence [PV+ and Somatostatin+ (SST+) cells], have significantly longer mIPSC mean inter-event interval in layer 2-3 pyramidal cells in the somatosensory cortex and hippocampal CA1 pyramidal cells (Berryer et al. 2016). Furthermore targeted expression of the light sensitive Channel rhodopsin-2 via Cre also revealed reduced amplitude of evoked IPSCs in Layer 5 pyramidal cells. Both findings are therefore suggestive of a potential reduction in GABAergic function which might have revealed itself in the SynGAP _deletion rat experiments as a decrease in AMPAR / $GABA_AR$ ratio, but given the literature also suggests increases in excitatory function, the ratio could have balanced out.

Alternatively, the fact that no such difference was revealed, may once again relate to the idea that SynGAP plays a particularly key role during development as evidenced by the numerous papers showing phenotypic differences in SynGAP haploinsufficiency models in the first two weeks of life which resolve by P21 (Clement et al. 2012; Clement et al. 2013; Ozkan et al. 2014).

In contrast to AMPAR / $GABA_AR$ ratios, AMPAR / NMDAR ratios which have been more extensively studied previously in SynGAP haploinsufficiency were also recorded and no difference between genotypes was observed. AMPAR / NMDAR ratios are increased in younger rats as discussed under 'Experimental age' (section 4.4.1) above (and shown by Clement et al. 2012; Clement et al. 2013), but experiments in adult mice have shown no difference in AMPAR / NMDAR ratios (Komiyama et al. 2002). The ratio of AMPAR / NMDAR in the developing brain of WT rats has been shown to increase over the first one to two weeks of life (Crair & Malenka 1995) and the unsilencing of AMPA receptors has been found to be relevant to LTP induction in young animals, but not mature animals (Abrahamsson et al. 2008; Hanse et al. 2013). Given SynGAP's role in AMPAR trafficking via its regulation of Ras and Rap (Chen et al. 1998; Kim et al. 1998; Zhu et al. 2002; Krapivinsky et al. 2004; Zhu et al. 2005; Derkach et al. 2007; Walkup et al. 2015) it makes sense that differences in AMPA / NMDA ratio in WT and *Syngap*$^{+/GAP}$ rats may well be more evident at younger ages; this would need to be verified in future experiments. As with the other experiments presented in this chapter, the experimental model and background strain of the rats may have been influential and their roles could be better evaluated if future AMPA / NMDA experiments in particular are completed at around P14 in future where this is comparable data in the literature.

The question of statistical power is again particularly relevant in these experiments. Using the calculator at http://biomath.info/power/ttest.htm, the minimum detectable difference between WT and *Syngap*$^{+/GAP}$ when using the current data and considering a statistical significance of 0.05 and power of 0.8 is 0.28 for AMPAR / $GABA_AR$ ratio and 10 for AMPAR / NMDAR ratio (Table 14). The observed differences between the means in this experiment were 0.0129 and 2 respectively, so the experiment was technically underpowered. The standard error of the mean between the data groups was much more consistent between groups than in other datasets though. The groups of data with $n \geq 7$ (*Syngap*$^{+/GAP}$ $GABA_AR$/AMPAR and WT AMPAR/NMDAR) passed a normality test and so the use of a power calculator which relies on the assumption of normally distributed data is more valid. However,

if the collected data is used for a future power calculation, the number of animals required per group for AMPAR / $GABA_AR$ is 341 and for AMPAR / NMDAR it is 31, neither of which is ethical or feasible to achieve.

Table 14 – Size of detectable difference in AMPAR / $GABA_AR$ and AMPAR / NMDAR ratios and future sample size calculations based on the current SynGAP rat data

Parameter	WT SEM and (sample size)	*Syngap*$^{+/GAP}$ SEM and (sample size)	Size of statistically detectable difference between groups*	Size of observed difference in means between groups	Sample Size (n) required per group if current data is used for power calculation
$GABA_AR$/AMPAR	0.06372 (7)	0.07806 (10)	0.28	0.0129	341
AMPAR/NMDAR	2.398 (8)	3.069 (6)	10	2	31

*calculated using http://biomath.info/power/ttest.htm

This therefore implies that although a difference could potentially be found between genotypes if large numbers of animals were used in the future, ethically and practically this isn't possible. So, it is reasonable to conclude that although the result is not statistically powerful, scientifically there was no meaningful difference in AMPAR / $GABA_AR$ and AMPAR / NMDAR ratios in P26-30 *Syngap*$^{+/GAP}$ rats.

4.4.3 Chapter Summary

This chapter details the first electrophysiological findings in a SynGAP rat model. Some of the data is somewhat surprising, particularly the lack of exaggeration in mGluR mediated hippocampal LTD in *Syngap*$^{+/GAP}$ rats and the reduction in frequency of mEPSCs from *Syngap*$^{+/GAP}$ rat cultures. The lack of mean difference in excitatory and inhibitory current data between genotypes is also rather unexpected, but the cumulative frequency distributions are perhaps suggestive of a trend in the predicted direction of excitation over inhibition.

As described, the background strain of the rats and variability within samples are factors that are likely to have influenced each dataset albeit to varying degree. Notwithstanding this, it would appear at the present time that there is little in the way of difference between WT and *Syngap*$^{+/GAP}$ rats in terms of hippocampal LTD, passive and active cell properties, excitatory and inhibitory currents and GABAR / AMPAR and AMPAR / NMDAR ratios.

5 CHAPTER FIVE: SYNGAP ISOFORM EXPERIMENTS

5.1 Key Findings

- Cortical cells co-transfected with Eα1 and eGFP tended to have larger and more frequent mEPSCs than in neighbouring control cells
- Hippocampal cells co-transfected with Eα1 and eGFP tended to have smaller and less frequent mEPSCs than in neighbouring control cells
- Expression of SynGAP Eα1 isoform may result in greater numbers of cortical cells completely lacking mEPSCs ('silent cells')
- Multiple problems with SynGAP isoform specific primers precluded interpretation of data regarding the existence or abundance of specific SynGAP isoforms in mice

5.2 Introduction

As described in the main introduction to this thesis, SynGAP is a complex gene with several N and C terminal isoforms which have been identified in various papers and are recognised by the notation of the isoform's N terminal followed by its C terminal e.g. Aα1, a system adopted in 2001 (Li et al. 2001).

McMahon et al. showed that different promoter regions exist for SynGAP A, B and C and promote the transcription of these isoforms from distinct transcription start sites (TSS). Multiple TSS exist for SynGAP A and SynGAP C, whereas SynGAP B has a single TSS (McMahon et al. 2012). McMahon and colleagues also identified high homology in intronic sequences suggestive of functional significance in regulating promoter activity. In contrast to the N terminal isoforms, McMahon noted that the C terminal isoforms are the result of alternative splicing.

5.2.1 Timeline of SynGAP isoform identification

As Table 15 shows, the first SynGAP paper (Chen et al. 1998) named the newly identified protein 'Synaptic ras GTPase-activating protein p135 SynGAP' or just 'p135 SynGAP'. The sequence of the protein published in that paper is now recognised as SynGAP Aα1. Chen and colleagues also identified what they believed to be two variants of p135 SynGAP, one an N terminal variant now recognised as

SynGAP B and the other a C terminal variant now recognised as SynGAP β. In the same year Kim and colleagues (Kim et al. 1998) identified a SynGAP protein when screening a yeast two–hybrid hippocampal cDNA library to find novel proteins that interact with the PDZ domains of the PSD 95/SAP90 family. The SynGAP protein they identified was Cα1 and they also found three different variants which they named SynGAP-a, SynGAP-b and SynGAP-c. These are now recognised as Aγ, Bα1 and Cα2 respectively.

Li et al. 2001 identified a transcript they named 'SynGAP-d'. The C terminal of this is now recognised as SynGAP β, but the N terminal was unique and later shown to be an artefact by McMahon and colleagues (McMahon et al. 2012, supplementary information). On designing primers to amplify SynGAP-d by RT-PCR, Li and colleagues found seven different sequences with minor differences in their C terminal sequences. These they named α1, α2, β (β1, β2, β3, β4) and γ.

Table 15- Timeline of the identification of different SynGAP isoforms

Study	Author's variant name	Isoform the variant is now recognised as	GenBank™ Accession Number
Chen et al. 1998	'Synaptic ras GTPase-activating protein p135 SynGAP' or 'p135 SynGAP'	SynGAP Aα1	AF048976.1
Chen et al. 1998		SynGAP B	AF053938.1
Chen et al. 1998		SynGAP β	AF055883.1
Kim et al. 1998	SynGAP	Cα1	AF050183
Kim et al. 1998	SynGAP-a	Aγ	AF058789.2
Kim et al. 1998	SynGAP-b	Bα1	AF058790.1
Kim et al. 1998	SynGAP-c	Cα2	AF050183.2
Li et al. 2001	C terminal isoforms α1, α2, β (β1, β2, β3, β4) and γ	C terminal isoforms α1, α2, β (β1, β2, β3, β4) and γ	n/a

5.2.2 Localisation of SynGAP isoforms

Some differences in the localisation of SynGAP isoforms have been reported which may indicate different isoform functions. C terminals α1, α2, β (β1, β2, β3, β4) and γ were found to be expressed in the brain using RT-PCR, but expression of γ was

markedly lower than that of α and β (Li et al. 2001). α and β were also specifically identified in the forebrain structures and cerebellum (Li et al. 2001; Moon et al. 2008), but whilst Li et al. found the expression profiles of α and β to be similar to each other in both the forebrain and cerebellum, Moon et al. noted that α1 was stronger in the cerebellar cortex, and β was stronger in the cerebellar medulla. In the dentate gyrus of the hippocampus Moon et al. showed that α1 formed two distinct immunoreactive layers in contrast to the homogeneous distribution of β.

Upon labelling hippocampal slices from 6-8 weeks old Wistar rats with fluorescent probes Moon et al. found the immunoreactive puncta for both SynGAPα1 and SynGAPβ overlapped with PSD-95 puncta. However the overlap was more intense with SynGAP α1 puncta. They also noted that a substantial fraction of β clusters did not co-localise with PSD-95 implying the presence of β in other sites. However on analysis of the synaptic plasma membrane fraction of 6 weeks old Wistar rat forebrain Li et al. found that whilst SynGAP α1 and β were both present in the post-synaptic density, SynGAP α1 alone was also found in other fractions including the post-synaptic raft, the synaptic plasma membrane and the synaptosome (Li et al. 2001). This discrepancy may reflect the different brain regions being examined.

Moon et al. went on to observe that α1 was predominantly present at excitatory post-synaptic sites in Sprague-Dawley rat hippocampal cultures whereas SynGAP β was present at both excitatory and inhibitory sites (Moon et al. 2008). Furthermore Li et al. reported that in Sprague-Dawley neocortical cultures β was localised in the dendrites including spines and also that it co-localised with PSD-95 (Li et al. 2001). This is consistent with the finding that PSD-binding motif on SynGAP α1 was not required for the localisation of SynGAP in dendritic spines (Vazquez et al. 2004; McMahon et al. 2012). However SynGAP β was also found to co-precipitate with CaMKII α sub-unit which the authors proposed as a mechanism for SynGAP β's strong localisation to the PSD in the absence of the QTRV domain by which SynGAP is known to interact with PSD-95 (Li et al. 2001). With regards to other C terminal isoforms, Tomoda et al. showed that GFP tagged SynGAP α2 was localised to extending axons but the GFP tagged SynGAP α1 was only localised to the cell

soma (Tomoda et al. 2004). In other later experiments, no SynGAP α2 mRNA was found on examination of developing thalamic ventral posterior medial nucleus tissue where it might have then localised to thalamo-cortical axons (Barnett et al. 2006).

5.2.3 SynGAP isoform abundance

Barnett and colleagues found on western blotting of homogenates of S1 (barrel) cortex, that in contrast to pan-syngap labelling (i.e. labelling of all isoforms) very little SynGAP α1 was present in the first week of life. Thereafter both SynGAP α1 and pan-SynGAP labelling dramatically increased during the second postnatal week. As the same authors saw complete failure of cellular segregation into barrels in layer 4 of the primary somatosensory cortex of *Syngap*$^{+/-}$ mice at P6/7, the implication is that isoforms other than α1 mediate barrel formation.

In an attempt to understand the developmental relevance of different isoforms in WT animals, McMahon et al. 2012 used quantitative reverse transcriptase-PCR to study their abundance in C57Bl6 mice using RNA isolated from forebrain and stimulated neuronal culture lysates. Primers complementary to Syngap variant-specific sequences were designed and total SynGAP levels peaked at P14 and were significantly different from the levels at P4 and P21, but the isoforms showed different expression profiles. Although they peaked at P14 the levels of N terminal isoform A were not statistically different from P4 to P14 to P21, but SynGAP B did show significant differences between its peak at P14 and the following time points (P4, P7, P21 and adulthood). Isoform C was expressed only at low levels up to P7 and then was dramatically up-regulated by P14 and wasn't significantly down regulated in adulthood as B was.

5.2.4 Differential functions of SynGAP isoforms

In addition to studying isoform abundance, McMahon and colleagues examined the impact of neuronal stimulation on SynGAP isoform expression. They found that the application of bicuculline (a $GABA_AR$ receptor antagonist) to increase network activity correlated with an up-regulation in SynGAP B and C 4 hours later, whereas SynGAP A was down-regulated. Overall the total SynGAP level did not change

indicating the changes in B and C offset that of A and which therefore suggested A is the most abundant isoform (McMahon et al. 2012).

They were also the first and so far only group to systematically examine the effects of different combinations of N and C terminal isoforms (A, B, C, α1 and α2) on cell function. They established that SynGAP α1 negatively regulates synaptic strength by increasing the number of silent cells (those that completely lacked mEPSCs during their recordings) and reducing the amplitude and frequency of mEPSCs when present. In the case of Aα1 they confirmed this was not due to alterations in postsynaptic morphology and found that the extent to which α1 affects synaptic strength is modulated by the N terminal isoform it is coupled with; Aα1 had a larger effect than Bα1 and Cα1. In contrast, the α2 isoform was associated with positive rather than negative alterations in synaptic strength (McMahon et al. 2012).

As discussed in the introduction to the previous chapter, other researchers have also examined the role of certain specific SynGAP isoforms in cultured neurons. Wang et al. (2013) found the knock down of alpha SynGAP in DIV 11-16 cultured cortical neurons resulted in increased mEPSC amplitude. In keeping with McMahon's work, a marked decrease in both amplitude and frequency of AMPAR mediated mEPSCs was observed in over-expression studies of GFP-tagged SynGAP Cα1isoform (Rumbaugh et al. 2006). However in the same work, deletion of the C terminal portion of SynGAP including the PDZ binding domain and also separate mutation of the GAP domain resulted in no difference in amplitude and frequency from untransfected neurons. This therefore implies the need for a functioning GAP domain and possibly the ability to interact via its PDZ binding domain for SynGAP to influence mEPSC frequency (Rumbaugh et al. 2006).

5.3 Aims and Hypothesis

In order to extend the SynGAP isoform work, this chapter details experiments to expand on the finding that distinct SynGAP isoforms can have a differential effect on synaptic strength (McMahon et al. 2012) by recording mEPSCs from cells transfected with the Eα1 isoform. It also includes experiments to examine the

abundance and relative expression of SynGAP isoforms including putative newly identified isoforms.

Based on the previous work of McMahon and colleagues (McMahon et al. 2012) it is hypothesised that

- SynGAP Eα1 isoform will be associated with a reduction in mEPSC amplitude and frequency
- SynGAP A will be the most abundant isoform in *Syngap*$^{+/-}$ mouse neocortex

5.4 Results

5.4.1 Identification of New SynGAP Isoforms

Owen Dando, Informatician in the Centre for Integrative Physiology, University of Edinburgh mapped mRNA-seq read sets to their respective genomes, examined for novel splice junctions at the SynGAP locus and thereby identified putative new SynGAP 5' variant forms A1 and G in addition to the known N terminal (A, B, C, E) and C terminal (α1, α2, β and γ) isoforms (Figure 42 and Figure 43). Dando also confirmed that there are two variants of SynGAP α2 (α2a and α2b). SynGAP α2a only differs from α1 by the addition of an extra 'G' nucleic acid and α2b only differs from α2a by the addition of an extra valine (coded for by GTG nucleic acid sequence). The extra G was also noted by Li and colleagues in four of their independent cDNA clones (Li et al. 2001).

It should be noted that SynGAP A1 is a different isoform to SynGAP A rather that being the A1 referred to by McMahon et al. 2012 which was a form of SynGAP A that was generated from a different transcription start site from the other A isoform they denoted 'A2' (McMahon et al. 2012).

Constructs of SynGAP isoforms Aα1, Bα1,Cα1, Eα1, Gα1 and Aα2, Bα2, Cα2, Eα2, Gα2 were made and their sequences confirmed by Sanger sequencing using Dando's sequences as a reference (Figure 43).

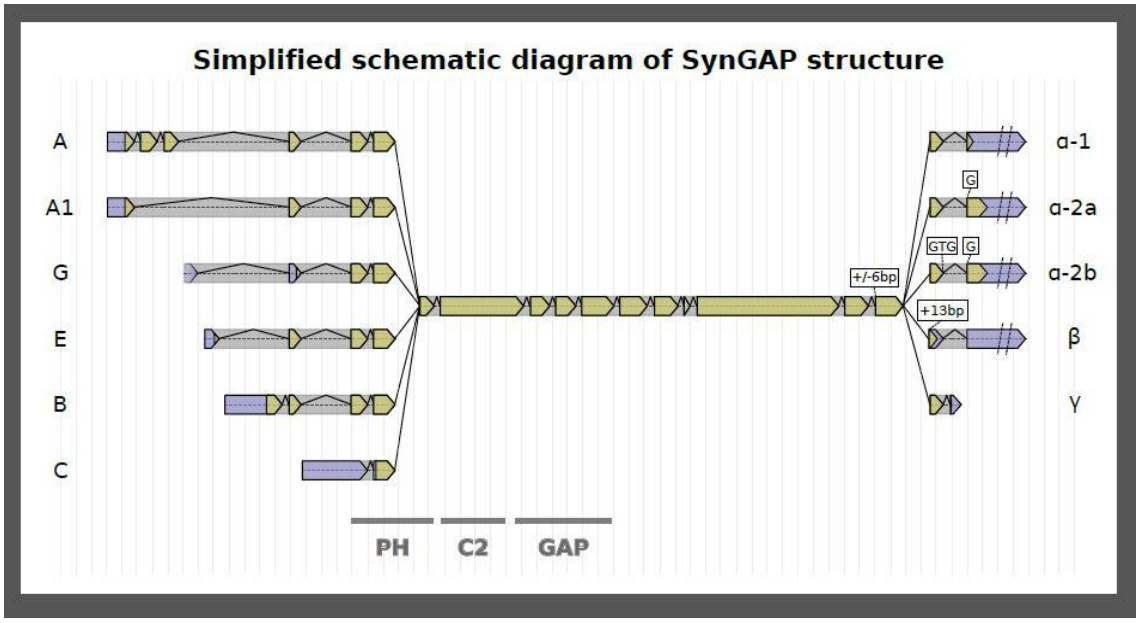

Figure 42 - Schematic of the SynGAP protein isoforms.

Courtesy of Owen Dando, Centre for Integrative Physiology, University of Edinburgh (personal correspondence) There are 6 N terminal isoforms (A, A1, B, C, E and G) and 5 C terminal isoforms (α1, α2a, α2b, β and γ).

SYNGAP CODING SEQUENCE

N Terminal Isoforms

A	ATGAGCAGGTCTCGAGCCTCCATCCATCGGGGGGAGCATCCCCGCGATGTCCTATGCCCCCTTCAGAGATGTACGGGGACCCCCTA
A1	
B	
C	
E	
G	
A	TGCACCGAACCCAATACGTTCATTCCCCGTACGATCGTCCTGGCTGGAACCCTCGGTTCTGCATCATCTCGGGGAACCAGCTG
A1	
B	
C	
E	
G	
A	CTCATGCTGGATGAGGATGAGATACACCCCCTTCTGATCCGCGACCGGAGGAGCGAGTCCAGCCGAAACAAACTGCTGAGAC
A1	ATGAGCAGGTCTCGAGCCTCC
B	ATGGGCTTAAGGCCT CCCACCCCGACCCCGTCAGGGGGCTCCGGCTCAGGTTCCTTGCCCCCTCCTTCCCA
C	
E	
G	
A	GCACCGTCTCTGTGCCAGTGGAGGGGCGGCCCCACGGCGAGCATGAATACCACTTGGGTCGCTCGAGGAGGAAGAGTGTCCC
A1	ATCCATCGGGGGAGCATCCCCGCGATGTCCTATGCCCCCTTCAGAGAATACCACTTGGGTCGCTCGAGGAGGAAGAGTGTCCC
B	CCGCCAGCCTCTCCGCCGCCGCTGCTCTTCTTGCTGCTTTCCGGGGGAATACCACTTGGGTCGCTCGAGGAGGAAGAGTGTCCC
C	
E	ATGTTCTCGCTGCATCTTCCGAGTGGGGGGAGTTATGAATACCACTTGGGTCGCTCGAGGAGGAAGAGTGTCCC
G	
A	AGGGGGGAAACAGTACAGCATGGAGGCCGCCCCCGCTGCGCCCTTCCGGCCCTCGCAAGGCTTCCTGAGCCGGAGGCTAAAA
A1	AGGGGGGAAACAGTACAGCATGGAGGCCGCCCCCGCTGCGCCCTTCCGGCCCTCGCAAGGCTTCCTGAGCCGGAGGCTAAAA
B	AGGGGGGAAACAGTACAGCATGGAGGCCGCCCCCGCTGCGCCCTTCCGGCCCTCGCAAGGCTTCCTGAGCCGGAGGCTAAAA
C	
E	AGGGGGGAAACAGTACAGCATGGAGGCCGCCCCCGCTGCGCCCTTCCGGCCCTCGCAAGGCTTCCTGAGCCGGAGGCTAAAA
G	ATGGAGGCCGCC CCCGCTGCGCCCTTCCGGCCCTCGCAAGGCTTCCTGAGCCGGAGGCTAAAA
A	AGCTCTATCAAACGTACAAAGTCACAACCCAAACTTGACCGGACCAGCAGCTTTCGACAGATCCTGCCTCGCTTCCGAAGTGC
A1	AGCTCTATCAAACGTACAAAGTCACAACCCAAACTTGACCGGACCAGCAGCTTTCGACAGATCCTGCCTCGCTTCCGAAGTGC
B	AGCTCTATCAAACGTACAAAGTCACAACCCAAACTTGACCGGACCAGCAGCTTTCGACAGATCCTGCCTCGCTTCCGAAGTGC
C	
E	AGCTCTATCAAACGTACAAAGTCACAACCCAAACTTGACCGGACCAGCAGCTTTCGACAGATCCTGCCTCGCTTCCGAAGTGC
G	AGCTCTATCAAACGTACAAAGTCACAACCCAAACTTGACCGGACCAGCAGCTTTCGACAGATCCTGCCTCGCTTCCGAAGTGC
A	TGACCATGACCGGGCCCGGCTGATGCAGAGCTTCAAGGAGTCACATTCCCACGAGTCCCTGCTGAGTCCCAGTAGTGCTGCTG
A1	TGACCATGACCGGGCCCGGCTGATGCAGAGCTTCAAGGAGTCACATTCCCACGAGTCCCTGCTGAGTCCCAGTAGTGCTGCTG
B	TGACCATGACCGGGCCCGGCTGATGCAGAGCTTCAAGGAGTCACATTCCCACGAGTCCCTGCTGAGTCCCAGTAGTGCTGCTG
C	ATGCAGAGCTTCAAGGAGTCACATTCCCACGAGTCCCTGCTGAGTCCCAGTAGTGCTGCTG
E	TGACCATGACCGGGCCCGGCTGATGCAGAGCTTCAAGGAGTCACATTCCCACGAGTCCCTGCTGAGTCCCAGTAGTGCTGCTG
G	TGACCATGACCGGGCCCGGCTGATGCAGAGCTTCAAGGAGTCACATTCCCACGAGTCCCTGCTGAGTCCCAGTAGTGCTGCTG
A	AGGCCTTGGAGCTCAACCTGGATGAAGACTCCATTATCAAGCCAGTACACAGCTCCATCCTGGGTCAGGAGTTCTGCTTTGAG
A1	AGGCCTTGGAGCTCAACCTGGATGAAGACTCCATTATCAAGCCAGTACACAGCTCCATCCTGGGTCAGGAGTTCTGCTTTGAG
B	AGGCCTTGGAGCTCAACCTGGATGAAGACTCCATTATCAAGCCAGTACACAGCTCCATCCTGGGTCAGGAGTTCTGCTTTGAG
C	AGGCCTTGGAGCTCAACCTGGATGAAGACTCCATTATCAAGCCAGTACACAGCTCCATCCTGGGTCAGGAGTTCTGCTTTGAG
E	AGGCCTTGGAGCTCAACCTGGATGAAGACTCCATTATCAAGCCAGTACACAGCTCCATCCTGGGTCAGGAGTTCTGCTTTGAG
G	AGGCCTTGGAGCTCAACCTGGATGAAGACTCCATTATCAAGCCAGTACACAGCTCCATCCTGGGTCAGGAGTTCTGCTTTGAG

Figure continued overleaf….

Common Sequence
GTAACAACATCATCTGGAACAAAATGCTTTGCCTGTCGGTCTGCAGCTGAAAGGGACAAATGGATTGAGAATCTGCAGAGGGCTGTA
AAACCCAACAAGGACAACAGCCGCCGAGTAGATAACGTGCTGAAGCTATGGATCATAGAGGCTCGAGAGCTGCCCCCCAAGAAGAG
ATATTACTGTGAGCTGTGCCTGGACGACATGCTGTATGCACGAACCACCTCCAAGCCCCGCTCGGCTTCAGGAGACACCGTCTTTTGG
GGCGAGCACTTTGAGTTTAACAACCTGCCTGCCGTCCGGGCCCTTCGGCTGCATCTGTACCGTGACTCAGACAAAAGCGGAAGAAG
GACAAGGCTGGCTACGTTGGCCTGGTGACTGTTCCAGTGGCCACCCTAGCTGGGCGCCACTTCACAGAGCAGTGGTACCCCGTGACCT
TGCCGACAGGCAGTGGGGGCTCTGGGGGCATGGGCTCGGGGGGAGGAGGAGGGTCAGGGGGTGGCTCAGGGGGCAAAGGGAAAGG
AGGTTGTCCTGCTGTGAGACTGAAAGCCCGTTACCAGACGATGAGCATCCTGCCCATGGAGCTGTATAAGGAGTTTGCAGAGTATGT
GACCAACCATTACCGGATGCTATGTGCAGTGCTGGAGCCTGCCCTGAATGTCAAAGGCAAGGAAGAGGTGGCCAGTGCACTGGTTCA
CATCCTGCAGAGCACAGGCAAGGCCAAGGACTTCCTTTCAGACATGGCCATGTCAGAGGTAGACCGATTCATGGAGCGGGAACACCT
CATATTCCGAGAGAACACGCTCGCCACTAAAGCCATAGAAGAGTATATGAGACTGATTGGCCAGAAATACCTCAAGGATGCCATTGG
GGAGTTCATTCGTGCTCTGTATGAATCTGAGGAGAACTGTGAAGTAGACCCCATCAAGTGCACAGCGTCCAGTCTGGCAGAGCACCA
GGCCAACCTGCGGATGTGCTGTGAGTTGGCCCTGTGCAAGGTGGTCAACTCCCATTGCGTGTTCCCGAGGGAGCTGAAGGAGGTGTTT
GCATCTTGGCGGCTGCGCTGCGCAGAGCGGGGCCGAGAGGACATTGCTGACAGGCTGATCAGCGCCTCGCTCTTCCTGCGCTTCCTCT
GCCCGGCCATTATGTCGCCCAGTCTATTTGGGCTTATGCAGGAGTACCCAGATGAGCAGACCTCACGAACCCTCACCCTCATCGCCAA
GGTCATCCAGAACCTGGCCAACTTTTCCAAGTTTACCTCAAAGGAGGACTTCCTGGGCTTCATGAATGAGTTTCTGGAGCTGGAGTGG
GGCTCTATGCAGCAGTTCTTGTATGAGATATCCAACCTGGACACCTTGACCAACAGCAGCAGTTTTGAGGGCTATATAGACTTGGGCC
GCGAGCTCTCCACACTTCACGCCCTGCTCTGGGAGGTGCTGCCCCAGCTCAGCAAGGAAGCCCTCCTGAAGCTGGGCCCACTGCCCCG
GCTCCTCAATGACATCAGCACAGCCCTGAGGAACCCTAACATCCAAAGGCAGCCAAGCCGCCAGAGTGAACGGACTCGGTCTCAGCC
CATGGTGCTGCGAGGGCCATCAGCCGAGATGCAGGGCTACATGATGCGGGACCTCAATAGCTCCATCGACCTTCAATCCTTCATGGCT
CGAGGCCTCAACAGCTCTATGGACATGGCTCGCCTCCCCTCCCCAACCAAGGAAAAACCACCACCACCACCACCCGGTGGGGGTAAA
GACCTTTTCTATGTGAGCCGGCCACCACTGGCCCGGTCCTCCCCAGCATACTGCACGAGCAGCTCGGACATCACAGAGCCAGAGCAG
AAGATGCTGAGTGTCAACAAGAGTGTGTCCATGCTGGACCTTCAGGGCGACGGGCCTGGAGGTCGCCTTAACAGTAGCAGTGTTTCC
AACCTGGCAGCTGTTGGGGACTTGTTGCATTCCAGCCAGGCCTCGCTGACAGCAGCTTTGGGGTTGCGGCCTGCACCTGCCGGGCGCC
TCTCCCAGGGGAGTGGCTCTTCCATCACAGCAGCTGGCATGCGCCTCAGCCAGATGGGGGTCACTACAGATGGTGTCCCCGCCCAGC
AACTGCGCATCCCCCTTTCCTTCCAGAACCCTCTCTTCCATATGGCTGCTGATGGGCCAGGGCCCCCAGCAGGCCATGGAGGGAGCAG
TGGTCATGGTCCACCTTCCTCCCATCACCACCACCACCACCATCACCACCACCGAGGGGGAGAACCCCCAGGGGACACTTTTGCCCCA
TTCCATGGCTATAGCAAGAGCGAGGACCTCTCTTCAGGGGTCCCTAAGCCCCCCGCCGCCTCCATCCTTCACAGCCACAGCTACAGCG
ACGAGTTTGGACCCTCTGGCACTGATTTTACCCGCCGGCAGCTCTCGCTTCAGGACAGTCTACAGCACATGCTCTCCCCTCCCCAGATT
ACCATCGGTCCCCAGAGGCCAGCTCCCTCAGGGCCGGGAGGGGGCAGCGGCGGGGGCAGCGGTGGGGGCCAGCCACCCCCCTTGCA
GAGGGGCAAGTCTCAACAGTTGACAGTGAGTGCCGCCCAGAAACCTCGGCCGTCTAGCGGGAACCTGTTGCAGTCCCCGGAGCCAAG
CTACGGACCTGCCCGTCCTCGGCAGCAGAGCCTCAGCAAAGAGGGCAGCATTGGGGGCAGCGGGGGCAGCGGGGGCGGAGGGGGTG
GGGGGCTCAAGCCCTCCATCACCAAGCAGCATTCCCAGACTCCATCCACGCTTAACCCCACAATGCCAGCCTCGGAGCGGACCGTAG
CCTGGGTCTCCAACATGCCTCACCTGTCGGCTGACATCGAGAGTGCACACATCGAGCGAGAAGAGTACAAGCTCAAGGAGTACTCCA
AGTCCATGGACGAAAGCCGGCTGGACAGGGTGAAGGAGTATGAGGAGGAGATACATTCGCTGAAGGAGAGGCTACACATGTCCAAC
CGGAAGCTGGAAGAGTATGAGCGGAGGTTGCTGTCCCAGGAAGAACAGACCAGCAAGATCCTGATGCAGTACCAAGCCCGCCTGGA
GCAGAGTGAGAAGCGCTTGAGACAGCAGCAGGTGGAGAAGGACTCCCAGATCAAGAGCATCATTGGCAG

C Terminal Isoforms

α1	GCTGATGCTGGTGGAGGAGGAGCTGCGTCGGGACCACCCCGCCATGGCTGAGCCGCTGCCTGAGCCCAAGAAGAGGCTGCTC
α2a	GCTGATGCTGGTGGAGGAGGAGCTGCGTCGGGACCACCCCGCCATGGCTGAGCCGCTGCCTGAGCCCAAGAAGAGGCTGCTC
α2b	GCTGATGCTGGTGGAGGAGGAGCTGCGTCGGGACCACCCCGCCATGGCTGAGCCGCTGCCTGAGCCCAAGAAGAGGCTGCTC
β	CCCGTCCCTTCAGGCTGATGCTGGTGGAGGAGGAGCTGCGTCGGGACCACCCCGCCATGGCTGA
γ	GCTGATGCTGGTGGAGGAGGAGCTGCGTCGGGACCACCCCGCCATGGCTGAGCCGCTGCCTGAGCCCAAGAAGAGGCTGCTC
α1	GACGCTCAGAGAGGCAGCTTCCCCCCTTGGGTCCAACAAACCCGCGTGTGA
α2a	GACGCTCACGAGAGGCAGCTTCCCCCCTTGGGTCCAACAAACCCGCGTGTGACGCTGGCCCCACCTTGGAACGGCCTGGCCCC
α2b	GACGCTCAGGTGGAGAGGCAGCTTCCCCCCTTGGGTCCAACAAACCCGCGTGTGACGCTGGCCCCACCTTGGAACGGCCTGG
β	
γ	GACGCTCAGCTCCTCATCAGGTAA
α1	
α2a	CCCAGCCCCACCCCCCCCACCCCGGCTGCAGATCACAGAGAACGGCGAGTTCCGGAACACCGCAGACCACTAG
α2b	CTGGCCCCCCCAGCCCCACCCCCCCCACCCCGGCTGCAGATCACAGAGAACGGCGAGTTCCGGAACACCGCAGACCACTAG
β	
γ	

Figure 43 – Mouse SynGAP Coding Sequence.

The unique portions of each N terminal isoform are highlighted in a different colour. The unique portions of the C terminal isoforms are highlighted in purple and the areas of common sequence between different C terminal isoforms are highlighted in other colours.

5.4.2 SynGAP Eα1 Isoform mEPSCs

Cortical and hippocampal cell cultures were prepared then mEPSC recordings were made from neurons co-transfected with SynGAP Eα1 isoform and eGFP or untransfected neurons on the same coverslips (controls). Recordings were also made from neurons on separate coverslips that had not been exposed to lipofectamine transfection ('untransfected' cells). The recordings were made in the presence of tetrodotoxin (300 nM) and picrotoxin (50 µM) to block spontaneous, action potential driven activity in order to unmask the miniature events. On examination of pooled data histograms for the recordings, the positive skew typical of mEPSC recordings was seen in the untransfected, control and Eα1 recordings in both the cortical and hippocampal cultures (Figure 44).

The mean untransfected cell mEPSC amplitude and frequency were 17.68 ± 1.4 pA and 0.88 ± 0.18 Hz (n = 38) in the cortical cultures and 21.9 ± 1.5 pA and 0.85 ± 0.16 Hz (n = 23) in the hippocampal cultures (Figure 45). As the cumulative frequency distributions in Figure 45 show, the mEPSC amplitude in cortical cells co-transfected with Eα1 and eGFP tended to be larger and the frequency higher than in neighbouring control cells. However, on analysis of mean data collated by n = cell (Figure 45), there was no statisitical difference in mEPSC amplitude (Cortex Control = 14.0 ± 2.3 pA n = 9, Cortex SynGAP Eα1 = 10.1 ± 2.9 pA n = 11, Mann-Whitney test between control and Eα1 p = 0.2905) or frequency (Cortex Control = 0.72 ± 0.37 Hz n = 9, Cortex SynGAP Eα1 = 0.28 ± 0.14 Hz n = 11, Mann-Whitney test between control and Eα1 p = 0.1718).

In hippocampal cells co-transfected with Eα1 and eGFP the mEPSC amplitude tended to be smaller and the frequency lower than in neighbouring control cells (Figure 45). However, once again there was no mean difference in mEPSC amplitude (Figure 45: Hippocampal Control = 23.1 ± 4.9 pA n = 8, Hippocampal SynGAP Eα1 = 18.3 ± 1.8 pA n = 11, Mann-Whitney test between control and Eα1 p = 0.3511) or frequency (Figure 45: Hippocampal Control = 0.87 ± 0.41 Hz n = 8, Hippocampal SynGAP Eα1 = 0.26 ± 0.07 Hz n = 11, Mann-Whitney test between control and Eα1 p = 0.3950).

McMahon and colleagues previously found that α1 C terminal SynGAP isoforms reduced the amplitude and frequency of mEPSCs in cultured forebrain neurons (McMahon et al. 2012). Therefore the mixed picture from the current separate cortical and hippocampal recordings is intriguing and warrants further exploration in the discussion below.

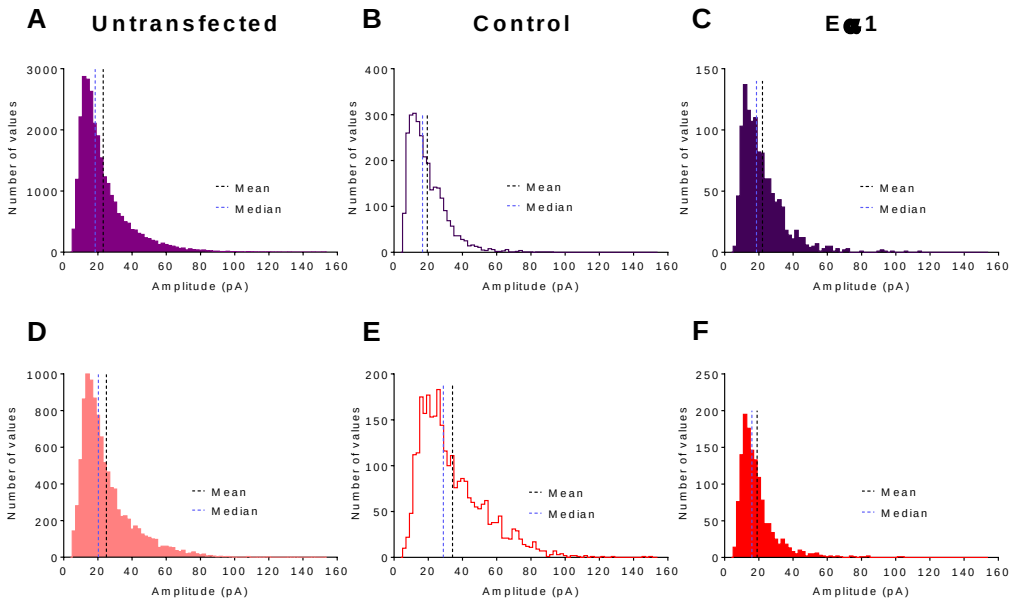

Figure 44 – The frequency distributions of mEPSC amplitude from untransfected, control and SynGAP Eα1 are positively skewed.

(A to C) The frequency distribution of the pooled mEPSC amplitudes from cortical untransfected (A), control (B) and SynGAP Eα1(C) recordings display the typical positively skewed distribution expected in mEPSC recordings (untransfected median = 18.46, untransfected mean = 23.12 pA, control median = 16.7 pA, control mean = 19.45 pA, SynGAP Eα1 median = 18.56 pA, SynGAP Eα1 mean = 22.05 pA).

(D to F) The frequency distribution of the pooled mEPSC amplitudes from hippocampal untransfected (D), control (E) and SynGAP Eα1 (F) recordings display the typical positively skewed distribution expected in mEPSC recordings (untransfected median = 20.31, untransfected mean = 24.97 pA, control median = 28.81 pA, control mean = 34.16 pA, SynGAP Eα1 median = 15.97 pA, SynGAP Eα1 mean = 18.98 pA).

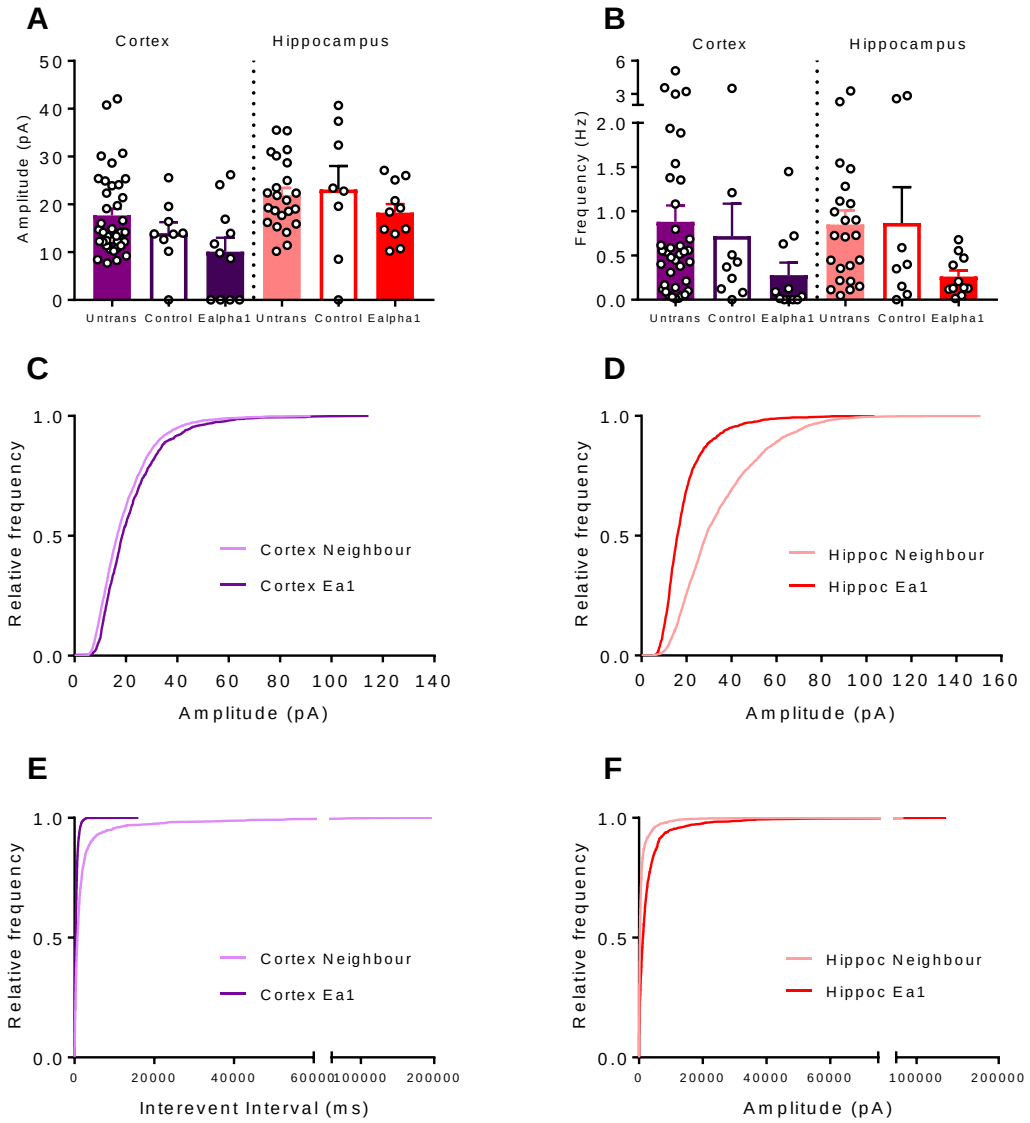

Figure 45 – There is no significant difference in the mean mEPSC amplitude or frequency in cortical and hippocampal neurons transfected with the SynGAP Eα1 isoform.

(A) There is no significant difference in mEPSC amplitude between control and SynGAP Eα1 recordings (Cortex Untransfected = 17.68 ± 1.4 pA *n* = 38, Cortex Control = 14.0 ± 2.3 pA *n* = 9, Cortex SynGAP Eα1 = 10.1 ± 2.9 pA *n* = 11, Mann-Whitney test between control and Eα1 *p* = 0.2905, Hippocampal Untransfected = 21.9 ± 1.5 pA *n* = 23, Hippocampal Control = 23.1 ± 4.9 pA *n* = 8, Hippocampal SynGAP Eα1 = 18.3 ± 1.8 pA *n* = 11, Mann-Whitney test between control and Eα1 *p* = 0.3511).

Legend continued overleaf…

Figure 45 legend continued…

(B) There is no significant difference in mEPSC frequency between control and SynGAP Eα1 recordings (Cortex Untransfected = 0.88 ± 0.18 Hz n = 38, Cortex Control = 0.72 ± 0.37 Hz n = 9, Cortex SynGAP Eα1 = 0.28 ± 0.14 Hz n = 11, Mann-Whitney test between control and Eα1 p = 0.1718, Hippocampal Untransfected = 0.85 ± 0.16 Hz n = 23, Hippocampal Control = 0.87 ± 0.41 Hz n = 8, Hippocampal SynGAP Eα1 = 0.26 ± 0.07 Hz n = 11, Mann-Whitney test between control and Eα1 p = 0.3950).

(C) mEPSC amplitude cumulative frequency distribution in cortical and (D) hippocampal cell cultures.

(E) mEPSC frequency cumulative frequency distribution in cortical and (F) hippocampal cell cultures.

The above mEPSC analyses included both cortical and hippocampal cells that had no identifiable mEPSCs during the recording period (a minimum of 5 minutes), so called 'silent cells' (Figure 46). α1 C terminal SynGAP isoforms have previously been shown to be specifically associated with higher proportions of silent cells in forebrain neuronal cultures (McMahon et al. 2012).

As Figure 46 shows, in the present experiment none of the untransfected cells were silent, whereas four Eα1 co-transfected cells were silent in the cortical cell recordings and 1 each of the cortical and hippocampal control recordings were silent (Cortex Control; mEPSCs n = 8, silent n = 1, Cortex Eα1; mEPSCs n = 7, silent n = 4, Hippocampus Control; mEPSCs n = 7, silent n = 1, Hippocampus Eα1: mEPSCs n = 11, silent n = 0). No statistical analysis of these numbers has been conducted due to the small numbers involved, but nevertheless it is suggestive of Eα1 having a silencing effect in the cortex like other α1 isoforms. Although further examination of the silent cells was not conducted in the present experiments, McMahon found that silent cells were viable, able to fire action potentials (in the absence of TTX) and didn't differ from controls in their holding currents or gross morphology (McMahon et al. 2012).

There is a risk that including the silent cell data would cause significant skewing of the statistical analysis. Figure 46 therefore presents the mean mEPSC amplitude and frequency data after excluding the silent cells. As with the full dataset, there is no significant difference in mean amplitude or frequency (Cortex Untransfected = 17.68 ± 1.4 pA, 0.88 ± 0.18 Hz n = 38, Cortex Control = 15.73 ± 1.7 pA, 0.8 ± 0.40 Hz n = 8, Cortex SynGAP Eα1 = 15.91 ± 2.6 pA, 0.44 ± 0.2 Hz n = 7, Mann-Whitney test between control and Eα1 amplitude p = 0.8665, Mann-Whitney test between control and Eα1 frequency p = 0.5358; Hippocampal Untransfected = 21.9 ± 1.5 pA, 0.85 ± 0.16 Hz n = 23, Hippocampal Control = 26.4 ± 4.2 pA, 0.99 ± 0.45 Hz n = 7, Hippocampal SynGAP Eα1 = 18.3 ± 1.8 pA, 0.26 ± 0.07 Hz n = 11, Mann-Whitney test between control and Eα1 amplitude p = 0.1259, Mann-Whitney test between control and Eα1 frequency p = 0.1509). However, one outlier in the cortical control data and two in the hippocampal control group have particularly high frequencies of

events which skews the data to make the difference between the control and Eα1 groups apparently more marked than it actually is. This is also true for the full dataset in which silent cells were included.

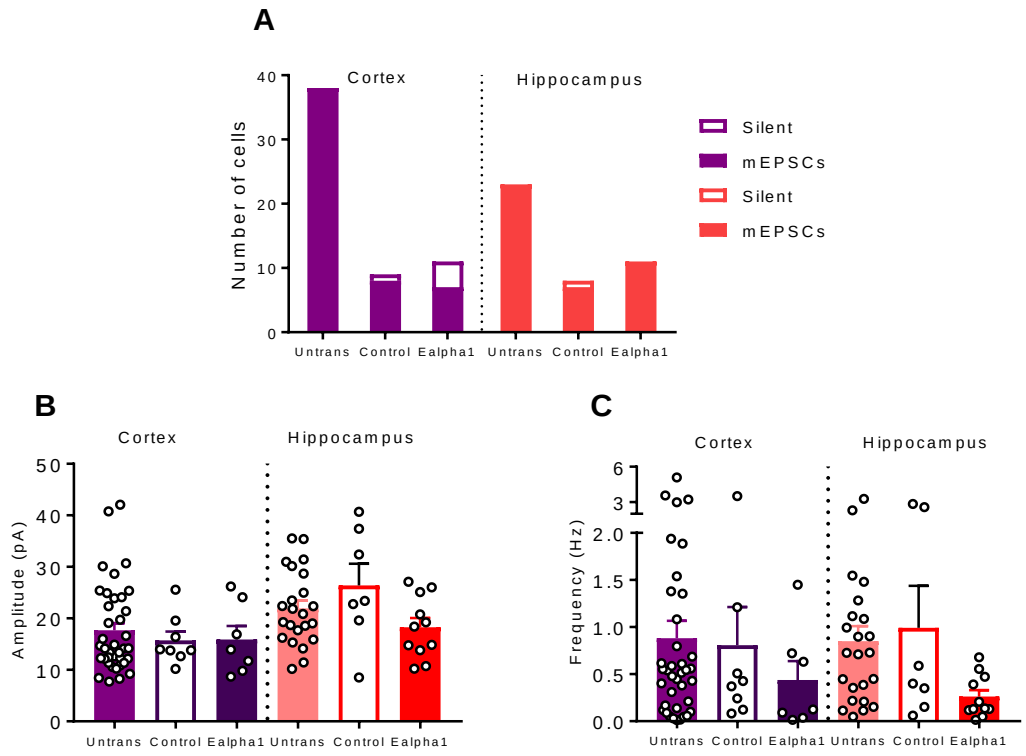

Figure 46 – There is no significant difference in mEPSC amplitude or frequency in cultures transfected with SynGAP Eα1 isoform when silent cells are excluded.

(A) A proportion of control and SynGAP Eα1 cells were 'silent' in cortical and hippocampal cultures (Cortex Untransfected; mEPSCs *n* = 38, silent *n* = 0, Cortex Control; mEPSCs *n* = 8, silent *n* = 1, Cortex Eα1; mEPSCs *n* = 7, silent *n* = 4, Hippocampus Untransfected; mEPSCs *n* = 23, silent *n* = 0, Hippocampus control; mEPSCs *n* = 7, silent *n* = 1, Hippocampus Eα1: mEPSCs *n* = 11, silent *n* = 0).

(B) There is no significant difference in mEPSC amplitude between the control and SynGAP Eα1 recordings in either cortical or hippocampal cultures when the unit of analysis is n = cell and silent cells are excluded (Cortex Untransfected = 17.68 ± 1.4 pA *n* = 38, Cortex Control = 15.73 ± 1.7 pA *n* = 8, Cortex SynGAP Eα1 = 15.91 ± 2.6 pA *n* = 7, Mann-Whitney test between control and Eα1 *p* = 0.8665, Hippocampal Untransfected = 21.9 ± 1.5 pA *n* = 23, Hippocampal Control = 26.4 ± 4.2 pA *n* = 7, Hippocampal SynGAP Eα1 = 18.3 ± 1.8 pA *n* = 11, Mann-Whitney test between control and Eα1 *p* = 0.1259).

Legend continues overleaf…

Figure 46 legend continued…

(C) There is no significant difference in mEPSC frequency between the control and SynGAP Eα1 recordings in cortical and hippocampal cultures when the unit of analysis is n = cell and silent cells are removed from the dataset (Cortex Untransfected = 0.88 ± 0.18 Hz *n* = 38, Cortex Control = 0.8 ± 0.40 Hz *n* = 8, Cortex SynGAP Eα1 = 0.44 ± 0.2 Hz *n* = 7, Mann-Whitney test between control and Eα1 *p* = 0.5358, Hippocampal Untransfected = 0.85 ± 0.16 Hz *n* = 23, Hippocampal Control = 0.99 ± 0.45 Hz *n* = 7, Hippocampal SynGAP Eα1 = 0.26 ± 0.07 Hz *n* = 11, Mann-Whitney test between control and Eα1 *p* = 0.1509).

5.4.3 SynGAP isoform abundance experiments

5.4.3.1 Primer Validation

OneStep RT-PCR was carried out and the product was run on an agarose gel to ensure the primer pair sets worked and only amplified one product (Figure 47).

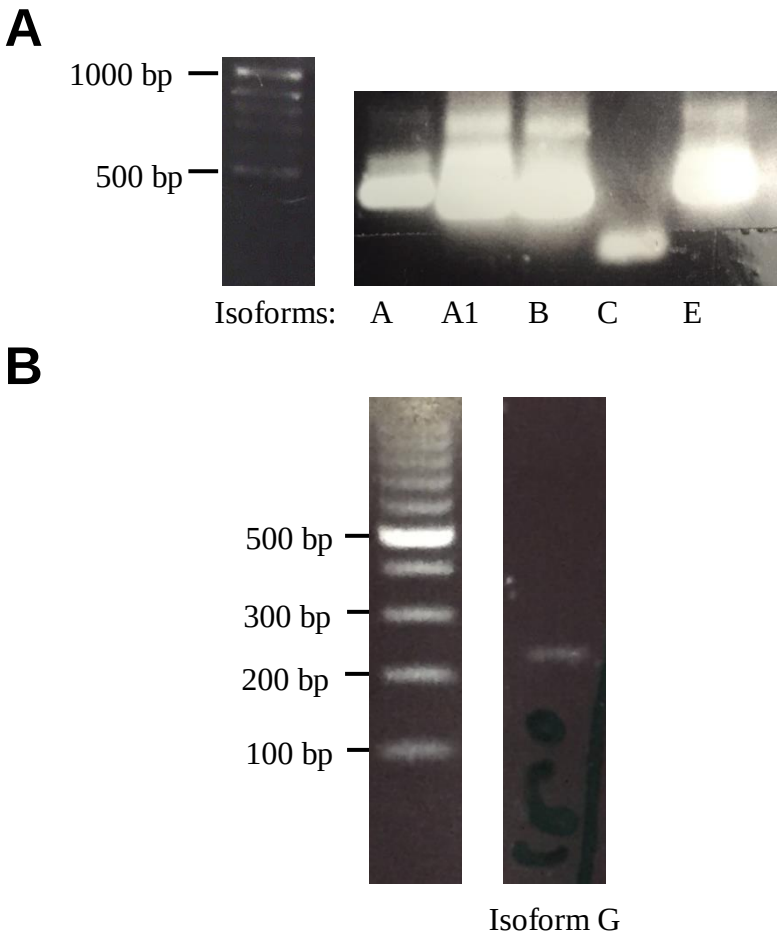

Figure 47 - Gels showing successful production and amplification of DNA from 1 µg of synthetic SynGAP isoform construct using OneStep RT-PCR.

Ladder panel is separate due to other samples present on the original gel between it and the SynGAP DNA.

Conventional two-step RT-PCR was then conducted using 6 ng of RNA for each experiment. The clean melting curves for each primer pair confirmed the amplification of just one product (Figure 48). The amplification plots showed similar amplification across the three replicate samples for each primer set except for isoforms B and E (Figure 49).

Standard curves were then constructed by conducting RT-PCR with increasing amounts of WT mouse neocortical RNA (Figure 50) in order to calculate the R^2 and primer pair efficiencies for each set of primers. Isoforms A, C and E had very good R^2 values (above 0.99), but the values for isoforms A1, B and GAPDH were lower, A1 considerably so (efficiency of 59.35%) (Table 16). The A1 primer pair was therefore discarded and will be re-designed.

There was no detectable product for primer pair G when using adult WT mouse neocortical tissue; hence no G data is presented with the melting plots amplification plots and standard curve data. In order to evaluate whether this lack of isoform G product was due to a physiological lack of G or an inability to amplify physiological levels of it using that particular primer pair, 1 μg of synthetic SynGAP G isoform construct was added to a OneStep qPCR reaction. Under these conditions an amplicon was generated and the melting curve and amplification plot were clean with no suggestion of non-specific target amplification (Figure 51). The amplification and melt plot graphs have a different appearance for the G isoform data when compared with the other isoforms as the MJ research DNA Engine Opticon PCR machine was used rather than the Applied Biosystems 7500 Real-Time PCR system. However it was later established that the G primer was not viable for reasons detailed in paragraph 5.5.2.4. It is therefore unclear exactly what the G primer pair amplified in Figure 51.

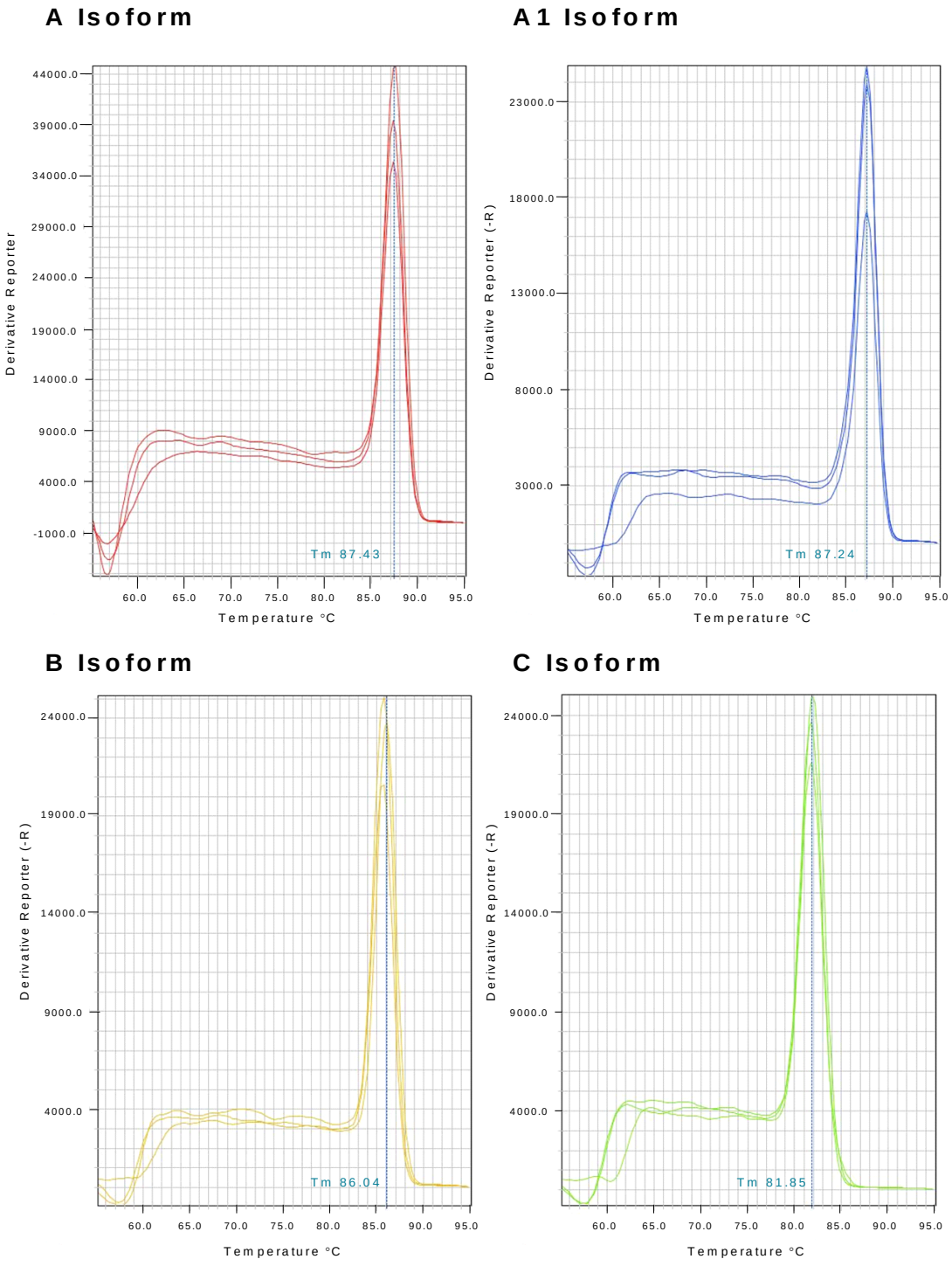

Figure 48 – SynGAP N terminal isoform primer melt plots.

(continued overleaf…)

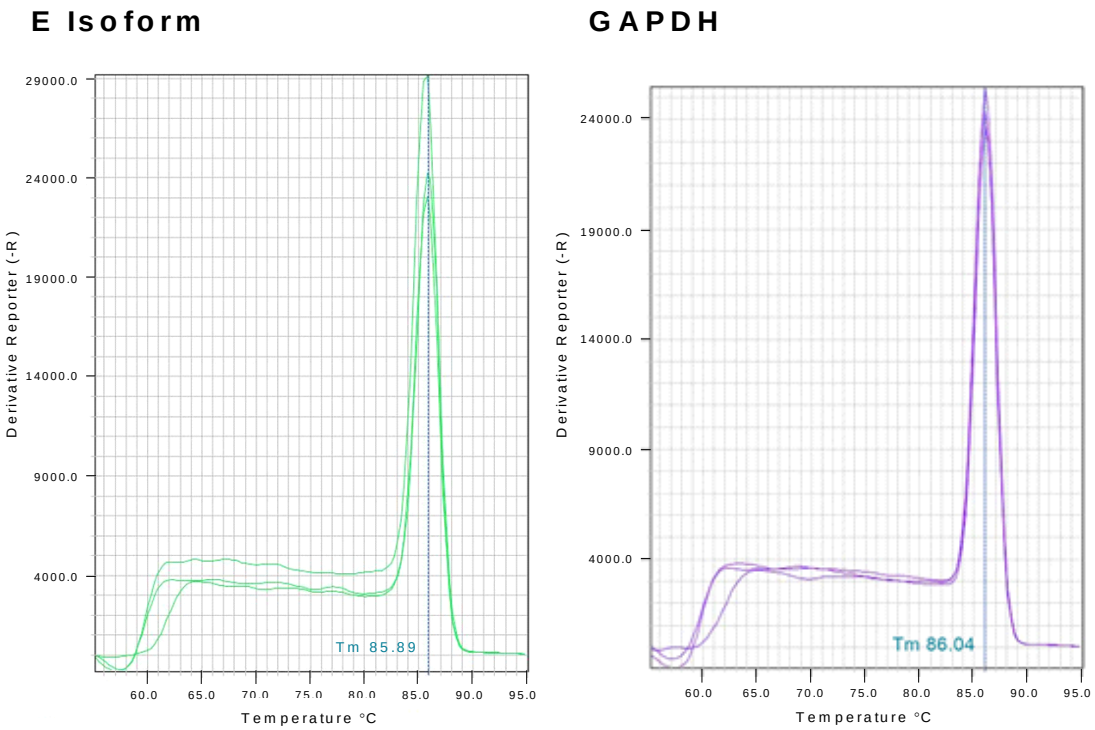

Figure 48 - SynGAP N terminal isoform primer melt plots continued.

Melt plots of each SynGAP isoform specific primer pair with melting temperature (Tm) shown in blue. 6 ng of cDNA used for each.

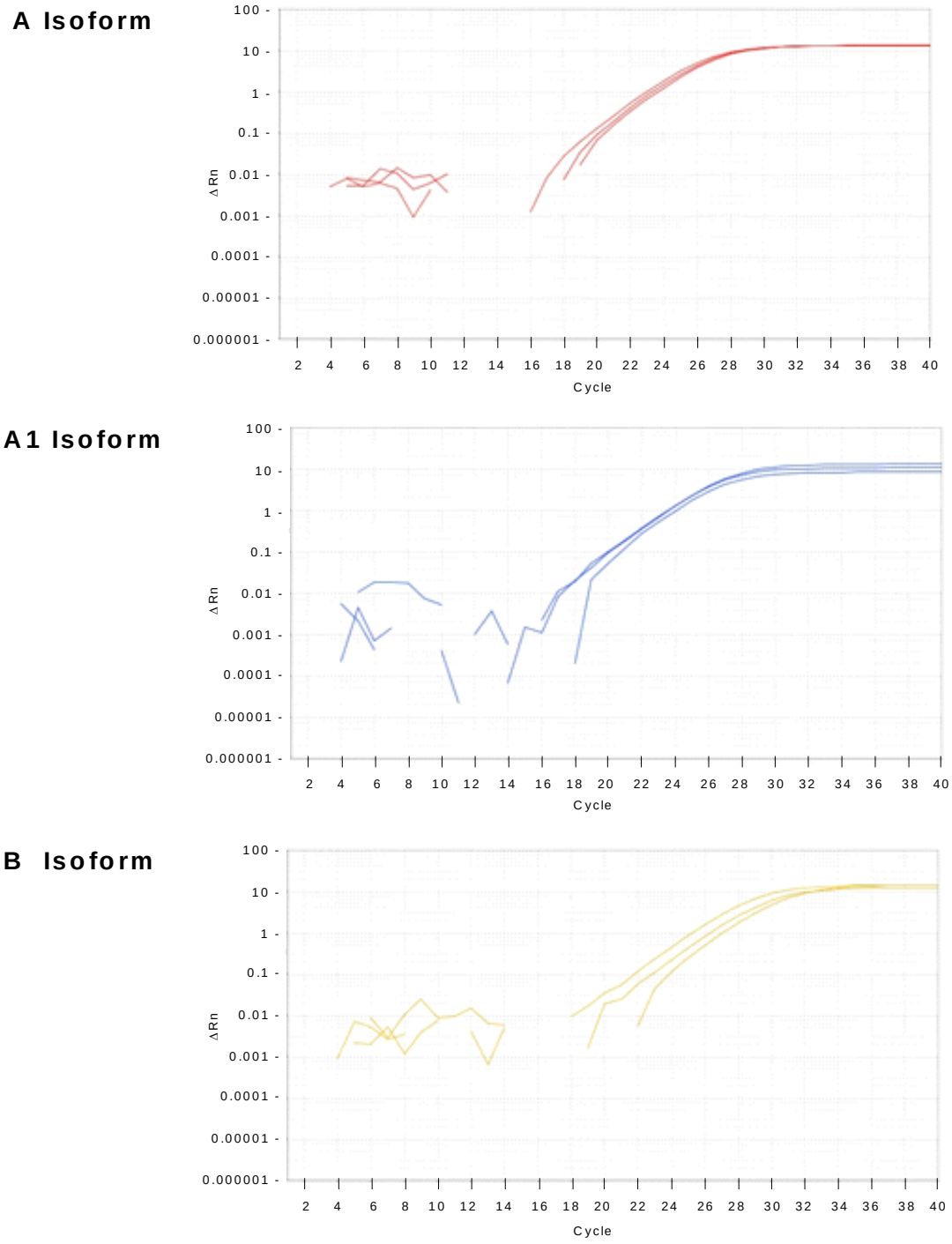

Figure 49 – Amplification plots for SynGAP N terminal isoform primers.

(continued overleaf…)

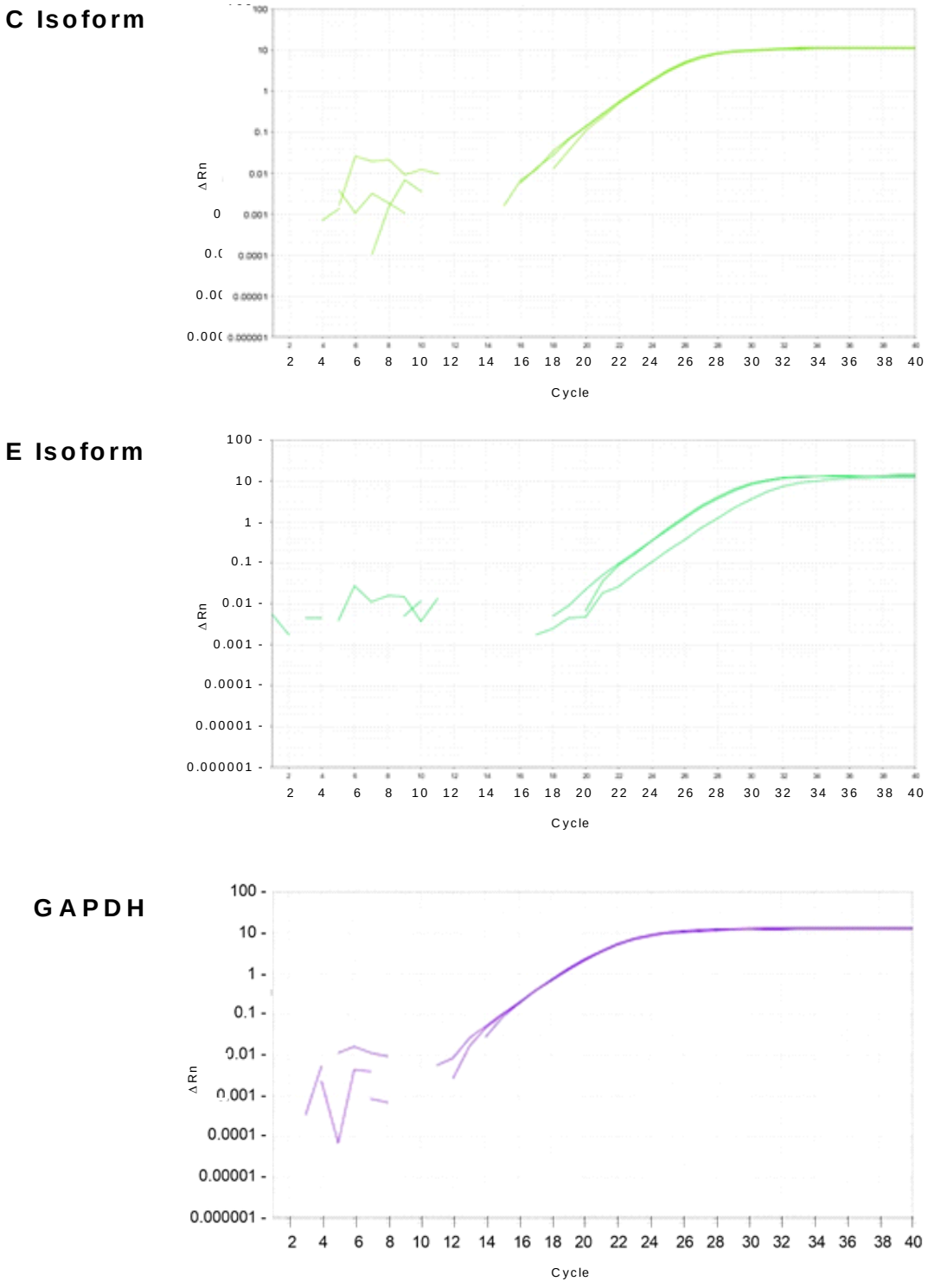

Figure 49 – Amplification plots for SynGAP N terminal isoform primers continued.

Amplification plots for each of the SynGAP isoform and the GAPDH control primer pair. 6 ng of cDNA used for each.

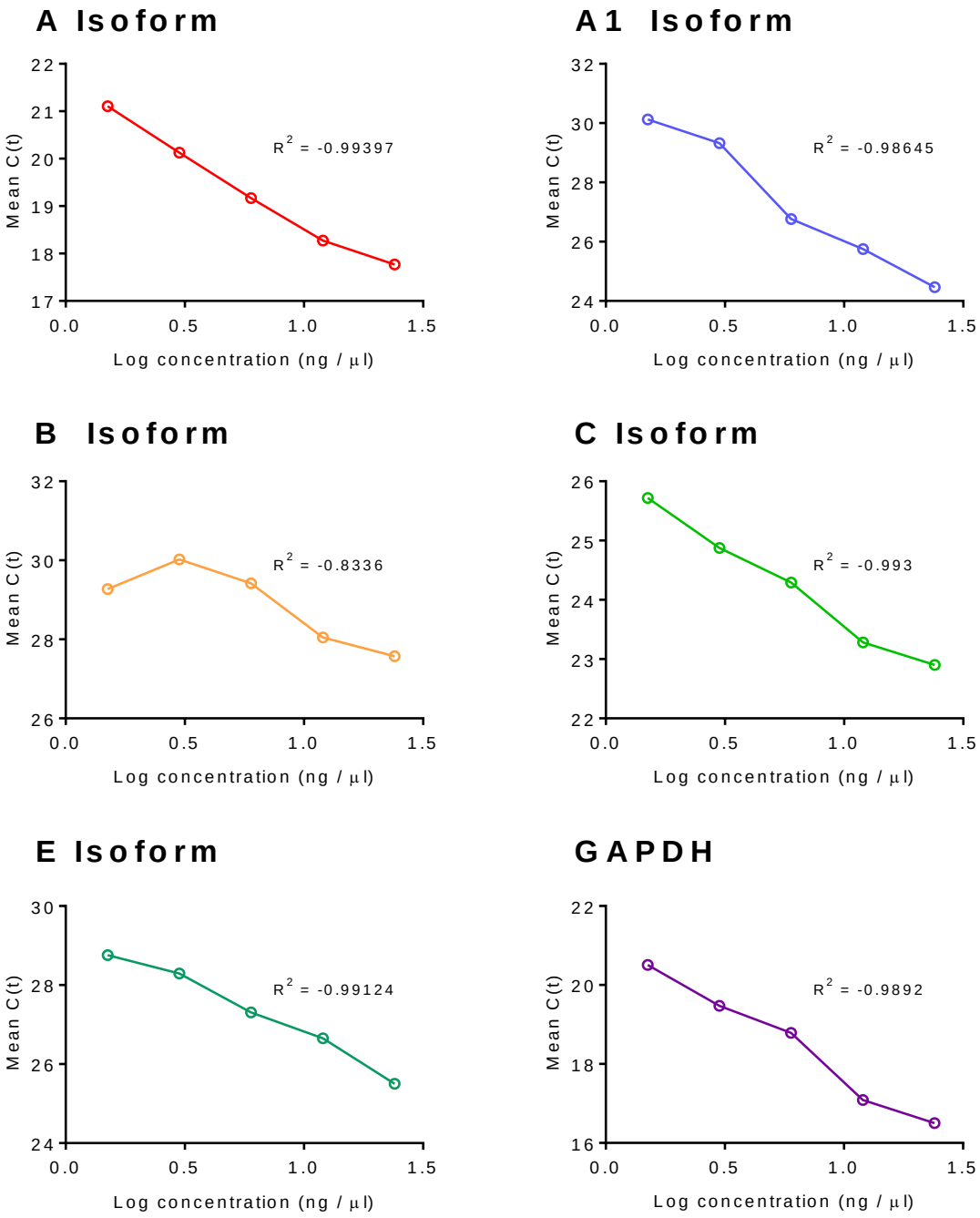

Figure 50 – Standard curves for SynGAP N terminal isoform and GAPDH control primer sets.

When the primer sets were evaluated, it was clear that aside from A1 (now discarded) all of them had efficiency values well over 100% (Table 16). Primer pair efficiency is calculated as $10^{(-1/\text{slope of standard curve})}-1$ and at 100% the template doubles after each thermal cycle during exponential amplification (Life Technologies 2012). High efficiencies can be due to the presence of inhibitors in the reactions or too much cDNA in the dilution series (BioTechniques 2011). High efficient values are therefore problematic and the potential impact of them on the RT-PCR data is explored in the discussion.

Table 16 – SynGAP isoform qPCR primers

Isoform	Forward Primer	Reverse Primer	R^2	Primer Pair Efficiency (%)
A	CGAGTCCAGCCGAAACAAAC	GGGACTCAGCAGGGACTC	-0.994	126.37
A1	CGATGTCCTATGCCCCCTTC	GGGACTCAGCAGGGACTC	-0.986	59.25
B	GCTCTTCTTGCTGCTTTCCG	GGGACTCAGCAGGGACTC	-0.833	202.05
C	AAGTGCTGACCATGACCG	GGGACTCAGCAGGGACTC	-0.993	160.89
E	TTCTCGCTGCATCTTCCGAG	GGGACTCAGCAGGGACTC	-0.991	134.03
G	CGGTGCGAGATGGAGGC	GGGACTCAGCAGGGACTC	-0.991*	188.28*
GAPDH Control	GGGTGTGAACCACGAGAAAT	CCTTCCACAATGCCAAAGTT	-0.989	94.85

*G primer results were obtained from separate qPCR in which 1 µg of RNA was added to the reaction. It therefore represents an overexpression state.

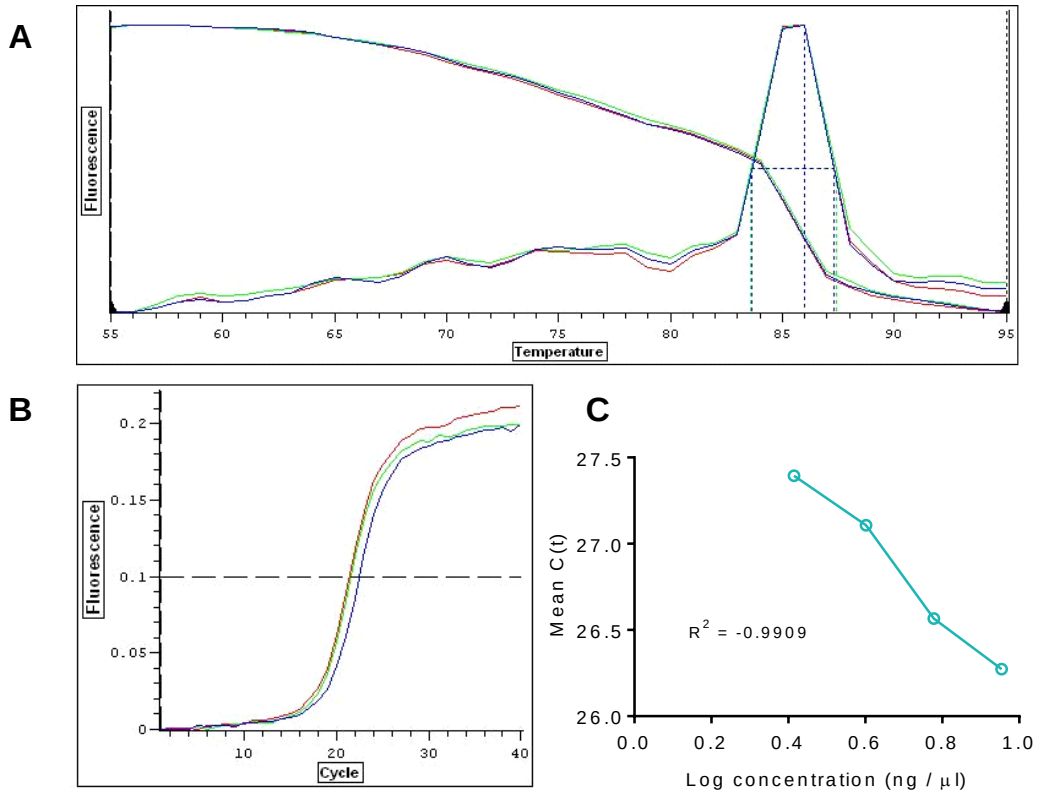

Figure 51 - G primer pair validation data using 1 µg of synthetic SynGAP G isoform construct.

(A) Melt plot.

(B) Amplification plot.

(C) Standard curve.

5.4.4 RNA "spike in" experiments

Prior to conducting experiments to compare the abundance of different SynGAP isoforms, so called 'pan SynGAP' primers, designed by McMahon and colleagues (McMahon et al. 2012) to amplify all known SynGAP isoforms, were used to check for the absence of SynGAP in the homozygous mouse neocortex. The forward primer sequence was CGAAGTGCTGACCATGAC and the reverse primer sequence was CGGCTGTTGTCCTTGTTG. As these were not newly designed primers, full validation was not conducted although their amplification and melt curve data were examined (Figure 52). Although the quantity was negligible compared to that in WT and *Syngap*$^{+/-}$, some mRNA was amplified in the *Syngap*$^{-/-}$ mice (Figure 52). As the amplification plot and melt curve show, this doesn't appear to be due to amplification of off target product as both graphs are indicative of a single amplicon. This issue is explored further in the discussion.

Thereafter a known amount of RNA was added to (or 'spiked' into) qPCR reactions using *Syngap*$^{-/-}$ mouse neocortex. This was repeated twice more, with different quantities of synthetic RNA used each time (Figure 53). Unfortunately, these experiments did not result in a clear pattern of results. The relative amounts of isoforms A and E amplified across the three spike-in experiments reflect the added quantities (i.e. more isoform added to the reaction resulted in greater amounts of amplicon). However, the amount of product for isoform C didn't follow the pattern of how much was added in; the highest amount of C was introduced in the third experiment but this resulted in the smallest amount of amplicon. Furthermore SynGAP B and G didn't amplify in any of the three experiments. It is possible that the amounts of B and G added in were too small to be amplified given the validation of their primers was conducted with larger amounts of synthetic RNA. Total or partial inhibition by other isoforms could perhaps explain the results for isoforms B, C and G which would be physiologically interesting. However, it may simply be that the primer sets and / or the synthetic RNA were not behaving as predicted under these particular experimental conditions. This is discussed further below.

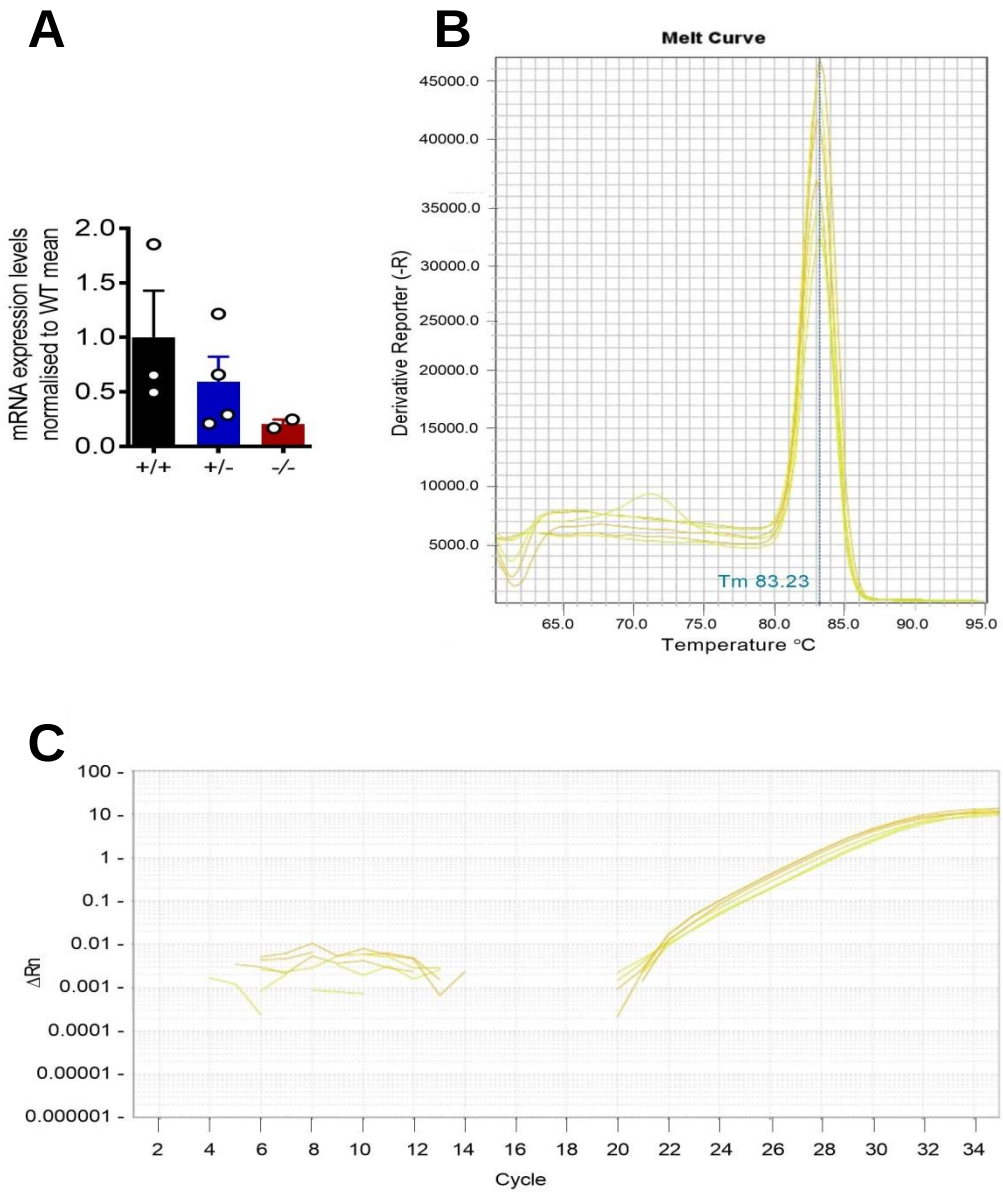

Figure 52 – RT-PCR of total SynGAP in *Syngap*$^{-/-}$ mice.

(A) Total SynGAP mRNA expression levels in WT, *Syngap*$^{+/-}$ and *Syngap*$^{-/-}$ mice using pan SynGAP primers designed to amplify all isoforms of the protein.

(B) Melting curve for pan SynGAP primers in in *Syngap*$^{-/-}$ mouse neocortical tissue showing one clear peak.

(C) Amplification plot for pan SynGAP primers in *Syngap*$^{-/-}$ mouse neocortical tissue showing similar amplification across triplicate repeats.

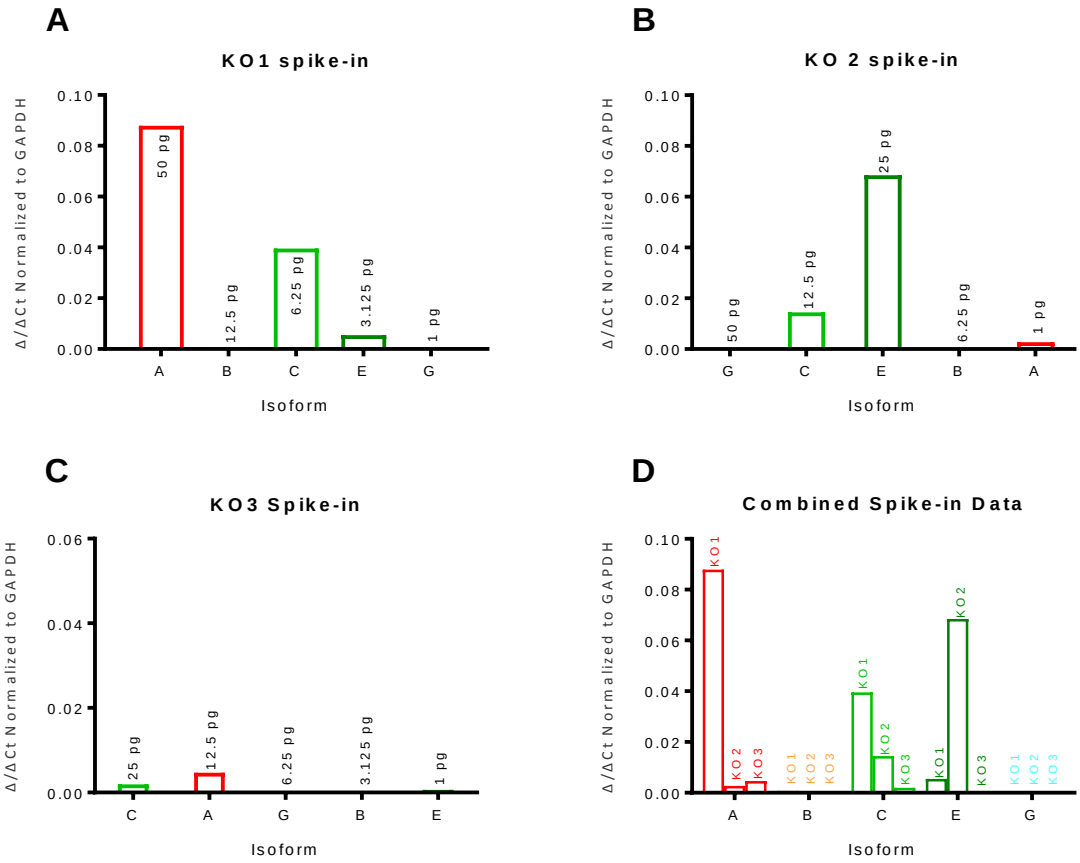

Figure 53 – Introducing known quantities of SynGAP isoforms into qPCR reactions did not result in a clear pattern of results.

A), B) and C) show the abundance of each SynGAP N terminal isoform following the 'spiking in' of the quantities of isoform cDNA noted on the graphs.

D) Combined data from panels A, B and C.

In addition to spiking in a mix of isoforms in one experiment, each isoform was also added to RT-PCR experiments individually in concentrations ranging from 0.1 pg – 100 pg (Figure 54). This was in an attempt to determine the physiological levels of isoform expression by comparing the Ct value at which each isoform was detected in WT mouse tissue with the concentration at which the same Ct value was seen in the synthetic "spike in" experiments. For example if isoform A had a Ct value of 24 in mRNA from WT tissue and the spiking in of 25 pg of synthetic SynGAP A resulted in a Ct value of 24, it is possible to conclude that there is 25 pg of SynGAP A mRNA in the WT tissue.

Unfortunately only isoforms A and E showed the expected change in abundance in relation to amount of RNA added to the mix. Isoform B was not detected at all and C did not vary consistently with the quantity introduced into the reaction. Therefore it wasn't possible to draw comparisons with WT tissue as the primers weren't behaving in a predictable or comparable manner.

Given this discrepancy in primer efficacy when different quantities of RNA were added, OneStep RT-PCR was used to evaluate the behaviour of each primer pair at different numbers of PCR cycles to see how similar the results were (Figure 54). Unfortunately this revealed considerable differences in results under similar experimental conditions. For example very little SynGAP C amplicon was seen under any of the experimental conditions, but in contrast, A, B and E were present at 25, 35 and 50 cycles. A, B and G clearly increased in abundance as more RNA was added at 25 cycles (although G isn't visible until 1000 pg is present), but this pattern is not very clear for E. Furthermore at 35 and 50 cycles A and E appear saturated with even the smallest amount of RNA (0.1 pg) and by 50 cycles B and G also appear saturated. This considerable lack of consistency in primer efficacy invalidates any attempt in this chapter to make conclusions between SynGAP isoform abundance.

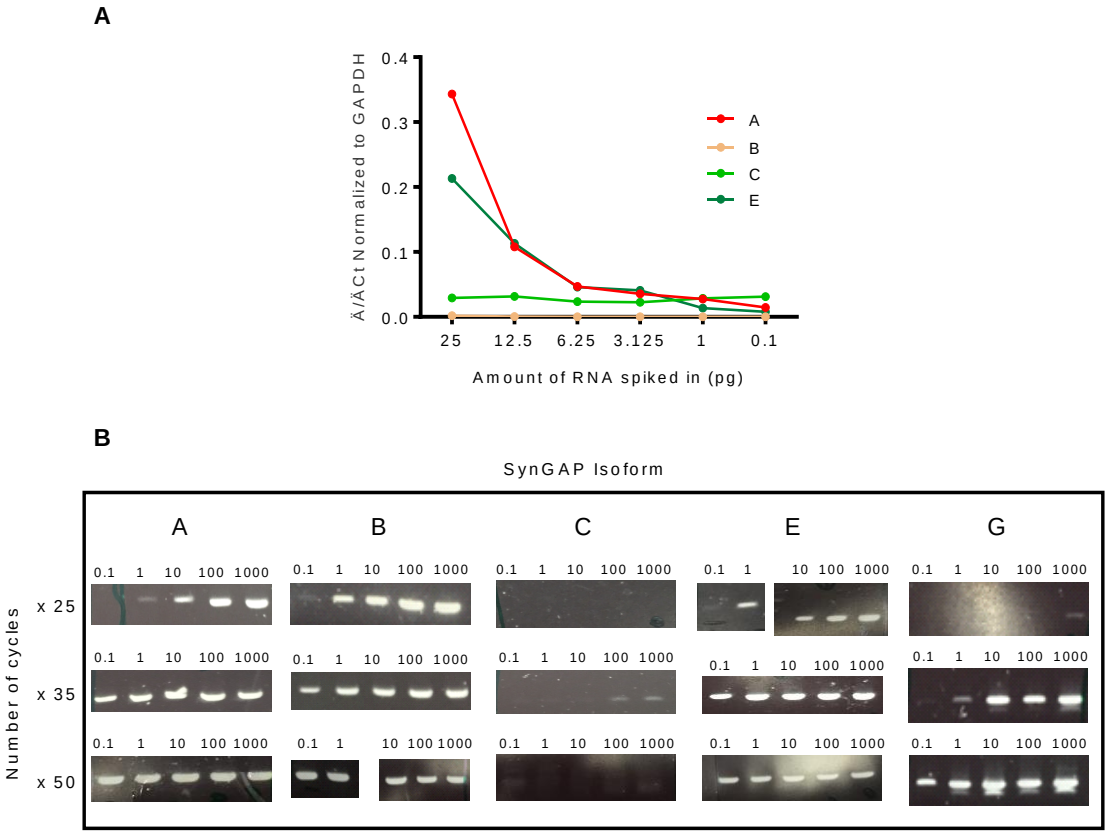

Figure 54 – The SynGAP isoform N terminal primers are not working in an equivalent manner making comparisons between their amplicons extremely difficult.

(A) Varying amounts of SynGAP isoform synthetic RNA were added individually to RT-PCR reactions with a view to comparing this data to that from WT mice to establish the physiological concentrations of each isoform in vivo. Only SynGAP A and E showed the expected decrease in abundance with reducing amounts of RNA. Isoform B wasn't detected and C did not vary with the amount of RNA added. Therefore it wasn't possible to make comparison with WT data.

(B) OneStep RT-PCR was carried out using increasing amounts of synthetic SynGAP isoform RNA (0.1, 1, 10, 100 and 1000 pg for each primer pair) and using three different number RT-PCR cycle numbers. The results show that the primers are not behaving in an equivalent manner to each other making comparisons between SynGAP isoforms invalid.

n.b. the gel images for SynGAP A and B at 35 cycles have been horizontally flipped as the concentrations RNA were loaded in the opposite order.

5.5 Discussion

The data in this chapter explores the role of the multiple SynGAP isoforms. The first part examines the effect on miniature post-synaptic currents of transfecting the previously unstudied SynGAP Eα1 isoform into neuronal cultures. The second presents the data from RT-PCR experiments investigating the different SynGAP N terminal isoforms.

5.5.1 SynGAP Eα1 mEPSC recordings

The data presented here is suggestive of SynGAP Eα1 resulting in more silent cells in the cortex (Figure 46). However in the cells that did have mEPSCs, no mean difference in mEPSC amplitude or frequency was seen when comparing cells co-transfected with SynGAP Eα1 and eGFP with their neighbouring control cells. This is true for both cortical and hippocampal cultures (Figure 45) and also when the silent cells are removed from the analysis (Figure 46). However, there was a tendency for cortical cells co-transfected with Eα1 and eGFP to have larger and more frequent mEPSCs, whereas hippocampal cells co-transfected with Eα1 and eGFP tended to have smaller and less frequent mEPSCs than neighbouring control cells (Figure 45). Discussion of why a lack of overall Eα1 effect was seen in contrast to data in other α1 isoforms (McMahon et al. 2012) is warranted. Given that these experiments were similar to mEPSC recordings from cultured neurons presented in Chapter 4, some repetition of the relevant factors here is inevitable.

5.5.1.1 Culture health

Poor culture health could have affected the quality or stability of the recordings, but the cultured neurons looked healthy when compared informally with other culture plates. Furthermore the following measures were taken to reduce the likelihood of unstable or poor quality recordings:

- Recordings were typically discarded if the holding current dropped below -100 pA
- Portions of each trace during which the access resistance was found to have exceeded 30 MΩ or varied by > 20%
- Portions of each trace with a root mean squared noise of >4 (calculated by Minianalysis Version 6 Software (Synaptosoft Inc.) were discarded

- Traces with less than 5 minutes of recording remaining thereafter were also discarded

However, it is worth noting that no silent cells were recorded from the completely untransfected coverslips. This is important as it means that silencing of cells in this context could be as a result of exposure to the lipofectamine transfection reagents rather than related to SynGAP Eα1.

5.5.1.2 Were the currents recorded typical of mEPSCs?

A lack of significance could be due to heterogeneity in the type of events being recorded. However, reassuringly, the frequency of untransfected recordings in this thesis (Cortical cultures 0.88 Hz, Hippocampal cultures 0.85 Hz) is in keeping with the published literature 0.2 – 2.5 Hz in rat culture or slice recordings (Turrigiano et al. 1998; De Simoni et al. 2003; Zhang et al. 2005; Sutton et al. 2006). It is acknowledged that the amplitudes recorded (Cortical cultures: 17.68 pA, Hippocampal cultures: 21.9 pA) are somewhat higher than the 11 – 15 pA in the literature though (Turrigiano et al. 1998; De Simoni et al. 2003; Zhang et al. 2005; Sutton et al. 2006).

I am however confident that, on balance, true mEPSCs were recorded because events were also manually reviewed to ensure they were fast rising and asymmetric and their amplitude distributions were found to have the expected positive skew (Figure 44) seen by other authors (Bekkers et al. 1990; McBain & Dingledine 1992; Wyllie et al. 1994).

5.5.1.3 Research protocol

McMahon and colleagues found that mouse SynGAP α1 C terminal isoforms were associated with a reduction in mEPSC amplitude and frequency. However, they recorded from mouse forebrain cultures, whereas the current recordings were made from separate rat cortical and hippocampal cultures into which mouse SynGAP Eα1 were transfected. Therefore, there could be an effect of species and type of cultured cell. SynGAP is highly conserved between species including portions of intronic

sequence which may regulate promoter activity (McMahon et al. 2012). There also appears to be conservation of sequence between mouse and rat for the putative new isoforms (personal correspondence from Owen Dando, Centre for Integrative Physiology, University of Edinburgh). It therefore seems unlikely that isoform specific effects would be drastically different between mice and rats, but it can't be ruled out.

McMahon and colleagues didn't differentiate between cortical and hippocampal recordings. This is interesting given the opposite trend in mEPSC amplitude and frequency found in the two brain areas in the current dataset. It isn't appropriate to combine the current cortical and hippocampal datasets here to see how they compare more directly to McMahon's work, as slightly different culturing methods were employed for the two cell types. Given that the hippocampal cells co-transfected with Eα1 and eGFP tended to have smaller and less frequent mEPSCs than neighbouring control cells, it may be that more of McMahon's recordings were derived from hippocampal cells. Alternatively it is entirely possible that the SynGAP Eα1 isoform has differential effects in different brain areas, but this cannot be confirmed or refuted with the present dataset.

Aside from this, the research protocol followed in the current work, mirrors McMahon's protocol closely (Table 17). Both used liposome mediated transfection and recorded from cells at the same day in vitro ages using identical external and internal recording solutions. There were minor difference in McMahon's inclusion criteria as she discarded cells with an access resistance > 28 MΩ rather than 30 MΩ, but accepted cells with a holding potential as negative as -150 pA (compared with the current -100 pA cut off) as long as they were stable. On balance I think the minor differences seen appear unlikely to account for the potential discrepancy in results.

Table 17 – SynGAP isoform mEPSC experimental procedures are similar to those of McMahon

Parameter	SynGAP Eα1 experiments	McMahon et al. experiments
Cell origin	Rat	Mouse
Brain region	Cortex and hippocampus	Forebrain
Age at culturing	DIV 20.5	DIV 17.5
Components of culture medium	**Cortical cultures (until feeding)** Neurobasal A, rat serum, Penicillin-streptomycin, B27 and Glutamine **Hippocampal (and cortical when fed)** Basal medium eagle, glucose solution, sodium pyruvate, N2 supplement, B27 supplement and penicillin-streptomycin solution or antibiotic-antimycotic	Neurobasal medium, B-27, Glutamax (L-alanyl-L-glutamine), Penicillin-Streptomycin
Transfection procedure	Lipofectamine 16 to 25 hours before recording	Liposome-mediated co-transfection with eGFP and SynGAP 16 to 36 hours before recording
Isoforms	Mouse Eα1	Mouse Aα1, Bα1,Cα1, Aα2, Bα2, Cα2
Age at recording	DIV 9 - 11	DIV 9 - 11
Recording solution	**Identical:** (in mM) NaCl 150, KCl 3, HEPES 10, $CaCl_2$ 2.5, $MgCl_2$ 1.3, glucose 10, glycine 0.05. 0.5 µM TTX, 50 µM picrotoxin	
Internal solution	**Identical:** (in mM) Cs gluconate 130, CsCl 10, HEPES 10, EGTA 0.1, glucose 10, sodium phosphocreatine 10, Mg ATP 4 and Na3GTP 0.5.	

5.5.1.4 Sample size

Could the lack of difference in mean amplitude or frequency in E α1 recordings be because the experiment was underpowered? As noted in Chapter 2, there was no previous published Eα1 research on which to base a power calculation. McMahon's Aα1 and Cα1 mEPSC amplitude data from her unpublished thesis and her 2012 Nature Communications paper (McMahon 2010; McMahon et al. 2012) were therefore used as proxy measures. The required group size in order to achieve an effect size of 0.05 and power of 0.8 was found to be between 23 and 127 cells in the Eα1 experiments depending on whether Aα1 or Cα1 data (Bα1 data fell between the two) was used. Therefore with group sizes of 7 – 11 for Eα1 transfected cells and neighbouring non-transfected cells, it is possible that this experiment would've observed a significant difference if the number of cells recorded from was higher.

When examining the Eα1data (with silent cells excluded) post-hoc using the power calculation and sample size software at http://biomath.info/power/ttest.htm, it was possible to assess how small a difference between the means could be identified for a significance level of 0.05 and power of 0.8. As Table 18 shows, the present body of

work is statistically underpowered as none of the observed mean values are larger than the minimum difference that could be detected.

However, the same caveats apply here as to the excitatory and inhibitory current data presented in Chapter 4; the use of power calculations is questionable as the data is a) not normally distributed and b) sampled from populations with different variances (Table 18).

Once again, the huge variation in the numbers of animals needed per group going forward if this current data is used for a power calculation, likely reflects the limitations of the power analysis and presents difficulties as it is not practical to use datasets as large as 156 let alone 22942. The predicted numbers for the hippocampal data are smaller than that for the cortical data though and so perhaps a pragmatic approach would be to increase the hippocampal group sizes to the point at which a statistical difference could be detected. A decision based on the experimental findings could then be made with regards to whether there was any merit in doing more cortical recordings. Perhaps a more robust hippocampal dataset could be used as the basis for a power calculation for cortical recordings as it could be argued that using data from other isoforms for power calculations is fundamentally flawed.

Finally it is again worthy of note that if the variance in the Eα1 data was consistently in the same direction compared to control, this might be informative, but the direction of variation changes between datasets, much like the Chapter 4 excitatory and inhibitory current data.

Table 18 – Size of detectable difference in SynGAP Eα1 mEPSC data and future sample size calculations based on the current SynGAP Eα1 data

Parameter	Control SEM and (sample size)	Eα1 SEM and (sample size)	Size of statistically detectable difference between groups*	Size of observed difference in means between groups	Sample Size (n) required per group if current data is used for power calculation
Cortical mEPSC amplitude	1.7 (8)	2.6 (7)	11 pA	0.18 pA	22,942
Hippocampal mEPSC amplitude	4.2 (7)	1.8 (11)	18 pA	8.1 pA	31
Cortical mEPSC frequency	0.4 (8)	0.2 (7)	1.7 Hz	0.36 Hz	156
Hippocampal mEPSC frequency	0.45 (7)	0.07 (11)	1.9 Hz	0.73 Hz	43

SEM = standard error of the mean, SD = standard deviation
*calculated using http://biomath.info/power/ttest.htm

5.5.1.5 Statistical analysis

The statistical measure (Mann-Whitney test) used to compare the Eα1 transfected cells with their neighbouring control cells was perhaps somewhat crude as it did not take into account the richness of the data with regards to factors such as transfection batch and culture batch. McMahon and colleagues overcame this by using a generalised linear mixed model statistical approach which could be considered for future Eα1 experiments. At the present time without employing a more complex analysis it is unclear whether this factor has led to a lack of mean statistical significance in the current dataset.

5.5.1.6 Control experiments

The current experiments compared Eα1 and eGFP co-transfected neurons to neighbouring neurons on the same coverslips. Expression of SynGAP Eα1 was taken to have occurred if the co-expressed eGFP was evident (i.e. if the neuron fluoresced green). Therefore neighbouring cells that weren't fluorescing were deemed not to have taken up the Eα1, but no objective measure was made of whether this assumption was true. If SynGAP Eα1 and eGFP were not equally expressed by cells that had been successfully transfected, this would therefore make the interpretation of Eα1 cell and control cell data difficult.

Furthermore, although the control cells had been bath exposed to lipofectamine transfection reagents, it was assumed that they had not been successfully transfected as they weren't expressing sufficient amounts of eGFP to fluoresce. It is not possible to know if this was because of some hitherto unidentified difference between them and successfully transfected cells that could potentially impact on mEPSC properties. Therefore for future experiments a β-globin plasmid could be co-transfected with GFP to act as a control. Control cells would then be more similar to experimental cells in so far as they would have taken up an external plasmid and they could also be positively identified as having undergone successful transfection if they fluoresce. Furthermore, samples could be taken from the cells to identify whether the construct was indeed being expressed. For example flow cytometry could be used to evaluate the expression of eGFP due to its fluorescent properties, but RT-PCR could be used to specifically ensure the gene of interest and not just its eGFP partner was being expressed.

5.5.1.7 Summary of Eα1 recording data

There is a suggestion that the SynGAP Eα1 isoform might, like other SynGAP isoforms have an impact on synaptic strength. However, the methodological issues described above make it difficult to draw definitive conclusions on this without further experiments.

5.5.2 SynGAP RT-PCR experiments

The initial OneStep RT-PCR confirmed the primer sets were able to amplify specific product (albeit using synthetic RNA), as did the presence of product in the two step RT-PCR experiments on WT neocortical tissue, except for SynGAP isoform G. However, these experiments could not evaluate the comparative efficacy of the primers and it wasn't until the RNA "spike in" experiments that it became clear that they may not be working in a comparable manner under the same experimental conditions. This was confirmed by the later OneStep RT-PCR reactions with varying amounts of RNA and numbers of PCR cycles. Hence drawing any conclusions from the RT-PCR experiments became extremely difficult. The relevant factors are now discussed in more detail below.

5.5.2.1 Sub-optimal predicted primer pair properties

Attempts were made to design the new primers to fit the following list of optimal parameters suggested by Dr Paul Baxter, Centre for Integrative Physiology, University of Edinburgh, based on his extensive RT-PCR experience:

- Primer length 17 – 23 bp
- Melting temperature 59 – 62.9°C
- Difference in melting temperatures of no more than 1°C
- Primer end is a cytosine or guanine
- Primers span an exon boundary
- Product (amplicon) length of 150 -250 bp

The primer pair properties were evaluated using the Sigma Aldrich OligoEvaluator™ (http://www.oligoevaluator.com/OligoCalcServlet). The amplicon length was estimated using the NCBI Blast tool (https://blast.ncbi.nlm.nih.gov/Blast.cgi) although it wasn't always possible to find a mouse transcript in which both the forward and reverse primer were found. Therefore for some primer pairs the amplicon length was estimated from a different species. Given that SynGAP is highly conserved between species (McMahon et al. 2012), these estimates are likely to be very similar to the hypothetical length in a mouse. Unfortunately no transcript with both the forward and reverse primer sites could be found for SynGAP E or G so it wasn't possible to estimate the amplicon length from Ensembl. For G this was because the forward primer was designed to be within the 5' untranslated region (UTR) of the isoform due to the short length of unique sequence available for G primer design. However, it was also later determined that there was a significant flaw in the design of the G primer (see paragraph 5.5.2.4). SynGAP E (as well as G) is a putative isoform so it is perhaps not surprising that the forward primer for it couldn't be identified in an existing SynGAP transcript. SynGAP sequence data from Owen Dando was therefore used to predict the amplicon length for isoforms E and G.

Whether each primer pair crossed an exon boundary was established by identifying the primer sites on the exon display on the Ensembl website

http://www.ensembl.org/Mus_musculus/Transcript/Exons?db=core;g=ENSMUSG00000067629;r=17:26941253-26972434;t=ENSMUST00000194598. The longest transcript (ENSMUST00000194598.5) was used except for isoform B and C (ENSMUST00000081285.8) and GAPDH (ENSMUST00000118875.7). As no transcript containing the E and G isoform forward primers could be identified it wasn't possible to determine whether they crossed an exon boundary, but once again this has become irrelevant for G due to the problems with its design (see paragraph 5.5.2.4).

The amount of unique sequence for some of the SynGAP isoforms is very short or non-existent which meant that it wasn't possible to ensure that all the melting temperatures fell in the desired range or that they didn't differ by more than 1°C. 1°C is particularly stringent though as commercial advice suggests a difference of 5°C is an acceptable range (Life Technologies 2012) within which the primers should melt and bind to the target sequence simultaneously. For the most part (except SynGAP E primer set) the current primers all fall within this more lenient cut off. Their melting temperatures were often predicted to be higher than was deemed optimal for RT-PCR conditions, but the reverse transcriptase enzyme used for the 2 step RT-PCR can be used to a temperature of 65°C and the enzyme mix for the OneStep PCR up to an annealing temperature of 68°C (Roche Applied Science 2010; Qiagen 2012). Furthermore commercial companies suggest a melting temperature between 50 and 65°C (BIO-RAD Laboratories 2006). The annealing temperature for the two step RT-PCR reactions was typically 55°C and given the advice that this should be 5°C lower than the primer melting temperature, this might have been a more important factor as all the SynGAP isoform primers had melting temperatures > 60°C. With an annealing temperature that is too low, primers can bind non-specifically to the template, but examination of the melt curves suggests this was not a problem as one clear product was amplified.

The amplicon length was considerably longer that the chosen ideal for many of the primer sets which was already more generous at its upper limit than the commercially suggested range of 50 – 200 bp (BIO-RAD Laboratories 2006; Qiagen

2011; Life Technologies 2012). Longer amplicons do not amplify as well as shorter ones which would lead to lower primer pair efficiencies, so given high primer pair efficiencies in this set of experiments, amplicon length wasn't clearly a problem unless it was masked by other more influential factors.

GC content of primers is recommended to fall in the range of 50-60% (BIO-RAD Laboratories 2006; Life Technologies 2012) although percentages up to 70% can be managed with adjustment of the thermocycling conditions (Roche Applied Science 2010). Therefore the GAPDH reverse primer's GC content of 45% is on the low side and the SynGAP G isoform forward primer is on the high side (70%). It is possible that this contributed to the lack of consistency of primer sets under the same conditions, but high GC content is more likely to lead to secondary structure formation and SynGAP G was not predicted to form secondary structures. It was in fact SynGAP E primer pair that was most at risk of this.

Which, if any, of the individual physiological properties adversely affected each primer pair is impossible to delineate from the current data. However, suffice to say there was considerable variation in the properties of the different primer sets which may have contributed to the lack of consistency in their efficacy.

Table 19 – SynGAP isoform RT-PCR primer pair properties

Isoform	Sequence	Primer Length (bp)	Melting Temperature (°C)	GC Percentage (%)	Predicted amplicon length (bp)	Span an exon boundary? (yes or no)	Secondary structure	Primer / Dimers
A	CGAGTCCAGCCGAAACAAAC	20	66.9	55	346	No	None	No
A1	CGATGTCCTATGCCCCCTTC	20	67.6	60	523	No	None	No
B	GCTCTTCTTGCTGCTTTCCG	20	66.3	55	296	No	None	No
C	AAGTGCTGACCATGACCG	18	62.5	55.6	76	No	None	No
E	TTCTCGCTGCATCTTCCGAG	20	67.9	55	306#	Couldn't be identified on exon view on Ensembl	Strong	No
G	CGGTGCGAGATGGAGGC	17	68.5	70.6	281#	Couldn't be identified on exon view on Ensembl	None	No
SynGAP reverse*	GGGACTCAGCAGGGACTC	18	62.6	66.7	-	No	None	No
GAPDH Forward	GGGTGTGAACCACGAGAAAT	20	63.8	50	120	No	Weak	No
GAPDH Reverse	CCTTCCACAATGCCAAAGTT	20	63.8	45		No	Very weak	No
Pan SynGAP Forward	CGAAGTGCTGACCATGAC	18	60.5	55.6	284	No	None	No
Pan SynGAP Reverse	CGGCTGTTGTCCTTGTTG	18	63.1	55.6		Yes (between exons 7 and 8)	None	No

*This reverse primer was used for all SynGAP isoform specific primer pairs # information derived from Owen Dando's data

5.5.2.2 Sub-optimal primer pair validation data

Ideally a primer pair will have an efficiency of 100% meaning the template doubles after each thermal cycle during exponential amplification (Life Technologies 2012). The A1 primer pair was discarded due to particularly low primer pair efficiency (59.25%) as any amplicon abundance determined using this primer pair may have significantly underestimated the amount of A1 isoform present.

SynGAP B isoform primer pair's standard curve was not straight seemingly due to a particularly low first data point and related to this (because primer pair efficiency = $10^{(-1/\text{slope of standard curve})}$ -1), it had an unacceptably high primer pair efficiency of 202.05%. Efficiencies in the range of 90-110% are reasonable (BIO-RAD Laboratories 2006; Life Technologies 2012) so the data for SynGAP B in particular, but also the other SynGAP isoforms was outwith this range. As mentioned above, high efficiencies can be due to the presence of inhibitors in the reactions, particularly reagents carried over from the reverse transcriptase step. They can also arise when too much cDNA was used in the dilution series for the standard curve (BioTechniques 2011). It might therefore be worth repeating the standard curves with lower concentrations and perhaps giving consideration to adding cDNA purification steps despite the Transcriptor First Strand cDNA Synthesis Kit instructions stating this isn't required (Roche Applied Science 2010).

In addition to the high efficiency, the B primer pair had a low R^2 value of 0.833. This is the extent to which the experimental data fit the standard curve and generally values less than 0.98 are deemed too low (BIO-RAD Laboratories 2006). The use of Isoform B primer pair was therefore questionable and in fact, there is an argument that all the SynGAP isoform primer pairs should've been re-evaluated to see if they could be better designed prior to RNA "spike in" experiments.

5.5.2.3 RNA used for primer validation

Use of the OneStep RT-PCR kit confirmed that the primers were able to successfully amplify their specific targets in synthetic RNA. However, further primer validation was carried out using two step RT-PCR on WT mouse neocortical tissue rather than

using synthetic RNA. No product was seen for isoform G and so 1 µg of synthetic RNA was used to establish if the problem lay with the reaction and primer pairs (i.e. the experiment didn't result in amplification of G isoform that was present) or in the RNA substrate (i.e. there was no G isoform present to amplify). The 1 µg experiments successfully generated an amplicon, suggesting there may not be any G isoform in the WT tissue. However, 1 µg is considerably higher than physiological levels of RNA so this could also have had a bearing on the results and it is also possible that the synthetic G isoform RNA's physiological properties cause it to behave differently under experimental conditions when compared to the WT tissue, something that was not evaluated.

5.5.2.4 There was an error in the SynGAP G forward primer design

Following the above experiments, it was determined that the design of the SynGAP G forward primer is flawed. On cross referencing the primer sequence again with Dr Dando's sequence information it was confirmed that the first part of the G forward primer (CGGTGCGAG) lies at the end of the first exon of G and is within the 5' (UTR) of the protein. However, it then became clear that the rest of the primer sequence (ATGGAGGC) is at the start of the coding region in exon 2, rather than at the actual start of exon 2 (which is a continuation of the 5' UTR). This means there is a gap between the two portions of sequence which is of course incompatible with a functioning primer. This primer will now need to be redesigned with the correct sequence information as a guide.

5.5.2.5 The behaviour of the SynGAP RT-PCR reactions is not consistent under similar experimental conditions

The relative amounts of isoforms A and E across the three "spike-in" experiments (Figure 53) reflect the quantity of RNA added (i.e. more synthetic RNA in = greater product produced) and they had the best R^2 and primer pair efficiencies perhaps adding weight to the argument that the data for the other isoforms is adversely affected by primer properties. The amount of product for isoform C didn't follow the pattern of how much was added in though and when synthetic SynGAP C RNA was introduced to RT-PCR individually at different concentrations, there was no appreciable change in the amount of amplicon detected (Figure 54). In addition to

this, SynGAP B was not detected either when probed for in the multi-spike in experiments (Figure 53) or when it was added in individually (Figure 54).

In principle these discrepancies in Isoforms B and C could be due to inhibition by other isoforms. However, in the case of C, the expression pattern in the multi-spike in experiments doesn't seem to relate to the abundance of any of the other isoforms. In the case of SynGAP B, the complete lack of product could just as easily reflect unexpected synthetic RNA or primer pair behaviour making conclusions about inhibition by other isoforms impossible.

In order for comparisons between the SynGAP isoforms to be made, the primer pairs for each one need to behave similarly under the same conditions. OneStep RT-PCR experiments conducted to better understand the comparability of the data for the different SynGAP isoforms made it abundantly clear that there is huge variation in the results (Figure 54). As noted, this could be due to the primer pairs behaving differently from one another. However the physiological properties of the synthetic SynGAP RNA constructs (e.g. melting temperature, GC content etc.) have also not previously been evaluated. If such properties vary between the constructs then this would also potentially skew the RT-PCR results. Furthermore, it is possible that due to varying levels of common sequence between the SynGAP isoforms, hybridisation occurred between PCR products, the primers and the target cDNAs in the RT-PCR experiments.

5.5.2.6 Some SynGAP appeared to be present in RT-PCR of *Syngap*$^{-/-}$ neocortical tissue

A further problem with the "spike-in" RT-PCR experiments is the possible presence of small amounts of SynGAP in *Syngap*$^{-/-}$ mice. The abundance is markedly less than that in WT and heterozygous mice, so it is possible that the explanation is the amplification of non-specific products. However, the melting curve for the pan syngap primer pair is clean suggesting a single amplicon (Figure 52). Furthermore the pan syngap reverse primer crosses an exon boundary (exon 7 to 8) and so contamination with genomic DNA is highly unlikely as it wouldn't be amplified by this primer set.

The SynGAP mice used in these experiments were those generated by Komiyama and colleagues by disrupting the C2 and GAP domains of the Syngap protein (Komiyama et al. 2002). They used Southern blotting to confirm the structure of the gene and reassuringly showed a lack of normal SynGAP DNA in the *Syngap*$^{-/-}$ mice. However, they did not probe in any further detail. The pan syngap primers used in the current RT-PCR experiments bind upstream from where Komiyama and colleagues inserted their target vector. Therefore SynGAP promoters may still be present in the mouse from which incomplete and likely non-functional SynGAP RNA transcripts can be made. These would serve as templates in the RT-PCR experiment and therefore explain the apparent presence of SynGAP amplicon in the *Syngap*$^{-/-}$ mice. The fact that the amplified levels are low can be explained by these non-functional transcripts undergoing nonsense mediated RNA decay, a mechanism by which cells can monitor mRNA quality and prevent the synthesis of truncated proteins that could have damaging effects such as dominant negative interactions (Brogna & Wen 2009). Nonsense mediated mRNA decay is triggered by premature translation-termination codons which are in abnormal contexts (Brogna & Wen 2009; Lykke-Andersen & Jensen 2015), something which could certainly have occurred following the disruption of the SynGAP DNA in the *Syngap*$^{-/-}$ mice.

5.5.3 Chapter summary

This chapter highlights some of the complexities of studying SynGAP isoforms, in particular the difficulties in designing successful, valid primers that are isoform specific due to the sequence homology between isoforms. Unfortunately it is therefore not possible to even cautiously draw inferences from any of the SynGAP isoform RT-PCR data in this chapter as factors related to the expression of different SynGAP isoforms cannot be isolated from factors related to the primer design, behaviour of the primers or synthetic RNA. Going forward with the RT-PCR experiments, each of the primer pairs needs to be re-designed in an attempt to make their intrinsic physiological properties more consistent and an examination of the intrinsic properties of the synthetic RNA would also be advantageous. If problems persist even with better primer validity, this may be suggestive of complex hybridisation between the different isoforms and their primers due to their common

sequence elements. As this will be impossible to control for or eliminate, it may be that RT-PCR will have to be abandoned as the technique to investigate SynGAP isoform abundance and other approaches such as RNA sequencing adopted instead.

However, on a more positive note, this chapter also expands on the previous systematic examination of the effect of SynGAP isoforms on synaptic strength (McMahon et al. 2012) and tentatively suggests that the Eα1 isoform may influence mEPSC amplitude and frequency like other isoforms. This statement is however made with caution given the differences seen were in cumulative frequency distributions and not mean data and further experiments are needed to come to firm conclusions about the role of Eα1.

6 CHAPTER SIX: CONCLUSIONS AND FUTURE DIRECTIONS

6.1 Concluding remarks

This thesis presents a variety of work which expands on the current knowledge of the functions of the SynGAP protein. This is of value for fundamental neuroscience given SynGAP's regulatory function in the brain, but it also adds to our understanding of the effects of altered SynGAP protein expression. In humans, SynGAP mutations are linked to intellectual disability, autism spectrum disorders and epilepsy so understanding the function of the SynGAP protein may in time help to better delineate the processes involved in these disorders.

Initial characterisation of the SynGAP_GAP deletion rat confirmed that deleting a portion of the SynGAP protein in rats would lead to death in homozygotes. Furthermore it showed that that there is no gross behavioural or developmental difference between WT and heterozygous rats. Western blot analysis confirmed the hypothesis that the mutant SynGAP would be present in various brain regions including the hippocampus and would be found to be comprised of multiple SynGAP isoforms. Developmental western blotting indicated a broadly similar pattern of SynGAP expression to that in WT mice.

Electrophysiological examination revealed some surprising findings, firstly the absence of the predicted exaggeration in hippocampal mGluR mediated LTD. Secondly, a decrease in the frequency of mEPSCs from cultured *Syngap*$^{+/GAP}$ neurons with no difference between *Syngap*$^{GAP/GAP}$ and WT neurons rather than the hypothesised increase. Moreover, no other definite electrophysiological differences were found between WT and *Syngap*$^{+/GAP}$ rats despite the prediction that changes indicative of increased excitability would be identified. This suggests that perhaps there is little in the way of cellular or synaptic phenotype in these animals.

The second major theme of this thesis was to expand on previous data indicating specific physiological effects of different SynGAP isoforms and to further explore

their expression. Unfortunately the sequence homology between isoforms heavily impacted on the primer design for RT-PCR experiments and the primers were shown to be functioning differently under comparable experimental conditions precluding the drawing of any firm conclusions about SynGAP isoform abundance and regulation. However observations of the impact of SynGAP isoform Eα1 on synaptic strength were tentatively more promising with some suggestion that this isoform does indeed play a role in synaptic strength regulation as other isoforms have previously been shown to do.

It is important however, that the major confounding variables and methodological difficulties identified in this thesis be addressed before consideration can be given to which future experiments to pursue.

6.1.1 Addressing confounding variables

Although various potentially confounding variables were identified in the results presented here, I believe the following are the most significant ones to be addressed in future research.

6.1.1.1 Difference in SynGAP rodent model

Comparisons between the current rat data and previous SynGAP mouse data are difficult due to the fact that the mouse models are full knock outs of the mutant *Syngap* allele with very little or no SynGAP protein expression whereas the rat model is a deletion in which mutant SynGAP is expressed.

Firstly, undertaking a GTPase assay such as those undertaken in early SynGAP research (Chen et al. 1998, Kim et al. 1998) to definitively establish the absence of GAP domain function in the SynGAP_GAP deletion rats would help to evaluate the difference as the GAP domain mediates SynGAP's enzymatic function.

Secondly, one could either engineer mice to have the SynGAP_GAP deletion or engineer rats to have a mutation resulting in knock out of the affected *Syngap* allele. Either genetic approach would be equally valid, but given the many advantages of studying rats over mice in conditions where learning, memory and sociability are of

particular interest, I would choose to engineer a knock out rat for comparison with the SynGAP_GAP deletion rat.

6.1.1.2 Background strain

As discussed in detail in Chapter 4, it has been difficult in this body of work to delineate which effects may be due to the alteration in SynGAP from those related to the background strain of the SynGAP_GAP deletion rats. The potential solutions would be to

1. Engineer rats with the same SynGAP mutation on different background strains
2. Conduct the same experiments presented here in groups of wild type rats from different background strains

Engineering a new genetically modified rat model is costly and time consuming so exploring the electrophysiological properties in WT rats from different background strains would be a pragmatic approach to delineating the role of strain versus *Syngap* mutation.

6.1.1.3 Developmental compensation

The work on altered SynGAP levels in rats has to date not been able to explore whether developmental compensation has played a role in the phenotypes or the lack thereof. Hence, going forward, repeating the experiments in conditions of acute SynGAP knockdown using a cre-loxP or siRNA approach would be of interest.

6.1.2 The challenges of SynGAP isoform specific primers

Given the similarity in sequence between SynGAP isoforms, primer design proved extremely challenging. It is possible that re-designing the primers again and attempting to adhere more closely to the parameters identified as important for good primer validity (Paragraph 2.3.4.3) may improve the comparability of primer sets. Examination of the intrinsic properties of the synthetic RNA may also be required to ensure they have similar melting temperatures, GC content etc. across different experimental conditions. If they don't have similar properties or if it is not possible to re-design the primers well enough, an alternative technique will need to be employed to examine SynGAP isoform abundance. Even if primer pair validity and

RNA intrinsic property problems are minimised, there could still be unpredictable hybridisation in the RT-PCR reactions due to the similarities between the different primers and RNA which would also mean that a different approach would be needed.

RNA sequencing is a potential alternative technique which has the advantage of having a high resolution with low background noise and the ability to identify new transcripts.

6.2 Future directions

Assuming the major methodological flaws in the data presented here have at some point in the future been addressed, where should SynGAP_GAP rat research proceed to next? SynGAP mouse research highlights many unanswered questions about the SynGAP_GAP deletion rat. Perhaps the most pressing are

1. Do the rats have a reduced seizure threshold and could they be experiencing subclinical seizures?
2. Do the rats display any behavioural deficits in learning and memory or social interaction?
3. Is there any evidence of altered brain circuitry in these rats?

In order to answer these questions and assuming unlimited funds and resources, I would plan to do the following

- EEG monitoring and an audiogenic seizure paradigm – these would both identify susceptibility to and presence of seizures, plus EEG may show other abnormal electrical rhythms as non-epileptic EEG abnormalities have been noted in humans with *SYNGAP1* ID (Mignot et al. 2016)
- A battery of behavioural tests including Morris water maze experiments and object-place-context tasks (for learning and memory), elevated plus maze (for measuring anxiety) and three chamber tests of social interaction
- Brain fMRI using a fear-conditioning paradigm developed in Edinburgh (Brydges et al. 2013). Further investigation of fear would be interesting given the reduced anxiety seen in various SynGAP mouse behavioural

experiments (Guo et al. 2009; Muhia et al. 2010; Clement et al. 2012; Ozkan et al. 2014; Berryer et al. 2016)

6.3 The ultimate goal

As a clinician, my patients are my primary focus and so my hope would be that robust phenotypes or biomarkers are identified in SynGAP rat models so that therapeutic options can be explored. To me the next logical step would be to administer drugs to the rats that act on the biochemical pathways that SynGAP regulates with a view to ameliorating those phenotypes. Some of these drugs are already licensed for human use including lovastatin which has been shown to reduce exaggerated protein synthesis via the ERK1/2 pathway in *Syngap*$^{+/-}$ mice (Barnes et al. 2015). This makes it more straightforward to progress to trialling them in people with *SYNGAP1* ID if positive effects are seen pre-clinically. As with rat research, clinical trials could perhaps involve EEG or fMRI as they translate easily to humans and can monitor identified biomarkers and so measure the temporal profile of drug treatment response. My ultimate hope is that the drugs tested would fully ameliorate the symptoms and difficulties experienced by patients with *SYNGAP ID* or at least result in a significant improvement in their quality of life.

Appendix 1

Presented here are the full images from which exerts have been used in the construction of figures in the main body of this thesis.

Genotyping Gels

Genotyping gel electrophoresis for 13 SynGAP Rat Pups - exert used in Figure 11.

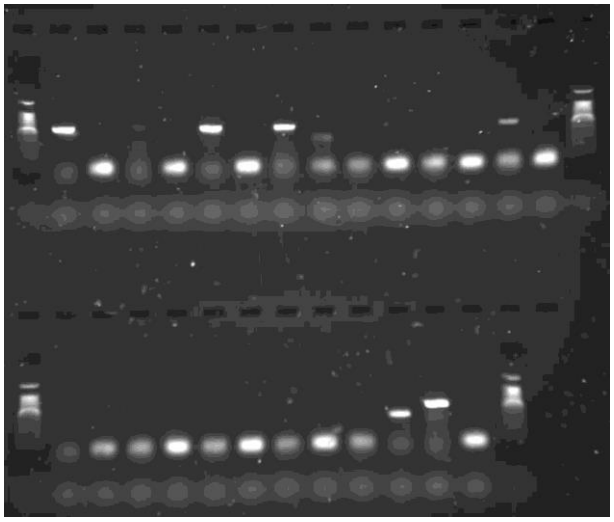

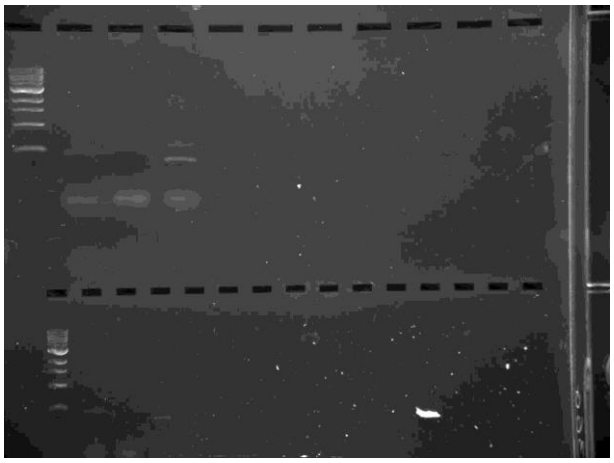

SynGAP cDNA amplification. Image cropped for used in Figure 12.

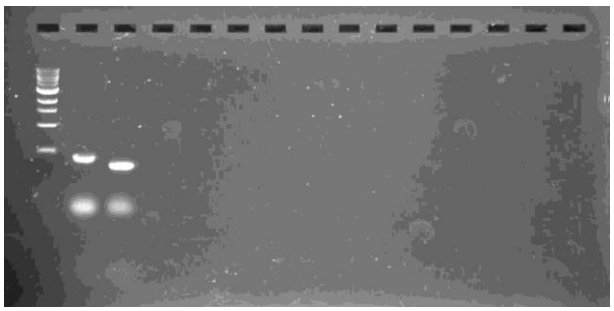

Re-amplification of SynGAP cDNA. Image cropped for used in Figure 12.

Hippocampal and neocortical western blots

P10 WT, *Syngap*$^{+/GAP}$ and *Syngap*$^{GAP/GAP}$ western blots

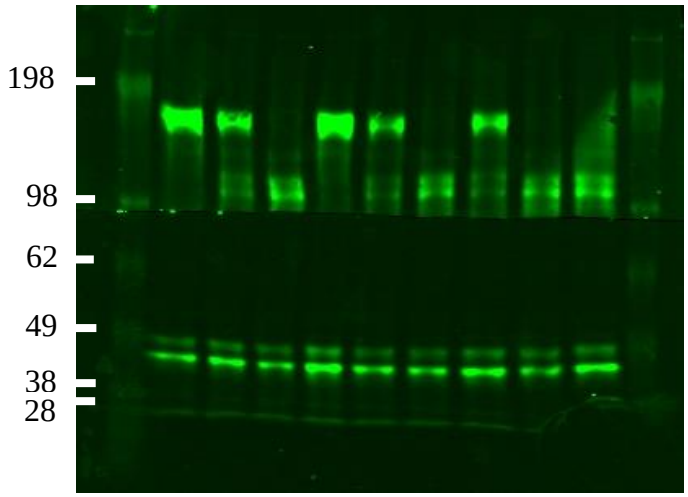

P10 hippocampus pan SynGAP isoform. Exert used in Figure 14.

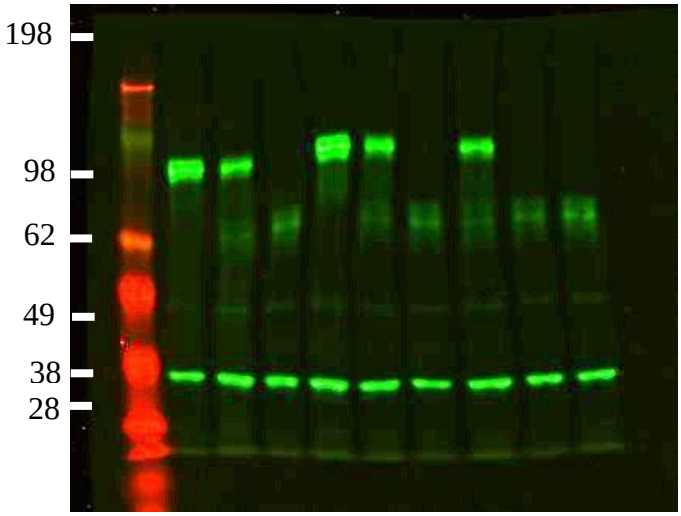

P10 neocortex pan SynGAP isoform. Exert used in Figure 14.

P20 hippocampal western blots

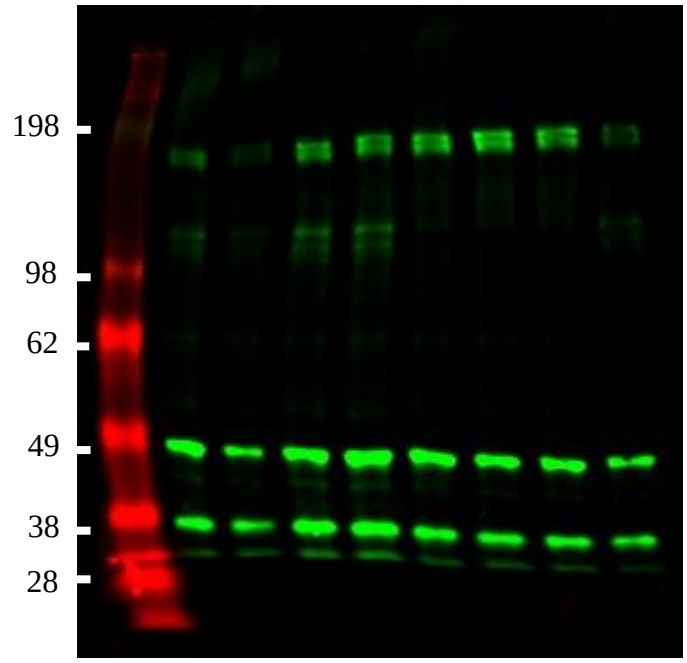

SynGAP A isoform antibody - exert used in Figure 16.

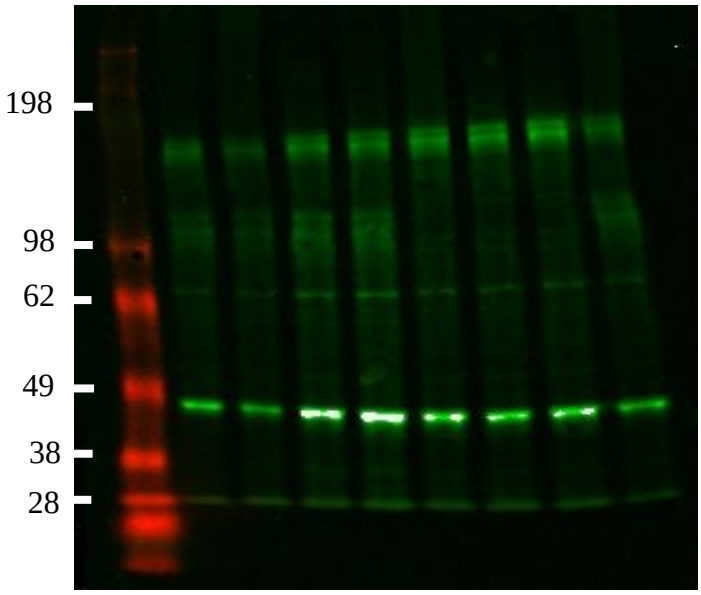

Pan SynGAP isoform antibody used for measurement of SynGAP bands only. Exert used in Figure 16.

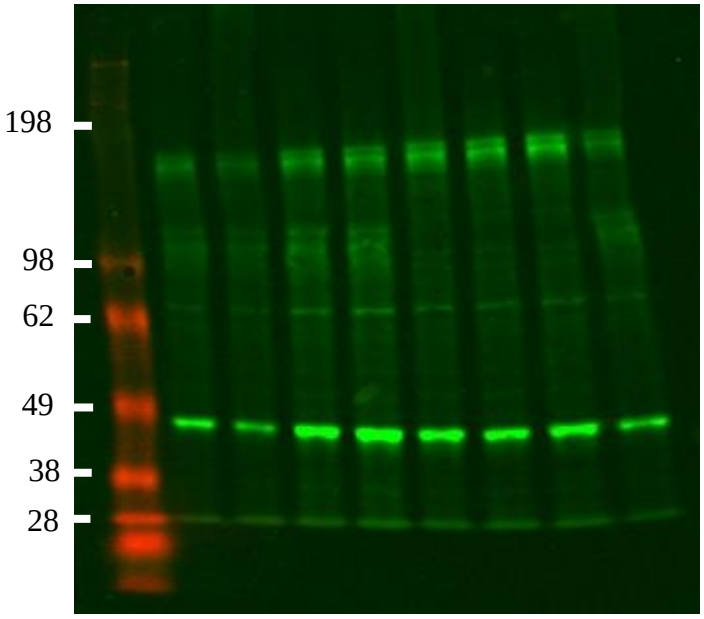

Pan SynGAP isoform antibody blot, used for measurement of beta actin bands only. Exert used in Figure 16.

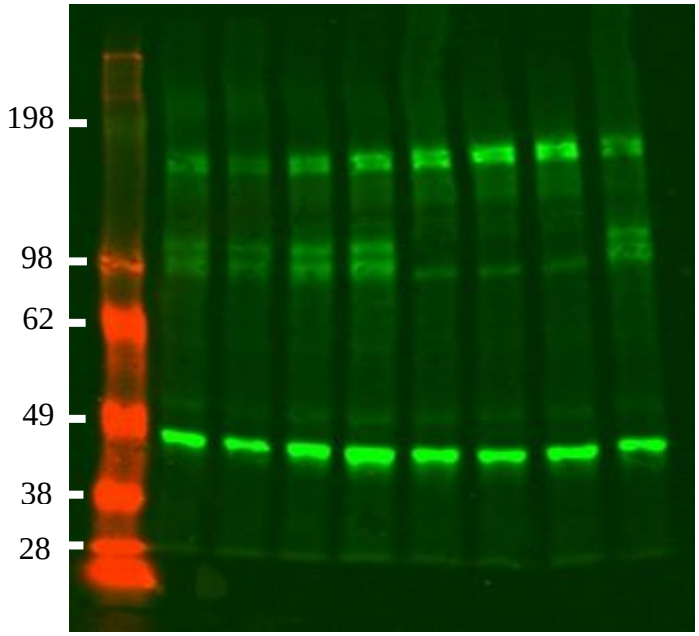

SynGAP alpha1 isoform antibody. Exert used in Figure 16.

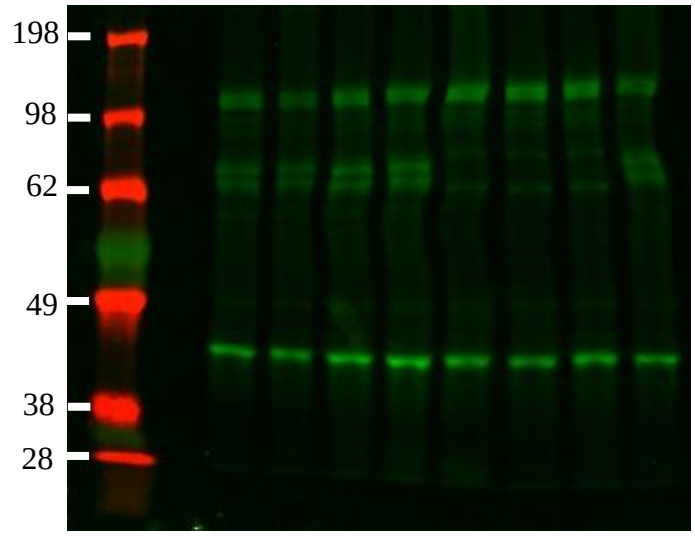

SynGAP alpha2 isoform antibody. Exert used in Figure 16.

P20 visual cortex western blots

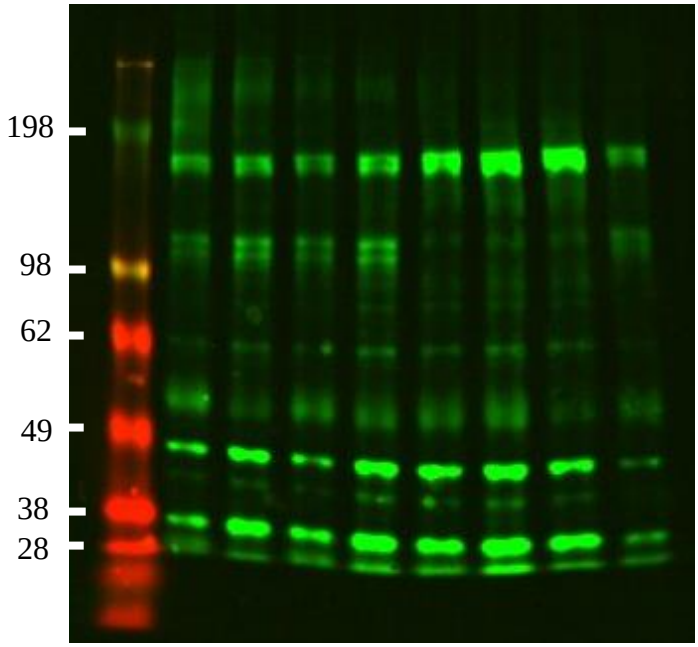

SynGAP A isoform antibody. Exert used in Figure 17.

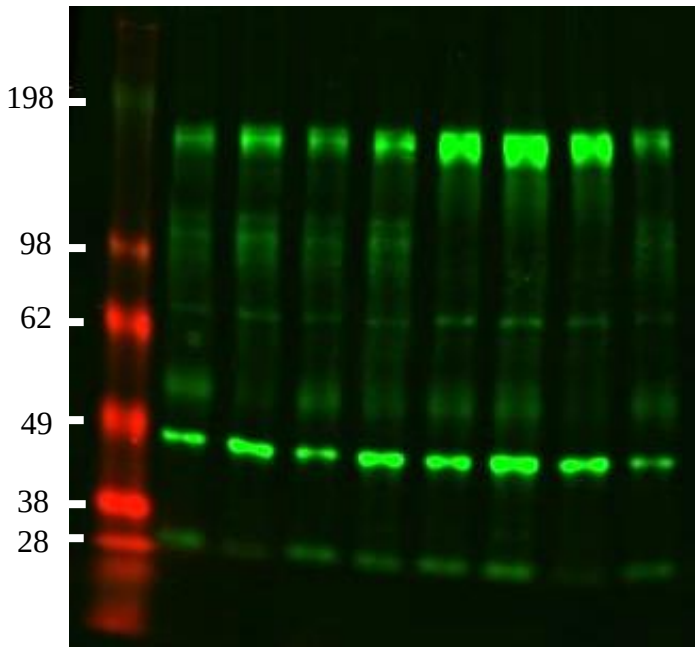

Pan SynGAP isoform antibody. Exert used in Figure 17.

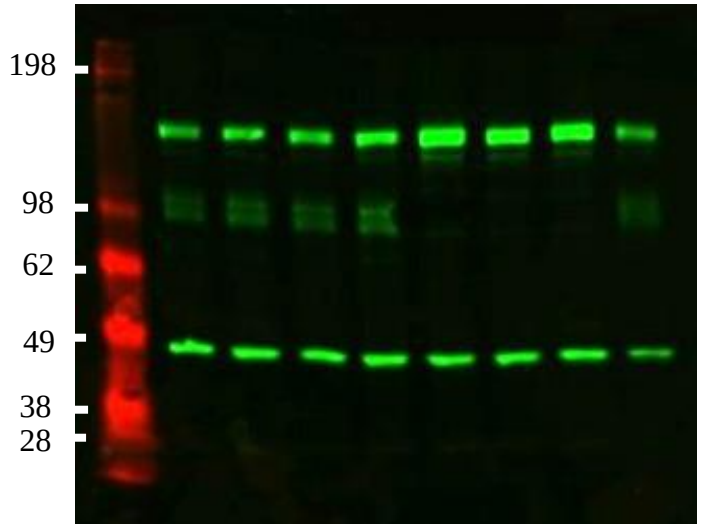

SynGAP alpha1 isoform antibody. Exert used in Figure 17.

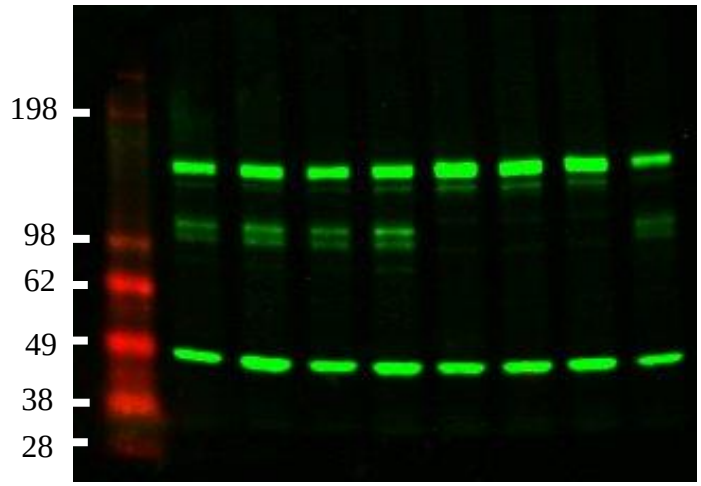

SynGAP alpha2 isoform antibody. Exert used in Figure 17.

Developmental western blots

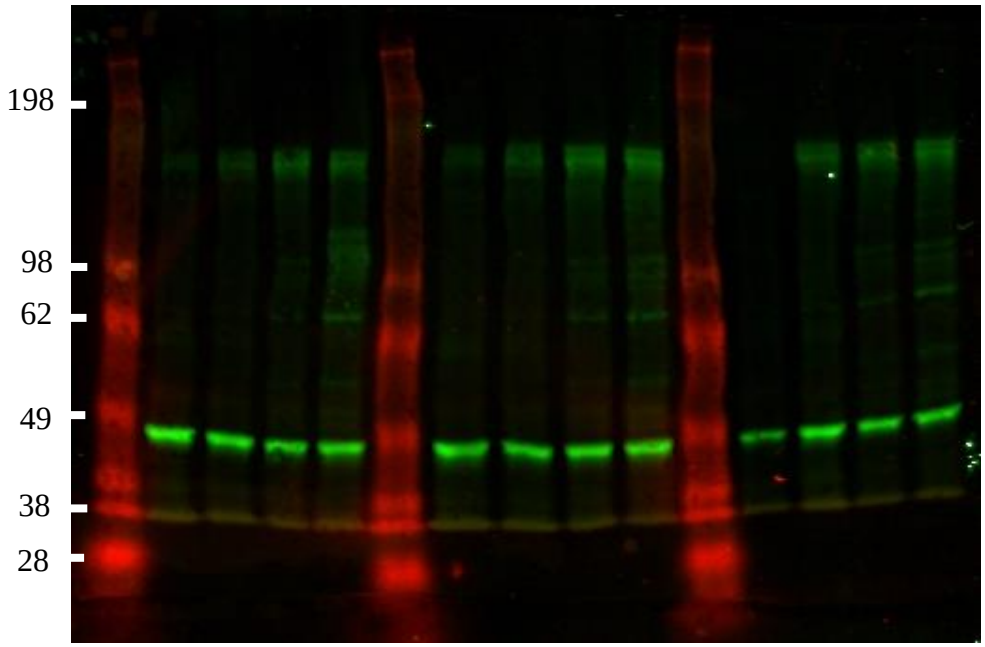

WT developmental western blot. Not presented in main thesis.

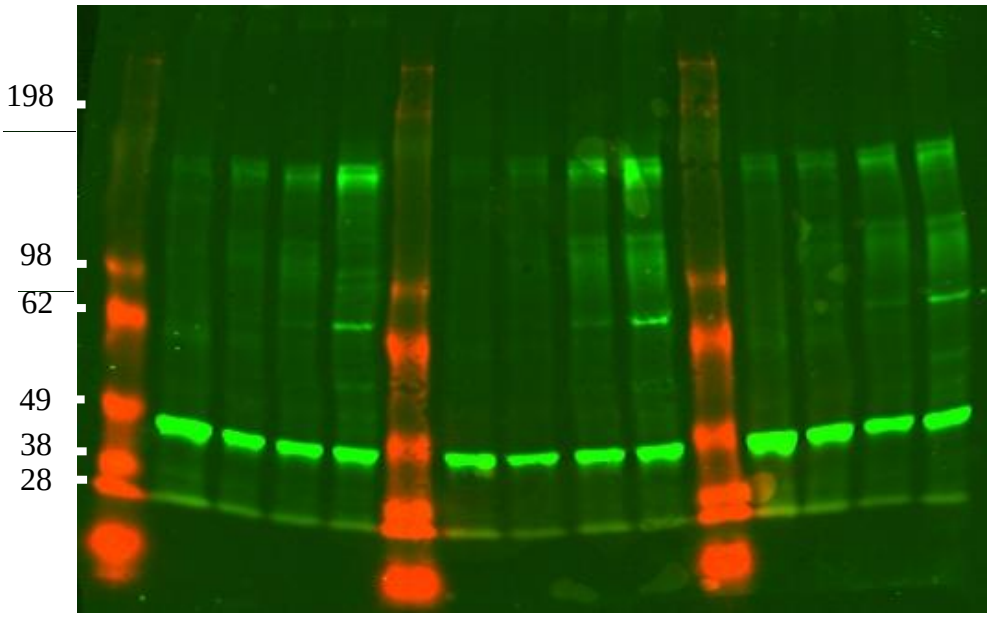

Heterozygous developmental western blot. Exert used in Figure 15.

RT-PCR Gels

Initial One Step RT-PCR gel to confirm the primer pairs were amplifying one product. Image cropped for use in Figure 47:

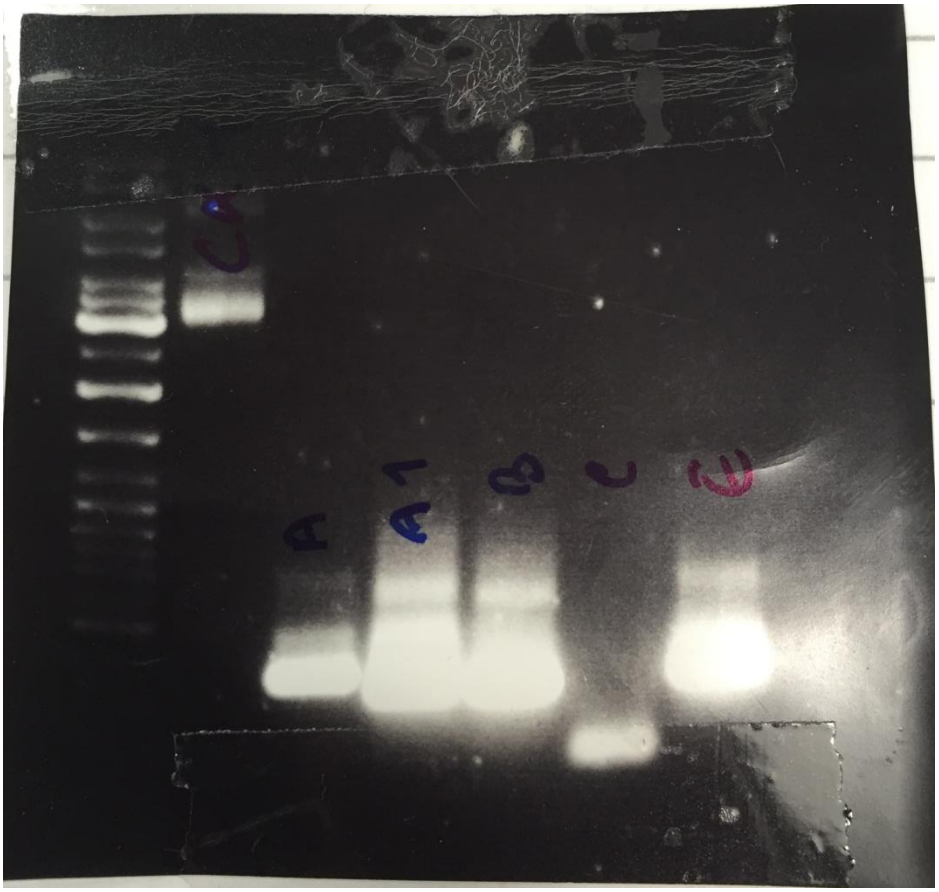

The following gels are from One Step RT-PCR to determine if the primer pairs were behaving in a similar manner to one another under varying experimental conditions – gels all used in Figure 54.

G isoform at 25, 35 and 50 cycles

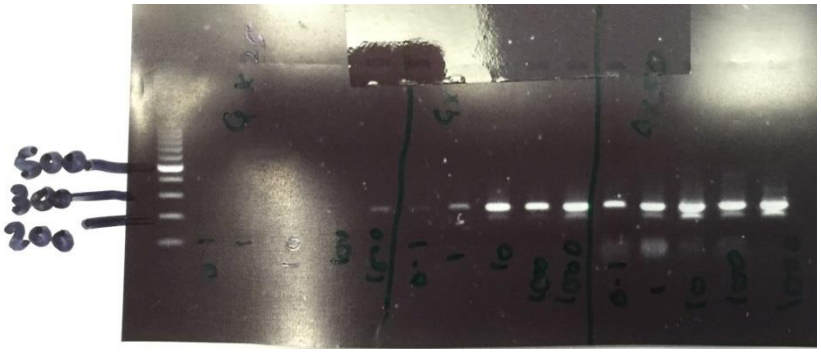

25 Cycles, Isoforms A, A1 (to be disregarded) B, C and E:

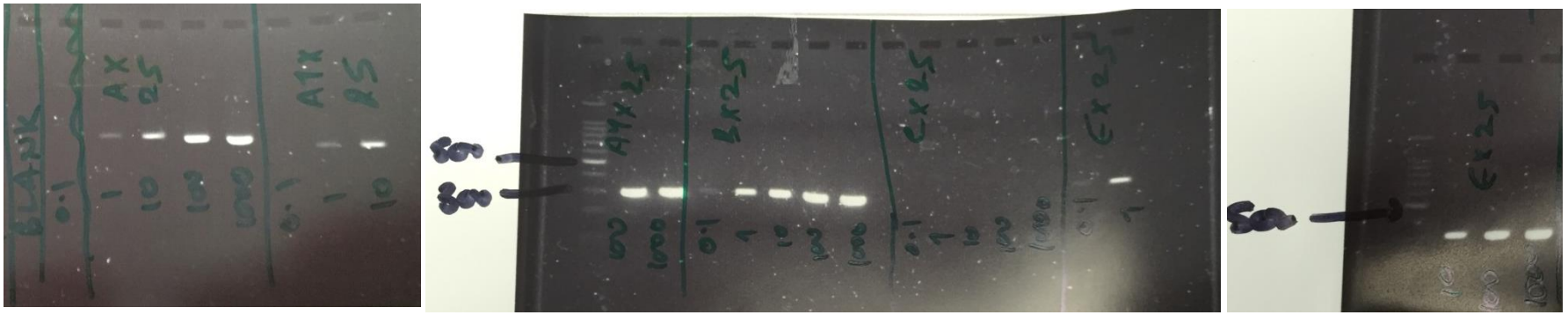

35 Cycles, Isoforms A, A1 (to be disregarded) B, C and E:

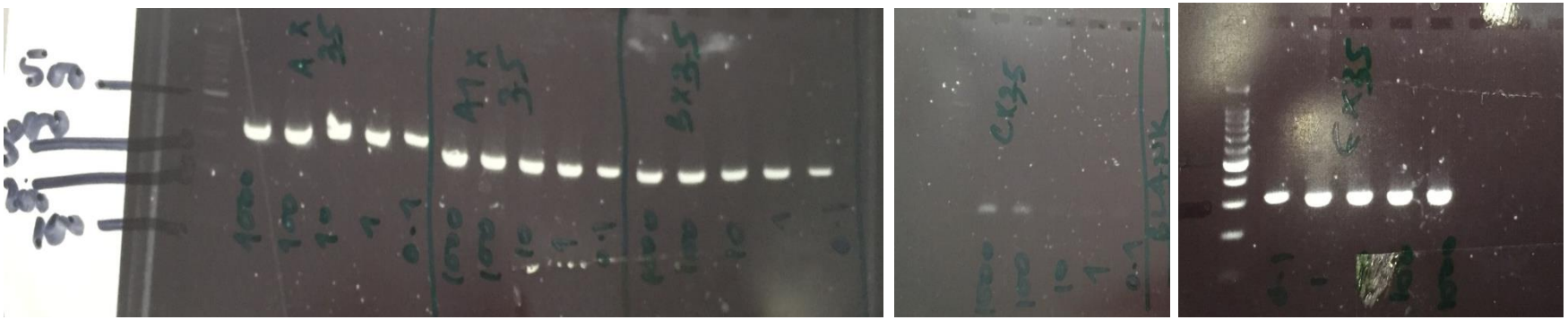

50 Cycles, Isoforms A, A1 (to be disregarded) B, C and E:

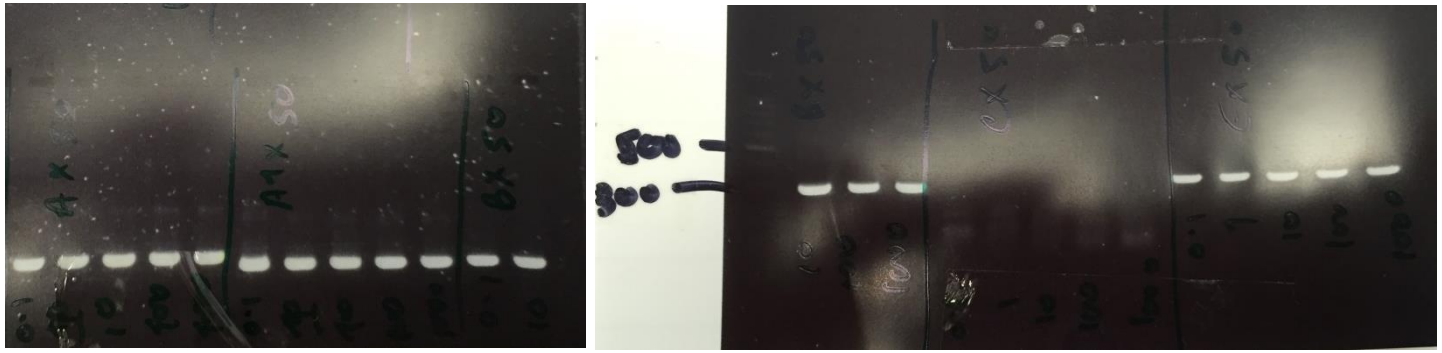

REFERENCES

Abrahamsson, T., Gustafsson, B. & Hanse, E., 2008. AMPA silencing is a prerequisite for developmental long-term potentiation in the hippocampal CA1 region. *Journal of neurophysiology*, 100(5), pp.2605–14.

Ahlemeyer, B. et al., 2003. Cytosine arabinofuranoside-induced activation of astrocytes increases the susceptibility of neurons to glutamate due to the release of soluble factors. *Neurochemistry International*, 42(7), pp.567–581.

Aldridge, G.M. et al., 2008. The use of total protein stains as loading controls: an alternative to high-abundance single protein controls in semi-quantitative immunoblotting. *Journal of Neuroscience Methods*, 172(2), pp.250–254.

APA, 2013. *Diagnostic and Statistical Manual of Mental Disorders (DSM–5)* 5th ed., American Psychiatric Association.

Araki, Y. et al., 2016. Phase Transition in Postsynaptic Densities Underlies Formation of Synaptic Complexes and Synaptic Article Phase Transition in Postsynaptic Densities Underlies Formation of Synaptic Complexes and Synaptic Plasticity. *Cell*, 166(5), p.1163–1175.e12.

Araki, Y. et al., 2015. Rapid Dispersion of SynGAP from Synaptic Spines Triggers AMPA Receptor Insertion and Spine Enlargement during LTP. *Neuron*, 85(1), pp.173–189.

Asperger, H. & Frith, U., 1991. Translation and Annotation of "Autistic psychopathy" in childhood. In *Autism and Asperger syndrome*. Cambridge University Press, pp. 37–92.

Auerbach, B.D., Osterweil, E.K. & Bear, M.F., 2012. Mutations causing syndromic autism define an axis of synaptic pathophysiology. , 480(7375), pp.63–68.

Banker, G.A. & Cowan, W.M., 1977. Rat Hippocampal Neurons in Dipsersed Cell Culture. *Brain research*, 126, pp.397–425.

Baraban, S.C. & Schwartzkroin, P.A., 1995. Electrophysiology of CA1 pyramidal neurons in an animal model of neuronal migration disorders: prenatal methylazoxymethanol treatment. *Epilepsy Research*, 22(2), pp.145–156.

Barnes, S.A. et al., 2015. Convergence of Hippocampal Pathophysiology in Syngap$^{+/-}$ and Fmr1$^{-/y}$ Mice. *Journal of Neuroscience*, 35(45), pp.15073–15081.

Barnett, M.W. et al., 2006. Synaptic Ras GTPase activating protein regulates pattern formation in the trigeminal system of mice. *The Journal of neuroscience*, 26(5), pp.1355–65.

Bear, M.F., Huber, K.M. & Warren, S.T., 2004. The mGluR theory of fragile X mental retardation. *Trends in neurosciences*, 27(7), pp.370–7.

Bekkers, J.M., Richerson, G.B. & Stevens, C.F., 1990. Origin of variability in quantal size in cultured hippocampal neurons and hippocampal slices. *Proceedings of the National Academy of Sciences of the United States of America*, 87(14), pp.5359–5362.

Benarroch, E.E., 2013. HCN channels Function and clinical implications. *Neurology*, 80, pp.304–310.

Bernards, A., 2003. GAPs galore! A survey of putative Ras superfamily GTPase activating proteins in man and Drosophila. *Biochimica et Biophysica Acta (BBA) - Reviews on Cancer*, 1603(2), pp.47–82.

Berryer, M.H. et al., 2016. Decrease of SYNGAP1 in GABAergic cells impairs inhibitory synapse connectivity, synaptic inhibition and cognitive function. *Nature communications*, 7, p.13340.

Berryer, M.H. et al., 2013. Mutations in SYNGAP1 cause intellectual disability, autism, and a specific form of epilepsy by inducing haploinsufficiency. *Human mutation*, 34(2), pp.385–94.

Betancur, C., 2011. Etiological heterogeneity in autism spectrum disorders: more than 100 genetic and genomic disorders and still counting. *Brain research*, 1380, pp.42–77.

BIO-RAD Laboratories, 2006. *Real-Time PCR Applications Guide*,

BioTechniques, 2011. BioTechniques Molecular Biology Technique Troubleshooting Forum. *BioTechniques*, 51(6), pp.401–402.

Bowden, J.B., Abraham, W.C. & Harris, K.M., 2012. Differential effects of strain, circadian cycle, and stimulation pattern on LTP and concurrent LTD in the dentate gyrus of freely moving rats. *Hippocampus*, 22(6), pp.1363–1370.

Braun, K. & Segal, M., 2000. FMRP involvement in formation of synapses among cultured hippocampal neurons. *Cerebral cortex (New York, N.Y. : 1991)*, 10(10), pp.1045–52.

Brewer, G.J. et al., 1993. Optimized Survival of Hippocampal-Neurons in B27-Supplemented Neurobasal(Tm), a New Serum-Free Medium Combination. *Journal of Neuroscience Research*, 35(5), pp.567–576.

Brogna, S. & Wen, J., 2009. Nonsense-mediated mRNA decay (NMD) mechanisms. *Nature Structural & Molecular Biology*, 16(2), pp.107–113.

Brugha, T.S. et al., 2016. Epidemiology of autism in adults across age groups and ability levels. *The British journal of psychiatry : the journal of mental science*, 209, pp.498–503.

Brydges, N.M. et al., 2013. Imaging Conditioned Fear Circuitry Using Awake Rodent fMRI. *PloS one*, 8(1), pp.4–10.

Carlisle, H.J. et al., 2008. SynGAP regulates steady-state and activity-dependent

phosphorylation of cofilin. *Journal of Neuroscience*, 28(50), pp.13673–13683.

Carroll, R.C. et al., 1999. Rapid redistribution of glutamate receptors contributes to long-term depression in hippocampal cultures. *Nature neuroscience*, 2(5), pp.454–60.

Carvill, G.L. et al., 2013. Targeted resequencing in epileptic encephalopathies identifies de novo mutations in CHD2 and SYNGAP1. *Nature genetics*, 45(7), pp.825–30.

Chen, H.J. et al., 1998. A synaptic Ras-GTPase activating protein (p135 SynGAP) inhibited by CaM kinase II. *Neuron*, 20(5), pp.895–904.

Chu, H.-Y. et al., 2010. Electrophysiological effects of SKF83959 on hippocampal CA1 pyramidal neurons: potential mechanisms for the drug's neuroprotective effects. *PloS one*, 5(10), pp.1–9.

Clement, J.P. et al., 2012. Pathogenic SYNGAP1 mutations impair cognitive development by disrupting maturation of dendritic spine synapses. *Cell*, 151(4), pp.709–23.

Clement, J.P. et al., 2013. SYNGAP1 links the maturation rate of excitatory synapses to the duration of critical-period synaptic plasticity. *The Journal of neuroscience : the official journal of the Society for Neuroscience*, 33(25), pp.10447–52.

Cooper, S.-A., 1999. The relationship between psychiatric and physical health in elderly people with intellectual disability. *Journal of Intellectual Disability Research*, 43(1), p.54.

Cooper, S.-A. & Smiley, E., 2009. Prevalence of intellectual disabilities and epidemiology of mental ill-health in adults with intellectual disabilities. In *Oxford textbook of psychiatry, volume 1*. pp. 825–829.

Cormier, R.J. & Kelly, P.T., 1996. Glutamate-induced long-term potentiation enhances spontaneous EPSC amplitude but not frequency. *Journal of neurophysiology*, 75(5), pp.1909–18.

Costa-Mattioli, M. & Monteggia, L.M., 2013. mTOR complexes in neurodevelopmental and neuropsychiatric disorders. *Nature neuroscience*, 16(11), pp.1537–43.

Cotman, C.W. & Nieto Sampedro, M., 1984. Cell biology of synaptic plasticity. *Science*, 225(1977), pp.1287–1294.

Crair, M.C. & Malenka, R.C., 1995. a Critical Period for Long-Term Potentiation At Thalamocortical Synapse. *Nature*, 375, pp.325–328.

Deacon, R.M.J. & Rawlins, J.N.P., 2006. T-maze alternation in the rodent. *Nature Protocols*, 1(1), pp.7–12.

Derkach, V.A. et al., 2007. Regulatory mechanisms of AMPA receptors in synaptic plasticity. *Nature Reviews Neuroscience*, 8, pp.101–113.

Dieckmann, F., Giovis, C. & Offergeld, J., 2015. The Life Expectancy of People with

Intellectual Disabilities in Germany. *Journal of Applied Research in Intellectual Disabilities*, (28), pp.373–382.

Dierssen, M. & Ramakers, G.J.A., 2006. Dendritic pathology in mental retardation: from molecular genetics to neurobiology. *Genes, brain, and behavior*, 5 Suppl 2(April 2005), pp.48–60.

Dittmer, A. & Dittmer, J., 2006. β-Actin is not a reliable loading control in Western blot analysis. *Electrophoresis*, 27(14), pp.2844–2845.

Edwards, F.A., Konnerth, A. & Sakmann, B., 1990. Quantal analysis of inhibitory synaptic transmission in the dentate gyrus of rat hippocampal slices: A patch-clamp study. *Journal of Physiology*, 430, pp.213–249.

Ehlers, M.D., 2000. Reinsertion or Degradation of AMPA Receptors Determined by Activity-Dependent Endocytic Sorting. *Neuron*, 28(2), pp.511–525.

Ellenbroek, B. & Youn, J., 2016. Rodent models in neuroscience research: is it a rat race? *Disease Models & Mechanisms*, 9(10), pp.1079–1087.

Emerson, E. & Baines, S., 2010. Health Inequalities & People with Learning Disabilities in the UK : 2010.

Fitzgerald, T.W. et al., 2015. Large-scale discovery of novel genetic causes of developmental disorders. *Nature*, 519(7542), pp.223–228.

Garreau De Loubresse, N. et al., 2014. Structural basis for the inhibition of the eukaryotic ribosome. *Nature*, 513, pp.517–523.

Graves, A., 2013. Hippocampal pyramidal neurons comprison two distinct types that are countermodulated by metabotropic receptors. *Neuron*, 76(4), pp.776–789.

Gray, L.E. et al., 1997. In Utero Exposure to Low Doses of 2,3,7,8-Tetrachlorodibenzo-p-dioxin Alters Reproductive Development of Female Long Evans Hooded Rat Offspring. *Toxicology and applied pharmacology*, 146(2), pp.237–44.

Gu, N., Vervaeke, K. & Storm, J.F., 2007. BK potassium channels facilitate high-frequency firing and cause early spike frequency adaptation in rat CA1 hippocampal pyramidal cells. *The Journal of physiology*, 580(Pt.3), pp.859–82.

Guo, X. et al., 2009. Reduced expression of the NMDA receptor-interacting protein SynGAP causes behavioral abnormalities that model symptoms of Schizophrenia. *Neuropsychopharmacology*, 34(7), pp.1659–72.

Hamdan, F.F. et al., 2011. De novo SYNGAP1 mutations in nonsyndromic intellectual disability and autism. *Biological psychiatry*, 69(9), pp.898–901.

Hamdan, F.F. et al., 2009. Mutations in SYNGAP1 in Autosomal Nonsyndromic Mental Retardation. *The New England journal of medicine*, 360, pp.599–605.

Hanse, E., Seth, H. & Riebe, I., 2013. AMPA-silent synapses in brain development and pathology. *Nature Reviews Neuroscience*, 14(12), pp.839–850.

He, C. et al., 2014. Neurophysiology of HCN channels : From cellular functions to multiple regulations. *Progress in Neurobiology*, 112, pp.1–23.

Heffron, D.S. & Mandell, J.W., 2005. Opposing roles of ERK and p38 MAP kinases in FGF2-induced astroglial process extension. *Molecular and Cellular Neuroscience*, 28(4), pp.779–790.

Herring, B.E. & Nicoll, R.A., 2016. Long-Term Potentiation: From CaMKII to AMPA receptor trafficking. *Annual review of physiology*, 78(1), pp.351–65.

Hershkowitz, N., Katchman, A.N. & Veregge, S., 1993. Site of synaptic depression during hypoxia: a patch-clamp analysis. *Journal of neurophysiology*, 69(2), pp.432–41.

Hovey, R.C. et al., 2011. Quantitative assessment of mammary gland development in female long evans rats following in utero exposure to atrazine. *Toxicological Sciences*, 119(2), pp.380–390.

Huber, K.M. et al., 2002. Altered synaptic plasticity in a mouse model of fragile X mental retardation. *Proceedings of the National Academy of Sciences of the United States of America*, 99(11), pp.7746–7750.

Huber, K.M. et al., 2001. Chemical Induction of mGluR5- and Protein Synthesis − Dependent Long-Term Depression in Hippocampal Area CA1 Chemical Induction of mGluR5- and Protein Synthesis – Dependent Long-Term Depression in Hippocampal Area CA1. *Journal of neurophysiology*, 86, pp.321–325.

Huber, K.M., Kayser, M.S. & Bear, M.F., 2000. Role for rapid dendritic protein synthesis in hippocampal mGluR-dependent long-term depression. *Science*, 288(5469), pp.1254–1257.

Iannaccone, P.M. & Jacob, H.J., 2009. Rats! *Disease Models & Mechanisms*, 2(5–6), pp.206–210.

Iossifov, I. et al., 2012. De Novo Gene Disruptions in Children on the Autistic Spectrum. *Neuron*, 74(2), pp.285–299.

Jeyabalan, N. & Clement, J.P., 2016. SYNGAP1 : Mind the Gap. *Frontiers in Cellular Neuroscience*, 10, pp.1–16.

Jonckers, E. et al., 2015. The power of using functional fMRI on small rodents to study brain pharmacology and disease. *Frontiers in Pharmacology*, 6, pp.1–19.

Kacew, S. & Festing, M.F.W., 1996. Role of Rat Strain in the Differential Sensitivity to Pharmaceutical Agents and Naturally Occurring Substances. *Journal of Toxicology and Environmental Health*, 47, pp.1–30.

Kaczorowski, C.C., Disterhoft, J. & Spruston, N., 2007. Stability and plasticity of intrinsic membrane properties in hippocampal CA1 pyramidal neurons: effects of internal anions. *The Journal of physiology*, 578(Pt 3), pp.799–818.

Kakeyama, M., Sone, H. & Tohyama, C., 2008. Perinatal exposure of female rats to 2,3,7,8-tetrachlorodibenzo-p-dioxin induces central precocious puberty in the offspring. *Journal of Endocrinology*, 197(2), pp.351–358.

Kamal, A. et al., 2014. Social isolation stress reduces hippocampal long-term potentiation: Effect of animal strain and involvement of glucocorticoid receptors. *Neuroscience*, 256, pp.262–270.

Kaneko, T., Li, L. & Li, S.S., 2008. The SH3 domain- a family of versatile peptide- and protein-recognition module. *Frontiers in Bioscience*, (May 1), pp.4938–4952.

Kanner, L., 1943. Autistic disturbances of affective contact. *Nervous Child*, 2, pp.217–250.

Karlsson, A. et al., 2011. Altered spontaneous synaptic inhibition in an animal model of cerebral heterotopias. *Brain Research*, 1383, pp.54–61.

Katchman, A.N., Vicini, S. & Hershkowitz, N., 1994. Mechanism of early anoxia-induced suppression of the GABAA-mediated inhibitory postsynaptic current. *Journal of neurophysiology*, 71(3), pp.1128–1138.

Keeley, R.J., Trow, J. & McDonald, R.J., 2015. Strain and sex differences in puberty onset and the effects of THC administration on weight gain and brain volumes. *Neuroscience*, 305, pp.328–342.

Kim, D. et al., 2013. TopHat2: accurate alignment of transcriptomes in the presence of insertions, deletions and gene fusions. *Genome Biology*, 14(4), p.R36.

Kim, J.H. et al., 1998. SynGAP: a synaptic RasGAP that associates with the PSD-95/SAP90 protein family. *Neuron*, 20(4), pp.683–91.

Kim, J.H. et al., 2003. The role of synaptic GTPase-activating protein in neuronal development and synaptic plasticity. *The Journal of neuroscience*, 23(4), pp.1119–24.

Kim, M.J. et al., 2005. Differential roles of NR2A- and NR2B-containing NMDA receptors in Ras-ERK signaling and AMPA receptor trafficking. *Neuron*, 46(5), pp.745–60.

Knuesel, I. et al., 2005. A role for synGAP in regulating neuronal apoptosis. *The European journal of neuroscience*, 21(3), pp.611–21.

Komiyama, N.H. et al., 2002. SynGAP regulates ERK/MAPK signaling, synaptic plasticity, and learning in the complex with postsynaptic density 95 and NMDA receptor. *The Journal of neuroscience*, 22(22), pp.9721–32.

Krapivinsky, G. et al., 2004. SynGAP-MUPP1-CaMKII synaptic complexes regulate p38 MAP kinase activity and NMDA receptor-dependent synaptic AMPA receptor

potentiation. *Neuron*, 43(4), pp.563–74.

Krepischi, A.C. V et al., 2010. A novel de novo microdeletion spanning the SYNGAP1 gene on the short arm of chromosome 6 associated with mental retardation. *American journal of medical genetics. Part A*, 152A(9), pp.2376–8.

Krumm, N. et al., 2014. A de novo convergence of autism genetics and molecular neuroscience. *Trends in Neurosciences*, 37(2), pp.95–105.

Kummer, K.K. et al., 2014. Differences in social interaction- vs. cocaine reward in mouse vs. rat. *Frontiers in behavioral neuroscience*, 8(October), p.363.

Lai, M.-C., Lombardo, M. V & Baron-Cohen, S., 2014. Autism. *The Lancet*, 383(9920), pp.896–910.

Lazic, S.E., 2010. The problem of pseudoreplication in neuroscientific studies: is it affecting your analysis? *BMC neuroscience*, 11(1), p.5.

Lemmon, M.A., 2008. Membrane recognition by phospholipid-binding domains. *Nature reviews: Molecular cell biology*, 9(2), pp.99–111.

Li, R. & Shen, Y., 2013. An old method facing a new challenge: re-visitng housekeeping proteins as internal reference control for neuroscience research. *Life Sciences*, 92(13), pp.747–751.

Li, W. et al., 2001. Characterization of a novel synGAP isoform, synGAP-beta. *The Journal of biological chemistry*, 276(24), pp.21417–24.

Li, X.G. et al., 1994. The Hippocampal Ca3 Network - An In-Vivo Intracellular Labeling Study. *Journal of Comparative Neurology*, 339(2), pp.181–208.

Life Technologies, 2012. Realtime PCR Handbook.

de Ligt, J. et al., 2012. Diagnostic exome sequencing in persons with severe intellectual disability. *The New England journal of medicine*, 367(20), pp.1921–9.

Lister, R. et al., 2013. Global epigenomic reconfiguration during mammalian brain development. *Science*, 341(6146), p.1237905.

Lüscher, C. et al., 1999. Role of AMPA Receptor Cycling in Synaptic Transmission and Plasticity. *Neuron*, 24(3), pp.649–658.

Luthi, A. et al., 1999. Hippocampal LTD Expression Involves a Pool of AMPARs Regulated by the NSF – GluR2 Interaction. *Neuron*, 24, pp.389–399.

Lykke-Andersen, S. & Jensen, T.H., 2015. Nonsense-mediated mRNA decay: an intricate machinery that shapes transcriptomes. *Nature Reviews Molecular Cell Biology*, 16(11), pp.665–677.

Magiati, I., Tay, X.W. & Howlin, P., 2014. Cognitive, language, social and behavioural outcomes in adults with autism spectrum disorders: A systematic review of longitudinal

follow-up studies in adulthood. *Clinical Psychology Review*, 34(1), pp.78–86.

Malik, R. & Chattarji, S., 2011. Enhanced intrinsic excitability and EPSP-spike coupling accompany enriched environment-induced facilitation of LTP in hippocampal CA1 pyramidal neurons. *Journal of Neurophysiology*, 107(5), pp.1366–1378.

Malinow, R. & Malenka, R.C., 2002. AMPA receptor trafficking and synaptic plasticity. *Annual review of neuroscience*, 25, pp.103–26.

Man, H. et al., 2000. Regulation of AMPA Receptor – Mediated Synaptic Transmission by Clathrin-Dependent Receptor Internalization. *Neuron*, 25, pp.649–662.

Manahan-Vaughan, D., 2000. Long-term Depression in Freely Moving Rats is Dependent upon Strain Variation, Induction Protocol and Behavioral State. *Cerebral Cortex*, 10(5), pp.482–487.

Maren, S., 1995. Sexually dimorphic perforant path LTD in urethane-anaesthetized rats. *Neuroscience letters*, 196, pp.177–180.

Maren, S., De Oca, B. & Fanselow, M.S., 1994. Sex differences in hippocampal long-term potentiation (LTP) and Pavlovian fear conditioning in rats: positive correlation between LTP and contextual learning. *Brain Research*, 661, pp.25–34.

Martin, D.P., Wallace, L. & Johnson, M., 1990. Cytosine Arabinoside Kills Postmitotic Neurons in a Fashion Resembling Trophic Factor Deprivation: Evidence That a Deoxycytidine-Dependent Process May be Required for Nerve Growth Signal Transduction. *Journal of Neuroscience*, 10(1), pp.184–193.

Matsuzaki, M. et al., 2004. Structure basis of long-term potentiation in single dendritic spines. *Nature*, 429(6993), pp.761–766.

Maulik, P.K. et al., 2011. Research in Developmental Disabilities Review article Prevalence of intellectual disability : A meta-analysis of population-based studies. *Research in Developmental Disabilities*, 32, pp.419–436.

McBain, C. & Dingledine, R., 1992. Dual-component miniature excitatory synaptic currents in rat hippocampal CA3 pyramidal neurons. *Journal of neurophysiology*, 68(1), pp.16–27.

McCormack, S.G., Stornetta, R.L. & Zhu, J.J., 2006. Synaptic AMPA Receptor Exchange Maintains Bidirectional Plasticity. *Neuron*, 50(1), pp.75–88.

McMahon, A., 2010. *An examination of multiple SynGAP isoforms in mammalian central neurons*. University of Edinburgh.

McMahon, A.C. et al., 2012. SynGAP isoforms exert opposing effects on synaptic strength. *Nature communications*, 3, p.900.

Mefford, H.C., Batshaw, M.L. & Hoffman, E.P., 2012. Genomics, Intellectual Disability,

and Autism. *New England Journal of Medicine*, pp.733–743.

Mignot, C. et al., 2016. Genetic and neurodevelopmental spectrum of SYNGAP1 -associated intellectual disability and epilepsy. *Journal of medical genetics*, 0, pp.1–12.

Montesinos, M., 2014. Pharmacological Intervention for Down Syndrome Cognitive Deficits : Emerging Drug Targets. *CNS & Neurological Disorders*, 13(1), pp.6–7.

Moon, I.S. et al., 2008. Differential distribution of synGAP alpha1 and synGAP beta isoforms in rat neurons. *Brain research*, 1241, pp.62–75.

Morrison, D.K., 2012. MAP kinase pathways. *Cold Spring Harbor Laboratory Press*, 4, pp.1–5.

Muhia, M. et al., 2009. Appetitively motivated instrumental learning in SynGAP heterozygous knockout mice. *Behavioral neuroscience*, 123(5), pp.1114–28.

Muhia, M. et al., 2010. Disruption of hippocampus-regulated behavioural and cognitive processes by heterozygous constitutive deletion of SynGAP. *The European journal of neuroscience*, 31(3), pp.529–43.

Muhia, M. et al., 2012. Molecular and behavioral changes associated with adult hippocampus-specific SynGAP1 knockout. *Learning & memory (Cold Spring Harbor, N.Y.)*, 19(7), pp.268–81.

Munir, K.M., 2016. The co-occurrence of mental disorders in children and adolescents with intellectual disability/intellectual developmental disorder. *Current Opinion in Psychiatry*, 29(2), pp.95–102.

Murphy, C. et al., 2016. Autism spectrum disorder in adults: diagnosis, management, and health services development. *Neuropsychiatric Disease and Treatment*, Volume 12, pp.1669–1686.

Nalefski, E.A. & Falke, J.J., 1996. The C2 domain calcium-binding motif: structural and functional diversity. *Protein Science*, 5(12), pp.2375–2390.

Nguyen, P. V, Duffy, S.N. & Young, J.Z., 2000. Differential maintenance and frequency-dependent tuning of LTP at hippocampal synapses of specific strains of inbred mice. *Journal of neurophysiology*, 84(5), pp.2484–2493.

Nosyreva, E.D. et al., 2006. Metabotropic Receptor-Dependent Long-Term Depression Persists in the Absence of Protein Synthesis in the Mouse Model of Fragile X Syndrome. , 95, pp.3291–3295.

Oberlander, J.G. & Woolley, C.S., 2016. 17β-Estradiol Acutely Potentiates Glutamatergic Synaptic Transmission in the Hippocampus through Distinct Mechanisms in Males and Females. *The Journal of neuroscience*, 36(9), pp.2677–90.

Oh, C. et al., 2000. Opposing Role of Mitogen-activated in the Regulation of

Chondrogenesis of Mesenchymes Opposing Role of Mitogen-activated Protein Kinase Subtypes , Erk-1 / 2 and p38 , in the Regulation of Chondrogenesis of Mesenchymes *. *The Journal of biological chemistry*, 275(8), pp.5613–5619.

Oh, J.S., Manzerra, P. & Kennedy, M.B., 2004. Regulation of the neuron-specific Ras GTPase-activating protein, synGAP, by Ca2+/calmodulin-dependent protein kinase II. *The Journal of biological chemistry*, 279(17), pp.17980–8.

Ojeda, S.R. & Skinner, M.K., 2006. Puberty in the rat. In *Knobil and Neill's Physiology of Reproduction*. Elsevier, pp. 2061–2126.

Opazo, P., Sainlos, M. & Choquet, D., 2012. Regulation of AMPA receptor surface diffusion by PSD-95 slots. *Current Opinion in Neurobiology*, 22(3), pp.453–460.

Ozkan, E.D. et al., 2014. Reduced cognition in Syngap1 mutants is caused by isolated damage within developing forebrain excitatory neurons. *Neuron*, 82(6), pp.1317–1333.

Palmer, M.J. et al., 1997. The group I mGlu receptor agonist DHPG induces a novel form of LTD in the CA1 region of the hippocampus. *Neuropharmacology*, 36(11–12), pp.1517–1532.

Parfitt, K.D. & Madison, D. V, 1993. Phorbol esters enhance synaptic transmission by a presynaptic, calcium-dependent mechanism in rat hippocampus. *Journal of Physiology*, 471, pp.245–268.

Parker, M.J. et al., 2015. De novo, heterozygous, loss-of-function mutations in SYNGAP1 cause a syndromic form of intellectual disability. *American Journal of Medical Genetics, Part A*, 167(10), pp.2231–2237.

Patja, K., Mölsä, P. & Iivanainen, M., 2001. Cause-specific mortality of people with intellectual disability in a population-based, 35-year follow-up study. *Journal of Intellectual Disability Research*, 45, pp.30–40.

Pena, V. et al., 2008. The C2 domain of SynGAP is essential for stimulation of the Rap GTPase reaction. *EMBO reports*, 9(4), pp.350–5.

Penzes, P. et al., 2011. Dendritic spine pathology in neuropsychiatric disorders. *Nature neuroscience*, 14(3), pp.285–93.

Penzes, P. et al., 2013. Developmental vulnerability of synapses and circuits associated with neuropsychiatric disorders. *Journal of Neurochemistry*, 126(2), pp.165–182.

Pinto, D. et al., 2014. Convergence of Genes and Cellular Pathways Dysregulated in Autism Spectrum Disorders. *The American Journal of Human Genetics*, 94, pp.677–694.

Pinto, D. et al., 2010. Functional Impact of Global Rare Copy Number Variation in Autism Spectrum Disorder. *Nature*, 466(7304), pp.368–372.

Pitler, T. a. & Alger, B.E., 1992. Postsynaptic spike firing reduces synaptic GABAA

responses in hippocampal pyramidal cells. *The Journal of neuroscience*, 12, pp.4122–4132.

Pláteník, J., Kuramoto, N. & Yoneda, Y., 2000. Molecular mechanisms associated with long-term consolidation of the NMDA signals. *Life Sciences*, 67(4), pp.335–364.

Porter, K. et al., 2005. Differential expression of two NMDA receptor interacting proteins, PSD-95 and SynGAP during mouse development. *The European journal of neuroscience*, 21(2), pp.351–62.

Prchalova, D. et al., 2017. Analysis of 31-year-old patient with SYNGAP1 gene defect points to importance of variants in broader splice regions and reveals developmental trajectory of SYNGAP1-associated phenotype: case report. *BMC Medical Genetics*, 18(1), p.62.

Qiagen, 2012. Qiagen OneStep RT-PCR Handbook. , (October).

Qiagen, 2011. QuantiTect® SYBR® Green PCR Handbook. , (July).

Qiu, J. et al., 2016. Evidence for evolutionary divergence of activity-dependent gene expression in developing neurons. *eLife*, 5, pp.1–15.

Rauch, A. et al., 2012. Range of genetic mutations associated with severe non-syndromic sporadic intellectual disability: an exome sequencing study. *Lancet*, 380(9854), pp.1674–82.

Redin, C. et al., 2014. Efficient strategy for the molecular diagnosis of intellectual disability using targeted high-throughput sequencing. *Journal of medical genetics*, 51(11), pp.724–36.

Roche Applied Science, 2010. Transcriptor First Strand cDNA Synthesis Kit, version 6.

Rodnina, M. V. & Wintermeyer, W., 2016. Protein Elongation, Co-translational Folding and Targeting. *Journal of Molecular Biology*, 428(10), pp.2165–2185.

Ropers, H.-H. & Hamel, B.C.J., 2005. X-linked mental retardation. *Nature Reviews Genetics*, 6(1), pp.46–57.

Routh, B. & Johnston, D., 2009. Anatomical and electrophysiological comparison of CA1 pyramidal neurons of the rat and mouse. *J Neurophysiol*, (102), pp.2288–2302.

De Rubeis, S. et al., 2014. Synaptic, transcriptional and chromatin genes disrupted in autism. *Nature*, 515(7526), pp.209–215.

Rubenstein, J.L.R. & Merzenich, M.M., 2003. Model of autism : increased ratio of excitation / inhibition in key neural systems. *Genes, brain, and behavior*, 2, pp.255–267.

Rumbaugh, G. et al., 2006. SynGAP regulates synaptic strength and mitogen-activated protein kinases in cultured neurons. *Proceedings of the National Academy of Sciences of the United States of America*, 103(12), pp.4344–51.

Sahin, M., 2012. Targeted treatment trials for tuberous sclerosis and autism: No longer a dream. *Current Opinion in Neurobiology*, 22(5), pp.895–901.

Saksela, K. & Permi, P., 2012. SH3 domain ligand binding: What's the consensus and where's the specificity? *FEBS Letters*, 586(17), pp.2609–2614.

Scheffzek, K. & Ahmadian, M.R., 2005. GTPase activating proteins: Structural and functional insights 18 years after discovery. *Cellular and Molecular Life Sciences*, 62(24), pp.3014–3038.

Senter, R.K. et al., 2016. The Role of mGlu Receptors in Hippocampal Plasticity Deficits in Neurological and Psychiatric Disorders: Implications for Allosteric Modulators as Novel Therapeutic Strategies. *Current neuropharmacology*, 14(5), pp.455–73.

Siddiqui, T.J. et al., 2010. LRRTMs and Neuroligins Bind Neurexins with a Differential Code to Cooperate in Glutamate Synapse Development. *Journal of Neuroscience*, 30(22), pp.7495–7506.

Sigma Advanced Genetic Engineering (SAGE) Laboratories, 2012. Project Plan for Generation of SynGAP1 Knockout Rat Model. , pp.1–8.

Sikkel, M.B., MacLeod, K.T. & Gordon, F., 2013. Letter regarding article, "Late sodium current inhibition reverses electromechanical dysfunction in human hypertrophic cardiomyopathy." *Circulation*, 128(10).

De Simoni, A., Griesinger, C.B. & Edwards, F.A., 2003. Development of rat CA1 neurones in acute versus organotypic slices: role of experience in synaptic morphology and activity. *The Journal of physiology*, 550(Pt 1), pp.135–47.

Snyder, E.M. et al., 2001. Internalization of ionotropic glutamate receptors in response to mGluR activation. *Nat Neurosci*, 4(11), pp.1079–1085.

Sot, B. et al., 2010. Unravelling the mechanism of dual-specificity GAPs. *The EMBO journal*, 29(7), pp.1205–14.

Staff, N.P. et al., 2000. Resting and active properties of pyramidal neurons in subiculum and CA1 of rat hippocampus. *Journal of neurophysiology*, 84(5), pp.2398–2408.

Stanko, J.P. et al., 2016. Differences in the Rate of in Situ Mammary Gland Development and Other Developmental Endpoints in Three Strains of Female Rat Commonly Used in Mammary Carcinogenesis Studies: Implications for Timing of Carcinogen Exposure. *Toxicologic Pathology*, 44(7), pp.1021–1033.

Stornetta, R.L. & Zhu, J.J., 2011. Ras and Rap Signaling in Synaptic Plasticity and Mental Disorders. *Neuroscientist*, 17(1), pp.54–78.

Stülpnagel, C. Von et al., 2015. SYNGAP1 Mutation in Focal and Generalized Epilepsy : A Literature Overview and A Case Report with Special Aspects of the EEG.

Neuropediatrics, 46, pp.287–291.

Sutton, M. a et al., 2006. Miniature neurotransmission stabilizes synaptic function via tonic suppression of local dendritic protein synthesis. *Cell*, 125(4), pp.785–99.

Takeuchi, T., Duszkiewicz, A.J. & Morris, R.G.M., 2014. The synaptic plasticity and memory hypothesis: encoding, storage and persistence. *Philosophical transactions of the Royal Society of London. Series B, Biological sciences*, 369(1633), p.20130288.

Thibault, O., Hadley, R. & Landfield, P.W., 2001. Elevated Postsynaptic $[Ca2+]_i$ and L-Type Calcium Channel Activity in Aged Hippocampal Neurons: Relationship to Impaired Synaptic Plasticity. *The Journal of neuroscience : the official journal of the Society for Neuroscience*, 21(24), pp.9744–9756.

Thomas, G.M. & Huganir, R.L., 2004. MAPK cascade signalling and synaptic plasticity. *Nature Reviews Neuroscience*, 5(3), pp.173–183.

Tian, Y. et al., 2012. Urethane suppresses hippocampal CA1 neuron excitability via changes in presynaptic glutamate release and in potassium channel activity. *Brain Research Bulletin*, 87(4–5), pp.420–426.

Tidyman, W.E. & Rauen, K.A., 2016. Pathogenetics of the RASopathies. *Human Molecular Genetics*, (916), pp.1–46.

Till, S.M. et al., 2015. Conserved hippocampal cellular pathophysiology but distinct behavioural deficits in a new rat model of FXS. *Human Molecular Genetics*, 24(21), pp.5977–5984.

Tomita, S. et al., 2005. Bidirectional synaptic plasticity regulated by phosphorylation of stargazin-like TARPs. *Neuron*, 45(2), pp.269–277.

Tomoda, T. et al., 2004. Role of Unc51.1 and its binding partners in CNS axon outgrowth. *Genes & development*, 18(5), pp.541–58.

Turrigiano, G.G. et al., 1998. Activity-dependent scaling of quantal amplitude in neocortical neurons. *Nature*, 391(6670), pp.892–896.

Tyrer, F., Smith, L.K. & Mcgrother, C.W., 2006. Mortality in adults with moderate to profound intellectual disability : a population-based study. *Journal of Intellectual Disability Research*, 51, pp.520–527.

Vazquez, L.E. et al., 2004. SynGAP regulates spine formation. *The Journal of neuroscience*, 24(40), pp.8862–72.

Vetter, I.R. & Wittinghofer, A., 2001. The guanine nucleotide-binding switch in three dimensions. *Science*, 294(5545), pp.1299–1304.

Vissers, L.E.L.M., Gilissen, C. & Veltman, J.A., 2015. Genetic studies in intellectual disability and related disorders. *Nature Reviews Genetics*, 17(1), pp.9–18.

bare, W.G. et al., 2016. A model for regulation by syngap-α1 of binding of synaptic proteins to PDZ-domain "slots" in the postsynaptic density. *eLife*, 5, pp.1–31.

Walkup, W.G. et al., 2015. Phosphorylation of synaptic GTPase-activating protein (synGAP) by Ca^{2+} /Calmodulin-dependent protein kinase II (CaMKII) and cyclin-dependent kinase 5 (CDK5) alters the ratio of its GAP activity toward ras and rap GTPases. *Journal of Biological Chemistry*, 290(8), pp.4908–4927.

Wang, C.-C., Held, R.G. & Hall, B.J., 2013. SynGAP regulates protein synthesis and homeostatic synaptic plasticity in developing cortical networks. *PloS one*, 8(12), pp.1–15.

Wang, J., 2013. Age-Dependent Structural Connectivity Effects in Fragile X Premutation.

Watabe, A.M., Zaki, P.A. & O'Dell, T.J., 2000. Coactivation of β-Adrenergic and Cholinergic Receptors Enhances the Induction of Long-Term Potentiation and Synergistically Activates Mitogen-Activated Protein Kinase in the Hippocampal CA1 Region. *The Journal of Neuroscience*, 20(16), pp.5924–5931.

Westermarck, J. et al., 2001. p38 Mitogen-Activated Protein Kinase-Dependent Activation of Protein Phosphatases 1 and 2A Inhibits MEK1 and Gene Expression p38 Mitogen-Activated Protein Kinase-Dependent Activation of Protein Phosphatases 1 and 2A Inhibits MEK1 and MEK2 Activity and Col. *Molecular and cellular biology*, 21(7), pp.2373–2383.

Whishaw, I.Q., 1995. A comparison of rats and mice in a swimming pool place task and matching to place task: Some surprising differences. *Physiology and Behavior*, 58(4), pp.687–693.

WHO, 2007. Atlas Global Resource for Persons with Intellectual Disabilities.

WHO, 1992. International Statistical Classification of Diseases and Related Health Problems 10th Revision. *World Health Organisation*. Available at: http://apps.who.int/classifications/icd10/browse/2016/en#/F70 [Accessed December 22, 2016].

Wijetunge, L.S. et al., 2013. Fragile X syndrome: From targets to treatments. *Neuropharmacology*, 68, pp.83–96.

Winder, D.G. et al., 1999. ERK plays a regulatory role in induction of LTP by theta frequency stimulation and its modulation by β-adrenergic receptors. *Neuron*, 24(3), pp.715–726.

Writzl, K. & Knegt, A.C., 2013. 6p21.3 microdeletion involving the SYNGAP1 gene in a patient with intellectual disability, seizures, and severe speech impairment. *American journal of medical genetics. Part A*, 161A(7), pp.1682–5.

Wyllie, D.J.A., Manabe, T. & Nicoll, R.A., 1994. A Rise in Postsynaptic Ca2+ Potentiates Miniature Excitatory Postsynaptic Currents and AMPA Responses in Hippocampal Neurons. *Neuron*, 12, pp.127–138.

Xiao, M.Y., Zhou, Q. & Nicoll, R.A., 2001. Metabotropic glutamate receptor activation causes a rapid redistribution of AMPA receptors. *Neuropharmacology*, 41(6), pp.664–671.

Yang, D.W. et al., 2004. Sexual dimorphism in the induction of LTP: Critical role of tetanizing stimulation. *Life Sciences*, 75(1), pp.119–127.

Zhang, J. et al., 2005. Amplitude/frequency of spontaneous mEPSC correlates to the degree of long-term depression in the CA1 region of the hippocampal slice. *Brain research*, 1050(1–2), pp.110–7.

Zhu, J.J. et al., 2002. Ras and Rap control AMPA receptor trafficking during synaptic plasticity. *Cell*, 110(4), pp.443–455.

Zhu, Y. et al., 2005. Rap2-JNK removes synaptic AMPA receptors during depotentiation. *Neuron*, 46(6), pp.905–916.

Zoghbi, H.Y. & Bear, M.F., 2012. Synaptic dysfunction in neurodevelopmental disorders associated with autism and intellectual disabilities. *Cold Spring Harbor perspectives in biology*, 4(3).

Zollino, M. et al., 2011. Integrated analysis of clinical signs and literature data for the diagnosis and therapy of a previously undescribed 6p21.3 deletion syndrome. *European journal of human genetics*, 19(2), pp.239–42.

Zucker, R.S., 1973. Changes in the Statistics of Transmitter Release During Facilitation. *Journal of Physiology*, 229, pp.787–810.